The Design, Synthesis and Characterisation of Amine Functionalised Silica Adsorbents for Post Combustion Carbon Capture

Christopher Mark Starkie, MSci

Thesis submitted to the University of Nottingham

for the degree of Doctor of Engineering

September 2015

Abstract

Amine functionalised silica adsorbents are promising materials for post combustion carbon capture. They exhibit high CO_2 equilibrium adsorption capacities and selectively adsorb CO_2 in the presence of water. A practical method of regenerating these materials in fossil fuel power stations is to utilise steam regeneration. There is a lack of understanding of the long term stability of amine functionalised silica in the presence of steam. This thesis explored the deactivation mechanism of impregnated and covalently tethered amine adsorbents under steam regeneration and humid adsorption conditions. The adsorbents were characterised using organic analysis and nitrogen sorption before and after aging. The effect of steam regeneration aging led to a significant decrease in the CO_2 adsorption uptakes of the adsorbents. Impregnated amine adsorbents were deactivated by leaching of the impregnated amine component from the largest pores of the support. Steam aging also led to diminished amine accessibility caused by amine polymer agglomerating within pores below 8 nm.

To address this issue of instability in the presence of steam amine impregnated silica adsorbents were post functionalised with organosilanes. Under certain conditions this silane functionalisation was shown to selectivity occur at the exterior and pore mouths of the adsorbent. The presence of silane coatings preserved the CO_2 adsorption capacities of the adsorbents after aging. A compromise exists between adsorbent stability and CO_2 uptake behaviour as silane functionalisation led to a reduction in the CO_2 uptake capacity. Post functionalisation of amine impregnated silica with hydrophobic silanes limits the intrusion of water within the pores of the adsorbent. This reduction in water intrusion limits the rate of solubilisation of the amine polymer, thus preventing leaching.

The impregnation of amine polymers onto porous silica supports typically leads to agglomerations and significant pore blocking. This limits the rate of adsorption and uptake capacity of the adsorbents. The introduction of amine-surfactant mixtures into the adsorbent was found to increase accessibility of the adsorption sites leading to enhanced rates of adsorption and CO_2 equilibrium uptakes. The addition of surfactants also yielded a reduction in the regeneration requirements of the adsorbents, by the formation of favourable thin films of amine within the pores of the adsorbent.

Acknowledgements

I would like to thank my supervisor for the first half of my studies, Trevor Drage. He gave me the freedom to experiment whilst offering guidance when needed. Sincere thanks are to be given to Ed Lester, who was a great replacement mentor, always offering good advice and support. Special thanks are given to my co-supervisor Sean Rigby. I fondly recall our marathon meetings, leaving with pages of notes and a head full of ideas. I am greatly indebted to my industrial supervisor Alvaro Amieiro, who gave constant support and encouragement throughout the process. I would also like to thank Johnson Matthey and Sue Ellis for giving me the opportunity to pursue my research ideas in their laboratories.

I would like to express my thanks to all my friends and colleagues at Johnson Matthey for all that they have done. In particular, Jon Bradley for sharing SSNMR knowledge and instrument time, Jamie Stevens for discussions on silica and Iain Hitchcock for his knowledge of gas sorption. Thanks should be extended to Linda Smith for help with vapour sorption, Chan Malde for assistance in rheology and Markus Knabber Buss for generous sorption instrument time.

I would also like to thank the University of Nottingham for providing me with this opportunity. Within Nottingham I would like to thank Lee Stevens and all the Nottingham EngDs for the laughter and support throughout the years.

I am grateful for the enduring support of my parents Richard and Linda and my brother John. I owe a great deal of thanks to Nichola. Thank you for everything over the past four years. You made the tough times good and the good times even better. One thing I had learned from this PhD is just how fortunate I am to be with you.

Contents

3 Experimental 79

List of figures

List of tables

Nomenclature

List of Acronyms:

3-APTES	3-aminopropyltriethoxysilane
AMSA	A type of mesoporous silica
BET	Brunauer–Emmett–Teller method of surface area determination
BJH	Barrett–Joyner–Halenda pore size distribution model
CHN	Organic analysis of the amount of carbon, hydrogen and nitrogen present in a substance
CP	Cross polarisation
DEA	Diethanolamine
$DeNO_x$	Nitrogen oxide removal technology
Diamine	3-2(aminoethyl)aminopropyltrimethoxysilane
DMAP	3-(dimethylamino)propyltrimethoxysilane
DRIFTS	Diffuse Reflectance Infrared Fourier Transform spectroscopy
DVS	Dynamic vapour sorption
EDA	Ethylenediamine
FGD	Flue gas desulfurisation
FTIR	Fourier transform infrared
HMS	Hexagonal mesoporous silica
IGCC	Integrated gasification combined cycle
ITQ-6	A type of mesoporous silica
KIT-6	A type of mesoporous silica
LDF	Linear driving force
MAP	3-(methylamino)propyltrimethoxysilane
MAS	Magic angle spinning
MCF	A type of Mesocellular silica foam

MCM-41	A type of mesoporous silica
MCM-48	A type of mesoporous silica
MEA	Ethanolamine
MOF	Metal organic framework
Monoamine	3-aminopropyltriethoxysilane
MSU-F	A type Mesocellular silica foam
MW	Molecular weight
PAA	Poly(allylamine)
PAMAM	Polyamidoamine
PAP	3-(phenylamino)propyltrimethoxysilane
PEG	Polyethyleneglycol
PEHA	Pentaethylenehexamine
PEI	Polyethyleneimine
PE-MCM-41	Pore expanded MCM-41
$\mathbf{p}\boldsymbol{K}_\mathbf{a}$	Logarithmic acid dissociation constant
$\mathbf{p}\boldsymbol{K}_\mathbf{b}$	Logarithmic base association constant
Pluronic 123	Poly(ethylene glycol)-block-poly(propylene glycol)-block-poly(ethylene glycol). Average MW 5800
SBA-12	A type of mesoporous silica
SBA-15	A type of mesoporous silica
SBA-16	A type of mesoporous silica
SSNMR	Solid state nuclear magnetic resonance
STEM	Scanning transmission electron microscope
TEM	Transmission electron microscopy
TEOS	Tetraethylorthosilicate
TEPA	Tetraethylenepentamine
TETA	Triethylenetetramine

TGA	Thermogravimetric analysis
TPD	Temperature programed desorption
Triamine	3-[2-(2-aminoethyl)aminoethyl]aminopropyltrimethoxysilane
VBC	vinylbenzylchloride
XRD	X-ray diffraction

List of symbols:

1°	Primary molecular site
2°	Secondary molecular site
3°	Tertiary molecular site
A	Pre exponential factor
C	BET constant
d	Lattice parameter (Å)
E_a	Activation energy (kJ mol^{-1})
E_{des}	Enthalpy of desorption (kJ mol^{-1})
I_0	Peak intensity at time = 0
I_t	Peak intensity at time t
K	Kelvin
n	Number of date points used in standard error calculation
P	Arbitrary scaling factor
P/P_0	Relative pressure
P_0	Saturation pressure (atm)
P_v	Pore volume (cm^3 g^{-1})
q_e	Equilibrium uptake
q_t	Uptake at time t
R	Ideal gas constant (8.315 J mol^{-1} K^{-1})
r_p	Pore radius (m)
t	Time (s)
T_1	Spin lattice relaxation time (ms)
$T_{1/2}$	Adsorption halftime (s)
v_1	Frequency factor (Hz)
V_m	Molar volume (dm^3)
x	Largest relative pressure point used to determine the BET surface area (0.3)
X_n	Number of 0.001K^{-1} steps away from the T_1 vs T^{-1} minima

List of Greek letters:

β	Heating rate (K min^{-1})
θ	Diffraction angle (2θ °)
Θ_c	Contact angle (°)
λ	Wavelength of Cuα X-ray radiation (0.154 nm)
σ	Standard deviation
σ	Shear stress (Pa)
η	Viscosity Pa S-$^{-1}$
Υ	Surface tension (mN m^{-1})
$\dot{\gamma}$	Shear rate (s^{-1})

CHAPTER 1

Introduction

There is a general consensus within the scientific community that anthropogenic emissions are a significant factor in the increasing global concentration of carbon dioxide (CO_2). CO_2 is a greenhouse gas, adsorbing thermal radiation from the surface of the Earth. Whilst this mechanism is responsible for maintaining the global temperatures required to sustain life on earth, increasing atmospheric concentrations of CO_2 have led to rising global temperature and potentially disastrous climate change. Global annual CO_2 emissions attributed to fossil-fuel use have increased by 80% from 21 to 38 Gt between 1970 and 2004 [1]. Of this, 13.4 Gt originates from stationary emissions sources such as power, cement production, refineries, iron and steel, petrochemicals and oil and gas processing [2]. More than $2/3^{rds}$ of these emissions are attributed to the power industry, $1/3^{rd}$ of which comes from coal combustion.

It is widely acknowledged that to sustainably meet the power demands of the future, alternative energy sources must be developed at scale. The colossal scale of change required will take several decades to implement, however several decades of ‘business as usual’ would lead to estimated global temperature increases of a few degrees Celsius [3]. This seemingly small change would lead to rising sea levels, increased ocean acidity and unpredictable global weather patterns. It is accepted that the usage of fossil fuels cannot be curtailed sharply without unacceptable consequences. Carbon capture and storage has been proposed as an essential component of future energy technology, allowing the utilisation of fossil fuels without the release of CO_2 into the atmosphere.

Carbon capture and storage can take several forms depending on process requirements. Oxyfuel combustion is the thermal conversion of fuel in a high O_2 atmosphere to yield a flue gas stream of CO_2 and H_2O allowing the CO_2 to be separated out, ready for storage. This process, however, bears a significant energy penalty from the air separation unit used to produce the necessary oxygen stream. There are many practical challenges around the control of the recirculating gas composition, the combustion stoichiometry and material corrosion issues created by the environmental conditions present inside the oxyfuel boiler [4,5]. Integrated gasification combined cycle (IGCC), often referred to as pre-combustion capture, is the gasification of carbon based fuel to generate a stream of H_2 and CO_2 at high pressure. The CO_2 is then separated and the hydrogen combusted to produce water. Such a process has a much greater complexity in comparison to a traditional power plant and hence carries additional risk and cost. The benefits of this system are improvements in efficiency and the production of a stream of CO_2 at high pressure [6].

Post combustion capture technologies using either liquid amine absorption or solid adsorbents are a promising technology option whereby the CO_2 is separated from a mixed composition flue gas. This process can be readily retrofitted to existing fossil fuel power plants. Liquid amine absorption processes have been long established in natural gas purification, using either aqueous solutions of ethanolamine (MEA) or chilled ammonia solvents [7]. Aqueous amine systems are the current lead post combustion capture technology but present a significant energy burden, typically 25-35 % of a plant's energy [8]. This is due to the aqueous solvent being limited to 30 wt% in order to minimise corrosion, resulting in significant energy expenditure through the heating of water during the regeneration process.

Additional issues are the leaching of amine to environment and the long term stability of the amine [9].

Adsorption processes are well known in the separation of mixtures of gases, manipulating the differences in the physisorption or chemisorption behaviour between adsorbate and adsorbent [10]. A wide range of solid adsorbents have been proposed for the adsorption of CO_2 using both chemisorption and physisorption to separate CO_2. Adsorbents that operate by physisorption include activated carbons, metal organic frameworks (MOFs), covalent organic frameworks and zeolites [11-13]. These are best suited to low temperature, high pressure CO_2 separations with their adsorption typically hindered in the presence of water [14]. MOFs can also be functionalised with amine groups to yield selective chemisorbents [15]. The lack of hydrothermal stability of many MOFS coupled with their typically low adsorption capacities at low CO_2 partial pressures can limit their application.

Metal oxides, lithium zirconates and hydrotalcites have also been investigated as selective CO_2 adsorbents offering good selectivity [16, 17]. These materials are suited to high temperature CO_2 capture, requiring high regeneration temperatures and associated stability issues are prevalent. Solid supported amines as CO_2 capture adsorbents are an intense area of study at present. They incorporate the amine chemistry of liquid systems offering selective chemisorption of CO_2 with a reduction in the regeneration requirements. Such materials appear to have variable hydrothermal stability and susceptibility towards oxides of sulphur and nitrogen.

1.1 Objectives of this Thesis

The principal objective of this thesis was to create impregnated amine adsorbents which would be stable to steam regeneration. This objective required an understanding of the degradation of amine functionalised adsorbents in the presence of water. To meet this aim a range of sorbents were aged in the presence of water for extended periods of time and the influence of the aging treatment characterised. The knowledge gained from this study was then applied to create steam stable adsorbents. Impregnated amine adsorbents were post-functionalised with a hydrophobic barrier coating. These adsorbents were then tested under steam regeneration conditions and structure activity relationship determined.

A second aim of this thesis was to understand the interactions of impregnated amines with impregnated additives. Binary mixtures of impregnated amines and surfactants were introduced into the pores of a silica support. Using a range of in-situ and ex-situ techniques the role that additives play on the pore structure and amine accessibility was investigated. A structure of the thesis is presented below:

Chapter 2 provides a comprehensive literature review of amine functionalised solid adsorbents relevant to this thesis.

Chapter 3 contains the experimental section of the thesis describing the materials and methods used in this thesis.

Chapter 4 investigates the role of surfactant additives and how they modify the CO_2 adsorption properties of impregnated amine adsorbents. A family of impregnated amine adsorbents bearing sodium dodecyl sulfate (SDS) and triethanolamine (TEA) were prepared and characterised by nitrogen adsorption to investigate the extent of pore blocking within samples. The mobility of the amine blend with the porous architecture was investigated using saturation recovery ^{1}H SSNMR. This was compared with viscosity measurements of the of the neat liquid amine-surfactant blends. The products formed during CO_2 adsorption were investigated by ^{13}C SSNMR and *in-situ* DRIFTS spectroscopy. The temperature dependence and regeneration requirements were investigated as well as the kinetics of the adsorption process. These findings allowed a further insight into how TEA and SDS influence the CO_2 adsorption of impregnated amine polymer.

The aim of Chapter 5 was to understand the stability of impregnated amine adsorbents in the presence of water under pseudo adsorption and desorption conditions. The difference in stability and capacity between covalently grafted and impregnated amines was explored. The role of amine molecular weight and pore size in degradation was also investigated. Adsorbents were aged under pseudo adsorption conditions consisting of 10 % H_2O/N_2, (1000 ml min^{-1}) at 75 °C for 24 h. To ascertain if the sorbents were stable to long term steam regeneration, the adsorbents were also aged under pseudo-steam regeneration conditions consisting of 66% H_2O/N_2, (100 ml min^{-1}) at 130 °C for 8 h, 0.1 g sorbent. The results of the aging and characterisation experiments are presented first, followed by a discussion of the cumulative findings. The mechanisms for support degradation are investigated and a mechanism for adsorbent degradation is presented.

Chapter 6 sought to develop new materials with an enhanced stability in the presence of steam. Hydrophobic silane groups were grafted onto exposed silica surfaces of the adsorbent particles. These sorbents were investigated to see if the coating affected the CO_2 adsorption under typical adsorption conditions. A range of coatings were studied to investigate influences with changes in structure. The sorbents were aged under pseudo desorption conditions (66% H_2O/N_2 at 130 °C for 8 h) and their stability and degradation pathway studied. The effect of the silane coating on adsorption capacity and kinetics under both dry and wet conditions is discussed as well as changes in the porosity of the materials. To understand the effect of the silane on the adsorption of water coating dynamic vapour sorption experiments were conducted and the findings correlated to the stability of the materials.

Chapter 7 summarises the main conclusions of the thesis and its impact on the advancement of solid adsorbents. This chapter presents preliminary results of novel surface polymerised silicas and develops contiguous ideas for future work.

Chapter 8 is an Appendix bearing supplementary information as marked in the respective chapters.

1.2 References

1. Core Writing Team, R. K. Pachauri, A. Reisinger, *Climate Change 2007 Synthesis Report: Contribution of Working Groups I, II and III to the Fourth Assessment Report of the Intergovernmental Panel on Climate Change.* IPCC, 2007.
2. B. Metz, O. Davidson, H. C. de Coninck, M. Loos, L. A. Meyer (eds.), *IPCC Special Report on Carbon Dioxide Capture and Storage. Prepared by Working Group III on the Intergovernmental Panel on Climate Change.* Cambridge University Press, Cambridge, Unitied Kingdom and New York, NY, USA, 2005.
3. B. Kirtman, S. B. Power, J.A. Adedoyin, G.J. Boer, R. Bojariu, I. Camilloni, F.J. Doblas-Reyes, A.M. Fiore, M. Kimoto, G.A. Meehl, M. Prather, A. Sarr, C. Schär, R. Sutton, G.J. van Oldenborgh, G. Vecchi, H.J. Wang, *Near-term Climate Change: Projections and Predictability. In: Climate Change 2013: The Physical Science Basis.* . Contribution of Working Group I to the Fifth Assessment Report of the Intergovernmental Panel on Climate Change [Stocker, T.F., D. Qin, G.-K. Plattner, M. Tignor, S.K. Allen, J. Boschung, A. Nauels, Y. Xia, V. Bex and P.M. Midgley (eds.)]. Cambridge University Press, Cambridge, United Kingdom and New York, NY, USA, pp. 953–1028, doi:10.1017/CBO9781107415324.023., 2013.
4. B. J. P. Buhre, L. K. Elliot, C. D. Sheng, R. P. Gupta, T. F. Wall, *Oxy-fuel combustion technology for coal-fired power generation.* Progress in Energy and Combustion Science, 2005. **31**(4): p. 283.
5. G. Scheffknecht. L. Al-Makhadmeh, U.S., J. Maier, *Oxy-fuel combustion - A review of the current state-of-the-art* Int. J. Greenhouse Gas Control, 2011. **5**(Supplement 1): p. S16.
6. J. D. Figueroa, T. Fout, S. Plasynski, H. Mcllvried, R. D. Srivastava, *Advances in CO_2 capture technology—The U.S. Department of Energy's Carbon Sequestration Program* Int. J. Greenhouse Gas Control, 2008. **2**: p. 9.
7. Rochelle, G.T., *Amine Scrubbing for CO_2 Capture.* Science, 2009. **325**: p. 1652.
8. S. Choi, J. H. Drese, C. W. Jones, *Adsorbent Materials for Carbon Dioxide Capture from Large Anthropogenic Point Sources.* ChemSusChem, 2009. **2**: p. 796.
9. C. J. Nielsen, H. Herrmann, C. Weller, *Atmospheric chemistry and environmental impact of the use of amines in carbon capture and storage (CCS)* Chem. Soc. Rev., 2012. **41**: p. 6684.
10. D. M. Ruthven, *Principles of Adsorption and Adsorption Processes.* John Wiley & Sons, New York, 1984.
11. C. Pevida, T. C. Drage, C. E. Snape, *Silica-templated melamine–formaldehyde resin derived adsorbents for CO_2 capture.* Carbon, 2008. **46**: p. 1464.
12. K. Sumida, D. L. Rogow, J. A. Mason, T. M. McDonald, E. D. Bloch, Z. R. Herm, T. Bae, J. R. Long, *Carbon Dioxide Capture in Metal-Organic Frameworks.* Chem. Rev., 2012. **112**: p. 724.
13. R. Dawson, E. Stöckel, J. R. Holst, D. J. Adams, A. I. Cooper, *Microporous organic polymers for carbon dioxide capture.* Energy Environ. Sci., 2011. **4**: p. 4239.

14. D. M. D'Alessandro, B. Smit, J. R. Long, *Carbon Dioxide Capture: Prospects for New Materials.* Angew. Chem., Int. Ed., 2010. **49**: p. 6058.
15. T. M. McDonald, W. R. Lee, J. A. Mason, B. M. Wiers, C. S. Hong, J. R. Long, *Capture of Carbon Dioxide from Air and Flue Gas in the Alkylamine-Appended Metal−Organic Framework mmen-Mg2(dobpdc).* J. Am. Chem. Soc., 2012. **134**: p. 7056.
16. J. Blamey, E. J. Anthony, J. Wang, P. S. Fennell, *The calcium looping cycle for large-scale CO_2 capture.* Progress in Energy and Combustion Science, 2010. **36**: p. 260.
17. J. Wang, L. Huang, R. Yang, Z, Zhang, J. Wu, Y. Gao, Q. Wang, D. O'Hare, Z. Zhong, *Recent advances in solid sorbents for CO_2 capture and new development trends.* Energy Environ. Sci., 2014. **7**: p. 3478.

CHAPTER TWO

The status and challenges of amine functionalised silica adsorbents for carbon capture

Ideal adsorbents for post combustion carbon capture are not explicitly defined as undoubtedly this will depend on the nature of the adsorption process. However, a set of guiding principal and desirable traits have been proposed in the literature [1, 2]. The principle aim of solid adsorbents is to reduce the energy penalty compared to liquid amine adsorption systems by *ca.* 30-50 %. This would be achieved by the sorbent having a minimum CO_2 working capacity of 3.0 mmol g^{-1} attainable under realistic flue gas conditions. Realistic flue gas conditions are presented in Table 2.1. Owing to the wide range of gas conditions, the adsorbents would need to be tailored to the specific flue gas compositions. The CO_2 adsorption capacity of a typical 30 % monoethanol amine liquid absorption system is 1 mmol g^{-1} [3, 4]. Hence solid adsorbents offer the potential for greater process intensification and a large reduction in the amount of material that is required to be regenerated. The target adsorption capacity of 3.0 mmol g^{-1} must be achieved with an incoming flue gas temperature of between 40 – 80 °C. The exact conditions are dependent on the fuel source and nature of the flue gas desulfurisation (FGD) and NO_x removal technology ($DeNO_x$).

The operating window between adsorption and desorption should be as narrow as possible with a target desorption temperature between 85 -140 °C. Such temperatures would allow the use of low grade heat or steam from the low pressure turbine cycle.

Table 2.1. Typical flue gas compositions of coal and natural gas fired power plants. Adapted from Drage *et. al.*[1].

Component	Coal (post FGD, $DeNO_x$)	Natural Gas
N_2	75-80 %	74-80 %
CO_2	12-15 %	3-5 %
H_2O	5-14%	7-10 %
O_2	3-4 %	12-15 %
SO_2	10-70 ppm	<10 ppm
NO_x	50-100 ppm	50 ppm
CO	<100 ppm	<5 ppm
Hg/As	ppb	0
Particulates	10-20 mg Nm^{-3}	None
Pressure	0.1 Mpa	0.1 Mpa

The conditions of regeneration ideally should be conducted in an atmosphere of pure CO_2, minimising the need for further separation [5]. Regeneration using low pressure steam is an attractive option for post combustion capture, with the condensation of water to yield pure streams of CO_2. The CO_2 adsorption should be rapid, with the capacity obtained in a matter of seconds to reduce the gas-solid contact time. The adsorbents are expected to be regenerable over thousands of cycles retaining their adsorption efficacy in the presence of water and other flue gas contaminants [6]. To be economical the adsorbent should be scalable so that in a full scale plant the price of the adsorbent should be that of a bulk chemical < \$ 5 kg^{-1}.

The challenge to develop the ideal adsorbent remains, and with such a stringent criteria no single adsorbent may be able to meet these demands. Differing adsorbents have different strengths and limitations and perhaps the adsorbents used in the future will be those which can be best integrated into a sorption process. The remainder of this section discusses the development of solid adsorbents with respect to these idealised targets.

2.1 Types of amine supported silica adsorbents

2.1.1 Amines physically adsorbed on the surface of silica

A scalable method of producing solid adsorbents is to impregnate a bare porous silica support with a CO_2 reactive amine polymer. Typically porous silica is dispersed in a solution of amine and volatile solvent, allowing the amine to diffuse inside the pores of the adsorbent. The solvent is gradually removed leaving the majority of the amine residing within the pores of the support where the interactions between the support and amine are maximised. The amine physically adsorbs onto the surface silica of the porous support through interactions of basic amine groups with the acidic surface silanol species.

Investigations into the dispersion of the amine by transmission electron microscopy (TEM) have shown that the distribution of the amine species is random, with a proportion of the amine located outside the pores of the adsorbent [7]. Typically neat amines or amine polymers show limited CO_2 adsorption capacity due to the slow rate of diffusion through the amine polymer [8]. Additionally the comparative rate of desorption of neat polyethyleneimine (PEI) was shown to be much slower than silica supported PEI [4]. The porous support provides a framework to disperse the amine enhancing the amine accessibility to the amine component leading to practical adsorbents. The wide applicability of the impregnation method allows a wide range of porous media and amines to be utilised.

Impregnated amine silica adsorbents were first reported by Xu *et al.* and designated as the molecular basket adsorbent [9]. The low molecular weight (MW) branched polyethyleneimine (PEI, MW 600) was impregnated within the pores of the mesoporous silica MCM-41. Branched PEI MW 600 is a commercially available hyperbranched viscous liquid polymer, with a high content of primary, secondary and tertiary amines. CO_2 adsorbs at nitrogen sites hence these polymers were chosen to maximise the number of amines suitable for adsorption. Low molecular weight branched PEI is featured in most of the impregnated adsorbent literature, owing to its favourable adsorption properties over other amines. Supported amine polymers must contain high levels of accessible amine component, giving a higher amount of CO_2 adsorption for a given amount of adsorbent. In turn this minimises the mass of sorbent that has to be heated and cooled during cycling. This higher density of CO_2 capture coupled with the lower specific heat capacity of silica compared to water allows solid adsorbents to regenerated with less energy input. Ideal impregnated amine species must have a negligible vapour so that volatile losses do not occur during either adsorption or regeneration.

2.1.1.1 Influence of the structure of polyethlyeneimine

Branched PEI contains a mixture of 1°, 2° and 3° amine sites, the proportion of which is determined by the degree of branching in the polymerisation. The ratio of 1°,2°, 3° is dependent on the synthesis used and in cases of commercial PEI can vary between batches. The ratio of 1°, 2° and 3° amines can be determined using inversely gated ^{13}C SSNMR. Harpe reported a 28:47:25 distribution and Hicks reporting a ratio of 42:33:25 for 1°,2° and 3° amines respectively [10, 11]. These studies suggest that commercially available PEI has a much lower proportion of tertiary amine groups than is often assumed. Owing to the differences in the CO_2 adsorption behaviour of 1°, 2° and 3°amines, changes is this ratio would lead to distinct differences in CO_2 adsorption uptake and kinetics. The adsorption mechanism of CO_2 is discussed at length in Section 2.5.

Drage *et al.* investigated the effect of PEI molecular weight on the performance of silica supported amines for CO_2 capture [12]. Lower molecular weight polymers included both linear PEI (MW 423) and branched PEI (600 MW and 1800 MW). Linear PEI appeared to be unstable over repeated cycling owing to volatile losses under regeneration conditions. Larger molecular weight PEI are more difficult to impregnate within porous media with pore blockages observed [13]. The viscosity of heavier molecular weight PEI is much greater thus leading to a reduction in the kinetics and equilibrium CO_2 adsorption capacity.

2.1.1.2 Variation of amine type

Other ethylenediamine polymers such as tetraethylenepentamine (TEPA) have been extensively studied as amines for CO_2 adsorption capacity [14-16]. Work by Qi found a significant increase in the CO_2 adsorption capacity of TEPA compared to the equivalent amount of PEI. This was attributed to the lower viscosity of the TEPA component leading to a greater number of accessible sites. However, the vapour pressure of TEPA is greater than that of PEI. Therefore volatile losses were observed with 50 % retention in its CO_2 adsorption capacity after 50 regeneration cycles (75 °C, N_2, 25 min). Pentaethylenehexamine supported on SBA-15 has also been explored, with similar adsorption behaviour to TEPA but with a marginal increase in stability [17]. That said, ethylenediamine impregnated SBA-15 was studied by Zheng *et. al.* who reported a degree of stability over 10 successive cycles. This could be due to the bidentate coordination of ethylenediamine to the surface of the silica [18]. Diethanolamine (DEA) utilised in liquid amine scrubber systems, has also been impregnated onto pore-expanded MCM-41 exhibiting fair CO_2 adsorption capacities [19]. This study did show a slight deactivation in CO_2 adsorption capacity after successive cycling, corresponding to leaching of the amine.

Chaikittisilp *et. al*. prepared low molecular weight poly(allylamine) (PAA) which features exclusively primary amine groups, albeit with a silightly lower nitrogen content than PEI (24 wt% vs 32 wt%) [20]. They noted that with increasing mass loadings of PAA and linear PEI the amine efficiency of the adsorbent decreased, whereas that of branched PEI increased. This could be due to the different structural confirmations adapted by branched and linear polymers. Adsorbents with homogenous nitrogen species could be beneficial owing to the differing stability of 1°, 2° and 3° amine groups (Section 2.8).

Fadhel *et al.* investigated the use of impregnated polyamidoamine (PAMAM) using different generations of step wise dendrimers [21]. Similar to PEI, the CO_2 adsorption of PAMAM was greatly increased upon impregnation onto silica. This is believed to be due to the support disrupting the internal hydrogen bonding network allowing the amines to react with CO_2. The PAMAM adsorbents were found to adsorb increasing amounts of CO_2 with increasing temperature. This suggested the adsorption was diffusion limited as the addition of heat improved the mobility of the polymer increasing the number of accessible sites.

2.1.1.3 The influence of amine loading

The extent of amine loading is a crucial factor in adsorbent design. With too low amine loading the CO_2 adsorption capacity is below the target levels. At higher levels of amine loading a reduction in amine efficiency, CO_2 adsorption capacity and kinetics is present [9]. Furthermore, amines residing on the exterior surface of the adsorbent behave similar to bulk amines. It has been suggested that additional amine can lead to the formation of a resistive amine film coating the exterior of the adsorbent, restricting access to the pores [17]. Linneen investigated the impregnation of TEPA on silica aerogels noting negligible accessible pore volume at 77 K for TEPA loadings of 90 wt % [22]. This coincided with a reduction in amine efficiency suggesting that a large proportion of the amine sites were inaccessible. Infrared spectroscopy investigations by Wilfong *et al.* highlighted that by increasing the TEPA loading from 12 to 37wt% the Si-OH signal decreased by 9% suggesting the TEPA was present in multilayers within the interior and exterior of the silica particle. They also noted a reduction in adsorption kinetics which was attributed to pore blockages [23].

2.1.2 Covalently tethered amine on silica adsorbents

Amines can be attached to solid supports though a covalent bond typically formed between a surface silanol and a silicon alkoxide. The covalent bond between the support and amine imparts greater stability as leaching due to volatile physisorbed amines is none existent. The adsorption rate of these materials is usually greater as the functionalisation occurs at the pore surface leaving the pore void unaffected. These materials are constructed using well known organic chemistry with a general scheme presented below in Figure 2.1. The silanol groups on the surface of the silica react with the silicon alkyoxide, releasing an alcohol dependent on the type of silicon ester used. Shorter esters such as methyl silicon esters tend to be more reactive than bulkier propyl esters on the basis of steric crowding of the electrophilic silicon centre.

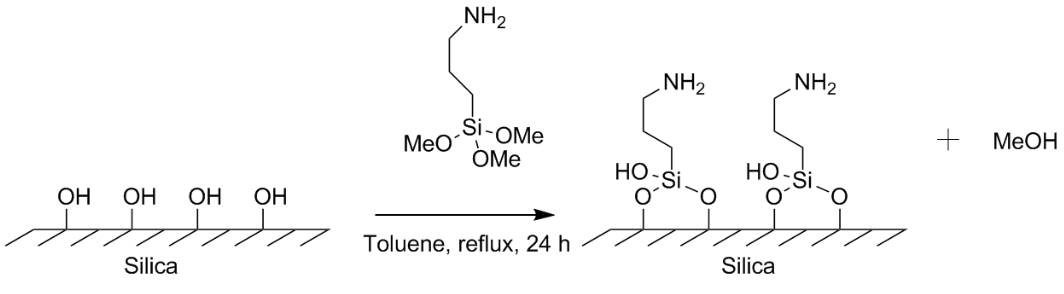

Figure 2.1. Schematic showing the grafting of 3-aminopropyltrimethoxysilane on a silica surface.

The concept of CO_2 adsorption on immobilised amine supports was first reported by Leal *et al.*, who prepared 3-aminopropyl immobilised on silica gel [24].

As is the case for impregnated adsorbents, the amount of amine loading and amine efficiency are critical variables in the performance of covalently tethered adsorbents. Figure 2.2 highlights the most commonly used amines grafted to the surface of porous silica supports.

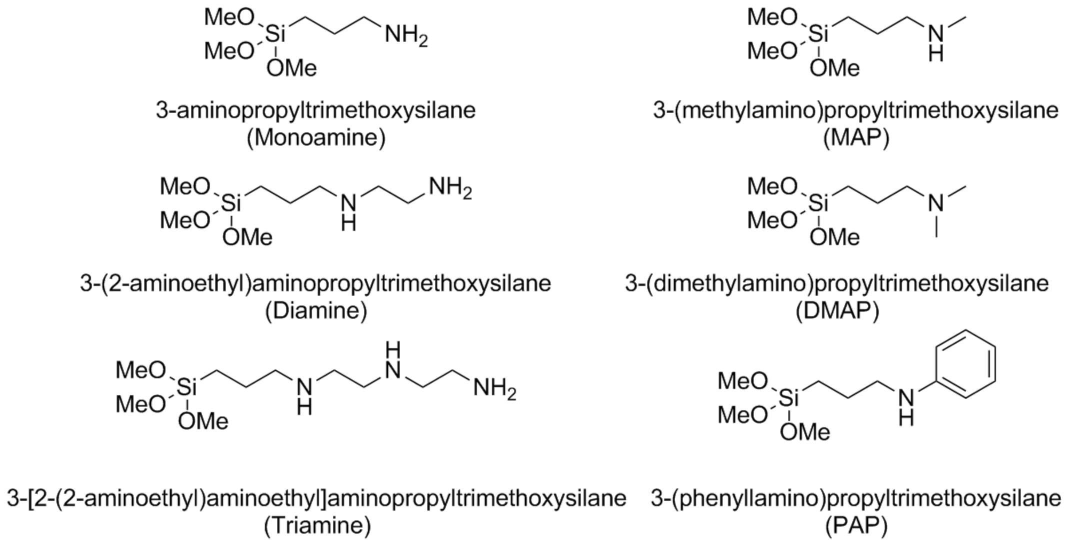

Figure 2.2. The most commonly used aminosilanes to functionalised porous silicas relevant to carbon capture.

2.1.2.1 Types of silane used to functionalise the surface of silica

Monoaminesilanes such as the frequently utilised 3-aminopropyltrimethoxysilane usually contain 1 primary amine head group. Diaminesilanes have one primary amine and one secondary amine in their structure while triaminesilanes feature two secondary amines and a terminal primary amine. Although a vast number of usable silanes are available many more can be envisaged; researchers of solid adsorbents are limited to those commercially available silanes to develop a low cost adsorbent. A large range of covalently tethered adsorbents have been prepared on a range of porous supports. The limiting factor affecting the deposition of silanes on the surface of the support is the number and accessibility of the surface silanols. The number of surface silanols is influenced by the silica preparation method. Van Der Voort *et al.* reported that the surface silanol density decreased with increasing calcination temperature [25]. They also reported an increase in silanol density arising from ethanol extraction of the templates as oppose to calcination.

Work by Knowles discovered that the pore curvature of the silica support affected the accessibility of the silanol groups, with a smaller extent of curvature leading to a greater silane loading [26]. This was caused by the slow reaction of surface silanols within the confines of small pores. The concentration of surface hydroxyl groups can be increased by hydrolysis of the siloxane bridges by hydrothermal treatment. However, conditions need to be strictly controlled to avoid hydrolysis of the silica structure [27]. This approach was completed by Wei *et al.* who boiled calcined SBA-16 in water for 2 h, leading to an increased in the CO_2 adsorption capacity after functionalisation with 3-aminopropyltriethoxysilane [28].

2.1.1.2 Effect of synthesis conditions

Synthesis conditions in the literature vary with the role and requirements of water in the system investigated [29, 30]. A critical point is present, as increasing levels of water led to homocondensation of the silanes independent of the support as well as increased multilayer surface condensation. The addition of small amounts of water during silane deposition has been shown to yield 30 % increase in silane loading and subsequently enhance the CO_2 uptakes [31]. In this work Harlick *et al.* also noted a reduction in silane grafting efficiency with increasing concentrations of silane loadings, with an efficiency below 25% for the highest loaded adsorbents. Huang *et al.* investigated the grafting of 3-aminopropyltriethoxysilane (3-APTES) using supercritical propane finding that increased amounts of amine loading could be incorporated into the structure leading to materials with a higher CO_2 adsorption capacity. The differences in material performance were modest and such high pressure techniques are likely to be able to produce adsorbents at scale for a target price of \$5 kg [32].

Sánchez-Vicente *et al.* investigated functionalised SBA-15 with 3-APTES grafted under supercritical CO_2 hypothesising that the grafted species would be either an alkylammonium carbamate or a carbamic acid [33]. This could be lead to the silane deposited in the optimum configuration to adsorb CO_2. The adsorbents produced using super critical CO_2 yielded very high amine efficiencies between 0.37 – 0.52 however the extent of amine loading and CO_2 adsorption capacity was similar to that of toluene grafted adsorbents.

2.1.3 Multistage tethering approaches to silica functionalisation

Alternative strategies towards the immobilisation of amines on silica surfaces include a two-step synthetic strategy; functionalisation with alkyl halide groups then subsequent substitution reaction with the required amine species. This method allows the use of more elaborate organic functionality to be introduced onto the support surface. Multistep approaches should be used with caution as each added step adds complexity and hence cost. This method has been successfully utilised by Kim *et al.* who successfully functionalised MCM-48 using the two step procedure shown in Figure 2.3. This allowed the incorporating of the sterically hindered pyrrolidine group [34].

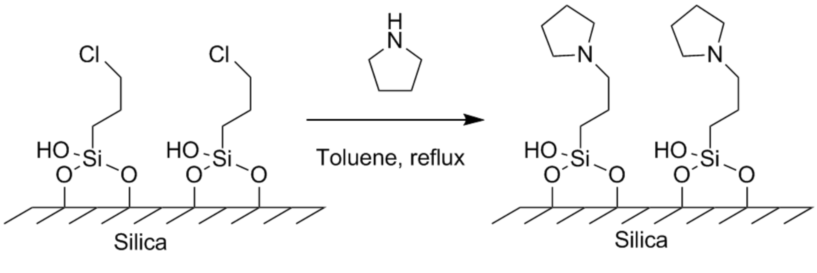

Figure 2.3. The two-stage grafting approach to surface amine functionalisation.

The stability of amine functionalised silica adsorbents has been improved by the grafting of PEI and TEPA to the surface using 3-glycidoxypropyltrimethoxyislane linkages [35]. It was found that covalently grafted PEI performed similarly to low levels of impregnated PEI, but the influence of water on the adsorbent stability was not investigated. The covalent attachment of PEI was improved upon by Du *et al.* first grafting polyacrylic acid to the surface of silica aerogels followed by subsequent functionalisation with PEI and TEPA [36]. They found that a high level of amine functionalisation could be grafted to the surface of the adsorbent. This lead to adsorbents with adsorption capacities of up to 3.80 mmol g^{-1} and no loss in capacity with repeated cycling.

Moschetta *et al.* described an alternative method to produce aminopropyl functionalised silica to yield aminopropyl groups with better spacing than those formed in solution [37]. They initially grafted alkylhalide silanes onto the surface followed by displacement with ammonia (100 °C, 1000 psi). These materials exhibited only a marginally improved CO_2 adsorption capacity, limiting the practical application of sorbents produced this way. However adsorbents produced via this method could utilise isotopically labelled ^{15}N and be used to investigate the mechanism of CO_2 adsorption.

2.1.4 Surface polymerised amine adsorbents

A limitation of covalently tethered amines is often the low amounts of amine that can be incorporated onto the surface of the silica. This low loading decreases the equilibrium adsorption capacity of the adsorbents. To address this issue polymerisation of reactive amines or their precursors within the pores of mesoporous silicas has been explored. This approach allows a greater amount of covalently bound material to be incorporated within the pores of an adsorbent. Step-wise chain growth of melamine dendrimers for CO_2 separation was first reported by Liang [38]. In this work SBA-15 was functionalised with aminopropyl groups with each generation built up using cyanuric chloride and ethylenediamine. The authors noted the material adsorbed CO_2 by a mixture of physisorption and chemisorption , with an enthalpy of adsorption reported between 50 – 70 kJ mol^{-1}. This is lower that the accepted value of ~90 kJ mol^{-1} [39]. The material performance was lower than expected which was attributed to amine inaccessibility either through crosslinking of the bidentate amines or steric crowding of the active sites. The CO_2 adsorption capacities were vastly decreased for the 4th generation adsorbents with nitrogen sorption showing negligible pore volume present. This is consistent with work by Acosta, who prepared and characterised melamine dendrimers on SBA-15 [40]. They found that for 8.2 nm pore diameter SBA-15 the dendrimers were limited to four generations after which the pores becomes saturated.

Chaikittisilp *et al*. investigated the stepwise growth of L-lysine on mesoporous silica for CO_2 adsorption [41]. The stepwise growth was achieved by the successive addition of *Z*-protected L-lysine N-carboxyanhydride to 3-APTES modified SBA-15 followed by a HBr/AcOH deprotection. These adsorbents exhibited reductions in pore volume and surface area with increased loading. The amine efficiency remained constant at 0.22 with increasing organic loading. This suggested that amine accessibility was not the limiting factor. The adsorption capacities of these adsorbents were similar to those achieved with well grafted APTES, which indicates that the deprotection approach may require optimisation.

Amines have been polymerised onto the surface of porous silicas by the polymerisation of aziridine onto a silica surface [11, 13, 42]. This leads to polyethlyeneimine covalently attached to the surface of the silica resulting in high levels of amine loading. For highly loaded materials the proportion of amine incorporated into the structure was low, with spontaneous polymerisation outside of the pores was observed. The average molecular weight of the PEI was proportional to the relative ratio of aziridine to silica used, with a typical PEI molecular weight of 6000 Daltons. The equilibrium CO_2 adsorption capacity was proportional to extent of amine loading with a maximum CO_2 adsorption capacity of 5.55 mmol g^{-1}. A lack of control is noted for porous systems owing to the high reactivity of the aziridine monomer. This leads to constriction at the pore mouths of the adsorbents leading to a large reduction in the adsorption kinetics and uptake capacities. The adsorption capacities of these materials were greater at 75 °C than at 35 °C, suggesting that the adsorption process is limited by the diffusion of CO_2 through the amine. These materials were shown to be stable is the presence of water, with their CO_2 capacities significantly enhanced in the presence of water vapour. Chaikittsilp investigated a vapour phase method of the synthesis of surface growth PEI sorbents noting that this method could be used to yield materials with greater amine loadings and lower average PEI molecular weights [43].

Work by Qi produced covalently tethered ethylenediamines by polymerising 2-methyl-2oxazoline in the presence of 3–iodopropyl functionalised silica [44]. The adsorbents were found to be stable under repeated cycling and exhibited high CO_2 adsorption. However, the long term stability of these adsorbents was not reported. This pathway appears to offer more control that using aziridine polymerisation and could provide a pathway for stable materials with high adsorption capacities.

2.2 CO_2 adsorption behaviour

Much of the literature of solid adsorbents focuses on the equilibrium CO_2 adsorption capacity of an adsorbent as an essential factor determining a materials suitability for CO_2 capture. Whilst this is a crucial aspect of adsorbent behaviour it often does not reflect achievable adsorption capacities under realistic adsorption conditions. The greater the uptake capacity of an adsorbent the more economical the process will be as less adsorbent is required to abate the same quantity of CO_2. This would lead to a smaller plant footprint and lower material handling requirements. Furthermore, regeneration would be more efficient as there is a lower amount of material to heat.

Given the long times required for amine impregnated adsorbents to reach their equilibrium CO_2 adsorption capacity, the working capacity is a more suitable measure of material performance. The working capacity of an adsorbent is defined as the difference in adsorption capacity between adsorption and desorption analysis conditions for a limited cycle time. Under realistic operating conditions it may be more economical to have short residence times at which point the adsorbent is far away from the equilibrium adsorption capacity.

For impregnated amine adsorbents the theoretical CO_2 adsorption capacity of the adsorbent is determined by the maximum amount of amine that can be constrained within the pores of the adsorbent. This can be calculated from the pore volume of the support and density of the amine polymer. In practical adsorbent preparations, as the fraction of the impregnated amine approaches the maximum, increasing amounts of amine are located at the exterior of the adsorbent where it behaves similar to bulk amine.

2.2.1 CO_2 adsorption on amine impregnated adsorbents

As shown in Figure 2.4, many impregnated adsorbents possess CO_2 equilibrium adsorption capacities in excess of the target requirement of 3 mmol g^{-1}. Owing to the wide range of analysis conditions used in the literature the capacities in Figure 2.4 were all recorded under 100 % CO_2 at 75 °C using a thermogravimetric analyser (TGA). There is a general trend with increasing PEI loading and equilibrium CO_2 adsorption capacity until the pores become filled. After this point the CO_2 adsorption falls drastically as amines become inaccessible. The values in Figure 2.4 represent equilibrium adsorption capacities often reported over 1 h of adsorption. The capacities measured at shorter times are much lower and hence a key area is to develop impregnated adsorbents with much faster adsorption kinetics.

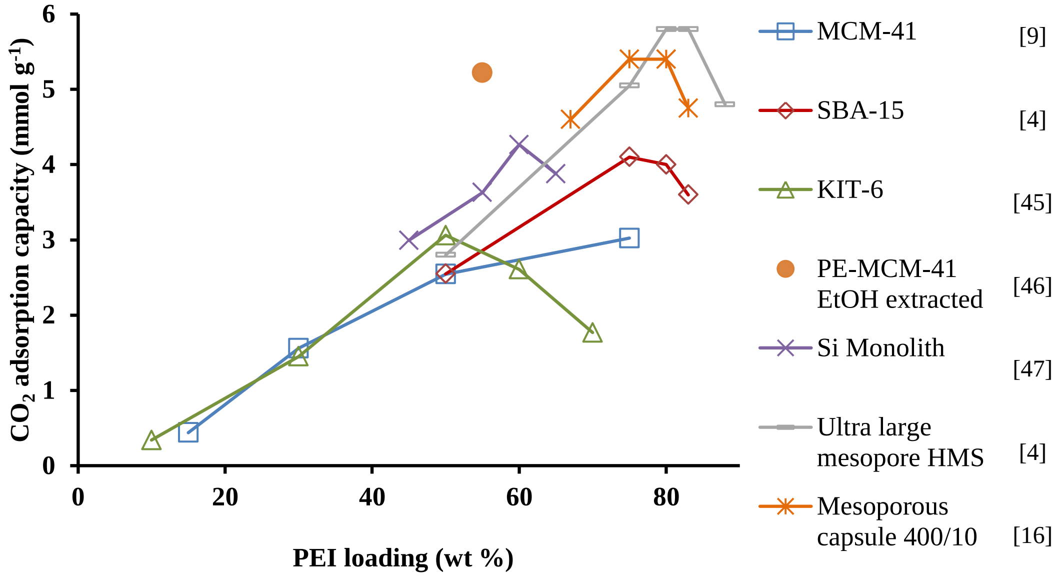

Figure 2.4. CO_2 adsorption capacities of PEI impregnated adsorbents measured under 100 % CO_2 at 75 °C using TGA.

The following section describes the factors that influence the CO_2 adsorption behaviour of amine impregnated silica adsorbents. Practical adsorption capacities often deviate significantly from the theoretical maximum adsorption capacities. This phenomenon was observed by Song *et al.* who impregnated MCM-41 with increasing loadings of PEI [8]. Increasing amounts of PEI led to a plateau in CO_2

adsorption at 80 wt% PEI, with increasing amounts yielding a decline in CO_2 adsorption capacity. Gas sorption experiments showed significant reduction in accessible pore volume and surface area suggesting that the pores were completely filled. At increasing loadings the amine deposited in multilayers on the exterior of the adsorbent particles forming a diffusive barrier of bulk PEI. Analogous results were reported by Wang who investigated the effect of PEI loading on SBA-15 [48]. The authors noted the maximum adsorption capacity was obtained with a PEI loading of 60 wt%. However the maximum amine efficiency was obtained with 30 wt% PEI attributed to the optimum dispersion of PEI within the pores of the adsorbent.

Similar reductions in amine efficiency with increasing amine loading were also observed by Linneen *et al.* [49]. They noted that as the TEPA loading surpassed 80 wt% no pore volume remained accessible at to N_2 at 77 K and the material exhibited a maximum CO_2 adsorption capacity of 5.5 mmol g^{-1}. Once the TEPA loading was increased to 90 wt% a reduction in the adsorption capacity was observed coupled with an increase in the rate of adsorption. This suggests that the amine was agglomerating on the surface of the particle restricting the diffusion of CO_2. For increasing concentrations of TEPA from 40 - 80 wt% the amine efficiency remained roughly constant suggesting that until this point the amine was filling the void spaces within the pores.

Wilfong *et al.* investigated the influence of TEPA film thickness on CO_2 adsorption behaviour using Diffuse Reflectance Infrared Fourier Transform spectroscopy (DRIFTS) [23]. They found that increasing the thickness of the amine film led to enhanced CO_2 amine interactions, which lead to the formation of an interconnected zwitterionic network of ammonium carbamate pairs. This network is thought to retard the diffusion of CO_2 leading to a decrease in amine efficiency. They rationalised that adsorbents with higher capacities and increased kinetics could be formed by using thinner films.

Srikanth and Chuang investigated the density of TEPA impregnated silica adsorbents using DRIFTS [50]. They found that increasing thicknesses of amine layers led to an increase in the regeneration requirements compared to thinner layers. Thin layers and binary impregnation mixtures appeared to increase the amount of CO_2 adsorbed as carbamic acid. This carbamic acid species was found to desorb at 25 °C whilst carbamates were desorbed at 75 °C under an inert gas flow. Increasing the film thickness would require the CO_2 to diffuse through a greater average distance of reactive amine, meaning a repeated readsorption is more likely.

2.2.2 CO_2 adsorption on binary mixtures impregnated on porous silica

Song *et al.* substituted a portion of the amine polymer component for the surfactant polyethylene glycol (PEG) [8]. This increased the adsorption capacity and rate of adsorption of impregnated amine adsorbents. As PEG alone does not adsorb appreciable quantities of CO_2 at 75 °C, it was rationalised that the presence of hydroxyl groups influenced the adsorption mechanism leading to the formation of bicarbonate species. This would lead to an increase in the amount of CO_2 adsorption due to the 1:1 molar ratio in the bicarbonate mechanism (see Section 2.5).

Based on their work of TEPA impregnated silicas with the addition of DEA, Yue proposed a different CO_2 adsorption mechanism in the presence of hydroxyl groups (Figure 2.5) [51]. They reported that substituting a proportion of impregnated TEPA for DEA resulted in an increased CO_2 uptake enhancement from 3.2 to 3.7 mmol g^{-1}. They suggested that two different carbonate species were formed, distinguishing two species during temperature programmed desorption and relating to carbamates and a bicarbonate species. In such a mechanism a neighbouring hydroxyl group abstracts a proton from the amine forming a bicarbonate species. However their work does not explain why on the basis of pK_a this seems unlikely to occur. In such a system the pK_a of the conjugate acid of propyl amine is approximately 10 whereas the pK_a of propanol is 16. This suggests that in any comparative system acid sites are more likely to be deprotonated by any nearby amine in preference to a hydroxyl group.

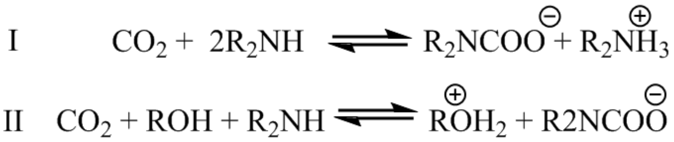

$$\text{I} \quad CO_2 + 2R_2NH \rightleftharpoons R_2NCO\overset{\ominus}{O} + R_2\overset{\oplus}{N}H_3$$

$$\text{II} \quad CO_2 + ROH + R_2NH \rightleftharpoons R\overset{\oplus}{O}H_2 + R2NCO\overset{\ominus}{O}$$

Figure 2.5. The reaction for carbamate formation (I). The reaction mechanism proposed by Yue *et al*. in the presence of a hydroxyl group(II) [51].

Yan reported the adsorption of amine impregnated silicas in which the pluronic 123 template within the pores had not been extracted [52]. In their contribution they proposed that the increases in CO_2 adsorption capacity were due to the swelling of PEI chains. It was suggested that the presence of the hydroxyl group led to a change in mechanism leading to a 1:1 ratio between amine and CO_2. However, when PEG was used with a much greater proportion of hydroxyl groups compared to pluronic 123, the synergistic effect on CO_2 uptake was less. This is despite an increase in hydroxyl group concentration of PEG compared to pluronic 123. They proposed that the addition of PEG hindered the adsorption of CO_2 relative to the incorporation of P123/PEI on silica. Work by Wang *et al.* screened a wide array of co-impregnated surfactants and polymeric amines on mesoporous silica supports [53]. They reported that a wide range of surfactant additives both with and without hydroxyl groups led to a modest increase in CO_2 adsorption capacity.

Recent work by Dao *et al.* explored the role of blends of impregnated amines and hydroxyl bearing groups [54]. Within this piece of work they noted an increase in CO_2 adsorption capacity with the addition of hydroxyl groups and related this to the mechanism proposed by Yue. It was noted that the optimal material performance was produced by blends of TEPA and amines with pendent hydroxyl groups. They investigated the role of non-hydroxyl bearing amines whereby the amine is much more basic than that of a hydroxyl, but did not witness a synergistic effect upon CO_2 adsorption. They did not rule out a change in mechanism but hypothesised that hydroxyl groups in close proximity could stabilise the carbamate formed via hydrogen bonding interaction.

Dao *et al*. optimised the impregnation conditions of TEPA and DEA supported mesocellular silica foam (MSU-F) adsorbents to yield a CO_2 adsorption capacity of 6.86 mmol g^{-1} under static adsorption conditions (100 kPa, 50 °C) [55]. This adsorbent exhibited an amine efficiency of 0.65 under dry conditions, which is attributed to extensive physisorption under the idealised analysis conditions. The aforementioned work suggests that the use of two impregnation partners on porous silica supports provides an important pathway of tuning adsorbent properties. Whilst increases in capacity are obtained for impregnated binary mixtures of adsorbents little work has been reported on their mechanism of action or the influence of such materials on kinetics.

Sanz *et al.* observed enhancements in the adsorption of CO_2 using PEI impregnated onto propylamine modified silica [56]. They rationalised that the tethered amine surface provided a better dispersion of the amines leading to increases in amine efficiency and adsorption kinetics.

These increases in adsorption capacity by impregnation of two species may be applicable to other amine supports. This would provide a simple method to further increase the adsorption capacity of many highly performing supports.

2.2.3 CO_2 adsorption on covalently tethered amines

As can be seen in Table 2.2, all covalently tethered amines fall below the target CO_2 uptake of 3 mmol g^{-1}. However these materials are still of interest as they typically have much faster CO_2 adsorption kinetics. Unlike impregnated adsorbents, CO_2 adsorption is rarely diffusion limited, hence a trade-off between capacity and kinetics can be made. For covalently tethered adsorbents the discrepancy between the observed CO_2 adsorption capacity and the measured CO_2 adsorption capacity is not directly proportional to the silane loading. The orientation of the amine groups is crucial as in most instances the amine groups initially physisorb parallel to the surface. This maximises the interactions between the amine group and the silica surface. This also brings the hydrolysable silyl ether groups in close proximity to the surface silanols facilitating hydrolysis. For low silane loadings the amine efficiency is greater than for high silane loadings. This is because higher silane loadings can lead to the formation of organosilane mutlilayers of amines, whereby a fraction of the amine is inaccessible [57].

Table 2.2. A comparison the covalently tethered adsorbents relevant to post combustion capture. Adapted from [58].

Support	Amine type	Amine loading (mmol g^{-1})	Ads. Temp. (°C)	CO_2 conc.[a] (%)	CO_2 uptake (mmol g^{-1})[b]	Amine eff. (a.u.)	Ref
Aerogel	MA	1.59	25	100	0.67	0.42	[58]
MCM-48	MA	2.30	25	100	2.05	0.89	[59]
AMSA	MA	2.17	25	10	1.95	0.90	[60]
AMSA	MA	2.17	50	10	1.19	0.55	[60]
SBA-15	MA	3.92	25	100[c]	1.80	0.46	[61]
Aerogel	MA	6.62	0	100	1.80	0.27	[62]
MCM-48	MA	2.28	25	100	1.68	0.74	[63]
Aerogel	MA	5.00	40	100[d]	1.80	0.36	[64]
Aerogel	DA	3.40	25	100	1.20	0.35	[58]
HMS	DA	4.57	20	90	1.34	0.29	[65]
SBA-15	DA	3.25	60	15	1.73	0.53	[66]
SBA-15	DA	5.16	45	100	1.86	0.36	[67]
Aerogel	TA	4.13	25	100	1.64	0.40	[58]
Aerogel	TA	7.40	25	100	2.61	0.35	[68]
Hydrated SBA-15	TA	5.80	60	15	1.80	0.31	[69]
PE-MCM-41	TA	7.95	25	5	2.65	0.33	[31]
PE-MCM-41	TA	7.80	70	5	2.28	0.29	[70]
SBA-15	TA	5.21	45	100	1.75	0.34	[71]
PE-MCM-41	TA	4.33	50	100	2.43	0.56	[72]
MCF	TA	4.00	75	15	1.30	0.33	[73]
SBA-15	TA	3.68	60	15	2.41	0.65	[66]
PE-MCM-41	TA	7.90	25	100	2.75	0.35	[74]
Templated silica	TA	5.18	25	100	1.74	0.34	[75]
SBA-12	MAP	2.17	25	10	0.98	0.45	[76]

Table 2.2. Continued

Support	Amine type	Amine loading (mmol g^{-1})	Ads. Temp. (°C)	CO_2 conc.[a] (%)	CO_2 uptake (mmol g^{-1})[b]	Amine eff. (a.u.)	Ref
SBA-15	MAP	1.92	60	15	0.25	0.13	[77]
SBA-15	DMAP	1.66	60	15	0.05	0.03	[77]
SBA-12	PAP	1.54	25	10	0.68	0.44	[76]

[a] In cases where the CO_2 concentration was below 100% either N_2 or He were used to dilute the CO_2. [b] Measured using either TGA, Gas sorption, GC or MS, this may have an influence on the reported capacity. [c] Measured under 0.1 atm. CO_2. [d] Measured under 0.15 atm. CO_2

2.2.3.1 The effect of amine structure on grafted amine adsorbents

The effect of amine structure has been investigated by a number of researchers. Both Hiyoshi and Ko compared the CO_2 adsorption of 1°, 2° and 3° grafted amine adsorbents on SBA-15 [69, 78]. They found that that the organic loading of the silane decreased with silane molecular weight, rationalising this with the increasing steric demands of the silane. The CO_2 adsorption capacities were measured to be 0.05, 0.25 and 0.66 mmol g^{-1} for 3°, 2° and 1° amine adsorbents respectively. The amine efficiencies also decreased in a similar manner with reported values of 0.03, 0.13 and 0.25 for the 3°, 2° and 1° amine adsorbents respectively. This was rationalised to be due the steric constraints of the additional methyl groups retarding the formation of a carbamate species. This pattern was observed more recently by Ko *et al.* who also noted a decrease in the enthalpy of CO_2 adsorption for the increasing number of methyl groups at the nitrogen [78]. In their work they observed a greater CO_2 uptake and amine efficiency for 2° aminosilanes than the previous study. From these observations it appears that the order of reactivity of amines for CO_2 adsorption follows the order of 1°< 2°< 3° amines.

Zelenak *et al*. studied the effect of amine basicity on CO_2 adsorption for a range of amines on SBA-12 [76]. It was reported that the higher the basicity of the amine the higher the uptake capacities, with the CO_2 adsorption following the order of basicity AP>MAP>PAP (Figure 2.3). In terms of basicity AP and MAP have very similar pK_b values. Although the electron donating effect of the methyl group should lead to a higher basicity, the steric demand of the methyl group reduces the observed basicity. In the instance of PAP, the basic lone pair of the nitrogen is delocalised within the aromatic π system resulting in PAP having a pK_b of 8.9 compared to a pK_b of ~4 for AP and MAP. The amine efficiency also echoed this trend in basicity, with SBA-12 AP having an efficiency of 0.49 compared to a theoretical maximum of 0.5 and SBA-12 MAP having a slightly lower efficiency of 0.45. However, SBA-12-PAP had a lower efficiency of 0.43 and a capacity ~60% of that of the AP functionalised silica. Given the general similarities in pK_b and CO_2 adsorption capacity, the principal factor affecting capture capacity is the steric requirement of the silane. Larger silanes such as PAP lead to a reduction in surface silane loading which inhibits the CO_2 uptake capacity of the materials. The CO_2 adsorption capacities were reported as 1.04, 0.98 and 0.68 mmol g^{-1} for AP, MP and PAP sorbents respectively at 25 °C. Desorption was completed without increasing the temperature, suggesting that for PAP sorbents a significant contribution of the CO_2 adsorption may come from physisorbed CO_2.

Brunelli *et al.* investigated the influence of the alkyl linker length on the CO_2 adsorption capacity of covalently tethered aminosilanes [79]. They found that the optimum length for CO_2 sorbents was a propyl carbon chain, however the CO_2 adsorption conditions were recorded at 400 ppm CO_2 at 25 °C yielding a maximum observed CO_2 adsorption capacity of 0.085 mmol g^{-1}. Negligible differences in the amine loading of the differing sorbents were reported as the amine loading was well below complete surface coverage. Increasing the amine linker length beyond a propyl chain led to a reduction in the CO_2 adsorption capacity, perhaps due to the amine interacting strongly with the surface silanols. Given the sparse coverage of amines, the shorter alkyl linkers may lack the flexibility and reach to form stable alkylammonium carbamate structures. Indeed work by Knowles *et al.* suggested that with sparse amine densities below 1 amine nm^{-2} there was negligible increases in CO_2 adsorption capture compared to the bare support [26]. This was rationalised as the amines were too isolated to form bidentate alkylammonium carbamate species, suggesting a certain geometric configuration is required for efficient CO_2 adsorption.

Hiyoshi *et al*. studied the difference between amine order and amine density, concluding that the amine coverage followed the order mono>di> triamine silanes [69]. The moles of silane deposited on the surface were proportional to the steric requirements of the silane. They reported that increasing levels of amine density resulted in a greater amount of alkylammonium carbamate, observed via infrared spectroscopy. This species is formed from the reaction of CO_2 with two surface bonded amines in close proximity.

In order to increase the nitrogen loading of covalently tethered adsorbents, silanes with increased nitrogen content have been grafted to the surface of silicas. Lineen compared grafted mono, diamino and triamino silanes on silica aerogel finding that triamines yielded the largest CO_2 adsorption capacities (2.61 mmol g^{-1}) [22]. They rationalised that the increased amount of amine incorporated into the silane led to the observed increase in the CO_2 adsorption capacity. There was only a marginal reduction in the amine efficiency with increasing nitrogen content suggesting good amine accessibility. Given the optimum adsorption conditions or adsorbent modifications, these adsorbents have the potential to become practical adsorbents. Unlike impregnated amine adsorbents they noted a reduction in the CO_2

adsorption capacities of the adsorbents with increasing temperature with the capacity reduced by ~45 % at typical flue gas temperatures.

2.2.4 CO_2 adsorption uptakes of surface polymerised adsorbents

The surface polymerisation of amines on the surface of silica is a recent development in amine silica adsorbents. Surface polymerised amine adsorbents possess large CO_2 adsorption capacities for covalently bound adsorbents, which is related to the significantly enhanced amine loading [13]. Covalently tethered amine adsorbents produced by the polymerisation of aziridine led to CO_2 adsorption capacities of up to 5.6 mmol g^{-1} at 25 °C under pure CO_2. Highly loaded adsorbents exhibited low amine efficiencies with approximately half of the amine sites occupied. This was related to the increased diffusional resistance of the support, a consequence of the uncontrolled nature of the polymerisation. For these adsorbents the CO_2 adsorption isotherms of the materials plateaued around 0.2 - 0.3 atm CO_2 suggesting that they may be suitable for flue gas concentrations. For aziridine polymerised materials formed from vapour deposition the CO_2 adsorption capacities under 10 % CO_2 at 25 °C of less than 1 mmol g^{-1} with very low amine efficiencies [43]. Unfortunately these adsorbents were not tested under realistic flue gas temperatures adding difficulty when comparing them to other adsorbents.

2.3 The effect of CO_2 partial pressure and adsorption temperature

For typical chemisorbents the equilibrium adsorption uptake will be dependent on the partial pressure of the system at a given temperature. At low pressures a typical adsorption isotherm conforms to Henry’s law with linear increases in CO_2 uptake vs pressure. As the pressure increases the isotherm increases in a non-linear manner towards saturation at high partial pressures. The adsorption isotherms of CO_2 over a range of pressures does not conform to common isotherm models such as the Langmuir or Freundlich adsorption isotherms At high partial pressures the isotherm departs from typical adsorption isotherms for chemisorption and does not reach a plateau at high partial pressures. The adsorbents typically exhibit a significant CO_2 adsorption at low partial pressures making them attractive adsorbents for post combustion carbon capture. This is due to the high heats of adsorption between the amine groups and CO_2. Serna-Guerro *et al.* suggested that this shape suggested a secondary physisorption contribution to the adsorbents at high partial pressures [80]. They remarked that the observed contribution of an adsorbents uptake is a combination of the both chemisorption and physisorption and developed a model to describe the behaviour of covalently tethered amine adsorbents [81].

2.3.1 Effect of CO_2 partial pressure and temperature for amine impregnated silica adsorbents

For polyamine impregnated mesoporous silica adsorbents the CO_2 adsorption isotherms are sensitive to changes in the adsorption temperature. The adsorption isotherms of impregnated amine adsorbents do not appear to follow the Langmuir adsorption isotherm as there is evidence of increasing CO_2 adsorption at higher pressures relating to physisorption. The adsorption isotherms do not appear to be greatly influenced by the nature of the amine with PEI, TEPA and ethylenediamine impregnated SBA-15 adsorbents found to give similar isotherm shapes [48, 54, 82]. Amine impregnated materials typically exhibit there optimum performance at 75 °C. At this temperature there is a balance between thermodynamics of CO_2 adsorption and the diffusion of CO_2 through the amine polymer [58].

Fauth *et al.* reported CO_2 adsorption isotherms for PEI impregnated upon APTES functionalised silica showed a reduction in the CO_2 adsorption capacity over all pressures as the temperature was increased from 40 - 120 °C [83]. They also noted that the increases in CO_2 capacity were linear above the pressure range ~ 0.4 atm CO_2 indicating that selective chemisorption would be the dominant mechanism under typical flue gas conditions of 0.15 atm of CO_2.

2.3.2 Effect of CO_2 partial pressure and temperature for covalently tethered amine adsorbents

Lineen *et al*. observed a slight reduction in the CO_2 adsorption amount with increasing adsorption temperatures for triamine grafted silica aerogels [58]. This is unusual as grafted materials are thought to not be diffusion limited. For a diffusion limited material, it is expected that increasing the temperature would lead to an enhanced rate of diffusion. Conversely as the temperature is increased the thermodynamic equilibrium is shifted is favour of a greater proportion of desorbed CO_2. It would be expected that if true equilibrium were established then the adsorption capacity of the adsorbents would be greater.

Knöfel *et al.* investigated high pressure CO_2 adsorption isotherms of diamine functionalised SBA-16 at 300 K from 1 – 35 bar [39]. They noted that the enthalpy of adsorption decreased from 90 kJ mol^{-1} at 1 bar approaching that of non functionalised silica which is known to only physisorb CO_2. The nature of the support appears to affect the physisorption of CO_2 on amine functionalised materials with Zukal *et al.* noting differences between amine loaded ITQ-6 and SBA-15 sorbents [84].

Wurzbacher *et. al.* reported the CO_2 adsorption isotherms of diamino grafted silica gel adsorbents at a range of temperatures and between 0 -0.6 P/P_0 [85]. They noted that at 25 °C there was a reasonable fit with the Freundlich model, which has been reported similarly for 3-APTES functionalised silicas below 0.6 P/P_0[80, 81, 84, 86]. Below these pressure ranges the physisorption of CO_2 is not expected to exert a significant contribution to the overall uptake. Between temperatures of 70 , 90, 110 °C they attempted to fit the Langmuir adsorption model with a reasonable fit attained at 110 °C. They rationalised at this temperature adsorbate-adsorbate interactions become insignificant. The fitting of models on similar materials between 25 - 55 °C found that no model fitted the data suggesting multiple adsorption processes were occurring [81]. Both authors observed a loss in adsorption capacity with increasing temperature.

2.4 Influence of the support on CO_2 adsorption

Given the restricted selection of amines used in solid adsorbents, variation of the support provides a pathway to influence the kinetics and capacities of the adsorbents. The role of the support in amine impregnated silica adsorbents is to act as a means to increase the dispersion and accessibility of the amine adsorbent. Son *et al*. investigated the influence of the silica structure, impregnating MCM-41, MCM-48, SBA-15, SBA-16 and KIT-6 with 50wt% PEI and observing differences in material performance [45]. They found that the CO_2 adsorption capacity was influenced by the pore size of the adsorbent, with the sequence of adsorption capacities correlating with pore size. It was also noted that the 3D pore connected structures of SBA-16 and MCM-48 possessed larger amine efficiencies than their 2D pore analogues. Increases in the rate of adsorption of total CO_2 adsorption capacity were also observed for TEPA functionalised supports with increasing pore sizes by Wang *et al* [87]. They noted the benefits of larger pore sizes were not sensitive to humidified CO_2. Different supports prepared by different synthesis routes may also have subtle differences in surface hydroxyl concentration. As well as pore structure, these differences in surface hydroxyl concentration may play a crucial role in the dispersion of impregnated amines.

2.4.1 The influence of support pore size

Zhang *et al.* produced a series of mesocellular silica foams with a range of pore volumes and pore sizes much larger than those studied by Son and Song [88]. These mesocellular silica foams typically consist of small particles perforated with mesoporous windows, which agglomerate to generate additional porosity [89]. They found a clear correlation between pore volume of the support and increasing CO_2 adsorption capacity with mesocellular silica foam (MCF) possessing a pore volume of 4.17 $cm^3\ g^{-1}$ exhibiting a CO_2 uptake of 6 mmol g^{-1}. These increases were thought to be due to a greater dispersion of PEI within the pores of the MCF. Interestingly they noted a shift in the maximum CO_2 adsorption capacity for highly loaded PEI adsorbents when going from 55 to 85 °C. This suggests that when PEI is sufficiently dispersed on a highly porous support the CO_2 is less dependent on the rate of diffusion of CO_2 through the polymer.

Zelenak *et al.* investigated the role of pore size for mesoporous silica adsorbents functionalised with 3-APTES [90]. They noted that the largest CO_2 adsorption capacity was obtained with the support with the largest pore size, lowest surface area but with the greatest density of amine sites. They rationalised that for the larger pore support more of the amines were accessible as the functionalising agent was able to diffuse freely through the pores. They also noted that the rate of uptake was faster for the 3D pore structure support SBA-12 rather than SBA-15 owing to greater pore connectivity.

2.4.2 The influence of the support pore length

The effect of pore length was investigated by Heydari-Gorji who investigated the channel length in a series of similar impregnated mesoporous silicas [91]. The total adsorption capacity and rate of adsorption was shown to be diffusion limited with the shortest channel lengths offering the highest adsorption capacities. This diffusion dependence was evidenced by increased CO_2 adsorption capacities with increases in adsorption temperature between the temperature range 25 - 75 °C. Whilst comparing pore lengths the authors investigated different silica morphologies with differing levels of macroporosity and channel orientation which could account for some of the differences observed.

2.4.3 The influence of hierarchical pore structures

The role of both macropores and mesopores in the form of hierarchical silica monoliths was investigated by Chen *et al*. [47]. They found that the higher pore volume allowed them to impregnate a greater amount of PEI within the pores of the adsorbent. This led to a greater CO_2 uptake capacity compared to purely mesoporous KIT-6 based sorbents. Furthermore this hierarchical structure was shown to increase the kinetics of adsorption for similarly loaded mesoporous supports. These differences could be accounted for by the increased amounts of pore volume remaining after impregnation.

Building on this understanding that supports featuring macroporosity or inherent mesoporosity generated between different porous grains, Qi *et. al.* investigated ultra large pore MCF as supports [4]. The support produced featured a bimodal pore size distribution with pores between 10-20 nm and 40+ nm. The CO_2 adsorption capacity was greater than 5.5 mmol g^{-1} attained with a PEI loading of 83 wt%. This correlates with other studies that the presence of greater pore volume leads allows more accessible amine to be loaded into the adsorbent.

Qi *et. al.* also investigated the use of hollow silica mesoporous capsules for CO_2 adsorption [16]. These materials consisted of 160 - 400 nm hollow spheres with a 20 – 40 nm porous shell consisting of 3 nm pores synthesised with a polystyrene co-template. It was believe such short channels mitigated issues associated with pore blockages present in longer pore structures. The adsorbents were impregnated with up to 86% TEPA or PEI leading to adsorption capacities of up to 7.9 $mmolg^{-1}$ under 10% CO_2, 75 °C. TEPA adsorbents exhibited much higher adsorption capacities owing to an increased number of adsorption sites under dry conditions. It was found core diameters of 160 nm were less efficient than those with a core diameter of 400 nm with the larger particles allowing the incorporation of a larger amount of amine. Whilst high capacities and favourable kinetics were reported the stability of such short pore lengths requires a thorough investigation. The authors presented a lack of stability over 100 dry adsorption and desorption cycles for the TEPA impregnated adsorbents. Furthermore there was a steady loss in performance with PEI adsorbents. However, the nature of this deactivation was not characterised. Both the ultra large pore MCF and hollow sphere particles show high capacities however the density of the resultant adsorbent is very low. Hence a comparison on a volumetric basis, used in commercial systems, may lead to a reduction in capacity. Furthermore the nanometre thick pore walls may be deformed during a particle forming process.

2.4.4. The influence of support surface energy on amine impregnated mesoporous silicas

Heydari-Gorji *et al.* increased the dispersion of PEI impregnated within the pores of pore-expanded MCM-41 by using long chain alkyl groups to modify the surface of the support [46]. The adsorbents pores were functionalised via selective removal of all but the most strongly adsorbed ionic surfactant used in the material synthesis. This led to surfaces covered with hydrophobic alkyl chains. The alkyl terminated silica had an increased rate of adsorption and increases in CO_2 adsorption capacity compared to a silanol populated pore surface. The alkyl modified materials showed a slight reduction in the adsorption capacity in the presence of water, potentially due to the increased hydrophobic nature of the adsorbent. In the presence of water, a highly hydrophobic adsorbent may led to the formation of a diffusive barrier of water over the surface of the adsorbent. However it is not clear whether the surface bound groups interacted with the PEI to form a blend as reported elsewhere [53, 92].

2.4.5 The influence of particle forming

A large proportion of the literature has investigated fine powders which may not be suitable for use in an adsorption process owing to pressure drop. Rezaei *et al.* investigated the effect of pelletisation pressure of impregnated and covalently tethered amine adsorbents [93]. They found that thicker walled commercial silica supports exhibited greater structural stability than templated mesoporous silicas such as SBA-15. It was found that pellets led to a slight reduction in surface area and pore volume of the adsorbent. Negligible losses in CO_2 uptakes were observed for the adsorbents upon pelletisation, however a reduction in the kinetics of adsorption was observed. This study suggests that at low forming pressures silica sorbent leads to stable adsorbents. Unfortunately no work was undertaken to under the mechanical strength of the particles and the likelihood of attrition in a fluidised bed configuration.

2.5 Structure and mechanism of CO_2 adsorption on amine functionalised silica adsorbents

The mechanism of CO_2 adsorption on amines can occur via several different mechanisms depending on the nature of the amine and presence of water. The adsorption of CO_2 in aqueous liquid phase is well characterised [94-96]. It is known that carbon dioxide reacts with aqueous solutions of primary and secondary amines leading to the formation of carbamates, carbonates and bicarbonates (Figure 2.6) [97].

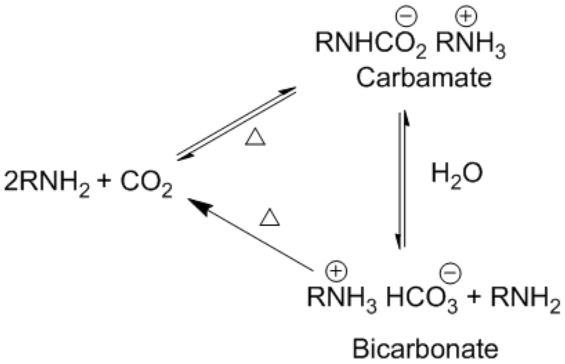

Figure 2.6. The mechanism of CO_2 adsorption in the presence of water for liquid amine adsorption systems.

Initially a carbamate is formed between one CO_2 molecule and two amine units [98]. This carbamate hydrolyses to form a bicarbonate and release one of the amine molecules, increasing the molar ratio between CO_2 capture and amine to 1:1 [96, 99, 100]. At low temperatures the equilibrium is in favour of the carbamates and bicarbonate products, whilst upon heating the equilibrium favours the evolution of CO_2. Efficient amine scrubbing solutions are those at which the proportion of bicarbonates is maximised. Furthermore the desorption of bicarbonates is believed to be faster leading to leaner CO_2 solutions after desorption [101].

The reaction of tertiary amines and CO_2 in aqueous solution proceeds via a different mechanism to primary and secondary amines. The tertiary amine acts as a base and reacts with carbonic acid formed by the dissolution of CO_2 in water (Figure

2.7) [102]. As the rate of carbonic acid formation is slow in the presence of water this adsorption mechanism is much slower than that of primary and secondary amines [103]. This reaction pathway is also possible for primary and secondary amines however owing to their lower basicity the carbamate/carbonate mechanism is more likely. This mechanism yields a 1:1 amine:CO_2 ratio making it an attractive option for CO_2 capture if the sluggish kinetics can be overcome.

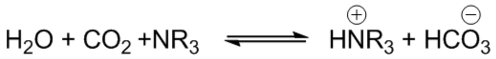

$$H_2O + CO_2 + NR_3 \rightleftharpoons \overset{\oplus}{H}NR_3 + HC\overset{\ominus}{O}_3$$

Figure 2.7. Tertiary amine adsorption in aqueous amine adsorption systems.

2.5.1 Mechanism of CO_2 adsorption on amine functionalised silicas under dry conditions

The mechanism of adsorbed CO_2 on amine functionalised silicas is still under debate with a wide variety of species observed by FTIR spectroscopy. The nature of the species formed was first investigated by Tsuda *et al.* who noted the formation of ammonium carbamate on 3-APTES modified silica gel using *ex-situ* FTIR spectroscopy [104]. This structure was thought to consist of two amines bonding to one CO_2 molecule (Figure 2.8, I). Later work by Leal investigated a similar 3-APTES functionalised silica gel observing bands at 1411 and 1385 cm^{-1} reporting them as the carbamate and bicarbonate respectively [24]. They also noted that ratio of the carbamate to bicarbonate changes compared when exposed to small amounts of water.

The species formed from the adsorption of CO_2 onto APTES functionalised SBA-15 was interpreted differently by Chang who assigned similar bands to bidentate and monodentate carbonates, observing the similar species under both dry and humid adsorption conditions [105]. Their experiments also agreed with those of

Khatri who observed the similar bands to Chang with a similar 3-APTES modified SBA-15 and agreed with the assignment by Chang [106]. This experiment was also completed with D_2O in place of water and led them to report similar bands which had been shifted due to the D/H exchange [107]. This conclusion is analogous to the species obtained in aqueous amine systems and consistent with the apparent increases in CO_2 adsorption uptakes.

Hiyoshi *et al.* also investigated 3-APTES functionalised SBA-15 assigning similar bands to Chaung and Khatari as carbamate bands [69]. The effect of amine surface coverage was also explored, with increasing density of amine leading to more alkylammonium carbamate formed. This was similar to that reported by Zheng *et al.* in their investigation into ethylenediamine functionalised SBA-15 [18]. Both groups of researchers noted that no new bands were formed under humid adsorption conditions.

Investigations by Fisher on TEPA impregnated β zeolite reported that only carbonate species were formed [108]. Conversely, Huang assigned bands to the presence of both bicarbonate and carbamate species whilst investigating 3-APTES functionalised MCM-48 [59]. FTIR investigations by Wang *et al.* on PEI/SBA-15 assigned the bands between 1320 – 1650 cm^{-1} as carbamates owing to the anhydrous conditions used and the high concentration of intra and inter molecular amine sites which would outcompete any residual water [109].

Work by Danon *et al.* showed evidence of surface bound silylpropylcarbamates formed on 3-APTES modified silica with sparse populations of amines compared to densely loaded aminopropyl surfaces [110]. This was achieved by the initial grafting of the bulky benzylimine (formed from the reaction of benzaldehyde and APTES) followed by acid deprotection. To confirm that the surface silanol formed an active carbamate species the remaining surface silanols of the amine functionalised material was capped with hexamethyldisilane. This capping of the surface silanols showed a significant reduction in the amount of silylpropylcarbamate formed. This study confirmed that in densely populated amine surface silicas a mixture of ammonium propylcarbamates are formed, with a strong bias towards ammonium propylcarbamates at high levels of amine loading (Figure 2.8, I). Instances where no second amine is in close proximity the propylamine can form a silylpropylcarbamate if a silanol is in close proximity (Figure 2.8, II). In the presence of isolated amine sites grafted aminopropyl groups do not adsorb CO_2.

2.5.2 Mechanism of CO_2 adsorption on amine functionalised silicas in the presence of water

Many researchers have reported an enhancement in CO_2 adsorption capacity in the presence of water [72, 80, 111-113]. The mechanism of CO_2 adsorption in the presence of water is currently not fully understood. Many have assumed that akin to liquid amine adsorption systems, the presence of water facilitates the formation of bicarbonate species. Such bicarbonate species react with CO_2 on a 1:1 ratio whereas in comparison the carbamate species requires two amines to one singly adsorbed CO_2 molecule. A shift towards the bicarbonate species would lead to a much higher adsorption capacity of the materials.

Bacsik *et al* investigated 3-APTES functionalised silica under both dry and humid adsorption conditions [114, 115]. The predominant species formed under both dry and humid CO_2 adsorption was alkylammonium carbamates and carbamic acid species (Figure 2.8 I and III, respectively). They found that the silylpropylcarbamates formed from the reaction carbamic acid and with a silanol group was slow under dry conditions and not observed in the presence of water (Figure 2.8, II). They also observed an increase in the proportion of primary amine groups in the presence of water vapour, suggesting the water disrupted the hydrogen bonding between the amine and the surface silnaols. The liberation of amines under humid adsorption conditions could explain the increases in capacity in the presence of water as no carbonates or bicarbonates were observed.

Didas *et al.* studied APTES modified SBA-15 by FTIR under humid adsorption conditions for different extents of amine coverage [116]. They found that for the least dense amine coverage a signal in which they assigned to the formation of a bicarbonate species was observed to slowly form after spectral contributions from fast forming species were removed. The band was assigned to the bicarbonate formation in correlation with measurements of previous literature reports (Figure 2.8 IV). Unfortunately no further characterisation was presented to confirm the formation of the bicarbonate species. Such species were not present on sorbents with medium or high aminopropyl coverage suggesting that this species only form when the more favourable carbamate species cannot be formed.

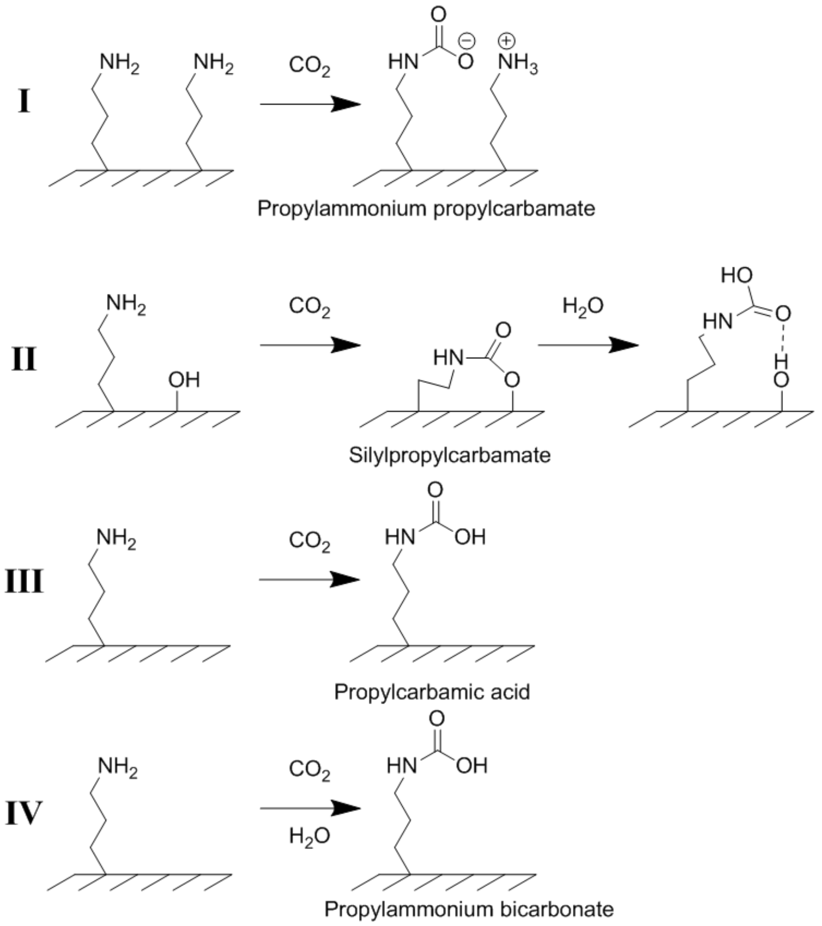

Figure 2.8. The species observed on the surface of amine functionalised silica under both wet and dry adsorption conditions.

Few experimental investigations into the mechanisms of impregnated polymeric amines have been conducted, with the currently agreed mechanism being that the dominant species are alkylammonium carbamates [23]. The effect of water in highly loaded amine adsorbents, be they impregnated or grafted is to liberate amine groups from the support surface or increase the flexibility of the amine polymers [117, 118].

Conversely to much of the prior work there has only been one recent example of an apparent bicarbonate formed in the present of impregnated adsorbents. Work by Hahn *et al.* proposed to observe the presence of a bicarbonate species via SSNMR exchange experiments [119]. In their work they observed a small amount of what was assumed to be bicarbonate formed under humid adsorption conditions. During the preparation of their sample for ^{13}C SSNMR they exposed the sorbent to dry $^{13}CO_2$ to increase the signal. This could have led to some of the amine becoming solvated in the solution reacting akin to liquid amine systems during the $^{13}CO_2$ purge.

While bicarbonate formation for some materials under certain conditions has been observed it is not suggested that this is the sole contribution to increased amine efficiency under humid conditions. Studies have suggested that water increases in CO_2 adsorption uptake via the formation of more carbamate species via the liberation of hydrogen bonded amines from the surface of the support [115]. For impregnated amine adsorbents the beneficial effect of water is to act akin to a plasticiser, increasing the mobility and in turn accessibility of the amines chains [117]. Given the complex nature of the CO_2 adsorption process it is sensible to think that the observation of increased capacities observed in experiments are convolutions of several of the effects discussed [115, 120, 121]. The concept of a doubling of efficiency of amine functionalised solid adsorbents in the presence of water is questionable. The only spectroscopic evidence to data suggests that bicarbonate formation yields only a marginal contribution to the CO_2 adsorption capacity. A possibility for future materials is to seek methods to form exclusively bicarbonate CO_2 adsorption products. Such materials would have an amine efficiency of one and required larger amine loadings to attain the target CO_2 capacity. It does appear that typical flue gas concentrations of water do not hinder the adsorption of CO_2. This is a key requirement for materials suitable for post combustion carbon capture.

2.6 Kinetics of CO_2 adsorption

In practical adsorption processes the kinetics of adsorption are a crucial factor for the implementation of economic adsorption systems. As defined by the sheer volumes of flue gas that are to be treated the estimated residence time of adsorbent particles in expected to be in the order of seconds [122]. Many adsorbents have been reported as having rapid kinetics with high CO_2 adsorption capacities reported under short time scales [16, 123]. Often the rate of adsorption is simply quantified as the amount adsorbed over a specific time period [124]. Such approach has limited value as it is highly dependent on the temperature, porosity, partial pressure, nature of the particles and analysis conditions used.

A model to accurately describe the kinetics and breakthrough of CO_2 adsorption would be of great utility in the design of solid adsorption CO_2 capture systems. Belmabkhout *et al.* used the linear driving force (LDF) model to represent the overall adsorption kinetics of CO_2 adsorption on MCM-41 finding a greater rate constant than zeolite 13X attributed to the larger pore diameter of the former [125]. Building upon this the same group applied a pseudo first order, pseudo second order, fractional order and Avrami kinetic models to grafted aminopropyl functionalised silica [126]. They found the fractional order kinetic model presented in Equation 2.1 to accurately describe the CO_2 adsorption.

$$q_t = q_e - \frac{1}{\left[((n-1)k_n/m)t^m + (1/q_e^{n-1})\right]^{1/(n-1)}} \qquad \text{Equation 2.1}$$

Where q_t is the uptake at time t, q_e is the equilibrium uptake, t is time, k_n, m and n are the model constants.

This was confirmed by Zhao *et al.* who applied the model to TEPA impregnated SBA-15 [82]. Whilst these models do accurately fit the experimental data caution should be applied with regard to the physical significance of the model. The model includes *m* and *n* values attributed to approximate the driving force and diffusional resistance respectively which vary between sample. The inclusion of these two terms yields a five variable model which has the flexibility to fit most adsorption data with little physical meaning.

Bollini *et al.* used a single site modified Langmuir model to investigate the effect of heat on the adsorption process of aminopropyl functionalised silica [127]. They noted that the CO_2 adsorption kinetics were somewhat insensitive to heat effects allowing the fitting of their models. However given the large enthalpy of adsorption of CO_2 reported to be 90 kJ mol^{-1} it could be expected that at greater flow rates or at a higher density of amine loading heat effects may become more important [128].

Further work by Bollini *et al.* compared the adsorption of zeolite 13X and 3-APTES grafted silica using a dual site Langmuir model and a simple diffusion into a sphere model [129]. They noted that in packed bed adsorption columns a characteristic tail of adsorption was due to the diffusion limitations of the adsorbent. Such a long adsorption tail is representative of sluggish CO_2 diffusion representing a significant proportion of the adsorption capacity of the adsorbent. This tail was only noted for highly loaded adsorbents suggesting that for optimised adsorbents a low amine loading may be beneficial.

Kalyanaraman *et al*. described a CO_2 adsorption model of PEI functionalised hollow fibre adsorbents using a two part LDF model accounting for surface PEI and bulk PEI [130]. Assuming a diffusion limited process they were able to model the temperature dependency of PEI based adsorbents. Using a non-isothermal model they qualitatively matched the experimental trend for heats effects and subsequent breakthrough. They concluded that diffusion of CO_2 through the polymer diffusion is the limiting factor.

Most of the models used to describe the adsorption of CO_2 assume the rate is diffusion limited and that the adsorption of CO_2 only occurs at a single site. Recent work by Abdollahi-Govar *et al.* developed a 3 site reversible non-isothermal mechanistic based model based around several reversible reactions between CO_2 and PEI [131].They found that the model whereby the CO_2 can adsorb onto PEI via three parallel mechanisms reversibly provided the best fit and applied this approach to both adsorption and desorption. Their model provides a poor fit at temperatures below 80 °C, possibly as a result of not accurately accounting for the diffusion limitations of the PEI polymer.

Work by Hahn *et al*. attempted to model the adsorption of amine impregnated SBA-15 under both wet and dry adsorption conditions [119]. They found that when the concentration of water increased beyond 5% in the flue gas the rate of CO_2 diffusion was reduced owing to a resistive film of water on the exterior of the adsorbent particle. They measured diffusion coefficients using the short time solution presented by Cavalcante *et al*. finding a linear correlation between the fractional uptake and square root of time suggesting temperature effects were not significant [132]. The diffusion coefficients they reported were faster than the aqueous amine systems by a factor of 1000 suggesting that solid adsorbents may be much faster than conventional amine adsorbent systems [133].

The kinetics of CO_2 adsorption onto impregnated amines is a complex process with many variables to take into consideration. As such the assumptions of many of the simple models described simply do not hold. Parameters that need to be accounted for include the changing viscosity of the amine polymer as a function of amount adsorbed. The significant heat of adsorption needs to be taken into account as well as the packing of the particles within the adsorption system.

2.7 Regeneration of solid adsorbents

2.7.1 Temperature swing adsorption

For solid adsorbents to be utilised in carbon capture systems the adsorbents must be stable for extended periods of times under flue gas conditions. Adsorbents can be regenerated through temperature swing adsorption. In such a process the sorbent is heated in the presence of sweep gas leading to an increase in adsorption temperature. Increasing the temperature causes the metastable carbamate species to decompose evolving CO_2 and regenerating the amine species. Purely thermal regeneration in the presence of CO_2 has been shown to degrade the adsorbents by the formation of urea species which is discussed in more detail in Section 2.8 [12]. The desorption temperature is typically around 373 K confirmed by Zheng *et al.* who observed the main weight loss peak at 373 K via TGA [18]. The precise temperature is adsorbent specific depending on the nature of the adsorbed species and pore structure. Generalisations with regard to the stability of impregnated adsorbents should be avoided as literature reports have noted both stability and lack of stability during mixed temperature and inert sweep regeneration [15, 82, 126, 134-137]. Structural changes of the porous supports have not been reported under dry conditions, with reduction in adsorption capacities due to the formation of inactive urea species.

2.7.2 Pressure swing regeneration

Decreasing the partial pressure of CO_2 during desorption shifts the equilibrium towards CO_2 desorption. Concentration swing desorption without an increase in sorbent temperature was reported by Xu *et al.* and by Son *et al.* [45] [138]. They noted that the adsorbent could be regenerated in a timely manner using an inert gas purge whilst maintaining the adsorption temperature at 348 K. Knowles *et al.* reported complete regeneration of 3-APTES functionalised silica using an inert gas sweep at 293 K [26]. Further reports have suggested that desorption under inert sweep conditions without the application of temperature did not lead to complete regeneration, suggesting that the application of temperature is a requirement [38, 76, 105, 135]. Eber *et al.* determined the optimal bed temperature for pressure swing adsorption to be dependent on the CO_2 with temperatures ranging from 60 – 80 °C [137]. For large scale CO_2 capture systems it would be uneconomical to desorb under an inert purge as high purity CO_2 is a requirement for efficient storage and hence would require further purification. Chaffee *et al.* suggested that a pressure swing process would be too costly given the volumes of sweep gas involved [139].

2.7.3 Vacuum swing regeneration

Vacuum swing adsorption has been proposed as a suitable CO_2 regeneration system with the spent adsorbent heated under the presence of vacuum. For vacuum swing adsorption the working capacity of the adsorbent is defined as the difference between the CO_2 adsorption uptake at 0.1 atm and vacuum conditions often assumed to be negligible [140]. Vacuum swing regeneration has been proposed for as an alternative regeneration strategy for adsorbents that operate by CO_2 physisorption such as zeolite 13X. Serna-Guerrero *et al.* compared temperature swing desorption and vacuum swing desorption of triamine functionalised silica, concluding that vacuum swing desorption may be more attractive where low temperature CO_2 adsorption is used [141]. Goeppert *et al.* investigated vacuum swing regeneration using PEI functionalised fumed silica for the capture of CO_2 from air using a combination of vacuum and heat. They reported that the sorbents were stable although only a limited number of cycles were measured [142]. Wurzbacher *et al.* found diamine functionalised silica to exhibit reversible CO_2 adsorption performance over 40 adsorption/desorption cycles using vacuum swing adsorption [85]. Vacuum swing adsorption would not be stable for impregnated amine adsorbents owing to the vapour pressure of the amines. Over time these amines could be removed from the support and enter the vacuum system.

2.7.4 Steam regeneration

In large scale power plants it seems sensible to use low grade steam to regenerate the adsorbents. The water and CO_2 mixture would be easy to separate yielding a stream of high purity CO_2. Only a small number of recent studies have considered the stability of solid adsorbents in the presence of steam or humid desorption conditions [11, 143]. Considering that polyethlyeneimine is water soluble and the lack of a formal covalent bond between the silica surface and impregnated amine polymers, one could anticipate that these adsorbents may be unstable over long timescales.

Amine silica sorbents were found to be regenerable in saturated steam at 106 °C with approximately two-thirds of the CO_2 removed in the first 3 minutes and negligible CO_2 evolved after 10 minutes [144]. Both impregnated PEI and grafted 3-APTES were subject to three cycles of steam aging. The impregnated PEI based adsorbent exhibiting no loss in CO_2 adsorption capacity whereas grafted 3-APTES led to a modest reduction in capacity over 3 cycles. The 3-APTES was covalently tethered to the surface of the adsorbent and as such is expected to have a greater stability. These findings suggest that changes in the support structure may arise from steam regeneration.

The stability of amine functionalised mesocellular silica foam adsorbents was explored using a water filled autoclave under various temperatures and autogenous pressure [145]. It was noted that exposure to steam at 106 °C for 24 h led to a significant reduction in adsorption capacity for impregnated and covalently tethered amines.

Work by Hammache *et. al.* investigated the cyclic stability of silica supported PEI (Cariact G10) adsorbents using a fixed bed reactor [146]. Deactivation was present after six adsorption and desorption cycles using steam regeneration of 90% H_2O/He, 105 °C. Under the cycling conditions they noted little change in the organic loading but a reduction in BET surface area and accessible pore volume, concluding that the amine may have agglomerated inhibiting access to the pores. Unlike previous reports no changes to the support were observed after exposure to identical conditions. This could be related to the choice of silica support as the silica gel used had thicker walls than the MCF used by Jones, a factor which has been related to increasing silica stability [147].

Wilfong *et al*. measured the stability of impregnated amines on silica before and after pumping water through a bed of the adsorbent to mimic condensation of steam within the pores [143]. A reduction in CO_2 adsorption capacity was observed due to the leaching of the amine species, with increased leaching inversely proportional to the amine molecular weight. Within the same study sealed autoclave aging experiments similar to those of Li, were used to investigate changes to thicker walled silica adsorbents. In their contribution no changes in the support were observed, with deactivation attributed to amine leaching [145].

2.8 Stability with respect to flue gas contaminants

Flue gas from coal fired powerstations comprises of approximately 15% CO_2, 5% H_2O, 4 % O_2 and ppm amounts of SO_x and NO_x. Post combustion capture sorbents need to be selective for CO_2 as well as exhibiting stability towards reactive contaminants found in the flue gas stream.

2.8.1 Stability in the presence of CO_2

The degradation of supported amine adsorbents in the presence of CO_2 was reported by Drage *et al.* who noted a loss of ~ 35% CO_2 adsorption capacity after regenerating PEI functionalised silicas in the presence of dry CO_2 for 1 hour [12]. They rationalised that this was due to the formation of a urea species formed between two amines in close proximity. Such urea species were found to be thermally stable and not removed with extended heating at 250 °C a temperature above practical use in post combustion carbon capture systems.

Further work is this area by Sayari *et al.* found that grafted primary amines, triamines and impregnated PEI led to reductions in capacity with successive cycling in the presence of CO_2 with an dry N_2 purge [72]. They confirmed the presence of a urea species which irreversibly bound to the adsorbent. They found that in the presence of humidified gases the formation of urea was inhibited and the materials appeared stable over repeated adsorption and desorption cycles. It was proposed that the presence of water led to the hydrolysis of the urea groups demonstrated by the restoration of a urea degraded adsorbent with a flow of humidified water for 24 h.

Building upon this work next Sayari *et al.* compared the stability of primary, secondary and tertiary amines to urea formation [148, 149]. They found that secondary amines were stable under the presence of dry CO_2 whereas primary amines or polyamines bearing primary, secondary and tertiary amine groups were unstable forming urea species. It was proposed that the urea formation could proceed via two reaction mechanisms (Figure 2.9). In route I the dehydration of carbamic acid leads to a formation of an isocyanate species which reacts further to from a urea species. Isocyanates cannot be formed on secondary amine sites however a primary or secondary amine could react with the isocyanate species to form a urea. Such a mechanism would explain the deactivation in cases whereby both primary amines and secondary amines were in neighbouring sites such as branched PEI species. The second mechanism is the direct conversion of ammonium carbamates to urea with the evolution of water. Such a mechanism appears less likely as no spectroscopic evidence of water evolution was observed. A range of both aliphatic and linear urea species were proposed depending on the geometric constraints of the amine.

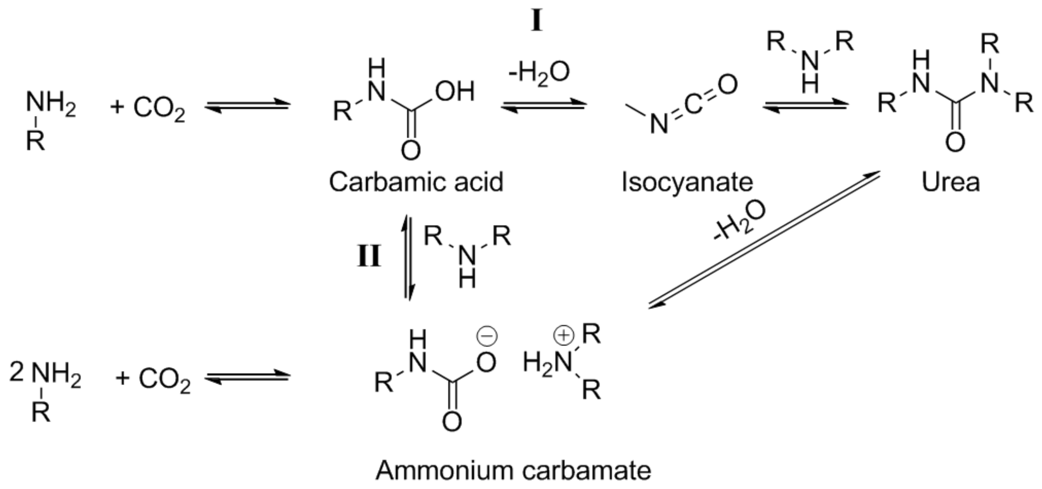

Figure 2.9. The two pathways for urea degradation. Adapted from [149].

Didas *et al.* investigated the effect of the aminosilane alkyl chain length on the likelihood of urea formation [150]. They found that the extent of urea formation was proportional to the CO_2 of the adsorbent with aminopropyl adsorbing the most CO_2 and also degraded the most in the presence of dry CO_2. They rationalised this activity on the extent of flexibility of the amine unit with ethylamine more likely to interact with surface silanols whereas longer propylsilane groups were more likely to interact with each other. This analysis assumes that the surface grafted amines align parallel to the surface, which is rarely the case [151]. Using density functional theory calculations they reported that the formation of an isocyanate provided the lowest energy pathway to urea formation. This was used to explain the requirement of primary amines for urea formation

2.8.2 Stability in the presence of O_2

Oxidative degradation of liquid amine systems is known to occur to yield a number of deactivation products [152, 153]. Bollini *et al.* and Heydari-Gojri *et al.* simultaneously reported investigations into the oxidative stability of differing amine functionalities [154, 155]. They both reported single component primary amine adsorbents have an increased stability over secondary amine species, however evidence of degradation was apparent. Furthermore tertiary amine species which were unreactive towards CO_2 under the dry conditions used were also unreactive to oxygen. For mixed amine bearing materials such as grafted diethylenetriamine the extent of oxidation degradation was greater suggesting a number of mechanisms may be in operation. This finding is significant given the popularity of secondary amine moieties in amine based solid adsorbents.

For liquid MEA systems it has been observed that in the presence of CO_2 the effects of SO_2 and O_2 were diminished compared to single component adsorption of flue gas contaminants. This is due to the greater solubility of CO_2 and MEA solutions coupled with the salting out of the carbonate product [156]. Heydari-Gorji *et al*. compared the simultaneous adsorption of CO_2 and O_2 with single component O_2 and CO_2 adsorption under dry and wet conditions. They found that the CO_2 out competed O_2 protecting the amine via the rapid formation of a carbamate product [148].

Hallenback *et al.* noted that a primary amine polymeric adsorbent was stable to 17 adsorption/desorption cycles using a thermal swing with an incoming gas stream containing 12 % CO_2, 4% O_2 and 84% N_2 [157]. This may be of the result of the oxidative degradation occurring at a much slower timescale in the presence of CO_2. The authors acknowledged the error in their measurements was approximately 8% suggesting degradation may be masked by the uncertainty in the measurement. Srikanth *et al.* investigated the oxidative stability of silica supported TEPA and polyethylene glycol in the presence air at 100 °C [50]. They noted that the secondary amine sites degraded at a greater rate than primary amine site also observing an increasing population of isolated amine sites allowing the formation of carbamic acid upon reaction with CO_2

The effect of the alkyl linker on the thermal and oxidative stability was investigated by Didas *et al.* [150]. They noted that aminosilanes with a methyl linker readily decomposed upon heating to 135 °C. The stability of aminosilanes with ethyl and propyl linkers were directly proportion to their CO_2 adsorption performance, with aminopropyl silanes adsorbing more CO_2 degrading faster in the presence of oxygen at elevated temperatures.

2.8.3 Stability in the presence of SO_x

The quantity of sulfur and nitrogen oxides is dependent on the fuel used and the flue gas treatment technology used. It is expected that plants fitted with post combustion capture would also utilise state of the art NO_x and SO_x treatment systems, however these methods still lead to ppm levels of SO_x and NO_x passing into the flue gas [157, 158]. The adsorbents used must be tolerant to these levels of contaminants.

Leal first reported the irreversible reaction between aminopropyl functionalised silica and and sulfur dioxide at 25 °C [24]. It was also noted that the quaternary ammonium halide adsorbed CO_2 reversibly and could easily be regenerated with the application of temperature at 92 °C. Similar reports of the CO_2 adsorption of primary amines sorbents being irreversible deactivated in the presence of SO_2 were reported by Furtado *et al*. and Khatri *et al.*[107, 159]. Khatri *et al*. used DRIFTS to characterise the deactivated species reported bands at 1108, 1200 and 1250 cm^{-1} as the stretches of sulfites and sulfate species formed on the aminopropyl groups.

A comprehensive study of the effects of single component NO, NO_2 and SO_2 adsorption on grafted 1°, 2°, 3° and mixed amine impregnated adsorbents was completed by Rezaei *et al.*[160]. They found that secondary amines adsorbed more SO_2 than primary amines with both leading to irreversible degradation. Tertiary amines were not found to adsorb significantly less SO_2 than primary and tertiary amines, although the stability of adsorbed species was not investigated owing to the lack of CO_2 adsorption between CO_2 under dry conditions. Similar bands to Khatri were observed on SO_2 aged adsorbents relating to the formation of sulfates or sulphite.

Tailor *et al.* investigated the reversible adsorption of SO_2 on dimethylaminopropyl functionalised pore expanded MCM-41 [161]. The adsorption capacity of SO_2 was found to be 2.12 mmol g^{-1} under dry conditions yielding an amine efficiency of 0.67 suggesting a 1:1 molar ratio. The SO_2 adsorption capacity was also found to increase in the presence of water vapour potentially due to the liberation of amine groups interacting with surface silanols. The materials were found to be stable over numerous cycles, regenerable at 130 °C with a nitrogen sweep gas. The materials exhibited excellent selectivity for SO_2 over CO_2 under both dry and wet gas conditions. Although the adsorption of CO_2 under humid conditions can occur in the presence of water it is limited owing to the low solubility of CO_2 in water.

Further work by Tailor *et al.* devised an SBA-15 impregnated tertiary amine polymer which adsorbed unto 4.68 mmol g^{-1} of SO_2 [162]. Using IR and SSNMR data they rationalised that the SO_2 formed a non-covalent adduct with the tertiary amine species. This is in agreement with studies of functionalised siloxanes and functionalised polyethylene glycols [163, 164]. The SO_2 adsorption capacity was considerably increased in the presence of water which could be accounted for by the increased mobility of the polymer chain. Unlike most impregnated polyamine adsorbents for CO_2 capture, increasing the adsorption temperature led to a reduction in SO_2 uptake. This could be related to the strong physisorbed nature of the SO_2 leading to lower equilibrium adsorption capacities. No competitive adsorption was found between SO_2/CO_2 with the SO_2 adsorption unaffected by the presence of CO_2.

Miller *et al.* investigated the adsorption of SO_2 over 1,3-phenylenediamine/SiO_2 system reporting the formation of both a sulfite and sulfate species [165]. At 50 °C they observed the oxidative degradation of the amine site to yield NO_2 groups leading to a reduction in the CO_2 adsorption capacity over multiple cycles.

Recent work by Fan *et al.* investigated grafted primary, secondary and tertiary silica/polymer composites in the presence of SO_2 [166]. Cycling of single component primary and secondary amines under 200 ppm/SO_2/10% CO_2/N_2 led to a successive reduction in the CO_2 adsorption capacity. Their findings agreed that tertiary amine sorbents reversibly adsorbed SO_2 with primary and secondary amines permanently losing 55 and 25% of their capacity respectively. Interestingly they noted that the SO_2 degraded primary amine sorbents were found to reversibly adsorb additional SO_2.

Building on their previous work Rezaei *et al* performed two component SO_2/CO_2, NO/CO_2 and NO_2/CO_2 co-adsorption experiments [167]. They found that in a stream of 200 ppm SO_2/ 10% CO_2 that CO_2 breakthrough occurred within 3 minutes whilst the breakthrough of SO_2 occurred after 90 mins. They found that at such concentrations of CO_2 the adsorbent gradually deactivated over 5 adsorption-desorption cycles suggesting that the sorbents may have limited lifetimes with SO_2 rich gas streams.

2.8.4 Stability in the presence of NO_x

Nitrogen oxides are present in both coal and gas fired powerstations and adsorbents need to be stable to both. Xu *et al.* investigated PEI impregnated MCM-41 for the separation of CO_2 from the flue gas on a natural gas fired boiler containing 7.4–7.7% CO_2, 14.6% H_2O, ~4.45% O_2, 200–300 ppm CO, 60–70 ppm NO_x, and 73–74% N_2 [138]. The adsorbent adsorbed approximately 3000 times more CO_2 than NO_x however the NO_x did not appear to be removed after regeneration suggesting NO_x needs to be reduced prior to CO_2 adsorption.

In their investigations between acid gases and primary, secondary and tertiary amines Rezaei *et al*. noted that none of the amines interacted with NO [160]. Most materials is this study adsorbed below 0.07 mmol g^{-1} NO under 200 ppm NO at 35 °C. They did note that highly loaded PEI sorbents adsorbed up to 0.35 mmol g^{-1} NO, possibility due to cooperative interactions from the densely packed amine sites. Primary amine bearing adsorbents were also found to adsorb slightly more NO than secondary and tertiary amines. Such low NO adsorption capacities are promising given that 85-95 % of the total NO_x generated from combustion is NO [168].

The same adsorbents adsorbed significantly more NO_2, up to 3.5 mmol g^{-1} NO_2 with little distinction of NO_2 uptake between primary, secondary and tertiary amines. This suggests that NO_2 reacts via a non-selective free radical mechanism. The NO_2 remained irreversibly bound to the surface leading to a reduction in CO_2 adsorption capacity of over 95%. IR spectroscopy showed the presence of N-N vibrational bands in the spectrum suggesting the formation nitrate compounds on the surface of the adsorbent.

In their NO/CO_2 and NO_2/CO_2 competitive adsorption experiments Rezaei *et al.* noted that the CO_2 adsorption was unaffected by the presence of NO even at high concentrations [167]. They also found that the impact of 20 ppm NO_2 over repeated cycles was minimal with an increasing effect at higher concentrations of NO_2. It appears that the alkylammonium products formed may protect the amines from NO_2 degradation. This suggests that under typical flue gas conditions of between 50 -100 ppm adsorbents may be stable, however longer term investigations need to be conducted.

2.9 Research challenges

Solid adsorbents have the potential to play a key role in mitigating climate change by the adsorption of CO_2 from flue gas streams. This Chapter has summarised the strengths and limitations of current research in amine functionalised solid adsorbents.

Polymeric amines impregnated on porous silicas feature straightforward preparation and high CO_2 adsorption capacities, often exceeding the target requirement of 3.0 mmol g^{-1} [4, 9, 16, 45, 46]. Often the maximum adsorption capacity is reported, typically achieved after equilibration for extended periods of time. Under practical adsorption conditions the adsorbent may only be exposed to the CO_2 for a matter of seconds [1, 122]. Owing to the often slow adsorption kinetics of impregnated amine adsorbents, the CO_2 uptake after a few seconds can be much lower that the equilibrium adsorption capacity [45]. There is a significant lack of accurate kinetic information that allows the comparison between the rates of uptakes of different adsorbents. The kinetics of PEI adsorption are complicated by the high heat of adsorption, range of adsorption sites and changes in amine mobility as the zwitterionic carbamate product is formed [50, 78, 169].

The long term durability of amine impregnated adsorbents in the presence of water has received limited attention in the literature [143-146, 170]. This is somewhat surprising given one of the benefits to amine impregnated silicas is their unhindered and often bolstered adsorption capacity in the presence of water [72, 80, 111, 113, 115]. Recent work has shown that impregnated amine adsorbents are unstable in the presence of steam with both support degradation and amine leaching being reported [143, 145]. Steam regeneration would be advantageous in capture systems, enabling the use of low grade waste steam [144]. Degradation of amine functionalised silica adsorbents in the presence of steam needs to be understood allowing for the development of steam stable adsorbents. Typically adsorbents displaying high adsorption capacities show adsorption capacities much greater than the required 3 mmol g^{-1}. However such adsorbents often have thin pore walls which have been associated with lower long term stability of silica adsorbents [147].

The role of the support relevant to amine impregnated adsorbents has been investigated. The role of the support is clear; high pore volumes and large pores lead to greater amine accessibility [88, 90]. By comparison only a handful of impregnated amine species have been investigated [12, 15, 17, 18, 20, 21]. It is often reported that the amine efficiency of the PEI is below 0.3 meaning 40% of the nitrogen content is unreactive. New polymers could be created with more efficient dispersion of amine groups or favourable CO_2 adsorption environments. Furthermore the physical properties of the polymer could be tailored to yield polymers with greater flexibility, thereby increasing amine efficiency.

Grafted amines offer rapid CO_2 adsorption, however most capacities reported have below the desirable 3.0 mmol g^{-1} [31, 58]. The highest adsorption capacities are found for triamine grafted amine materials thought to be due to the increased nitrogen loading. Advances in silane preparation are required to enable the use of potentially more selective or active amine components. A greater understanding of the interactions between CO_2 and solid adsorbents could led to adsorbents with greater amine efficiencies by exclusive formation of bicarbonate or carbamic acid species.

Adsorbents prepared by the surface polymerisation of amines are a new area of amine incorporation and have been shown to yield high amine loadings and adsorption capacities [11, 13, 43]. Owing to diffusion limitations of the amines within the pores of the adsorbents, a greater proportion of the amine is typically located around the pore mouths. This leads to the creation of diffusion limiting films reducing the uptake of CO_2. To date no through study has presented rapid kinetic data on the order of seconds for surface polymerised adsorbents.

From a critical evaluation of the literature there are several knowledge gaps that must be investigated to determine the most appropriate solid adsorbents for post combustion carbon capture. These include:

1) Long term stability in the presence of water, enabling the use of stream regeneration.

2) Greater understanding of the kinetics of CO_2 adsorption to enable the design and application of superior adsorbents.

3) Greater understanding of the kinetics of CO_2 desorption allowing optimum regeneration conditions to be defined.

4) Stability with respect to common flue gas contaminants, oxygen, CO_2, NO_x and SO_x.

5) Methods of producing adsorbents at scale and low cost to meet the demands of a new market that could be created.

6) Improving the kinetics of impregnated adsorbents to ensure they have applicability in practical adsorption systems.

7) Improving the capacity of grafted adsorbents so that they can become economically competitive with liquid amine adsorption systems.

8) Improving the control of surface polymerised adsorbents allowing the grafting of high amine loadings without severely hampering the kinetics of adsorption.

9) Optimisation of the amine chemistry and support properties to narrow the temperature window between adsorption and desorption.

10) Understanding the behaviour of impregnated amines within porous silica supports.

2.10 References

1. T. C. Drage, C.E.Snape, L. A. Stevens, J. Wood, J. Wang, A. I. Cooper, R. Dawson, X. Guo, C. Satterley, R. Irons, *Materials challenges for the development of solid sorbents for post-combustion carbon capture.* 2012, 2012. **22**: p. 2815.
2. A. Samanta, A. Zhao, G. K. H. Shimizu, P. Sarkar, R. Gupta, *Post-Combustion CO_2 Capture Using Solid Sorbents: A Review.* Ind . Eng. Chem. Res., 2011. **51**: p. 1438.
3. S. Choi, J. H. Drese, C. W. Jones, *Adsorbent Materials for Carbon Dioxide Capture from Large Anthropogenic Point Sources.* ChemSusChem, 2009. **2**: p. 796.
4. G. Qi, L. Fu, B. H. Choi, E. P. Giannelis, *Efficent CO_2 sorbents based on silica foam with ultra-large mesopores.* Energy Environ. Sci., 2012. **5**: p. 7369.
5. T. C. Drage, K. M. Smith, A. Arenillas, C. E. Snape, *Developing strategies for the regeneration of polyethylenimine based CO_2 adsorbents.* Energy Procedia, 2009. **1**: p. 875.
6. S. Sjostrom, H. Krutka, *Evaluation of solid sorbents as a retrofit technology for CO_2 capture. Fuel*, 2010. **89**(1298).
7. R. Sanz, G. Calleja, A. Arencibia, E. S. Sanz-Pérez, *Amino functionalized mesostructured SBA-15 silica for CO_2 capture: Exploring the relation between the adsorption capacity and the distribution of amino groups by TEM.* Microporous and Mesoporous Materials, 2012. **158**: p. 309.
8. X. Xu, C.S., J. M. Andresen, B. G. Miller, A. W. Scaroni, *Preparation and characterization of novel CO_2 "molecular basket" adsorbents based on polymer-modified mesoporous molecular sieve MCM-41. Microporous and Mesoporous Materials*, 2003. **62**: p. 29.
9. X. Xu, C. Song, J. M. Andresen, B. G. Miller, A. W. Scaroni, *Novel Polyethyleneimine-Modified Mesoporous Molecular Sieve of MCM-41 Type as High Capacity Adsorbent For CO_2 Capture. Energy & Fuels*, 2002. **16**: p. 1463.
10. A. von Harpe, H. Petersen, Y. Li, T. Kissel, *Characterisation of commerically available and synthesized polyethyleneimines for gene delivery. J. Controlled Release*, 2000. **69**: p. 309.
11. J. C. Hicks, J. H. Drese, D. J. Fauth, M. L. Gray, G. Qi, C. W. Jones, *Designing Adsorbents for CO_2 Capture from Flue Gas-Hyperbranched Aminosilicas Capable of Capturing CO_2 Reversibly.* J. Am. Chem. Soc., 2008. **130**: p. 2902.
12. T. C. Drage, A. Arenillas, K. M Smith, C. E. Snape, *Thermal Stability of Polyethylenimine Based Carbon Dioxide Adsorbents and Its Influence on Selection of Regeneration Strategies.* Microporous and Mesoporous Materials, 2008. **116**: p. 504.
13. J. H. Drese, S. Choi, R. P. Lively, W. J. Koros, D. J. Fauth, M. L. Gray, C. W. Jones, *Synthesis-Structure-Property Relationships for Hyperbranched Aminosilica CO_2 Adsorbents. Adv. Funct. Mater.*, 2009. **19**: p. 3821.
14. M. Yao, Y. Dong, X. Hu, X. Feng, A. Jia, G. Xie, G. Hu, M. Luo, *Tetraethylenepentamine-Modified Silica Nanotubes for Low-Temperature CO_2 Capture.* Energy Fuels, 2013. **27**: p. 7673.

15. S. Liu, W. Hsio, W. Sie, *Tetraethylenepentamine-modified mesoporous adsorbents for CO2 capture: effects of preparation methods.* Adsorption, 2012. **18**: p. 431.
16. G. Qi, Y. Wang, L. Estevez, X. Duan, N. Anako, A. A. Park, W. Li, C. W. Jones, E. P. Giannelis, *High efficiency nanocomposite sorbents for CO_2 capture based on amine-functionalized mesoporous capsules.* Energy Environ. Sci., 2011. **4**(444).
17. L. Wei, Z. Gao, Y. Jing, Y. Wang, *Adsorption of CO_2 from Simulated Flue Gas on Pentaethylenehexamine-Loaded Mesoporous Silica Support Adsorbent.* Ind . Eng. Chem. Res., 2013. **52**: p. 14965.
18. F. Zheng, D. N. Tran, B. J. Busche, G. E. Fryxell, R. S. Addleman, T. S. Zemanian, C. L. Aardahl, *Ethylenediamine-Modified SBA-15 as Regenerable CO_2 Sorbent.* Ind . Eng. Chem. Res., 2005. **44**: p. 3099.
19. R. S. Franchi, P. J. E. Harlick, A. Sayari, *Applications of Pore-Expanded Mesoporous Silica. 2. Development of a High-Capacity, Water-Tolerant Adsorbent for CO_2.* Ind . Eng. Chem. Res., 2005. **44**: p. 8007.
20. W. Chaikittislip, R. Khunsupat, T. T. Chen, C. W. Jones, *Poly(allylamine)-Mesoporous Silica Composite Materials for CO_2 Capture from Simulated Flue Gas or Ambient Air.* Ind . Eng. Chem. Res., 2011. **50**: p. 14203.
21. B. Fadhel, M. Hearn, A. Chaffee, *CO_2 adsorption by PAMAM dendrimers: Significant effect of impregnation into SBA-15.* Microporous and Mesoporous Materials, 2009. **123**: p. 140.
22. N. Linneen, R. Pfeffer, Y. S. Lin, *CO_2 capture using particulate silica aerogel immobilised with tetraethylenepentamine.* Microporous and Mesoporous Materials, 2013. **176**: p. 123.
23. W. C. Wilfong, C. S .Srikanth, S. C. Chuang, *In Situ ATR and DRIFTS Studies of the Nature of Adsorbed CO_2 on Tetraethylenepentamine Films.* ACS Appl. Mater. Interfaces, 2014. **6**: p. 13617.
24. O. Leal, C. Bolivar, C. Ovalles, J. José García, Y. Espidel, *Reversible adsorption of carbon dioxide on amine surface-bonded silica gel.* Inorg. Chim. Acta, 1995. **240**: p. 183.
25. P. Van Der Voort, I. Gillis-D'Hamers, K. C. Vrancken, E. F. Vansant, *Effect of porosity on the disribution and reactivity of hydroxyl groups on the surface of silica gel.* J. Chem. Soc., Faraday Trans., 1991. **87**: p. 3899.
26. G. P. Knowles, J. V. Graham, S. W. Delaney, A. L. Chaffee, *Aminopropyl-functionalised mesoporous silicas as CO_2 adsorbents.* Fuel Process. Technol., 2005. **86**: p. 1435.
27. R. K. Iler, *The Chemistry of Silica.* John Wiley & Sons, New York, 1979.
28. J. Wei, J. Shi, H. Pan, W. Zhao, Q. Ye, Y. Shi, *Adsorption of carbon dioxide on organically functionalized SBA-16.* Microporous and Mesoporous Materials, 2008. **116**: p. 394.
29. N. Gartmann, C. Schütze, H. Ritter, D. Brühwiler, *The Effect of Water on the Functionalization of Mesoporous Silica with 3-Aminopropyltriethoxysilane.* J. Phys. Chem. Lett., 2009. **1**: p. 379.
30. R. Kishor, A. K. Ghoshai, *APTES grafted mesoporous silica KIT-6 for CO_2 adsorption* Chemical Engineering Journal, 2015. **262**: p. 882.
31. P. J. E. Harlick, A. Sayari., *Applications of Pore-Expanded Mesoporous Silica. 5. Triamine Grafted Material with Exceptional CO_2 Dynamic and Equilibrium Adsorption Performance.* Ind . Eng. Chem. Res., 2007. **46**: p. 446.

32. C. Huang, W. Klinthong, C. Tan, *SBA-15 grafted with 3-aminopropyl triethoxysilane in supercritical propane for CO_2 capture.* J. Supercrit. Fluids, 2013. **77**: p. 117.
33. Y. Sánchez-Vicente, L.A. Stevens, C. Pando , M. José Torralvo , C. E. Snape, and A.C. T. C. Drage, *A new sustainable route in supercritical CO_2 to functionalize silica SBA-15 with 3-aminopropyltrimethoxysilane as material for carbon capture.* Chemical Engineering Journal, 2015(264): p. 886.
34. S. Kim, J. Ida, V. V. Guliants, J. Y. S. Lin, *Tailoring Pore Properties of MCM-48 Silica for Selective Adsorption of CO_2.* J. Phys. Chem. B, 2005. **109**: p. 6287.
35. H. Kassab, M. Maksoud, S. Aguado, M. Pera-Titus, B. Albena, L. Bonnevoit, *Polyethylenimine covalently grafted on mesostructured porous silica for CO_2 capture.* RSC Adv., 2012. **2**: p. 2508.
36. Y. Du, Z. Du, W. Zou, H. Li, J. Mi, C. Zhang, *Carbon dioxide adsorbent based on rich amines loaded nano-silica.* Journal of Colloid and Interface Science, 2013. **409**: p. 123.
37. E. G. Moschetta, M. A. Sakwa-Novak, J. L. Greenfield, C. W. Jones, *Post-Grafting Amination of Alkyl Halide-Functionalized Silica for Applications in Catalysis, Adsorption, and ^{15}N NMR Spectroscopy.* Langmuir, 2015. **32**: p. 2218.
38. Z. Liang, B. Fadhel, C. J. Schneider, A. L. Chaffee, *Stepwise growth of melamine-based dendrimers into mesopores and their CO_2 adsorption properties.* Microporous and Mesoporous Materials, 2008. **111**: p. 536.
39. C. Knöfel, J. Descarpentries, A. Benzaouia, V. Zelenak, S. Mornet, P. L. Llewellyn, V. Hornebecq *Functionalised micro-/mesoporous silica for the adsorption of carbon dioxide.* Microporous and Mesoporous Materials, 2006. **99**: p. 79.
40. E. J. Acosta, C. S. Carr, E. E. Simanek, D. F. Shantz, *Synthesis of Melamine-Based Dendrimers on Amine-Functionalised SBA-15 Leading to Complex Hybrids with Controllable Chemistry and Porosity.* Adv. Funct. Mater., 2004. **16**: p. 985.
41. W. Chaikittislip, J. D. Lunn, D. F. Shantz, C. W. Jones, *Poly(L-lysine) Brush–Mesoporous Silica Hybrid Material as a Biomolecule- Based Adsorbent for CO_2 Capture from Simulated Flue Gas and Air.* Chem. Eur. J., 2011. **17**: p. 10556.
42. H. J. Kim, J. H. Moon, J. W. Park, *A Hyperbranched Poly(ethyleneimine) Grown on Surfaces.* Journal of Colloid and Interface Science, 2000. **227**: p. 247.
43. W. Chaikittislip, S. A. Didas, H. Kim, C. W. Jones, *Vapor-Phase Transport as A Novel Route to Hyperbranched Polyamine-Oxide Hybrid Materials.* Chem. Mater., 2013. **25**: p. 613.
44. G. Qi, L.Fu, E. P. Giannelis, *Sponges with covalently tethered amines for high-efficiency carbon capture.* Nat Commun, 2015. **5**: p. 5796.
45. W. Son, J. Choi, W. Ahn, *Adsorptive removal of carbon dioxide using polyethyleneimine-loaded mesoporous silica materials. Microporous and Mesoporous Materials*, 2008. **113**: p. 31.
46. A. Heydari-Gorji, Y. Belmbkhout, A. Sayari, *Polyethyleneimine-Impregnated Mesoporous Silica: Effect of Amine Loading and Surface Alkyl Chains on CO_2 Adsorption.* Langmuir, 2011. **27**: p. 12411.

47. C. Chen, S. Yang, W. Ahn, R. Ryoo, *Amine-impregnated silica monolith with a hierarchical pore structure: enhancement of CO_2 captire capacity.* Chem. Commun., 2009. **1**: p. 3627.
48. X. Wang, X. Ma, C. Song, D. R. Locke, S. Siefert, R. E. Winans, J. Möllmer, M. Lange, A. Möller, R. Gläser, *Molecular basket sorbents polyethylenimine–SBA-15 for CO_2 capture from flue gas: Characterization and sorption properties.* Microporous and Mesoporous Materials, 2013. **169**: p. 103.
49. N. N. Linneen, R. Pfeffer, Y. S. Lin, *Amine Distribution and Carbon Dioxide Sorption Performance of Amine Coated Silica Aerogel Sorbents: Effect of Synthesis Methods.* Ind . Eng. Chem. Res., 2013. **52**: p. 14671.
50. C. S. Srikanth, S. S. C. Chuang, *Infrared Study of Strongly and Weakly Adsorbed CO_2 on Fresh and Oxidatively Degraded Amine Sorbents.* J. Phys. Chem. C, 2013. **117**: p. 9196.
51. M. B. Yue, L. B. Sun, Y. Cao, Z. J. Wang, Y. Wang, Q. Yu, J. H. Zhu, *Promoting the CO_2 adsorption in the amine-containing SBA-15 by hydoxyl group.* Microporous and Mesoporous Materials, 2008. **114**: p. 74.
52. W. Yan, J. Tang, Z. Bian, J. Hu, H. Liu, *Carbon Dioxide Capture by Amine-Impregnated Mesocellular-Foam-Containing Template. Ind . Eng. Chem. Res.*, 2012. **51**: p. 3653.
53. J. Wang, D. Long, H. Zhou, Q. Chen, X. Liu, L. Ling, *Surfactant promoted solid amine sorbents for CO_2 capture. Energy Environ. Sci.*, 2012. **5**: p. 5742.
54. D. S. Dao, H. Yamada, K. Yogo, *Large-Pore Mesostructured Silica Impregnated with Blended Amines for CO_2 Capture. Ind . Eng. Chem. Res.*, 2013. **52**: p. 13810.
55. D.S. Dao, H. Yamada, K. Yogo, *Response Surface Optimisation of Impregnation of Blended Amines into Mesoporous Silica for High-Performance CO_2 Capture.* Energy & Fuels, 2015. **29**: p. 985.
56. R. Sanz, G. Calleja, A. Arencibia, E. S. Sanz-Pérez, *Development of high efficiency adsorbents for CO_2 capture based on a double-functionalization method of grafting and impregnation.* J. Mater. Chem. A., 2013. **1**: p. 1956.
57. E. P. Plueddemann, *Silane Coupling Agents Second Edition.* Springer Science+Business Media New York, 1991.
58. N. N. Linneen, R. Pfeffer, Y. S. Lin, *CO_2 adsorption performance for amine grafted particulate silica aerogels.* Chemical Engineering Journal, 2014. **254**: p. 190.
59. H. Y. Huang, R. T. Yang, D. Chinn, C. L. Munson, *Amine-Grafted MCM-48 and Silica Xerogel as Superior Sorbents for Acidic Gas Removal from Natural Gas.* Ind . Eng. Chem. Res., 2003. **42**: p. 2427.
60. S. Ciu, W. Cheng, X. Shen, M. Fan, T. Russell, *Mesoporous amine-modified SiO_2 aerogel: a potential CO_2 sorbent.* Energy Environ. Sci., 2011. **4**: p. 2070.
61. S. Hao, H. Chang, Q. Xiao, Y. Zhong, W. Zhu, *One-pot synthesis and CO_2 adsorption properties of ordered mesoporous SBA-15 materials functionalized with APTMS.* J. Phys. Chem., 2011. **115**: p. 12873.
62. K. Wörmeyer, M. Alnaief, I. Smirnova, *Amino functionalised Silica-Aerogels for CO_2 -adsorption at low partial pressures.* Adsorption, 2012. **18**: p. 163.
63. M. Gil, I. Tiscornia, Ó. de la Iglesia, R. Mallada, J. Santamaría, *Monoamine grafted MCM-48: an efficient material for CO2 removal at low partial pressures,.* Chem. Eng. J., 2011. **175**: p. 291.

64. R. Begag, H. Krutka, W. Dong, D. Mihalcik, W. Rhine, G. Gould, J. Baldic, P. Nahass, *Superhydrophobic amine functionalized aerogels as sorbents for CO_2 capture.* Greenhouse Gases Sci. Technol., 2010. **3**: p. 30.
65. G.P. Knowles, S. W. Delaney, A. L. Chaffee, *Diethylenetriamine[propyl(silyl)]-Functionalized (DT) Mesoporous Silicas as CO_2 Adsorbents.* Ind . Eng. Chem. Res., 2006. **45**: p. 2626.
66. F Chang, K. Chao, H. Cheng, C. S. Tan *Adsorption of CO_2 onto aminegrafted mesoporous silicas.* Sep. Purif. Technol., 2009. **70**: p. 87.
67. A. Olea, E. S. Pérez, A. Arencibia, R. Sanz, G. Calleja, *Amine-functionalized pore-expanded SBA-15 for CO_2 adsorption.* Adsorption, 2013. **19**: p. 589.
68. E. S. Sanz-Pérez, M. Oilvares.-Marín, A. Arencibia, R. Sanz, G. Calleja, M. M. Maroto-Valer, *CO_2 adsorption performance of amino-functionalised SBA-15 under post-combustion conditions.* Int. J. Greenhouse Gas Control, 2013. **17**: p. 366.
69. N. Hiyoshi, K. Yogo, T. Yashima, *Adsorption characterisitics of carbon dioxide on organically functionalised SBA-15.* Microporous Mesoporous Mater., 2005. **84**: p. 357.
70. R. Serna-Guerrero, Y. Belmabkhout, A. Sayari, *Influence of regeneration conditions on the cyclic performance of amine-grafted mesoporous silica for CO_2 capture: An experimental and statistical study.* Chemical Engineering Science, 2010. **65**: p. 4166.
71. G. Calleja, R. Sanz, A. Arencibia, E.S. Sanz-Pérez, *Influence of drying conditions on amine-functionalized SBA-15 as adsorbent of CO_2.* Top. Catal. , 2011. **54**: p. 135.
72. A. Sayari, Y. Belmabkhout, *Stabilization of Amine-Containing CO_2 Adsorbents: Dramatic Effect of Water Vapor. J. Am. Chem. Soc.*, 2010. **132**: p. 6312.
73. S. Liu, C. Wu, H. Lee, S. liu, *Highly Stable Amine-modifed Mesoporous Silica Materials for Efficent CO_2 Capture.* Top. Catal., 2009. **53**: p. 210.
74. Y. Belmabkhout, N. Heymans, G. De Weireld , A. Sayari, *Simultaneous adsorption of H_2S and CO_2 on triamine-grafted pore-expanded mesoporous MCM-41 silica.* Energy Fuels, 2011. **25**: p. 1310.
75. S. Kim, W. Son, J. Choi, W. Ahn, *CO_2 adsorption using amine-functionalized mesoporous silica prepared via anionic surfactant-mediated synthesis.* Microporous and Mesoporous Materials, 2008. **115**: p. 497.
76. V. Zelenak, D. Halamova, L. Gaberova, E. Bloch, P. Llewellyn, *Amine-modified SBA-12 mesoporous silica for carbon dioxide capture: Effect of amine basicity on sorption properties.* Microporous and Mesoporous Materials, 2008. **116**: p. 358.
77. N. Hiyoshi, K. Yogo, T. Yashima, *Adsorption characteristics of carbon dioxide on orgnically functionalised SBA-15.* Microporous and Mesoporous Materials, 2005. **84**: p. 357.
78. Y. G. Ko, S. Shin, U. S. Choi, *Primary, secondary, and tertiary amines for CO_2 capture: Designing for mesoporous CO_2 adsorbents.* Journal of Colloid and Interface Science, 2011. **361**: p. 594.
79. N. A. Brunelli, S. Didas, K. Venkatasubbaiah, C. W. Jones, *Tuning Cooperatitivity by Controlling the Linker Length of Silica-Supported Amines in Catalysis and CO_2 Capture.* J. Am. Chem. Soc., 2012. **134**: p. 13950.

80. R. Serna-Guerrero, E. Da'na,A.Sayari, *New Insights into the Interactions of CO_2 with Amine-Functionalized Silica. Ind . Eng. Chem. Res.*, 2008. **47**(23): p. 9406.
81. R. Serna-Guerrero, Y. Belmabkhout, A. Sayari, *Modeling CO_2 adsorption on amine-functionalized mesoporous silica: 1. A semi-empirical equilibrium model.* Chemical Engineering Journal, 2010. **161**: p. 173.
82. A. Zhao, A. Samanta, P. Sarkar and R. Gupta, *Carbon Dioxide Adsorption on Amine-impregnated Mesoporous SBA-15 Sorbents: Experiemental and Kinetics Study. Ind . Eng. Chem. Res.*, 2013. **52**: p. 6480.
83. D. J. Fauth, M. L. Gray, H. W. Pennline, *Investigation of Porous Silica Supported Mixed-Amine Sorbents for Post-Combustion CO_2 Capture.* Energy Fuels, 2011. **26**: p. 2483.
84. A. Zukal, I. Dominguez, J. Mayerova, J. Cejka, *Functionalization of Delaminated Zeolite ITQ-6 for the Adsorption of Carbon Dioxide.* Langmuir, 2009. **25**: p. 10314.
85. J. A. Wurzbacher, C. Gebald, A. Steinfeld, *Separation of CO_2 from air by temperature-vacuum swing adsorption using diamine-functionalized silica gel.* Energy Environ. Sci., 2011. **4**: p. 3584.
86. H. Y. Huang, R. T. Yang, D. C. Curtis, L. Munson, Amine-Grafted MCM-48 and Silica Xerogel as Superior Sorbents for Acidic Gas Removal from Natural Gas, Ind. Eng. Chem. Res., 2003. **42**: p. 2427.
87. L. Wang, M. Yao, X. Hu, G. Hu, J. Lu, M. Luo, M. Fan, *Amine-modified ordered mesoporous silica: The effect of pore size on CO_2 capture performance.* Applied Surface Science, 2015. **324**: p. 286.
88. H. Zhang, A. Goeppert, M. Czaun, G. K. S. Prakash, G. A. Olah., *CO_2 capture on easily regenerable hybrid adsorbents based on polyamines and mesocellular silica foam. Effect of pore volume of the support and polyamine molecular weight.* RSC Adv., 2014. **4**: p. 19403.
89. P. Schmidt-Winkel, W. W. Lukens Jr., P. Yang, D. I. Margolese, J. S. Lettow, J. Y. Ying, G. D. Stucky, *Microemulsion Templating of Siliceous Mesostructed Cellular Foams with Well-Defined Ultralarge Mesopores.* Chem. Mater., 2000. **12**: p. 686.
90. V. Zeleňák, M. Badaničováa, D. Halamováa, J. Čejkab, A. Zukalb, N. Murafac, G. Goerigkd, *Amine-modified ordered mesoporous silica: Effect of pore size on carbon dioxide capture.* Chemical Engineering Journal, 2008. **144**(2): p. 336-342.
91. A. Heydari-Gorji, Y. Yang, A. Sayari, *Effect of the Pore Length on CO_2 Adsorption over Amine-Modified Mesoporous Silicas.* Energy & Fuels, 2011. **25**: p. 4206.
92. C. M. Starkie, A. Amieiro.-Fonseca, S. P. Rigby, T. C. Drage, E. H. Lester, *Surfactant Mediated CO_2 Adsorption; the Role of the Co-impregnation Species. Energy Procedia*, 2014. **63**: p. 2323.
93. F. Rezaei, M. A. Sakwa.-Novak, S. Bali, D. M. Duncanson, C. W. Jones, *Shaping amine-based solid CO_2 adsorbents: Effects of pelletization pressure on the physical and chemical properties.* Microporous and Mesoporous Materials, 2015. **204**: p. 34.
94. P. V. Danckwerts, *The Reaction of CO_2 With Ethanolamines.* Chemical Engineering Science, 1979. **34**: p. 443.

95. G. F. Versteeg, L. A. J. Van Dijck, W. P. M. Van Swaaij, *On The Kinetics Between CO_2 and Alkanolamines Both in Aqueous and Non-aqueous Solutions. An Overview.* Chem. Eng. Comm., 1996. **144**: p. 113.
96. M. Caplow, *Kinetics of Carbamate Formation and Breakdown.* J. Am. Chem. Soc., 1968. **90**: p. 6795.
97. R. J. Hook, *An Investigation of Some Sterically Hindered Amines as Potential Carbon Dioxide Scrubbing Compounds.* Ind . Eng. Chem. Res., 1997. **36**: p. 1779.
98. G. Sartori, D. W. Savage, *Sterically hindered amines for carbon dioxide removal from gases.* Ind . Eng. Chem. Fundam., 1983. **22**: p. 239.
99. S. P. Ewing, D. Lockshon, W. P. Jencks, *Mechanism of cleavage of carbamate anions.* J. Am. Chem. Soc., 1980. **102**: p. 3072.
100. A. K. Chakraborty, G. Astarita., K. B. Bischoff, Carbon dioxide absorption in aqueous solutions of hindered amines, 1986. **41**: p. 997.
101. P. Tontiwachwuthlkul, A. Meisen, C. J. Lim, *Solubility of CO_2 in 2-Amino-2-methyl-1-propanol Solutions* J. Chem. Eng. Data, 1991. **36**: p. 130.
102. T. L. Donaldson, Y. N. Nguyen, *Carbon Dioxide Reaction Kinetics and Transport in Aqueous Amine Membranes.* Ind. Eng. Chem. Fundam., 1980. **19**: p. 260.
103. F. A. Chowdhury, H. Yamada, T. Higashii, K. Goto, M. Onoda, *CO_2 Capture by Tertiary Amine Adsorbents: A Performance Comparison Study.* Ind . Eng. Chem. Res., 2013. **52**: p. 8323.
104. T. Tsuda, T.Fujiwara, Y. Taketani, T. Saegusa, *Amino Silica Gels Acting as a Carbon Dioxide Absorbent.* Chemistry Letters, 1992. **21**: p. 2161.
105. A. C. C. Chang, S. C. Chuang, M. Gray, Y. Soong, *In-Situ Infrared Study of CO_2 Adsorption on SBA-15 Grafted with γ-(Aminopropyl)triethoxysilane.* Energy & Fuels, 2003. **17**: p. 468.
106. R. A. Khatri, S. S. C. Chuang, Y. Soong, M. Gray, *Carbon Dioxide Capture by Diamine-Grafted SBA-15: A Combined Fourier Transform Infrared and Mass Spectrometry Study.* Ind . Eng. Chem. Res., 2005. **44**: p. 3702.
107. R. A. Khatri, S. S. C. Chuang, Y. Soong, M. Gray, *Thermal and Chemical Stability of Regenerable Solid Amine Sorbent for CO_2 Capture.* Energy & Fuels, 2006. **20**: p. 1514.
108. J. C. Fisher II, J. Tanthana, S. S. C. Chuang, *Oxide-supported tetraethylenepentamine for CO_2 capuire.* Environ. Prog. Sustainable Energy, 2009. **28**: p. 589.
109. X. Wang, V. Schwartz, J. C. Clark, X. Ma, S. H. Overbury, X. Xu, C. Song, *Infrared Study of CO2 Sorption over "Molecular Basket" Sorbent Consisting of Polyethylenimine-Modified Mesoporous Molecular Sieve.* J. Phys. Chem. C, 2009. **113**: p. 7260.
110. A. Danon, P. C. Stair, E. Weitz, *FTIR Study of CO_2 Adsorption on Amine-Grafted SBA-15: Elucidation of Adsorbed Species.* J. Phys. Chem. C, 2011. **115**: p. 11540.
111. D. J. N. Subagyono, M. Marshall, G. P. Knowles, A. L. Chaffe, *CO_2 adsorption by amine modified siliceous mesostructured cellular foam (MCF) in humidified gas.* Microporous and Mesoporous Materials, 2014. **186**: p. 84.
112. P. Bollini, S. A. Didas, .C. W. Jones, *Amine-Oxide Hybrid Materials for Acid Gas Separations. J. Mater. Chem.*, 2011. **21**: p. 15100.

113. C. Gebald, J. A. Wurzbacher, A. Borgschulte, T. Zimmermann, A. Steinfeld, *Single Component and Binary CO_2 and H_2O Adsorption of Amine-Functionalized Cellulose. Environ. Sci. Technol.*, 2014. **48**: p. 2497.

114. Z. Bacsik, R. Atluri, A. E. Garcia-Bennett, N. Hedin, *Temperature-Induced Uptake of CO_2 and Formation of Carbamates in Mesocaged Silica Modified with n-Propylamines.* Langmuir, 2010. **26**: p. 10013.

115. Z. Bacsik, N. Ahlsten, G. Zhao, A. E. Garcia-Bennett, B. Martín-Matute. *Mechanisms and Kinetics for Sorption of CO2 on Bicontinuous Mesoporous Silica Modified with n-Propylamine.* Langmuir, 2011. **27**(17): p. 11118-11128.

116. S. A. Didas, M. A. Sakwa-Novak, G. S. Foo, C. Sievers and C. W. Jones, *Effect of Amine Surface Coverage on the Co-Adsorption of CO_2 and Water: Spectral Deconvolution of Adsorbed Species.* J. Phys. Chem. Lett., 2014. **5**: p. 4196.

117. D. S. Mebane, J. D. Kress, C. B. Storlie, D. J. Fauth, M. L.Gray, K. Li, *Transport, Zwitterions, and the Role of Water for CO_2 Adsorption in Mesoporous Silica-Supported Amine Sorbents. J. Phys. Chem. C*, 2013. **117**(26617).

118. Y. Fan, Y. Labreche, R. P Lively, W. J. Koros, C. W. Jones, *Dynamic CO_2 Adsorption Performance of Internally Cooled Silica Supported Poly(ethylenimine) Hollow Fiber Sorbents.* AICHE J., 2014. **60**: p. 3878.

119. M. W. Hahn, M. Steib, A. Jentys and J. A Lercher, *Mechanism and Kinetics of CO_2 Adsorption on Surface Bonded Amines.* J. Phys. Chem. C, 2015. **119**: p. 4126.

120. X. Wang, V. Schwartz, J. C. Clark, X. Ma, S. H. Overbury, Z. Xu, C. Song, *Infrared Study of CO_2 Sorption over "Molecular Basket" Sorbent Consisting of Polyethyleneimine-Modified Mesoporous Molecular Sieve.* J. Phys. Chem. C, 2009. **113**: p. 7260.

121. B. Aziz, G. Zhao, N. Hedin, *Carbon Dioxide Sorbents with Propylamine Groups-Silica Functionalised with a Fractional Factorial Design Approach.* Langmuir, 2011. **27**: p. 3822.

122. W. Zhang, H. Liu, C. Sun, T. C. Drage, C. E. Snape, *Performance of Polyethyleneimine-silica adsorbent for post-combustion CO_2 capture in a bubbling fluidized bed.* Chemical Engineering Journal, 2014. **251**: p. 293.

123. D. J. N. Subagyono, Z. Liang, G. P. Knowles, A. L. Chaffe, *Amine modified mesocellular siliceous foam (MCF) as a sorbent for CO_2.* Chem Eng Res Des, 2011. **89**: p. 1647.

124. R. Sanz, G. Calleja, A. Arencibia, E. S. Sanz-Pérez, *CO_2 Uptake and Adsorption Kinetics of Pore-Expanded SBA-15 Double-Functionalized with Amino Groups.* Energy & Fuels, 2013. **27**: p. 7637.

125. Y. Belmabkhout, R. Serna-Guerrero, A. Sayari, *Adsorption of CO_2 from dry gases on MCM-41 silica at ambient temperature and high pressure. 1: Pure CO_2 adsorption.* Chemical Engineering Science, 2009. **64**: p. 3721.

126. A. Heydari-Gorji, A. Sayari, *CO_2 capture on polyethyleneimine-impregnated hydrophobic mesoporous silica: Experimental and kinetic modeling.* Chemical Engineering Journal, 2011. **173**: p. 72.

127. P. Bollini, N. A. Brunelli, S. A. Didas, C. W. Jones, *Dynamics of CO_2 Adsorption on Amine Adsorbents. 1. Impact of Heat Effects.* Ind. Eng. Chem. Res., 2012. **51**: p. 15145.

128. M. A. Alkhabbaz, P. Bollini, G. S. Foo, C. Sievers, C. W. Jones, *Important Roles of Enthalpic and Entropic Contributions to* CO_2 *Capture from Simulated Flue Gas and Ambient Air Using Mesoporous Silica Grafted Amines.* J. Am. Chem. Soc., 2014. **136**: p. 13170.
129. P. Bollini, N. A. Brunelli, S. A. Didas, C. W. Jones, *Dynamics of* CO_2 *Adsorption on Amine Adsorbents, 2. Insights into Adsorbnet Design* Ind . Eng. Chem. Res., 2012. **51**: p. 15153.
130. J. Kalyanaraman, Y. Fan, R. P. Lively, W. J. Koros, C. W. Jones, M. J. Realff, Y. Kawajiri, *Modeling and experimental validation of carbon dioxide sorption on hollow fibers loaded with silica-supported poly(ethylenimine).* Chemical Engineering Journal, 2015. **259**: p. 737.
131. A. Abdollahi-Govar, A. D. Ebner, J. A. Ritter, *New Kinetic Model That Describes the Reversible Adsorption and Desorption Behavior of* CO_2 *in a Solid Amine Sorbent.* Energy & Fuels, 2015. **29**: p. 4492.
132. C. L. Cavalcante, D. M. Ruthven, *Adsorption of Branched and Cyclic Paraffins in Silicalite .2 Kinetics.* Ind . Eng. Chem. Res., 1995. **34**: p. 185.
133. E. D. Snijder, M. J. M. Riele, G. F. Versteeg, W. van Swaaij, *Diffusion Coefficients of Several Aqueous Alkanolamine Solutions.* Chem. Eng. Data, 1993. **38**: p. 475.
134. A. Goeppert, S. Meth, G. K. S. Prakash, A. Olah, *Nanostructured silica as a support for regenerable high-capacity organoamine-based CO2 sorbents.* Energy Environ. Sci., 2010. **3**: p. 1949.
135. M. L. Gray, Y. Soong, K. J. Champagne, H. Pennline, J. P. Baltrus, R. W. Stevens Jr., R. Khatri, S. S. C. Chuang, T. Filburn, *Improved immbilized carbon dioxide capture sorbents.* Fuel Process. Technol., 2005. **86**: p. 1449.
136. A. Sayari, Y. Belmabkhout, E. Da'na, *Deactivation of Supported Amines: Does the Nature of Amine Matter?* Langmuir, 2012. **28**: p. 4241.
137. A. D. Ebner, M. L. Gray, N. G. Chisholm, Q. T. Black, D. D. Mumford, M. A. Nicholson, J. A. Ritter, *Suitability of a Solid Amine Sorbent for* CO_2 *Capture by Pressure Swing Adsorption.* Ind . Eng. Chem. Res., 2011. **50**: p. 5634.
138. X. Xu, C. Song, J. M. Andresen, B. G. Miller, A. W. Scaroni, *Adsorption separation of carbon dioxide from flue gas of natural gas-fired boiler by a novel nanoporous "molecular basket" adsorbent.* Fuel Process. Technol., 2005. **86**: p. 1457.
139. A. L. Chaffee, G. P. Knowles, Z. Liang, J. Zhang, P. Xiao, P. A. Webley, CO_2 *capture by adsorption: materials and process development.* Int. J. Greenhouse Gas Control, 2007. **1**: p. 11-18.
140. N. Hedin, L. Andersson, L. Bergström, J. Yan *Adsorbents for the post-combustion capture of* CO_2 *using rapid temperature swing or vacuum swing adsorption.* Appl. Energy, 2013. **104**: p. 418.
141. R. Serna-Guerrero, Y. Belmabkhout, A. Sayari, *Triamine-grafted pore-expanded mesoporous silica for* CO_2 *capture: Effect of moisture and adsorbent regeneration strategies.* Adsorption, 2010. **16**: p. 567.
142. A. Goeppert, M. Czaun, R. B May, G. K. S. Prakash, G. A. Olah, S. R. Narayanan, *Carbon Dioxide Capture from the Air Using a Polyamine Based Regenerable Solid Adsorbent.* J. Am. Chem. Soc., 2011. **133**: p. 20164.
143. W. C. Wilfong, B. W. Kail, M. L. Gray, *Rapid Screening of Immobilized Amine* CO_2 *Sorbents for Steam Stability by Their Direct Contact with Liquid* H_2O*.* ChemSusChem, 2015. **8**: p. 2041.

144. W. Li, S. Choi, J. H. Drese, M. Hornbostel, G. Krishnan, P. M. Eisenberger, C. W. Jones, *Steam-Stripping for Regeneration of Supported Amine-Based CO_2 Adsorbents. ChemSusChem*, 2010. **3**: p. 899.
145. W. Li, P. Bollini, S. A. Didas, S. Choi, J. H. Drese, C. W. Jones, *Structural Changes of Silica Mesocellular Foam Supported Amine-Functionalized CO_2 Adsorbents Upon Exposure to Steam.* ACS Appl. Mater. Interfaces, 2010. **2**: p. 3363.
146. S. Hammache, J. S. Hammache, M. L. Gray, D. J. Fauth, B. H. Howard, H. W. Pennline, *Comprehensive Study of Steam on Polyethyleneimine on Silica for CO_2 Capture.* Energy & Fuels, 2013. **27**: p. 6899.
147. R. Mokaya, *Improving the Stability of Mesoporous MCM-41 Silica via Thicker More Highly Condensed Pore Walls.* J. Phys. Chem. B, 1999. **103**: p. 10204.
148. A. Heydari-Gorji, A. Sayari, *Thermal, Oxidative, and CO_2 - Induced Degradation of Supported Polyethyleneimine Adsorbents.* Ind . Eng. Chem. Res., 2012. **51**: p. 6887.
149. A. Sayari, A. Heydari.-Gorji, Y. Yang, *CO_2-Induced Degradation of Amine-Containing Adsorbents: Reaction Products and Pathways.* J. Am. Chem. Soc., 2012. **134**: p. 13834.
150. S. A. Didas, R. Zhu, N. A. Brunelli, D. S. Sholl, C. W. Jones, *Thermal, Oxidative and CO_2 Induced Degradation of Primary Amines Used for CO_2 Capture: Effect of Alkyl Linker on Stability.* J. Phys. Chem. C, 2014. **118**: p. 12302.
151. R. K. Iler, *The Chemistry of Silica.* John Wiley & Sons, 1979.
152. H. Lepaumier, D. Picq, P. L. Carrette, *New amines for CO_2 capture. I. Mechanisms of amine degradation in the presence of CO_2.* Ind . Eng. Chem. Res., 2009. **48**: p. 9061.
153. G. S. Goff, G. T. Rochelle, *Monoethanolamine degradation:O_2 mass transfer effects under CO_2 capture conditions.* Ind . Eng. Chem. Res., 2004. **43**: p. 6400.
154. P. Bollini, S. Choi, J. H. Drese, C. W. Jones, *Oxidative Degradation of Aminosilica Adsorbents Relevant to Postcombustion CO_2 Capture.* Energy & Fuels, 2011. **25**: p. 2416.
155. A. Heydari-Gorji, Y. Blmabkhout, A. Sayari, *Degradation of Amine-Supported CO_2 Adsorbents in the Presence of Oxygen Containing Gases.* Microporous and Mesoporous Materials, 2011. **145**: p. 146.
156. I. J. Uyanga, R. O. Idem, *Studies of SO_2- and O_2-induced degradation of aqueous MEA during CO_2 capture from power plant flue gas streams.* Ind . Eng. Chem. Res., 2007. **46**: p. 2558.
157. A. P. Hallenbeck, J. R. Kitchin, *Effects of O_2 and SO_2 on the Capture Capacity of a Primary-Amine Based Polymeric CO_2 Sorbent.* Ind . Eng. Chem. Res., 2013. **52**: p. 10788.
158. F. Rezaei, A. A. Rownaghi, S. Monhexi, R. P. Lively, C. W. Jones, *SO_x/NO_x Removal from Flue Gas Streams by Solid Adsorbents: A Review of Current Challenges and Future Directions.* Energy & Fuels, 2015. **Article ASAP**.
1590. A. M. B. Furtado, D. Barpaga, L. A. Mitchell, Y. Wang, J. B. DeCoste, G. W. Peterson, M. D. LeVan, *Orgnaoalkoxysilane-Grafted Silica Composites for Acidic and Basic Gas Adsorption.* Langmuir, 2012. **28**: p. 17450.

160. F. Rezaei, C. W. Jones, *Stability of Supported Amine Adsorbents to SO_2 and NO_x in Postcombustion CO_2 Capture. 1. Single-Component Adsorption.* Ind . Eng. Chem. Res., 2013. **52**: p. 12192.
161. R. Tailor, A. Ahmadalinezhad, A. Sayari, *Selective removal of SO_2 over tertiary amine-containing materials.* Chemical Engineering Journal, 2014. **240**: p. 462.
162. R. Tailor, M. Abboud, A. Sayari, *Supported Polytertiary Amines: Highly Efficent and Selective SO_2 Adsorbents.* Environ. Sci. Technol., 2014. **48**: p. 2025.
163. L. L. Vasileva, F. N. Dultsev, A. K. Milekhin, *IR spectral study of SO_2 adsorption on polysiloxane layers containing tertiary amino groups.* J. Struct. Chem., 1996. **37**: p. 142.
164. D. Yang, M. Hou, H. Ning, J. Zhang, J. Ma, B. Han, *Efficent SO_2 capture by amine functionalized PEG.* Phys. Chem. Chem. Phys., 2013. **15**: p. 18123.
165. D. D. Miller, S. S. C. Chuang, *Experimental and Theoretical Investigation of SO_2 Adsorption over the 1,3-Phenylenediamine/SiO_2 System.* J. Phys. Chem. C, 2015. **119**: p. 6713.
166. Y. Fan, F. Rezaei, Y. Labreche, R. P. Lively, W. J. Koros, C. W. Jones, *Stability of amine-based hollow fiber CO_2 adsorbents in the presence of NO and SO_2.* Fuel, 2015. **160**: p. 153.
167. F. Rezaei, C. W. Jones, *Stability of Supported Amine Adsorbents to SO_2 and NO_x in Postcombustion CO_2 Capture. 2. Multicomponent Adsorption.* Ind . Eng. Chem. Res., 2014. **52**: p. 12103.
168. S. Barman, L. Philip, *Integrated System for the Treatment of Oxides of Nitrogen from Flue Gases.* Environ. Sci. Technol., 2006. **45**: p. 1035.
169. D. S. Mebane, J. D. Kress, C. B. Storlie, D. J. Fauth, M. L.Gray, K. Li, *Transport, Zwitterions, and the Role of Water for CO_2 Adsorption in Mesoporous Silica-Supported Amine Sorbents.* J. Phys. Chem. C, 2013. **117**: p. 26617.
170. W. Chaikittislip, H. Kim, C. W. Jones, *Mesoporous Alumina-Supported Amines as Potential Steam-Stable Adsorbents for Capturing CO_2 from Simulated Flue Gas and Ambient Air.* Energy Fuels, 2011. **25**: p. 5528.

CHAPTER THREE

Experimental

3.1 Materials

The following chemicals were used as received:

Pluronic 123, 3-aminpropyltriethoxysilane, triethoxy(octyl)silane, triethoxyphenylsilane, hexadecyltrimethoxysilane, tetraethylorthosilicate, tetraethylenepentamine, toluene, methanol, acetone, 4-vinylbenzylchloride, ethanol, 37% hydrochloric acid, butylamine, Davisil 22 silica , Davisil 60 silica, Davisil 150 silica were purchased from Sigma-Aldrich. Sodium dodecyl sulfate, triethanolamine, branched polyethyleneimine with molecular weights of 600 (PEI 600) and 1800 (PEI 1800), ethylenediamine, 1H,1H,2H,2H-perfluorodecylltriethoxysilane were purchased from Alfa Aesar. Sodium hydroxide was purchased from Fisher Scientific. 4,4-azobis(4-cyanovaleric acid) functionalised silica was supplied by Dr James Stevens of Johnson Matthey. Nitrogen, carbon dioxide, helium, CO_2 15 % CO_2/N_2 were purchased from BOC. Deionised water was produced using a Millipore IQ II.

3.2 Characterisation of commercial polyethyleneimine

Solution NMR was conducted on a JEOL GSX 270 MHz NMR spectrometer and referenced to chloroform proton signal. Inversely gated ^{13}C NMR experiments were used to characterise the distribution of 1°, 2° and 3° amine sites in the commercial polyethyleneimine (PEI 600 and PEI 1800) used in this study. In a typical experiment approximately 10 mg of polymer was dissolved is deuterated chloroform (0.8 ml) with the addition of chromium (III) acetylacetonate (200 µl, 0.1 M) as a relaxation agent. Data acquisition was collected over 30000 scans. The ^{13}C NMR spectrum of branched PEI consisted of eight carbon environments between 39-

58 ppm (Figure 3.1). The positions of these peaks are related to the 8 carbon environments of branched PEI (Figure 3.2).

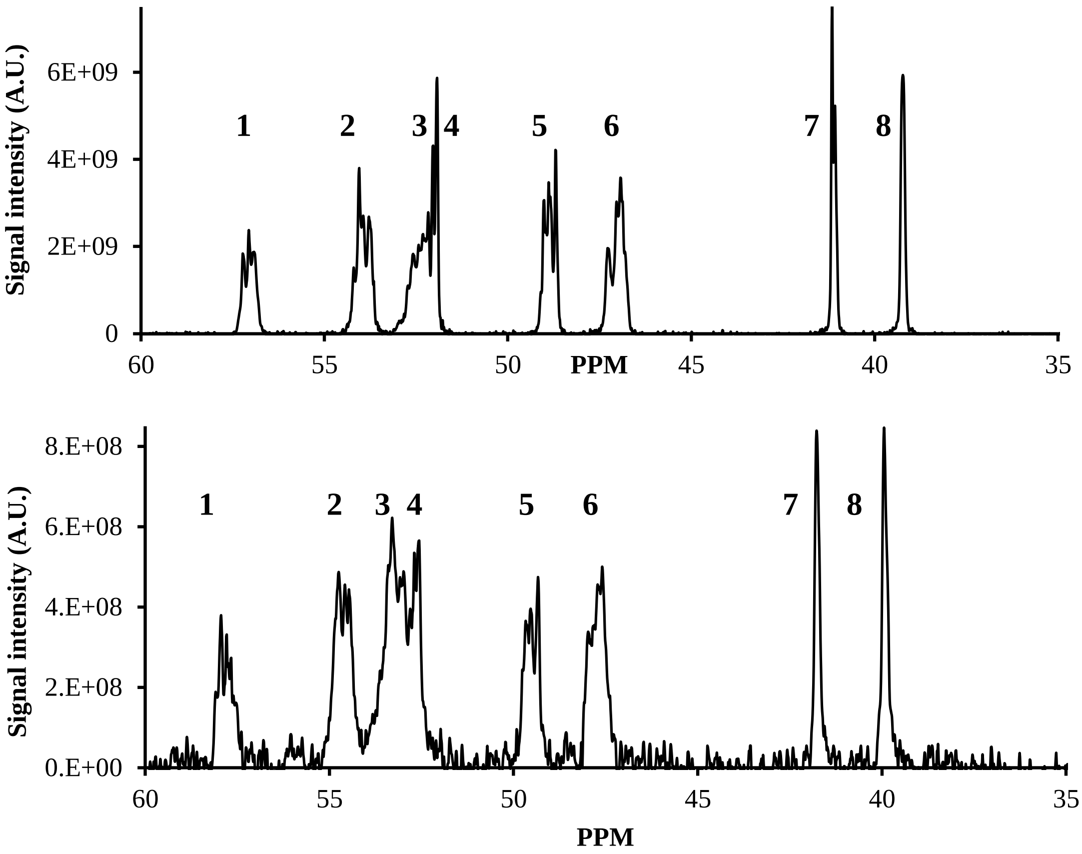

Figure 3.1. Inversely gated ^{13}C NMR of PEI 600 (top) and PEI 1800 (bottom).

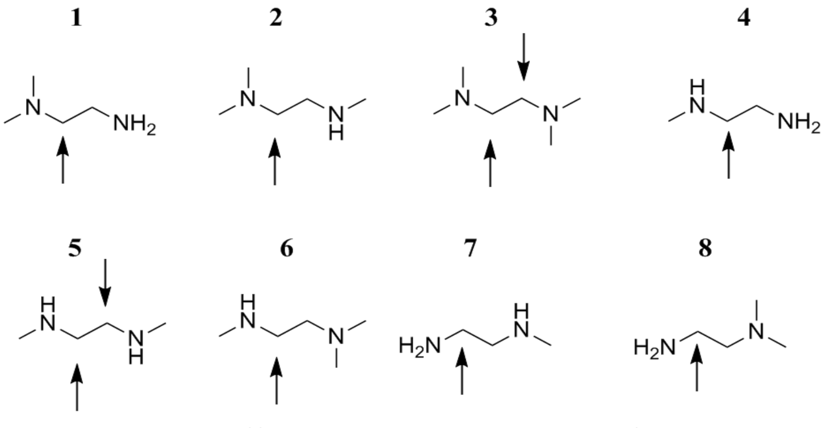

Figure 3.2. The 8 different carbon environments of branched PEI.

Owing to the overlap in the signals observed at 53 ppm, peak shape fitting was completed using Fityk 0.9.8 [1]. The ^{13}C spectra of PEI 600 gave three signals present between 52 and 53 ppm consistent with literature reports [2, 3]. These were deconvoluted to yield two sharp signals at 51.9 and 52.1 ppm, 2° amine sites with the broader signal at 52.5 ppm corresponding to a 3° amine site (Figure 3.3). The ^{13}C spectra of PEI 1800 presented two peaks overlapping peaks between 52-54 ppm. These were deconvoluted to a peak at 52.6 ppm corresponding to a 2° amine and another at 53.2 ppm for a 3° amine site (Figure 3.4).

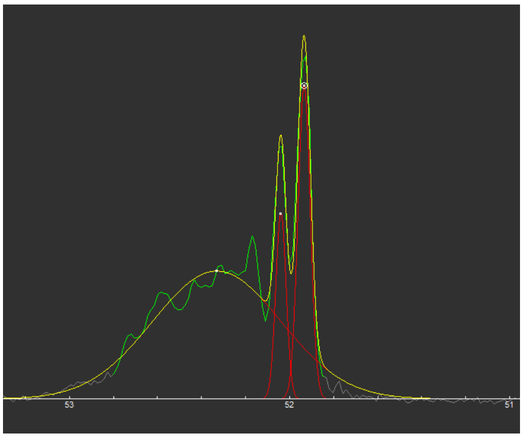

Figure 3.3. Spectra deconvolution of overlapping peaks between 52-53 ppm. The raw data is in green, fitted peaks in red and the overall area of integration in yellow.

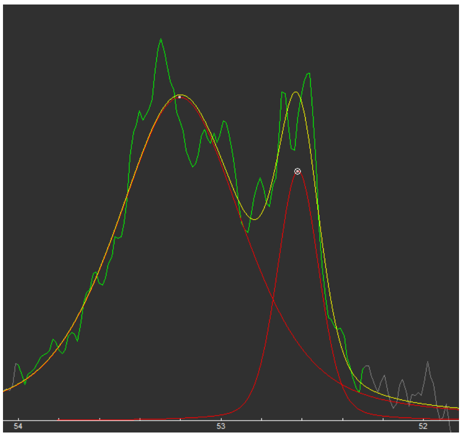

Figure 3.4. Spectra deconvolution of overlapping peaks between 52-53 ppm. The raw data is in green, fitted peaks in red and the overall area of integration in yellow.

The ratio of 1°, 2° and 3° amine from the integrals of the ^{13}C spectra were used with Equation 3.1 to obtain the distribution of 1°:2°:3° amines (Table 3.1).

$$1^{o}:2^{o}:3^{o} = (I_7 + I_8):\frac{(I_4+I_5+I_6)}{2}:\frac{(I_1+I_2+I_3)}{3} \qquad \text{Equation 3.1}$$

Where I_x is the integral of peak x, where, x is the assignment given in Figure 3.2. The fraction of 1°, 2° and 3° amines in PEI 600 and PEI 1800 agree well with reported values [2, 3].

Table 3.1. The proportion of 1°:2°:3° amines of the polyethyleneimines used in this study.

Amine	1°	2°	3°	Polydispersity index[a]
PEI 600	39	36	25	1.08
PEI 1800	38	32	30	1.14

[a] Provided by Alfa Aesar

3.3 CO_2 adsorption using a fixed bed reactor

CO_2 adsorption experiments were conducted in a fixed bed reactor shown in Figure 3.5. The rig consisted of a series of computer controlled mass flow controllers feeding into an oven to preheat the gases. The gas could either by sent over the adsorbent dry or bubbled through a pair of stainless steel water bubblers yielding a vapour laden gas flow. The water content of the gas was adjusted using a needle valve to adjust the fraction of wet and dry gas that passed through the sample. The sorbent filled tube was inserted into a computer controlled furnace with a thermocouple penetrating into the sample. After passing through the adsorbent bed the gas flowed through heated lines to an online MKS 2030 Multigas IR detector. This detector could simultaneously measure the CO_2 and H_2O concentrations in the gas stream. The IR data were recorded at 1 s intervals with a resolution of 0.5 cm^{-1} with the analysis chamber maintained at 191 °C +/- 0.5 °C.

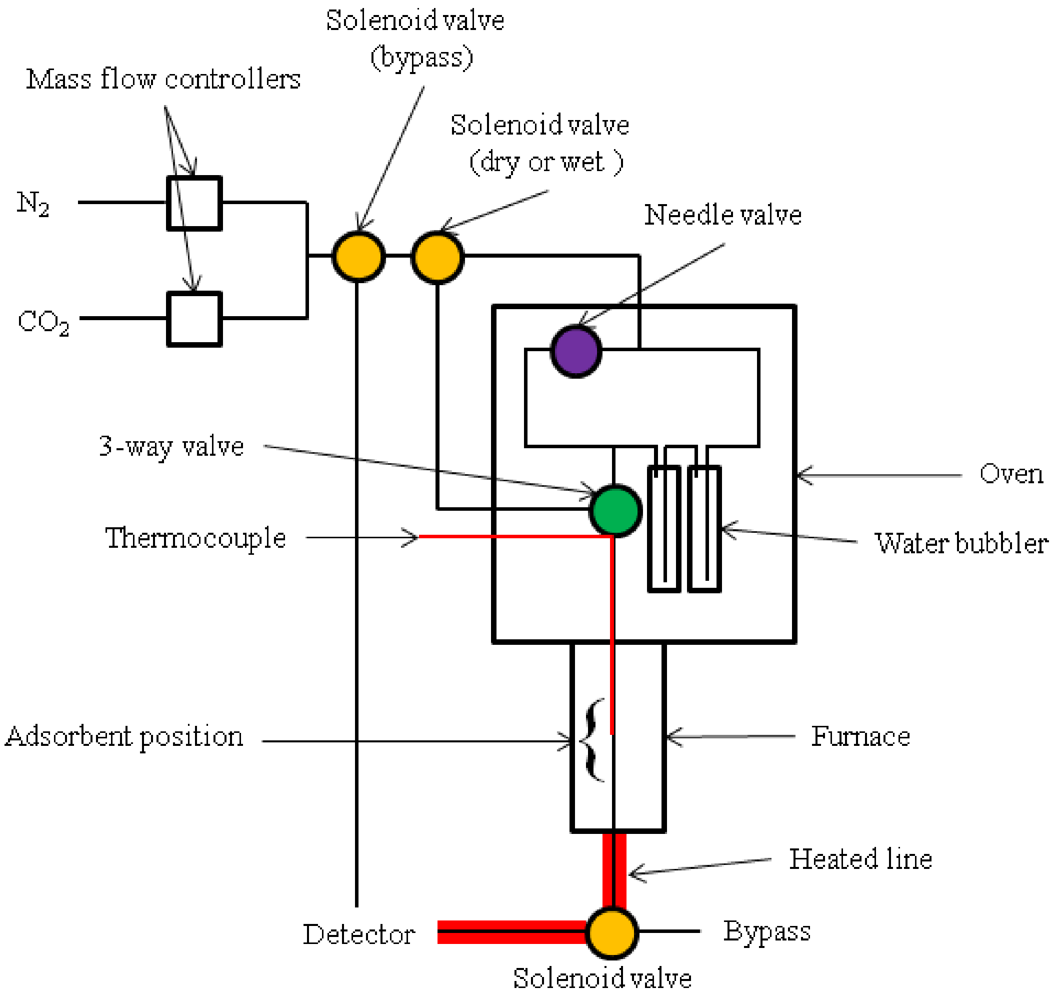

Figure 3.5. Schematic of the fixed bed CO_2 adsorption reactor used in this study.

The volume of tubing before the bypass solenoid and to the detector inlet was determined to be 50.7 cm^3. For an empty reactor tube the signal response time attributed to the dead volume was determined to be 3 s with a flow rate of 1000 ml min^{-1}. The effect of the detector signal between changing from the bypass to adsorption flow was measured experimentally. A 15 s delay was present upon switching between gas flows due to the internal volume of the detector (~200 ml). This profile was subtracted from experimental data to account for the detector response Figure 3.6.

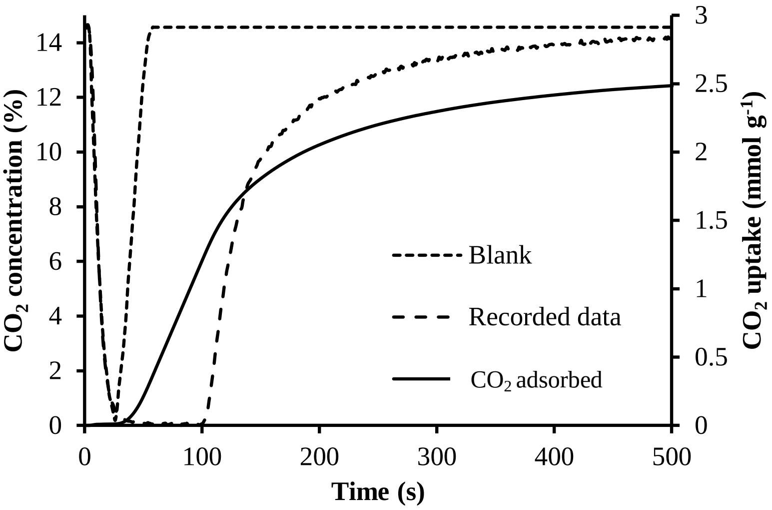

Figure 3.6. The CO_2 subtraction used to determine the CO_2 adsorption capacities in the fixed bed reactor.

For a typical CO_2 adsorption experiment 10 cm^3 (~8 g of 250-355 µm particles) of the adsorbent was supported on ~0.2 g of quartz wool inside a 3/8'' x 16'' stainless steel tube. The weight of the adsorbent was measured at the end of the experiment to obtain a CO_2 free, dry mass. Under dry adsorption conditions the adsorbent was first dried under a nitrogen flow (1000 ml min^{-1}) at 120 °C for 60 min. This was to remove any moisture or preadsorbed CO_2. The adsorbent was allowed to equilibrate at 75 °C for 60 minutes. The gas flow was then diverted to bypass the reactor, and the gas stream changed to 15% CO_2 / N_2. The gas path was switched to pass 15% CO_2 / N_2 over the sample. The amount of CO_2 adsorbed was calculated by the difference between the incoming CO_2 concentration and that measured after passing through the sample. Equation 3.2 was used to calculate the CO_2 adsorbed.

$$CO_2 adsorbed = \sum \frac{(C_{inlet} - C_{outlet}) MW_{CO_2}}{60 V_m} \qquad \text{Equation 3.2}$$

Where C_{inlet} is the incident CO_2 concentration, C_{outlet} is the CO_2 concentration measured by the detector, V_m is the molar volume of the gas. The adsorption was deemed complete when the detector signal returned to the inlet gas concentration. The variability in the detector signal was +/-0.1 %. The error in the CO_2 uptake measurement was estimated by measuring CO_2 uptake of S-PEI 4 times and calculating the standard error using Equation 3.3.

$$Standard\ Error = \frac{\sigma}{\sqrt{n}} \qquad \text{Equation 3.3}$$

Where σ is the standard deviation and n is the number of data points. The standard error was determined to +/- 3.7 %. This is uncertainty is similar to that reported for other breakthrough adsorption rigs [4].

For a typical CO_2 adsorption experiment in the presence of water, the bubblers were filled with deionised water. The water was purged with N_2 (1000 ml min^{-1}) for 10 min to remove dissolved CO_2 and O_2. Then 10 cm^3 (~8 g of 250-355 µm particles) of the adsorbent was supported on quartz wool and placed in a 3/8’’x 16’’ stainless steel tube. The weight of the adsorbent was measured at the end of the experiment to obtain a CO_2 free, dry mass. The sorbent was subjected to flow of N_2 (1000 ml min^{-1}) and the sorbent heated to 120 °C for one hour. The sorbent was then allowed to cool to 75 °C. The adsorbent gas flow was then directed through the bubblers until the adsorbent was saturated. This was determined when the outlet concentration of water was constant. The needle valve that partitioned the wet and dry gas streams was adjusted so the outlet concentration of water was 10%. The gas flow was then diverted from the sample and changed to 15% CO_2. Once a stable baseline of 15% CO_2 was obtained the gas flow was then switched back to the sample and the CO_2 uptake measured.

3.4 CO_2 adsorption using a thermogravimetric analyser

The CO_2 adsorption capacity was measured using a TA instruments Q600 thermogravimetric analyser (TGA) connected to nitrogen and 15% CO_2/N_2. Approximately 20 mg of the sorbent was loaded in a pre-weighed platinum pan and placed onto an autosampler. The analysis was computer controlled with a typical measurement programme being:

1) Change flow to N_2 (100 ml min^{-1})

2) Hold for 5 minutes

3) Ramp to 120 °C, rate 5 °C min^{-1}

4) Hold at 120 °C for 30 min

5) Cool to 75 °C (or other required adsorption temperature)

6) Equilibrate at 75 °C

7) Switch gas flow to 15% CO_2/N_2 (100 ml min^{-1})

8) Hold for 90 min

9) Repeat steps 1-8 once

The sequence was repeated for cycling experiments. The amount of CO_2 adsorbed was taken as the difference in mass between of the dry adsorbent before and after exposure to CO_2 at 75 °C. The data recorded was corrected for the CO_2 adsorption of a blank sample pan. The error in the balance and temperature control was given by the manufacturer to be +/-0.1%.

3.5 Volumetric CO_2 adsorption experiments

Volumetric CO_2 adsorption isotherms were obtained on a Quantachrome Autosorb iQ2. A sample was placed into a pre-weighed gas sorption cell. The sample filled gas sorption cell was heated to 100 °C for 1 hour before increasing the temperature to 130 °C for 3 hours under virtual vacuum to remove any pre-adsorbed gases. After drying the cell was weighed to yield the dry mass of the sample. The sample was then reattached to the gas sorption unit onto the analysis port and a virtual vacuum applied to remove any CO_2 adsorbed during weighing of the sample. The analysis was completed at 313.15 K using a heated Dewar filled with ethyleneglycol. The Vectordose analysis programme was used with the pressure decay measured at 1 second intervals. The experimental parameters are given in Table 3.2. A low dosage volume was used to minimise heat effects.

Table 3.2. The analysis parameters used in the CO_2 adsorption experiments.

Relative pressure range	Dose volume (cm^3 g^{-1})
0.0001-0.3	0.5
0.3 – 0.99	2.0

3.6 Determination of organic loading

A Perkin Elmer Diamond TGA was used to determine the organic loading of the adsorbents. Approximately 15 mg of the adsorbent was loaded onto a tared alumina pan and held at 40 °C for 2 min to stabilise. The sample was then heated from 40 – 950 °C under 100 ml min^{-1} air at a rate of 10 °C min^{-1}. The mass loss and heat flow were referenced to an internal identical alumina pan. The amine loading was determined by calculating the mass loss per gram and dividing by the molecular weight of the average amine repeating unit. The error in the balance and temperature control was given by the manufacturer to be +/-0.1%.

3.7 Nitrogen sorption

Nitrogen adsorption–desorption isotherms were obtained on a Quantachrome Autosorb 1-C at -196 °C. A sample was placed into a pre-weighed gas sorption cell. The filled gas sorption cell was heated to 100 °C for 1 hour before increasing the temperature to 130 °C for 3 hours under virtual vacuum to remove any pre-adsorbed species. After drying, the cell was weighed to yield the dry mass of the sample. The sample was then reattached to the gas sorption unit and sample analysis begun. A total of 83 adsorption and desorption points were collected from 0.0255 to 0.9961 P/P_0. Equilibration times of 6 minutes were used with a tolerance band of 0.01.

The specific surface area of the adsorbents was calculated by the Brunauer–Emmett–Teller (BET) method. The pore size distributions were calculated from the adsorption branch isotherm using the Barrett–Joyner–Halenda (BJH) adsorption model and are referred to henceforth as BJH PSD. This pore size model is widely used in the characterisation of amine functionalised silica adsorbents [5-10].

Using an approach similar to Gibson *et al*. the extent of pore blocking was calculated as ratio of the observed pore volume and theoretical pore volume [11]. The inaccessible pore volume can be quantified using Equation 3.4, where $v_{measured}$ is the pore volume determined experimentally, $v_{support}$ is the volume of the bare support and v_{organic} is the volume occupied by the impregnated amine.

$$Inaccessible\ pore\ volume = 1 - \frac{V_{measured}}{V_{support} - V_{organic}} \qquad \text{Equation 3.4}$$

With a tolerance set to 0, the error in the amount adsorbed for each data point was 0.03 cm^3g^{-1}. The cumulative error taken from the fortieth adsorption point is given by Equation 3.5. This percentage error was then used to estimate the upper and lower limits of the pore volume which would be linearly affected by changes in the volume of gas adsorbed at P/P_0 0.995.

$$Error\ (\%) = \frac{number\ points * approximate\ error}{Volume\ adsorbed\ at \frac{P}{P_0} = 0.995} \qquad \text{Equation 3.5}$$

All BET fits gave coefficients of determination greater than 0.999 thus providing a poor comparison of the errors between samples. The error in the BET surface area measurement was calculated using Equation 3.6 [12]. Where c is the BET C constant and x is the largest relative pressure used for the BET fit (0.3 P/P_0).

$$Error\ (\%) = 1 - \frac{cx}{cx + (1-x)} \qquad \text{Equation 3.6}$$

3.8 Water sorption

Water sorption isotherms were measured at 25 °C on a Quantachrome Autosorb 1-C gas sorption instrument. For a typical analysis the required amount of adsorbent was placed into a pre-weighed gas sorption cell and attached to the gas sorption machine. The filled gas sorption cell was heated to 100 °C for 1 hour before increasing the temperature to 130 °C for 3 hours under virtual vacuum to remove any pre-adsorbed species. The samples were backfilled with helium and weighed to obtain a dry mass. The cell was then reattached to the analysis port. The sample was then evacuated and heated to 130 °C for a further 3 h to ensure that any moisture adsorbed during the weighing stage was removed. The adsorption was then completed between 0.05 – 0.9 P/P_0 with a manifold temperature of 50 °C. An equilibration time of 3 mins and a tolerance of 0.02 were used.

3.9 Temperature programmed desorption

Temperature programmed desorption was conducted on a Micromeritics Autochem II RS232 fitted with a 1 ml sample loop and a liquid nitrogen filled CryoCooler. The desorbed species were measured using a thermal conductivity detector and an online MKS Cirrus 2 mass spectrometer. Approximately 0.15 g of sorbent was supported on quartz wool in a pre-weighed u-shaped quartz cell. In a typical experiment the following programme was used.

1) Change flow to He (50 ml min^{-1})

2) Ramp to 120 °C at a rate of 5 °C min^{-1}

3) Hold for 60 min

4) Ramp to 60 °C at a rate of 5 °C min^{-1}

5) Switch gas flow to CO_2 (50 ml min^{-1})

6) Hold for 60 min

7) Ramp to 0 at a rate of 5 °C min^{-1}

8) Switch to He (50 ml min^{-1})

9) Hold for 2 min

10) Start data recording

11) Ramp to 150 °C at the specified heating rate

After the experiment the adsorbent was cooled to room temperature and weighed allowing the dry mass of the adsorbent to be measured.

3.10 Diffuse reflectance infrared Fourier transform spectroscopy

Diffuse reflectance infrared Fourier transform spectroscopy (DRIFTS) was conducted using a Perkin Elmer S 100 FTIR spectrometer modified with a Harrick Scientific diffuse reflection accessory. In a typical experiment the adsorbent was ground to a fine powder and placed into the sample holder. For single beam characterisation spectra the adsorbent was diluted with KBr as required. The sorbent was packed down and the surface levelled before being encased in the low pressure reaction cell. A flow of He (200 ml min^{-1}) was passed through the cell and the cell heated to 130 °C at a rate of 2 °C min^{-1} to remove any adsorbed CO_2. The cell was cooled down to 75 °C and the spectrum of the fresh adsorbent measured. For single spectra, spectra were recorded in single beam mode referenced to KBr with 64 scans at a resolution of 4 cm^{-1}. For continuous measurements such as *in-situ* monitoring of the adsorbent during CO_2 adsorption, a background of the adsorbent under helium was used. For *in-situ* DRIFTS measurements spectra were continuously recorded with 32 scans at a resolution of 4 cm^{-1}.

3.11 Powder X-ray diffraction

Powder X-ray diffraction (PXRD) data were collected by Dr Edward Bilbé from Johnson Matthey. Data were collected on a Bruker AXS D8 using Cu $K\alpha_{1+2}$

radiation using a knife edge over the sample to scan between 0.5 to 10 °2θ with a 0.022 ° step size at ambient temperature (23 °C). The d-spacing was determined using Equation 3.7.

$$n\lambda = 2d\sin\theta \qquad \text{Equation 3.7}$$

Where n is an integer, λ is the wavelength of radiation (1.54 Å for Cu $K\alpha_{1+2}$), θ is the angle between the incident radiation and the surface of the solid and d is the spacing between layer of atoms.

3.12 Solid state nuclear magnetic resonance

Solid state nuclear magnetic resonance (SSNMR) data collection of ^{13}C and ^{29}Si spectra were acquired by Dr Jonathon Bradley from Johnson Matthey.

SSNMR spectra were acquired at a static magnetic field strength of 9.4T (v_0(^{1}H) = 400.16 MHz) on a Bruker Avance III console using TopSpin 3.1 software. A widebore Bruker 4 mm BB/1H WVT MAS probe tuned to ^{1}H (v_0(^{1}H) = 400.16 MHz) and either ^{13}C (v_0 (^{13}C) = 100.6 MHz) or ^{29}Si (v_0 (^{29}Si) = 79.5 MHz) was used. Spectra were referenced to either alanine (^{13}C, 20:5 ppm) or kaolinite (^{29}Si, -91:3 ppm). Powdered samples were packed into zirconia MAS rotors with plastic caps, with the sample mass determined by the difference in rotor mass before and after packing. All spectra were recorded using cross polarisation (CP) with magic angle spinning (MAS) at 10,000 Hz. A contact time of 1 ms was used for the ^{13}C experiments, and 5 ms for the ^{29}Si experiments. Spectra were collected between 2000 - 10000 scans depending on the sample.

For mobility measurements the activation energy of molecular motion was measured using a saturation recovery pulse sequence ^{1}H SSNMR experiment. The spin-lattice relaxation times (T_1) were measured between 23 - 110 °C, temperatures relevant to the CO_2 adsorption process. Twelve recovery times between 5 – 10240 ms were used at each temperature with the T_1 calculated from the peak intensity using Equation 3.8.

$$I_t = I_0 + Pe^{\left(\frac{-t}{T_1}\right)} \qquad \text{Equation 3.8}$$

Where I_t is the signal intensity at delay time t, I_0 is the signal intensity at time 0, P is an arbitrary scaling factor and T_1 is the spin lattice relaxation time. Topspin 3.1 was used to calculate the T_1 values with a typical plot of I_t vs t given in Figure 3.7.

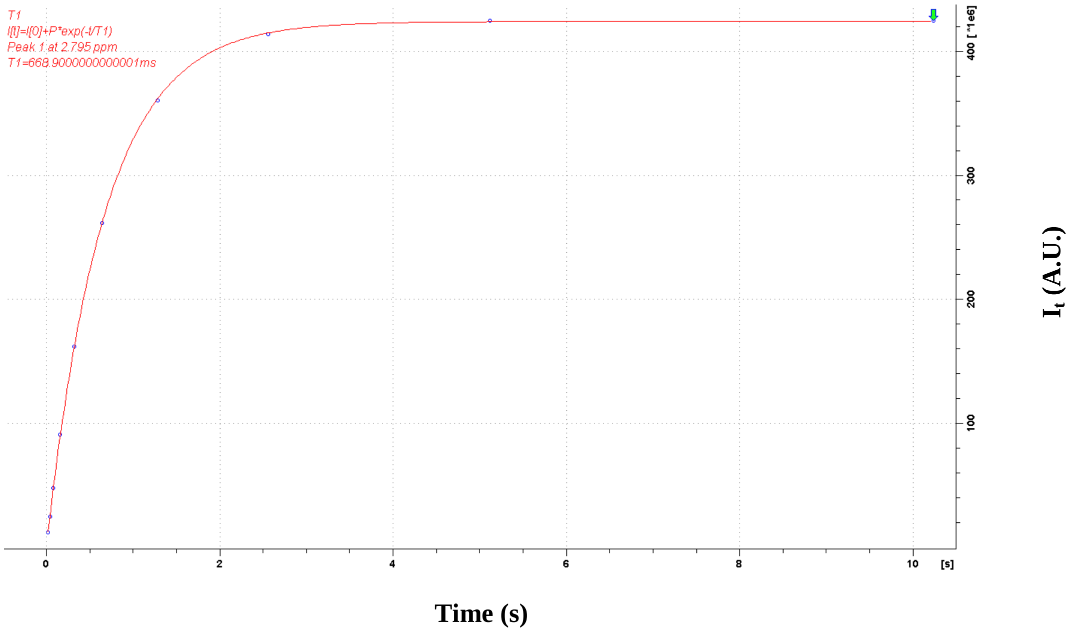

Figure 3.7. A plot of peak intensity as a function of correlation time with Equation 3.8 fitted to the data to yield the time constant for sorbent A at 40 °C.

For a thermally activated process the activation energy, E_a can be obtained from T_1 as a function of temperature (Equation 3.9) [13].

$$T_1 = Aexp\left(\frac{E_a}{RT}\right) \qquad \text{Equation 3.9}$$

Where R is the ideal gas constant, T is the temperature and A is a constant (pre-exponential factor). This can be re-arranged to yield Equation 3.10, which allows the activation energy of motion to be quantified.

$$lnT_1 = \frac{E_a}{RT} + lnA \qquad \text{Equation 3.10}$$

A plot of T_1 vs 1/T was constructed and a relative activation energy of motion can be obtained by fitting of Equation 3.10 to a tangent. To yield a more representative fit a second order polynomial was fitted to the data (appendix A2). The derivative of this function was determined allowing the gradient to be obtained at 0.001 increments from the minimum. This method allowed the calculation of the relative activation energies to motion of adsorbents A –F (section 4.7).

3.13 Shear viscosity measurements

Shear viscosity was measured using a TA instruments AR 2000 rotational rheometer in a 4cm parallel plate configuration. The following programme was used to determine the viscosity:

1) Pre-shear at a shear rate ($\dot{\gamma}$) = 50 s^{-1}

2) Heat to 30 °C at a rate of 2 °C min^{-1}

3) Pre-shear at a shear rate $\dot{\gamma}$ = 50 s^{-1} for 2 min

4) Measurement 1, 60 s

5) Heat to 50 °C at a rate of 2 °C min^{-1}

6) Pre-shear at a shear rate $\dot{\gamma}$ = 50 s^{-1} for 2 min

7) Measurement 2, 60 s

8) Heat to 70 °C at a rate of 2 °C min^{-1}

9) Pre-shear at a shear rate $\dot{\gamma}$ = 50 s^{-1} for 2 min

10) Measurement 3, 60 s

11) Heat to 90 °C at a rate of 2 °C min^{-1}

12) Pre-shear at a shear rate $\dot{\gamma}$ = 50 s^{-1} for 2 min

13) Measurement 4, 60 s

14) Heat to 100 °C at a rate of 2 °C min^{-1}

15) Pre-shear at a shear rate $\dot{\gamma}$ = 50 s^{-1} for 2 min

16) Measurement 5, 60 s

The viscosity was calculated using the Newtonian flow model (Equation 3.11)

$$n = \sigma / \dot{\gamma} \qquad \text{Equation 3.11}$$

Where n is the viscosity, σ is the shear stress and $\dot{\gamma}$ is the shear rate.

3.14 CHN analysis

CHN analysis was by conducted by Laura Stead of Johnson Matthey using an Exeter analytical Inc. CE 440 Elemental Analyser. The combustion was completed in triplicate with the average values reported. Approximately 3mg of sample was used in each experiment with the combustion completed in pure oxygen at 975 °C. The error in the CHN measurements was supplied by the manufacturer to be +/-0.3 %.

3.15 Pseudo-adsorption aging experiments

Aging under 10% H_2O/N_2, 1000 ml min^{-1}, 75 °C, 24 h was conducted using the same test rig as the CO_2 adsorption experiments (section 3.2, Figure 3.5). In a typical experiment 8 g (250-355 μm particles) of adsorbent was supported on quartz wool in a 3/8‘‘ x16 ’’ stainless steel reactor with a thermocouple inserted into the centre of the sample. A flow of nitrogen (1000 ml min^{-1}) was passed over the adsorbent and the temperature ramped to 130 °C at a rate of 5 °C min^{-1} and held for 60 min. The sorbent was cooled to 75 °C under a flow of nitrogen and equilibrated for 60 min. The CO_2 adsorption uptake was then measured under dry conditions with a regeneration step under a flow of N_2 (1000 ml min^{-1}) at 120 °C for 60 min. This was followed by analysis under wet conditions (section 3.3). The sorbent was then regenerated under N_2 (1000 ml min^{-1}) at 120 °C for 60 min, followed by cooling to 75 °C. The adsorbent was held at this temperature for 24 h under a flow of 10% H_2O/N_2 (1000 ml min^{-1}). The reactor was isolated and the water in the bubblers refilled after 12 hours to ensure the water level remained at its optimal level, providing a steady flow of 10% water. After aging the sorbent was tested for wet CO_2 adsorption capacity. The adsorbent was regenerated and dried at 120 °C for 1 h under a flow of N_2 (1000 ml min^{-1}) before cooling down to 75 °C before measurement of the CO_2 adsorption capacity.

3.16 Pseudo steam regeneration aging experiments

Desorption aging experiments were conducted in a fixed bed reactor (Figure 3.8). Approximately 0.1 g of sorbent was supported on quartz wool and a thermocouple inserted inside a quartz glass reactor tube. The rig consisted of an oven to preheat the gasses with the sample held within a computer controlled furnace. The sorbent was dried under a flow of N_2 (100 ml min^{-1}) for 1 h at 130 °C. The adsorbent was then maintained at this temperature and a syringe pump filled with deionised water, pumped water (9.9 ml min^{-1}) into the oven held at 130 °C. This lead to the formation of a steady flow of 66% H_2O/N_2, 100 ml min^{-1}, evidenced by the steady pressure signal with a typical pressure backdrop of approximately 0.2 bar. This provided a steam mass flow rate of 100 g steam per gram of adsorbent per hour. After 8 h the pump was turned off with the flow of nitrogen maintained and the sample allowed to cool to room temperature over 2 h before the sample was removed.

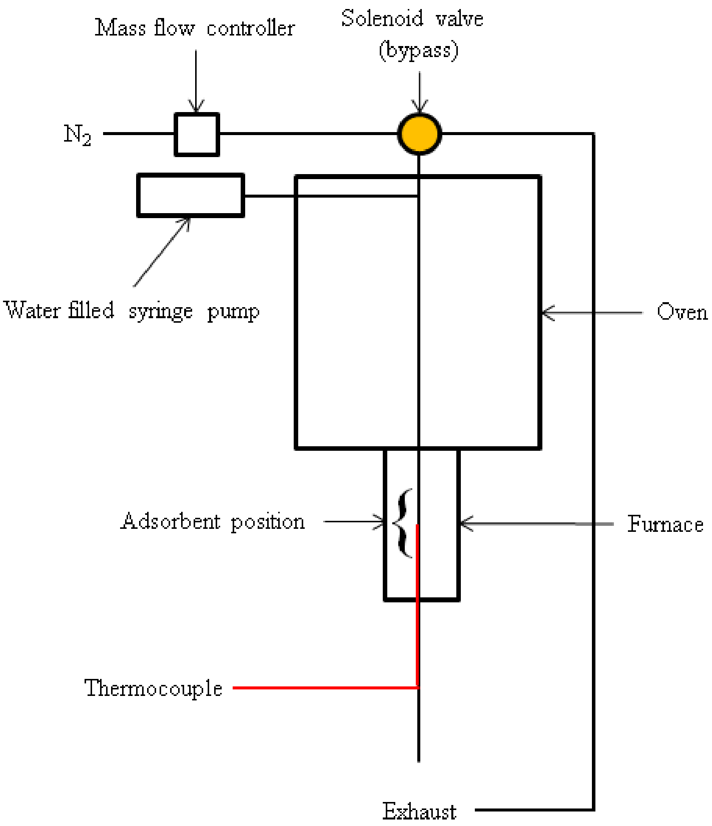

Figure 3.8. Schematic of the fixed bed reactor using to mimic steam regeneration conditions.

3.17 Electron microscopy

Scanning transmission Electron Microscope (STEM) images were collected by Yuan Zhao from Johnson Matthey, on a Hitachi HD-2000 Scanning Transmission Electron Microscope operated at 200 kV. The powder samples were mounted onto a holey carbon film coated copper TEM grid and coated in carbon.

3.18 Dynamic vapour sorption

Data acquisition for dynamic vapour sorption was conducted by Linda Smith of Johnson Matthey on a TA instruments Q5000 SA Moisture Sorption Analyser. In a typical procedure 3mg of the adsorbents was weighed into a metalised quartz pan. The mass increases were referenced an internal blank pan. The error in the balance and temperature control was given by the manufacturer to be +/-0.1%. The analysis was computer controlled with a typical measurement programme being:

1) Change flow to N_2 (100 ml min^{-1})

2) Ramp to 60 °C (5 °C min^{-1})

3) Hold for 360 min

4) Set relative humidity to 30 % RH

5) Hold for 1 hour

6) Set relative humidity to 33 % RH

7) Hold for 1 hour

8) Set relative humidity to 87 % RH

9) Hold for 1 hour

10) Set relative humidity to 90 % RH

11) Hold for 1 hour

3.19 Preparation of SBA-15

Synthesis of SBA-15 was prepared in a similar manner to Zhao *et. al.* with the same batch of SBA-15 used throughout the study [14]. Briefly Pluronic 123 (P123, triblock copolymer (EO)20(PO)70(EO)20, MW 4,800, 80.0g) was dissolved in aqueous hydrochloric acid (1.33 M, 3000 ml) with vigorous stirring at 35 °C. After complete dissolution of the Pluronic 123, tetraethoxyorthosilicate (TEOS, 182 ml) was added dropwise and the mixture stirred at 35 °C for 24 h. After 24 h the solution was statically heated at 85 °C for 48 h. The white solid was then dried in an oven at 105 °C for 2 h before heating in a furnace to 600 °C for 6 h to obtain a white solid powder.

3.20 General method for producing amine impregnated adsorbents

A table of the adsorbents prepared in this study is given in Table 3.3. To the desired quantity of amine was added pre-dried silica to ensure a final amine weight loading of 33 wt%. To this was added methanol (4 ml per gram of silica) without stirring. The flask was mixed using a tumbling motion of a rotary evaporator for 2 hours at 40 °C with the appearance changing from aggregates to a free flowing powder in solution. A gentle vacuum was applied (240 mbar) to gradually remove the solvent. After the solvent was removed, the flask was heated to 60 °C and the pressure decreased to 20 mbar to dry the adsorbents for 4 hours. The flask was cooled to room and the pressure increased to ambient. The adsorbent was collected as a free flowing white powder. TEPA based adsorbents were noted as having a yellow appearance. Binary mixtures of amine adsorbents were prepared in a similar manner with the silica added to a pre-weighed mixture of amine and surfactant additive.

Table 3.3: The impregnated amine adsorbents prepared in this study.

Support	Amine	Additive	Organic Loading (%)	Abbreviation
SBA-15	PEI 600	-	40	SBA-15 PEI
SBA-15	TEPA	-	40	SBA-15 TEPA
Davisil 60	PEI 600	-	33	S-PEI
Davisil 60	TEPA	-	33	S-TEPA
Davisil 60	PEI 600	SDS	33 (80:20)[a]	S-PEI-SDS
Davisil 60	PEI 600	TEA	33(80:20)[a]	S-PEI-TEA
Davisil 60	TEPA	SDS	33(80:20)[a]	S-TEPA-SDS
Davisil 60	TEPA	TEA	33(80:20)[a]	S-TEPA-TEA
Davisil 60	PEI 1800	-	33	S-PEI-H
Davisil 22	PEI 600	-	33	S-PEI-SP
Davisil 150	PEI 600	-	33	S-PEI-LP

[a] ratio of amine to additive

3.21 General method for the post functionalisation of S-PEI with organosilanes

The dry mass of S-PEI was determined to be 95% using TGA analysis. S-PEI (10 g, 33wt% PEI 600) was washed with methanol (20 ml) three times. TGA analysis after this treatment was found to reduce the organic loading of the particle by less than 0.5%. The required amount of silane (see Table 3.4) was dosed onto the S-PEI in 50 µm aliquots with the particles mechanically mixed between doses. The flask was attached to a rotary evaporator and the pressure reduced to 240 mbar at 40 °C for 1h with the flask rotating at 120 rpm. The pressure was reduced further to 20 mbar and the temperature increased to 60 °C for 6 hours. The flask was cooled to room temperature and the solids washed with toluene (3 x 30 ml). The adsorbent was dried under vacuum at room temperature for 18 h to yield a dry white free flowing powder.

The different amounts of silane loading are given in Table 3.4. The external surface area of the Davisil 60 support was measured to be 81 m^2 g^{-1}. This represented approximately 15 % of the total surface area of 516 m^2 g^{-1}. Assuming concentration of hydroxyl groups of 2 mmol g^{-1} silica this leaves 0.33 mmol g^{-1} hydroxyl groups at the support surface. Hence the addition of silane amounts were calculated to yield a silane coverage of 0.33, 0.6 and 1 mmol g^{-1}.

Table 3.4. The amounts of silane used in the synthesis of silane coated adsorbents.

Starting material	Silane	Silane loading (ml)	Abbreviation
S-PEI	Trimethoxy(octyl)silane	0.85	S-PEI-O-L
S-PEI	Trimethoxy(octyl)silane	1.55	S-PEI-O-M
S-PEI	Trimethoxy(octyl)silane	2.58	S-PEI-O-H
S-PEI	1H,1H,2H,2H-Perfluorodecylltriethoxysilane	1.44	S-PEI-F-L
S-PEI	1H,1H,2H,2H-Perfluorodecylltriethoxysilane	2.61	S-PEI-F-M
S-PEI	1H,1H,2H,2H-Perfluorodecyltriethoxysilane	4.35	S-PEI-F-H
S-PEI	Hexadecyltrimethoxysilane	1.29	S-PEI-H-L
S-PEI	Hexadecyltrimethoxysilane	2.34	S-PEI-H-M
S-PEI	Hexadecyltrimethoxysilane	3.90	S-PEI-H-H
S-PEI	Triethoxyphenylsilane	0.82	S-PEI-P-L
S-PEI	Triethoxyphenylsilane	1.49	S-PEI-P-M
S-PEI	Triethoxyphenylsilane	2.48	S-PEI-P-H

3.22 Synthesis of 3-aminopropyl functionalised silica

Davisil 60 (10.0 g, 250-355 μm particles) was placed in two neck round bottom flask fitted with a septum and a condenser leading to a vacuum gas manifold. The silica was held under vacuum at 100 °C for 1 h to remove preadsorbed water. The vessel was allowed to cool to room temperature and charged with nitrogen. The silica was dispersed in anhydrous toluene (150 ml) with stirring. To this was added 3-aminopropyltriethoxysilane (4.68 ml, 20 mmol) and the mixture heated to reflux for 18 h. To this was added water (0.71 ml, 40 mmol) and the mixture refluxed for a further 6 hours. The solution was cooled to room temperature and the solid recovered by filtration and washed with toluene (3 x 100 ml), methanol (3 x 100 ml), water (3x 100 ml) and methanol (3 x 100 ml). The adsorbent was dried under vacuum at room temperature for 18 h to yield a white free flowing solid.

3.23 Polymerisation of 4-vinylchlorobenzene on silica

To a 2 necked round bottom flask fitted with a septum and a condenser leading to a vacuum gas manifold was added 4,4-azobis(4-cyanovaleric acid) functionalised silica (0.5 g, 0.4 mmol g^{-1} of 4,4-azobis(4-cyanovaleric acid)). To this was added isopropanol (20 ml) and stirred. The flask was evacuated and backfilled with nitrogen 3 times. The inhibitor (*tert*-butylcatechol) present in 4-vinylbenzylchloride was removed by passing the liquid through a plug of alumina. The required amount of 4-vinyl4-vinylbenzylchloride was then added to the flask and the mixture heated to reflux with stirring for 24 h (see Table 3.5). After 24 h the solution was allowed to cool and the solids collected by filtration. The solids were washed with toluene (3 x 100 ml), isopropanol (3 x 100 ml), water (3x 100 ml) and methanol (3 x 100 ml). The material was dried under vacuum at room temperature for 18 hours to yield an off white free flowing powder.

Table 3.5. The amount of vinylbenzylchloride used to produced surface polymerised adsorbents.

Material	Loading of vinylbenzylchloride (wt%)[a]	Amount of vinylbenzylchloride (ml)
S-Poly 0.25 VBC	0.25	0.14
S-Poly 0.5 VBC	0.50	0.27
S-Poly 1 VBC	1.00	0.54
S-Poly 2 VBC	2.00	1.08
S-Poly 4 VBC	4.00	2.16

[a] wt% relative to the mass of the 4,4-azobis(4-cyanovaleric acid) functionalised silica

3.24 Ethylenediamine functionalisation of poly(4-vinylchlorobenzene) modified silica

To a 2 necked round bottom flask fitted with a septum and a condenser leading to a vacuum gas manifold was added S-Poly-x (0.5g), where x represents wt% loading of vinylbenzylchloride. The flask was then evacuated and backfilled with nitrogen 3 times. To this was added ethanol (30ml) and sodium hydroxide (see Table 3.6 for amounts) with stirring. To this was added ethylenediamine (5 times molar excess w.r.t to vinylbenzylchloride) and the mixture heated to reflux for 24 h. The mixture was allowed to cool to room temperature and the solids collected by filtration. The solids were washed with toluene (3 x 100 ml), isopropanol (3 x 100 ml), water (3x 100 ml) and methanol (3 x 100 ml). The material was dried under vacuum at room temperature for 18 hours to yield an off white free flowing powder.

Table 3.6. Quantities of materials used to produce ethylenediamine functionalised polyvinylbenzylchloride modified silica.

Material	Amount of ethylenediamine (ml)[a]	Amount of sodium hydroxide (g)[b]
S-Poly VBC 0.25 EDA	0.53	0.07
S-Poly VBC 0.5 EDA	1.07	0.14
S-Poly VBC 1 EDA	2.13	0.284
S-Poly VBC 2 EDA	4.26	0.568
S-Poly VBC 4 EDA	8.52	1.136

[a] A 5 times molar equivalent w.r.t maximum vinylbenzylchloride loading. [b] 1 molar equivalent w.r.t. maximum vinylbenzylchloride loading.

3.25. References

1. Wojdyr, M., *Fityk: a general-purpose peak fitting program.* J. Appl. Cryst., 2010. **43**: p. 1126.
2. A. von Harpe, H. Peterson, Y. Li, T. Kissel, *Characterisation of commerically available and synthesized polyethyleneimines for gene delivery. J. Controlled Release*, 2000. **69**: p. 309.
3. J. H. Drese, S. Choi, R. P. Lively, W. J. Koros, D. J. Fauth, M. L. Gray, C. W. Jones, *Synthesis-Structure-Property Relationships for Hyperbranched Aminosilica CO_2 Adsorbents. Adv. Funct. Mater.*, 2009. **19**: p. 3821.
4. D. J. Fauth, M. L. Gray, H. W. Pennline, *Investigation of Porous Silica Supported Mixed-Amine Sorbents for Post-Combustion CO_2 Capture.* Energy Fuels, 2011. **26**: p. 2483.
5. D. S. Dao, H. Yamada, K. Yogo, *Large-Pore Mesostructured Silica Impregnated with Blended Amines for CO_2 Capture. Ind . Eng. Chem. Res.*, 2013. **52**: p. 13810.
6. V. Zeleňák , M. Badanićová, D. Halamová, J. Čejka, N. Murafa, G. Goerigk, *Amine-modified ordered mesoporous silica: Effect of pore size on carbon dioxide capture.* Chemical Engineering Journal, 2008. **144**(2): p. 336-342.
7. N. Linneen, R. Pfeffer, Y. S. Lin, *CO_2 capture using particulate silica aerogel immobilised with tetraethylenepentamine.* Microporous and Mesoporous Materials, 2013. **176**: p. 123.
8. G. Qi, L.F., B. H. Choi, E. P. Giannelis, *Efficent CO_2 sorbents based on silica foam with ultra-large mesopores.* Energy Environ. Sci., 2012. **5**: p. 7369.
9. J. Wei, J. Shi, H. Pan, W. Zhao, Q. Ye, Y. Shi, *Adsorption of carbon dioxide on organically functionalized SBA-16.* Microporous and Mesoporous Materials, 2008. **116**: p. 394.
10. N. Hiyoshi, K. Yogo, T. Yashima, *Adsorption characteristics of carbon dioxide on orgnically functionalised SBA-15.* Microporous and Mesoporous Materials, 2005. **84**: p. 357.
11. J. A. A. Gibson, A. V. Gromov, S. Brandani, E. E. B. Campbell, *The effect of pore structure on the CO_2 adsorption efficiecy of polyamine impregnated porous carbons. Microporous and Mesoporous Materials*, 2015. **208**: p. 129.
12. T. Allen, *Particle size measurement.* Chapman & Hall, London, 1981.
13. D. C. Apperley, R.K.H., P. Hodgekinson, *Solid-State NMR: Basic Principles & Practice* Momentum Press New York, 2012.
14. D. Zhao, Q. Huo, J. Feng, B. F. Chmelka, G. D. Stucky, *Nonionic Triblock and Star Diblock Copolymer and Oligomeric Surfactant Syntheses of Highly Ordered, Hydrothermally Stable, Mesoporous Silica Structures. J. Am. Chem. Soc.*, 1998. **120**: p. 6024.

CHAPTER FOUR

The role of surfactant additives in amine impregnated silica adsorbents

4.1 Introduction

Whilst a high adsorption capacity is a requirement for the solid adsorbents this needs to be balanced with adsorption kinetics, regeneration requirements and adsorbent stability. This contribution explores polymeric amines and surfactant additives co-impregnated onto silica supports. As described in Section 2.2.2, the addition of surfactant species has been shown to enhance the CO_2 adsorption capacities of impregnated amine adsorbents. The mechanism of how surfactants promote CO_2 adsorption is poorly understood. Yue *et al.* proposed a change in adsorption mechanism in the presence of hydroxylated surfactants [1]. However no spectroscopic evidence was presented. Dao *et al.* suggested that enhancements in uptake were related to increased rates of CO_2 diffusion through the adsorbent [2]. This chapter builds upon previous work by Starkie *et al.* and explores the mechanism of action of SDS and TEA additives in amine impregnated solid adsorbents [3].

4.2 Selection of silica support

Deviating from previous work Davisil 60 was used in place of SBA-15 as a silica support [3]. The cause of this substitution was the requirement to test these materials in a packed bed reactor. This required the material to be of a set particle size between 250-355 μm to avoid variable back pressures between samples. This would disrupt the measurements obtained by the online infrared-analyser. Furthermore, approximately 8 g of sample was required for each experiment with a high level of consistency between samples. At present there is no practical method of preparing large amounts of SBA-15 with controlled particle size and excellent consistency between batches. Hence lower grade silicas such as Davisil 60 are more likely to be utilised in carbon capture. A comparison of the properties of SBA-15 and Davisil silica is given below in Table 4.1.

Table 4.1. A comparison of support properties for Davisil 60 and SBA-15.

Sample	**Surface area (m^2 g^{-1})**	**Mean pore size (nm)[a]**	**Pore Volume (cm^3 g^{-1})[b]**	**Particle size (µm)**
SBA-15	743.0 +/- 49.7	6.2	0.98 +/- 0.02	1-100
Davisil 60	516.4 +/- 14.0	8.3	0.78 +/- 0.02	250-355
SBA-15 40wt% PEI	191 +/- 12.4	4.7	0.04 +/- 0.02	1-100
Davisil 60 33 wt% PEI	96.7 +/- 7.0	6.1	0.20 +/- 0.02	250-355

[a] BJH PSD [b] See Section 3.7 for BET and Pore volume error calculation.

SBA-15 has greater pore volume and larger surface area than Davisil 60 as well as microporous channels between the larger 6 nm pores. The evidence of micropores was established using t- plot analysis with the micropore volume corresponding to approximately 16% of the pore volume. Similar textural properties have been reported with SBA-15 prepared under similar conditions [4]. The lower surface area and pore volume implies that less amine polymer could be incorporated into the Davisil 60 support. Therefore a reduction in CO_2 equilibrium adsorption capacity could be anticipated. The pore size of SBA-15 is around 6 nm with a narrow pore size distribution. Davisil 60 has a larger average pore size with a wider pore size distribution. Work by Zelenak *et al.* on the effect of pore size found that larger pores tended to have faster and greater CO_2 adsorption. It was also noted and that below a critical pore diameter of 3.5 nm, the rate of CO_2 adsorption is limited by the sluggish diffusion into these pores [5]. This work also noted the importance of pore connectivity between the primary channels of the supports. SBA-15 possesses 2-D pore connectivity whereas the Davisil has random pore connectivity. Scanning transmission electron microscopy images (STEM) images of the SBA-15 and Davisil silica supports are presented in Figure 4.1.

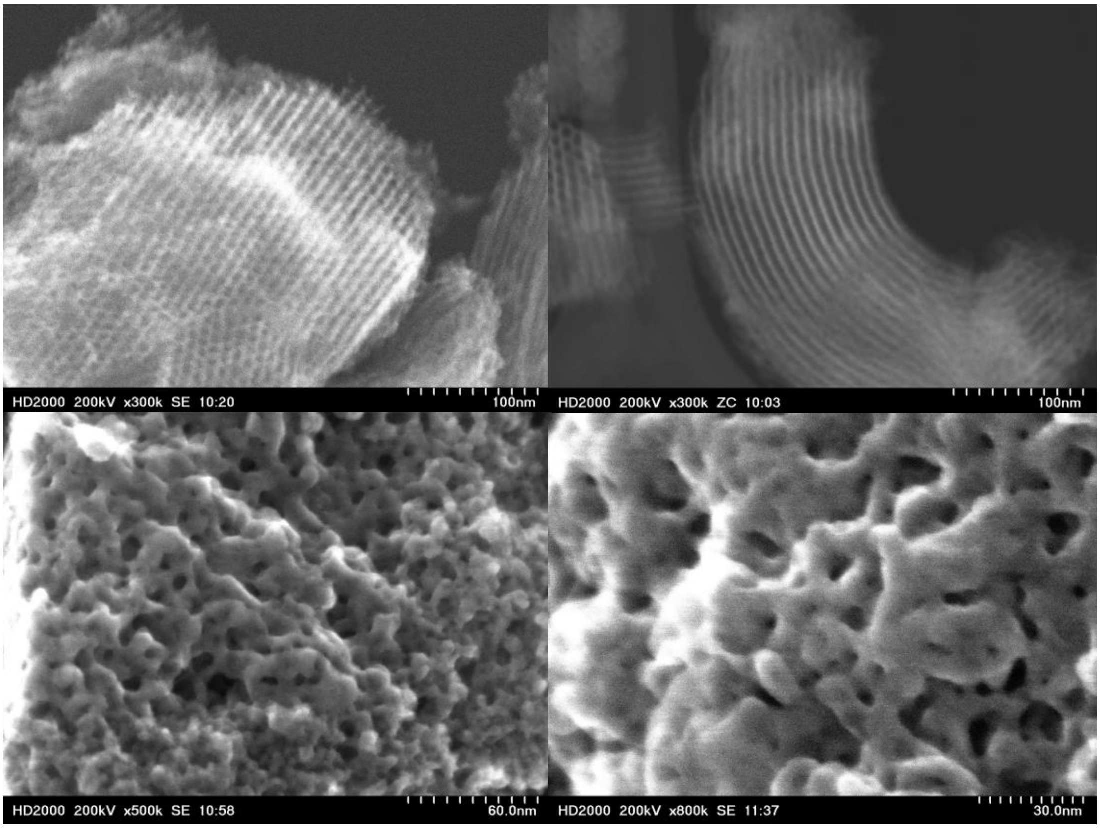

Figure 4.1. STEM images of SBA-15 (top) and Davisil 60 (bottom).

The ordered porous nature and hexagonal wormlike chains of SBA-15 are evident. The pore size can be measured to be approximately 6 nm, similar to that measured by gas adsorption. By contrast Davisil 60 has an irregular porous architecture with a wide range of pore sizes.

Upon impregnation of PEI into the supports the pore size, surface area, pore volume decrease accordingly (Table 4.1). Davisil 60 has a larger pore size distribution of which it can be assumed that smaller pore sizes would offer an increased level of interaction with the PEI species and as a result the PEI would preferentially bind within these smaller pores. As such the apparent reduction in average pore size is much less than that of SBA-15 supported adsorbents.

Power X-ray diffraction (PXRD) of SBA-15 and Davisil 60 before and after amine impregnation is given in Figure 4.2. The diffraction pattern of SBA-15 shows peaks at 0.9 and 1.8 ° relating to the (100) and (110) planes respectively. The evidence of these peaks confirms the hexagonal p6mm morphology of the structure [6]. In agreement with several literature sources the intensity of the peaks decreased with the addition of organics [7]. The retention of the lattice spacing indicates that the structure is unaltered during amine impregnation. Davisil has a broad feature in the diffraction pattern with a peak maximum at 0.945 ° corresponding to an average *d* spacing of 92.5 Å. The incorporation of PEI into the pores of Davisil also leads to a significant reduction in signal intensity with the incorporation of PEI. This suggests that there are no changes in structure upon amine impregnation.

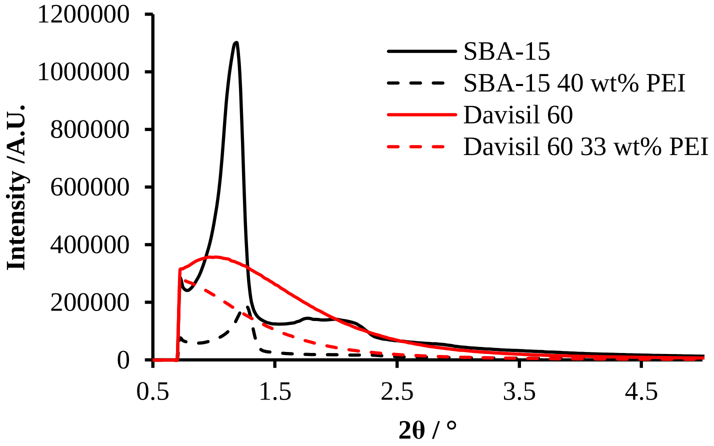

Figure 4.2. Powder X-ray diffraction patterns of hexagonal mesoporous silica (SBA-15) before and after PEI impregnation and Davisil 60 before and after PEI impregnation.

4.3 Selection of amine

PEI 600, PEI 1800 and TEPA were selected as the amines of choice with the characteristics of both amines used given in Table 4.2. The ratio of primary, secondary and tertiary amines was determined by quantitative ^{13}C NMR of the commercial PEI 600 and PEI 1800 samples (Section 3.2). The ratios reported agree well with other commercial low MW PEI sample analysed by Kissel and Drese who found a typical composition of (31-44): (33-39) : (23-31) for 1°, 2° and 3° amine sites [8, 9]. This ratio is important as primary and secondary amines are believed to react with CO_2 to form a zwitterionic product in a ratio of two amines to one CO_2 molecule under dry conditions. Tertiary amines however are thought to adsorb CO_2 only under wet conditions via the deprotonation of carbonic acid. Therefore to establish the true potential of the adsorbents accurate accounting of the primary, secondary and tertiary amine ratios is essential.

Table 4.2. The ratio of primary secondary and tertiary amines of the amines used in this study.

Amine	**Average MW (Daltons)[a]**	**Amine ratio 1°:2°:3°**	**Polydispersity (a.u.)**
PEI	600	39:36:25[b]	1.08
PEI	1800	38:32:30[b]	1.14
TEPA	189	40:60:0	N.D.[c]

[a] stated number average molecular weight determined by supplier. [b] determined by quantitative ^{13}C NMR. c) TEPA is a mixture of triethylenetetramine, tetraethylenepentamine and pentaethylenehexamine with minor impurities. The batch used in this study had a TEPA content of 54% as reported by the manufacturer.

The pore volume of the SBA-15 support used was 0.98 cm^3 g^{-1} meaning that the total amount of amine that could be incorporated into the structure was 50 wt% for PEI and 49 wt% for TEPA. To ensure amine accessibility SBA-15 supported adsorbents were prepared with a fixed amine loading of 40 wt% total organic content. Owing to the lower pore volume and pore accessibility of Davisil 60 the amine loading was maintained at 33 wt%. Table 4.3 gives the amine loadings and theoretical maximum CO_2 adsorption capacities of the adsorbents.

Table 4.3. The theoretical maximum CO_2 adsorption capacity under dry adsorption conditions.

Sorbent	Amine loading (mmol g^{-1})	Maximum CO_2 uptake (mmol g^{-1})[a]
SBA-15 40wt% PEI	9.49	3.80[b]
SBA-15 40wt% TEPA	9.49	4.75
Davisil 60 33 wt% PEI	7.84	3.13[b]
Davisil 60 33 wt% TEPA	7.84	3.92

[a] Assuming exclusive aklylammonium carbamate formation [b]Assuming 3° amine sites are unreactive.

Low molecular weight amines commonly used in carbon capture such as monoethanolamine are not suitable for use in solid adsorbents owing to their high vapour pressures. Linear PEI was not suited to this study owing to the solid form of the amine at the adsorption temperature. Higher molecular weight PEI was considered but has been shown to exhibit slower CO_2 diffusivity and lower uptakes [9].

4.4 Comparing the properties of SBA-15 and Davisil 60 impregnated amine adsorbents

The organic loading of the polymeric amines was determined by TGA with the results summarised in Table 4.4. The mass loss from TGA can be portioned into three regimes. Mass loss between 25- 170 °C can be attributed to desorption of water, CO_2 and residual solvent species. Mass loss between 170 - 250 °C can be attributed to the combustion of organic species with further mass losses above 250 °C due to the combustion of carbonised species (Figure 4.3).The mass loss by TGA and position in the maximum of the first derivative are consistent with the introduction of organics into the pores of the silica at the target loadings. Additional TGA data can be found in appendix A1-A3.

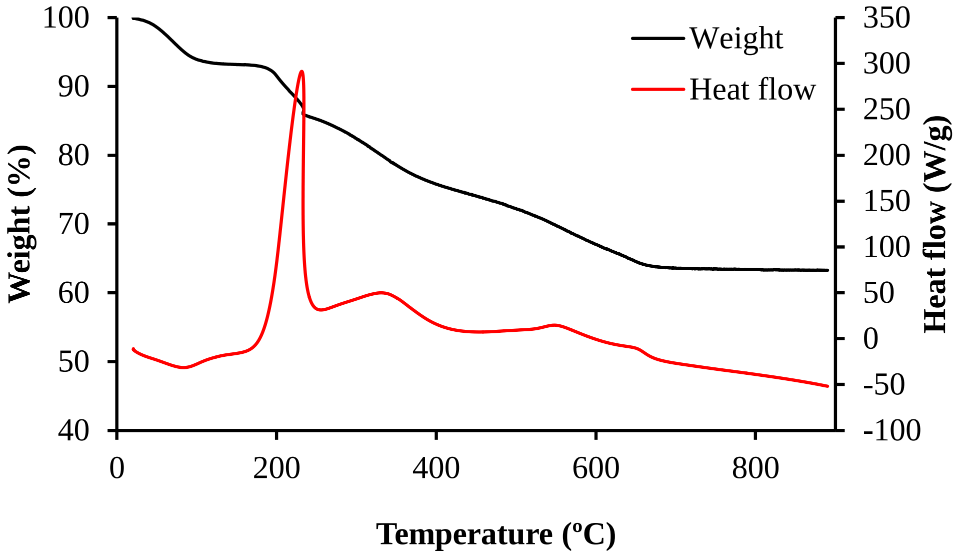

Figure 4.3. Determination of the organic loading of Davisil 60 33 wt% PEI using TGA. Heating rate (β) = 10 K min^{-1}, under air (100 ml min^{-1}).

Table 4.4. Determination of the organic loading using TGA.

Sample	Organic loading by TGA (%)	Peak heat flow (°C)
SBA-15 40 wt% PEI	40.1	227.4
SBA-15 40 wt% TEPA	39.4	223.4
Davisil 60 33wt% PEI	32.8	237.7
Davisil 60 33 wt% TEPA	32.6	232.1

The CO_2 uptakes of PEI 600 and TEPA on SBA-15 and Davisil 60 were measured using the method described in Section 3.4 with the results presented below in Table 4.5. The adsorption capacities of the Davisil supported adsorbents are slightly lower than those of the SBA-15 adsorbents due to the lower amine loading. The amine efficiency is defined at the moles of CO_2 adsorbed over the moles of amine adsorption sites. Under dry conditions a maximum amine efficiency of 0.5 is possible owing to the requirement of 2 amines to react with 1 CO_2. The amine efficiency of the Davisil 60 adsorbents is similar to SBA-15. This could be due to the lower amine loading and slightly larger average pore size. Typically the amine efficiency is inversely proportional to the amine loading [10].

Table 4.5. Equilibrium CO_2 adsorption capacities of SBA-15 and Davisil supported amine adsorbents measured at (75 °C, 100 % CO_2, 100ml min^{-1}).

Sorbent	CO_2 adsorption capacity (mmol g^{-1})	Amine efficiency (a.u)
SBA-15 40% PEI	2.64	0.27
SBA-15 40% TEPA	3.21	0.33
Davisil 60 33% PEI	2.32	0.29
Davisil 60 33% TEPA	2.56	0.33

The uptake profiles of the comparative adsorbents are shown in Figure 4.4. This gives rise to two regimes of CO_2 adsorption. Firstly there is an initial rapid stage of adsorption where CO_2 rapidly adsorbs onto the surface amine species. This is followed by much slower adsorption thought to be due to the diffusion of CO_2 through the layers of amine polymer [11]. From inspection of Figure 4.4 it is clear that Davisil is a good potential support candidate for CO_2 adsorption and as such was taken forward as a support for the remainder of the investigation.

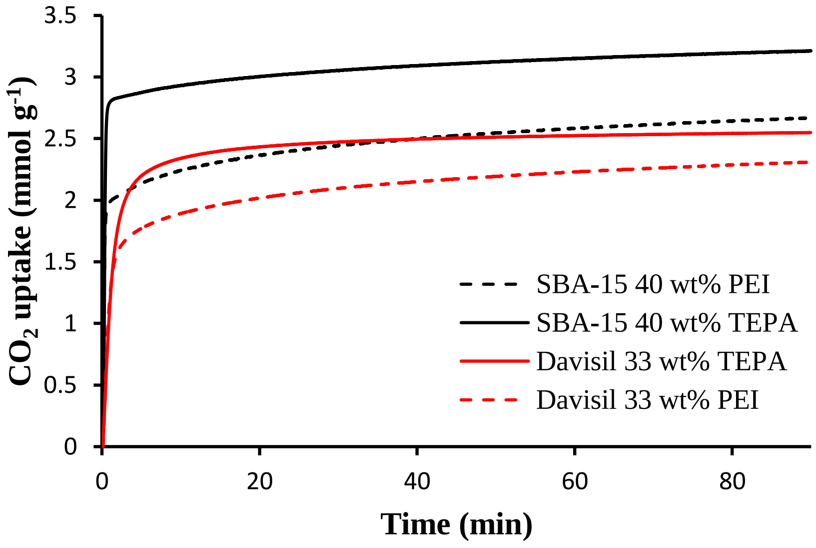

Figure 4.4. TGA results comparing Davisil and SBA-15 supported amines measured under CO_2 (100%, 100 ml min^{-1}, 75 °C).

4.5 Design of adsorbents

Binary polymeric amine and surfactant mixtures were co-impregnated upon Davisl 60 in accordance with the ratios presented in Table 4.6. Similar compositions have been shown to enhance the CO_2 adsorption compared to single component amine adsorbents [3]. Triethanaolamine (TEA) was chosen to investigate the role of hydroxyl group additives on CO_2 adsorption. Sodium dodecyl sulfate (SDS) was chosen as recent work suggested that templated silica structures where the template had been partially extracted showed significant increases in CO_2 adsorption capacities [12]. A description of the adsorbent synthesis is provided in Section 3.20.

Table 4.6. The binary polymeric amine surfactant compositions used in this study.

Designation	Support	Amine	Additive	Amine :Surfactant ratio
A	Davisil 60	PEI[a]	None	1:0
B	Davisil 60	PEI[a]	SDS	80:20
C	Davisil 60	PEI[a]	TEA	80:20
D	Davisil 60	TEPA	None	1:0
E	Davisil 60	TEPA	SDS	80:20
F	Davisil 60	TEPA	TEA	80:20

[a] MW 600

4.6 Determination of organic components

The presence of the amine polymer and surfactant within the confines of the porous support was confirmed by TGA, elemental analysis, DRIFTS, SSNMR and nitrogen sorption. The TGA results shown below in Table 4.7 show a shift in the maximum signal of first derivative indicating that the combustion is no longer representative of the pure amine component. The maximum of the first derivative appears to decrease with the inclusion of both SDS and TEA suggesting that the addition of the surfactant additive reduces the thermal stability of the adsorbent. The weight loss determined by TGA confirmed the target loading of 33 wt% organic content. The results from the CHN analysis are given below in Table 4.7. The experimentally derived CHN results appear to yield higher amounts of C and H than predicted. As a consequence the N loading was found to be lower. This was consistent amongst all samples. This was a consequence of the materials adsorbing CO_2 and H_2O from the atmosphere.

Table 4.7. Thermogravimetric and elemental analysis for binary surfactant polymeric adsorbents.

Sample	**Organic loading (%)[a]**	**Max. of first derivative (°C)**	**%C (Calc.%)[b]**	**%H (Calc.%)[b]**	**%N (Calc.%)[b]**
A	32.8	227.4	(17.89) 18.24	(4.47) 4.52	10.21 (10.44)
B	33.0	203.8	(18.34) 18.61	(4.33) 4.36	8.14 (8.78)
C	32.9	213.4	(18.23) 18.73	(4.42) 4.0	8.92 (9.40)
D	32.6	223.4	(16.78) 17.44	(4.02) 4.17	11.87 (12.32)
E	32.9	193.1	(16.66) 17.62	(3.77) 3.85	8.84 (9.74)
F	32.8	203.4	(16.55) 16.87	(3.86) 4.12	9.68 (10.37)

[a] Determined by TGA [b] Calculated values are in parenthesis.

^{13}C SSNMR was used to confirm the presence of the organic species with the spectra recorded presented in Figure 4.5. Sorbent A exhibited two broad peaks centred at 40 and 47 ppm, relating to the 8 distinct carbon sites of the PEI backbone. These peaks suggest that the PEI has not degraded during the impregnation process. Sorbent D yielded peaks between 38-53 ppm representing the carbon backbone of the TEPA species. Sorbents B and E exhibited additional peaks corresponding to the impregnation of SDS [13]. The peak at 14.6 ppm was indicative of the terminal CH_3 group with the peaks between 22 -34 ppm corresponding to the CH_2 units of the SDS with the peak at 6.17 ppm due to carbon at a position α to the sulfate group. Sorbent C and F exhibited an additional peak at 58.9 ppm related to the carbon α to the hydroxyl group in TEA [13]. The inclusion of the surfactant additives and amine impregnation onto the support does not appear to have changed the structure of the amine in any way.

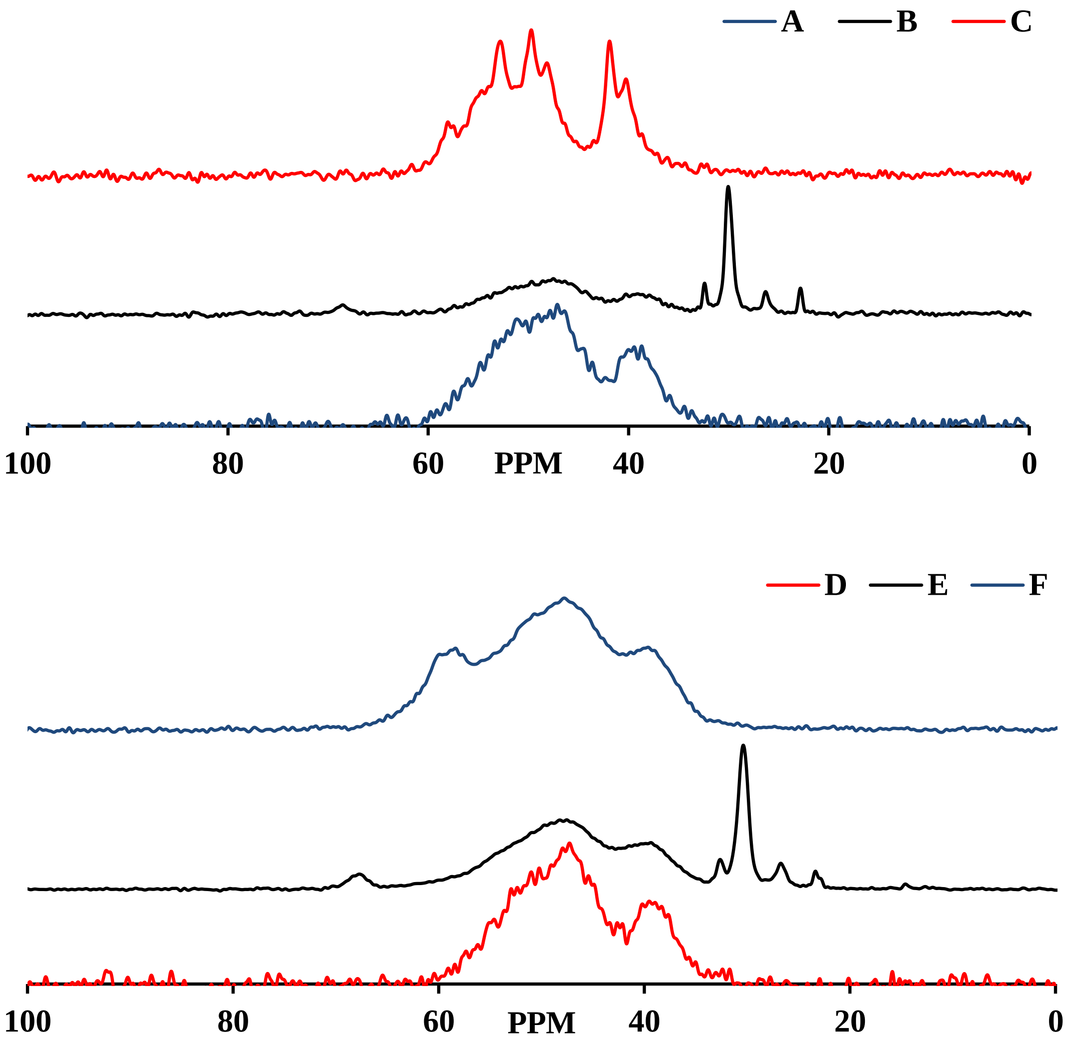

Figure 4.5. ^{13}C SSNMR of sorbents A-C (top) and D-F (bottom).

DRIFT spectra of all of the additives and their components are summarised in Table 4.8 with the spectra given in appendix A4.

Table 4.8. Infrared bands assignments for adsorbents A-F.

Wavenumber (cm^{-1})	Assignment	Species	Reference
3750	Si-OH	Silica	[14, 15]
3660	O-H str	Silica	[15]
3360, 3290	N-H str	PEI/TEPA	[16]
2931	C-H str	PEI/TEPA	[15, 16]
2810,2880	C-H str	PEI/TEPA	[15, 16]
2360, 2349	CO_2 str	Gas phase CO_2	[6]
1630	H-O-H bend	Adsorbed water	[15]
1601	N-H def	PEI/TEPA	[15]
1468	CH_2 bend	TEPA/PEI	[7]
1410	C-N str	PEI/TEPA	[7]
1270 (br.)	Si-O-Si	Silica	[6]
3300 (br.)	O-H	TEA	[13]
2933	C-H	SDS	[13]
1250	S=O	SDS	[13]

Upon impregnation of PEI on the silica support the bands accounting for surface bound water and surface silanols are reduced. Appearance of NH_2 and NH species is given by bands at 3360 and 2390 cm^{-1} respectively. Further confirmation of the NH species is provided by the accompanying NH deformation at 1601 cm^{-1}. The hydrocarbon backbone is present characterised by CH stretches at 2931 and 2810 cm^{-1} and the CH deformation at 1459 cm^{-1}. Similar bands were observed for TEPA impregnated samples. When 20% of the amine was replaced with TEA there was an increase in the bands at 3300 cm^{-1} assigned to the O-H stretches of the TEA. Substituting 20% of the amine with SDS did not lead to any significant changes in the IR bands.

4.7 Influence of surfactant addition on porous structure

The porous structure of the adsorbents were characterised by nitrogen sorption (Figure 4.6). Type IV isotherms typical of mesoporous substrates were obtained for all impregnated adsorbents. The porous properties of sorbents A-F are summarised in Table 4.9. All samples show a lower surface area, mean pore size and pore volume relative to the unfunctionalised support indicating that the PEI is contained within the pores of the support. The experimentally determined pore volume is significantly lower than that of the theoretical calculation (Table 4.9). This suggests that a fraction of pores have become inaccessible after amine impregnation. This is similar to similar to adsorbents characterised by Sanz who found that the impregnation of amines on silicas is not uniform [18]. The increase in accessible pore volume and larger average pore size of B compared to A suggests that the addition of SDS provides a better dispersion of the amine. Given the potential error in the measurements differences in pore volume and surface area could not be established between adsorbents A and C at 77 K.

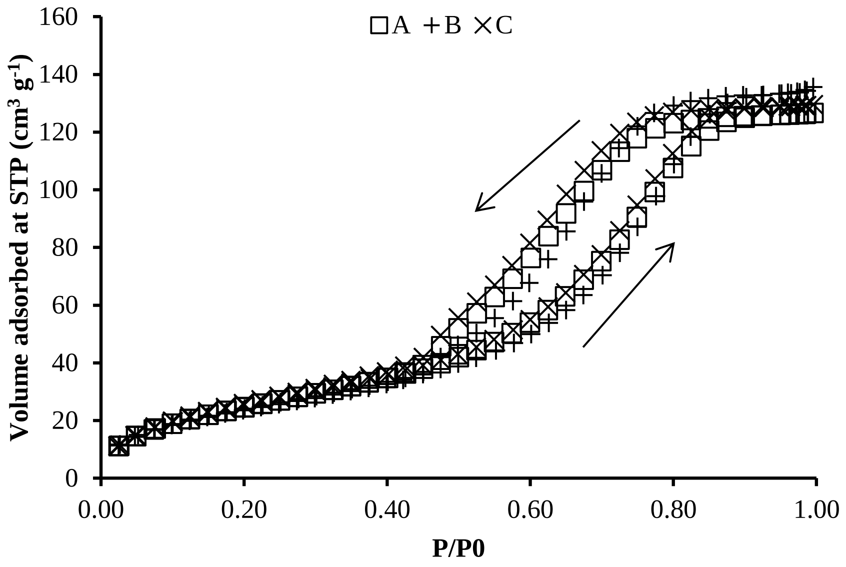

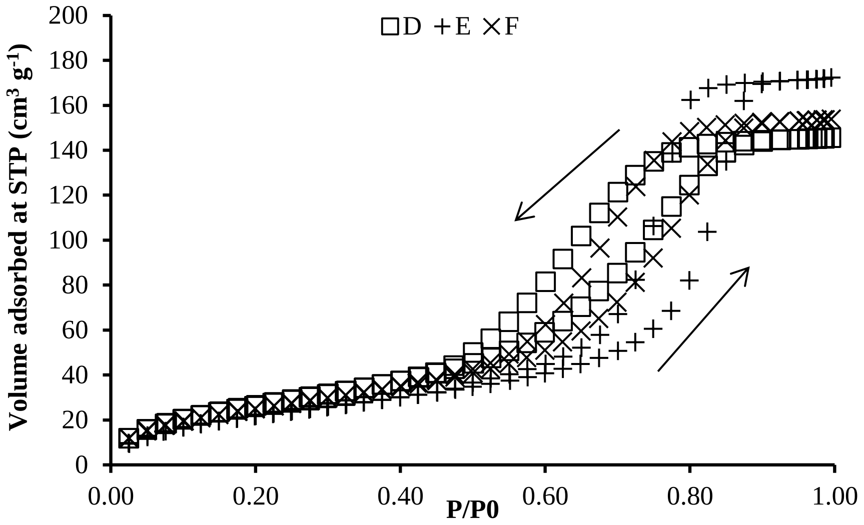

Figure 4.6. Nitrogen sorption isotherms for the as prepared adsorbents A-C (top) and D-F (bottom).

A lower inaccessible pore volume was found for TEPA based adsorbents compared to those based on PEI. This is likely to be attributed to the lower viscosity and smaller molecular size of the TEPA molecules. Increases in pore volume are observed for both E and F relative to D, suggesting the addition of SDS and TEA improves the dispersion for TEPA based adsorbents.

Table 4.9. A summary of the pore structure information obtained using nitrogen at 77 K.

Sorbent	BET Surface area ($m^2\ g^{-1}$)	Average pore size (Å) [a]	Pore Volume ($cm^3\ g^{-1}$)	Blocked volume (%)
Davisil 60	516 +/- 14	90	0.785 +/- 0.02	N/A
A	96 +/- 7.0	75	0.196 +/- 0.02	56
B	90 +/- 5.5	83	0.210 +/- 0.02	53
C	99 +/- 7.4	74	0.198 +/- 0.02	55
D	103 +/- 7.5	74	0.225 +/- 0.02	50
E	94 +/- 6.3	85	0.240 +/- 0.02	47
F	95 +/- 6.8	77	0.235 +/- 0.02	48

a) Determined using the BJH adsorption PSD model

4.8 Determination of the activation energy for motion by SSNMR

The mobility of the polymeric amines and surfactant mixtures within the pores of the support were determined using a saturation recovery pulse sequence ^1H SSNMR experiment. The spin-lattice relaxation times (T_1) were obtained from spectra recorded between 23 - 110 °C; temperatures relevant to the CO_2 adsorption process. Spectra of fully recovered samples with a delay time of 10240 ms are given in Figure 4.7.

Single component adsorbent A shows a single peak centred at 3.2 ppm corresponding to the averaged signal of the PEI protons. As the temperature increases the full width half maximum (FWHM) of all peaks decreases suggesting the impregnated polymers are now more mobile. Sample B has a broad peak between 6.17 -5.82 ppm which shifts as a function of temperature which is assigned to CH_2-SO_3Na. Additional peaks at 3.5, 1.36 and 0.9 ppm are assigned to N-CH_2, CH_2 and CH_3 respectively. For adsorbent C, peaks at 5.1, 3.9 and 2.9 ppm, assigned to HO-CH_2, N-CH_2 and O-CH_2 of TEA. Sample D features a single peak at 2.5 ppm relating to single component TEPA signals. Samples E and F exhibit analogues bands to B and C respectively.

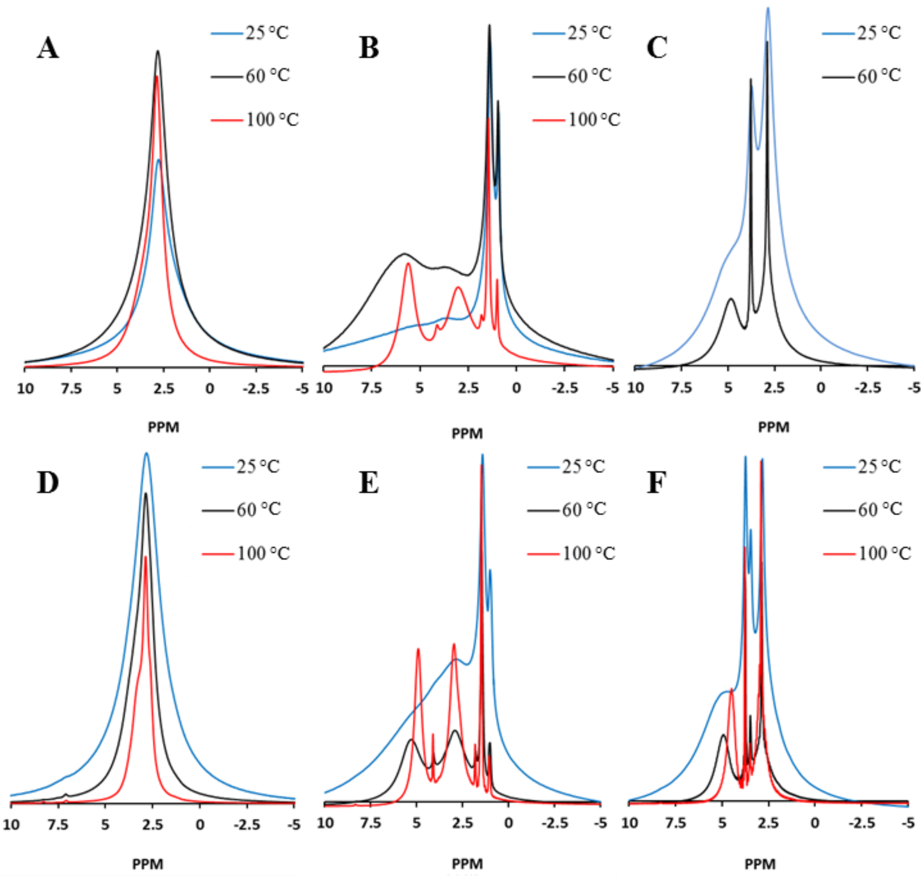

Figure 4.7. Variable temperature MAS ^{1}H SSNMR of adsorbents A-F.

The relative quantification of the mobility of the organic components of A-F was completed using the method outlined in Section 3.12. Plots of T_1 vs T^{-1} yielded a single minima across the temperature ranges (Appendix A5). It is not clear what type of motion this relates to; rotational or translational motion. A comparison of the activation energies as a function of 0.001 K^{-1} increments from the minimum of the T_1 vs T^{-1} plot (x_n) is presented in Figure 4.8.

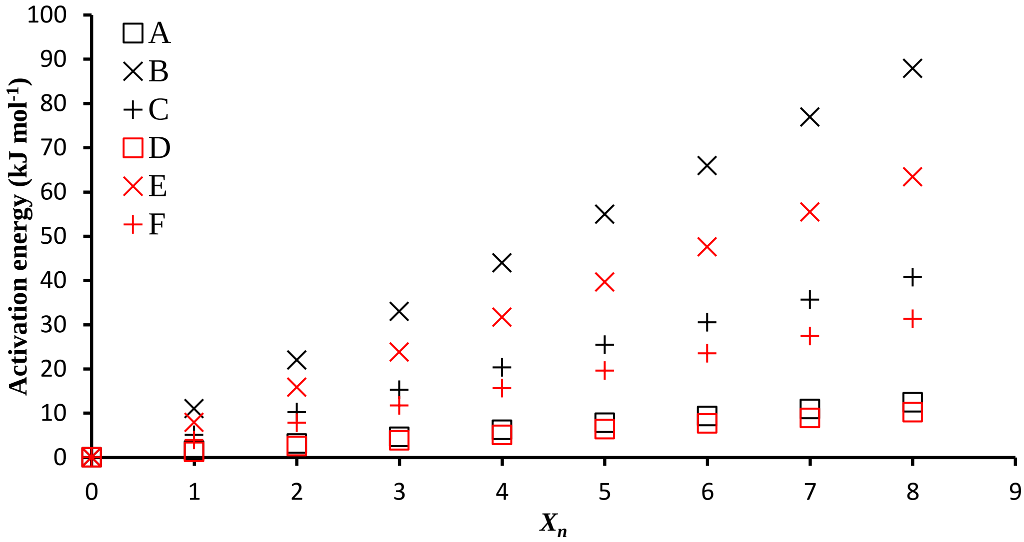

Figure 4.8. Activation energy of motion for adsorbent A-F determined at 0.001 K^{-1} (x_n) steps from the minima.

A linear relationship is observed which is expected for a second order polynomial. The magnitude of the activation barriers presented in Figure 4.8 agree well with activation energies of lithium polymer electrolytes determined by T_2 correlation measurements [19]. Sorbents D-F with the lower molecular weight amine TEPA exhibit lower activation energies towards motion then PEI based adsorbents A-C. This can be attributed to the lower molecular weight of the TEPA units having a lower sum of interactions to overcome. Binary surfactant-amine sorbents appear to have a larger activation energy of motion irrespective of the nature of amine or surfactant. The incorporation of SDS led to the largest increases in activation energy for both PEI and TEPA based adsorbents. The introduction of TEA in sorbents leads to an increase in the activation energy of motion albeit to a lesser extent than of SDS. These findings suggest that the incorporation of SDS and TEA into the impregnation mixture may lead to an adsorbent with increased viscosity. This would lead to a slower rate of CO_2 diffusion through the amine polymer-surfactant blend.

4.9. Shear viscosity of amine-surfactant blends

To confirm the findings from Section 4.8, the shear viscosity of neat binary amine mixtures present in adsorbents A-F was measured. These are referred to as compositions A-F in this section. The shear viscosity method used was described in experimental Section 3.13 and the results presented in Figure 4.9. The viscosity of composition A rapidly decreased with increasing temperature until 55 °C at which point the rate of decrease slowed. This could be attributed to a conformational change in the polymer structure similar to that observed during the VT ^{1}H SSNMR experiments. The viscosity of compositions B and C followed a similar temperature response to composition A. However, the magnitude of the viscosity measured for B and C was greater than A at all temperatures.

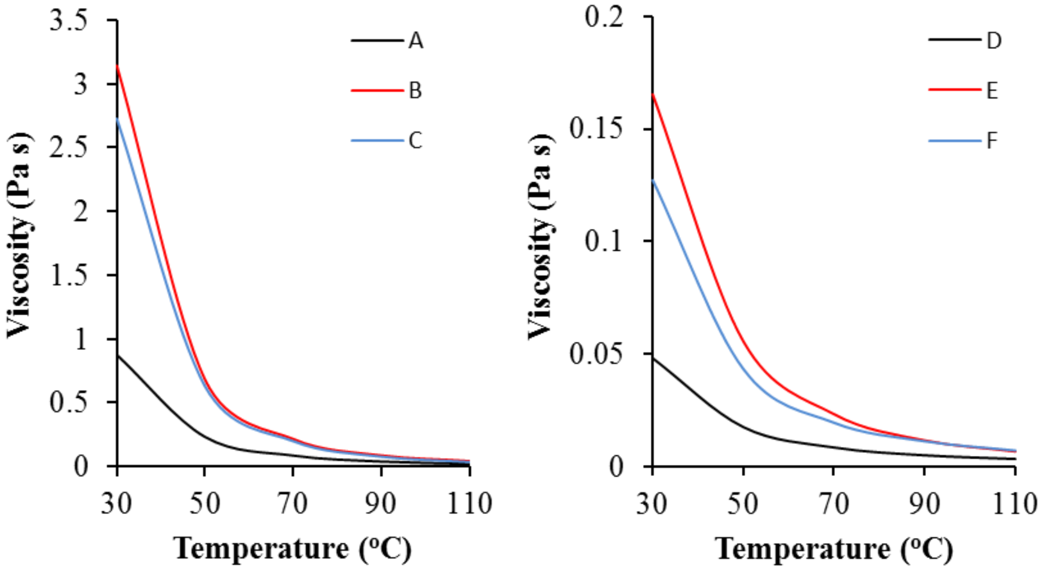

Figure 4.9. The change in viscosity as a function of temperature for the neat amine-surfactant compositions A-C (left) and D-F (right).

The viscosity of TEPA compositions were an order of magnitude lower than PEI compositions, attributed to the lower molecular weight and absence of polymer branching. Furthermore, the difference between the final and initial viscosity of PEI compositions were much greater than the TEPA compositions. The viscosity of compositions D, E and F decreased rapidly until 55 °C, at which point the rate of decreased slowed. Similar to Composition B, the inclusion of SDS in composition E led to a significant increase in viscosity which decreased rapidly with temperature. Composition F possessed a greater viscosity over all temperatures studied than composition D. The order of the viscosities correlated with the activation energies of motion determined by ^{1}H SSNMR. As an analogous calculation the activation energy of viscous flow was determined. The viscosity followed an Arrhenius dependency for all samples with a plot of $ln\eta$ as a function of T^{-1} yielding a straight line in accordance with Equation 4.1 (Figure 4.10)

$$ln\eta = lnA + \left(\frac{E_a}{R}\right)\frac{1}{T} \qquad \text{Equation 4.11}$$

Where η is the viscosity, A is the pre exponential factor, E_a is the activation energy, R is the ideal gas constant and T is the temperature. This allowed the quantification of the activation energy E_a for viscous flow of for the differing compositions with the data summarised below in Table 4.10.

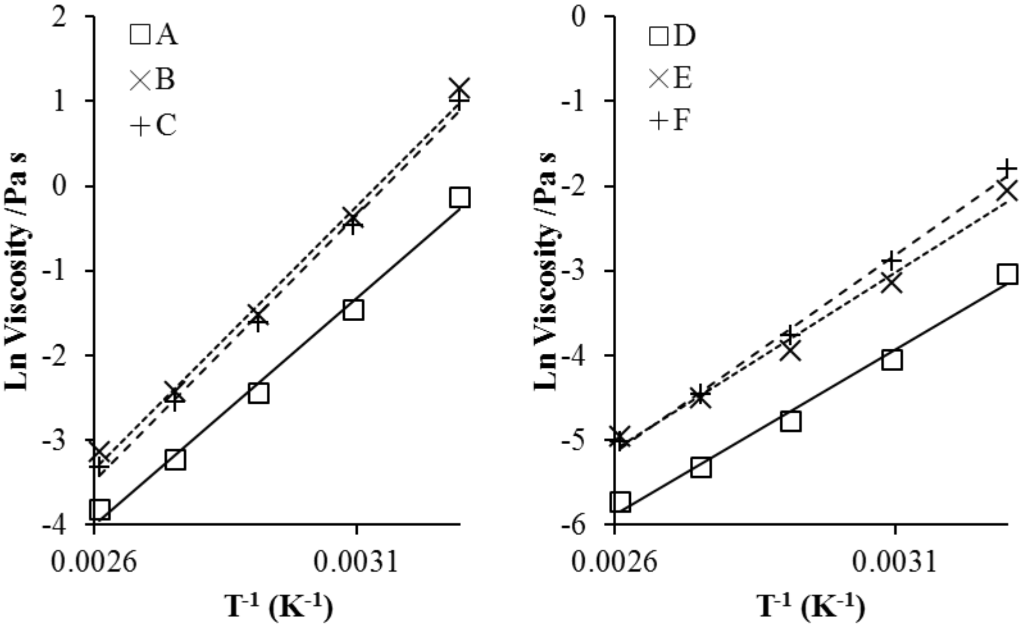

Figure 4.10. Arrhenius dependency of the viscosity of compositions A-F.

Table 4.10. The activation energy of viscous flow for compositions A-F.

Adsorbent	**Ea (kJmol^{-1})**	**R^2**
A	44.54	0.9929
B	52.14	0.9968
C	51.64	0.9933
D	32.423	0.9879
E	38.93	0.9885
F	34.84	0.9962

From this is can be seen that E_a for composition D is much lower than composition A. Relative to composition A, the addition of SDS increased the E_a by 17 % whilst the addition of TEA increased E_a by 15%. The E_a of TEPA based adsorbents was influenced to a lesser extent by the presence of additives. The incorporation of SDS and TEA led to a 20 and 7% increase in E_a respectively. The trend in activation energies established using shear viscosity between adsorbents A-F qualitatively agrees with the relationship determined by T_1 relaxation times in Section 4.8. These increases in activation energy of motion suggest that diffusion through PEI/TEPA-surfactant mixtures may be slower. This is an intriguing observation as typically a decrease in the rate of diffusion would lead to a lower equilibrium adsorption capacity. However, numerous reports have presented that the inclusion of similar additives led to increased CO_2 adsorption capacities [1, 21]. The following section will investigate the CO_2 adsorption uptakes of these adsorbents to ascertain if this is the case for adsorbents A-F.

4.10 CO_2 adsorption under dry conditions

The adsorption capacity of sorbents A-F were measured in the fixed bed adsorption reactor described in Section 3.3. CO_2 adsorption experiments were conducted at 75 °C, with a flow of 15% CO_2/N_2 (1000 ml min^{-1}). CO_2 uptake profiles are given in Figure 4.11 with the equilibrium adsorption capacities reported in Table 4.11. Given the design of the adsorption apparatus a quasi- linear region in CO_2 uptake between 0 and 50 s is observed. The slight sigmoidal shape in this region can be attributed to the distribution of residence times. Given the similar mass of adsorbent used, same base support and same conditions it was thought that this would provide a sensible comparison between adsorbents to aid material development. Differences in adsorbent porosity as defined in Section 4.6.2 may contribute differences in breakthrough shape.

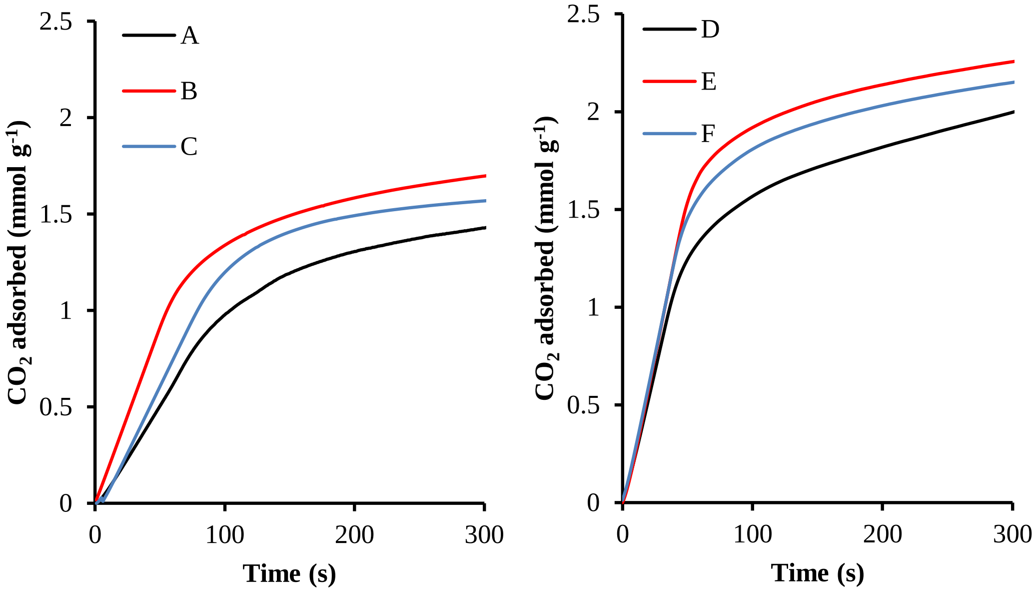

Figure 4.11. CO_2 adsorption experiments for sorbents A-F conducted in a packed bed reactor at 75 °C, 15% CO_2.

Table 4.11. CO_2 adsorption capacity of the adsorbents measured under 15% CO_2/N_2 at 75 °C.

Sorbent	Dry uptake (mmol g^{-1})[a]	Amine efficiency
A	1.70	0.21
B	1.95	0.31
C	1.79	0.28
D	2.36	0.30
E	2.47	0.37
F	2.42	0.37

[a] The error for CO_2 adsorption experiments was determined to be +/- 3.7 % (Section 3.3)

The CO_2 adsorption capacities of A and D were improved by the substitution of amine for either SDS or TEA. The extent of increase appeared greater for SDS than TEA. These findings suggest that the inclusion of a surfactant additive yields an increase in amine accessibility. The uptake capacities of the TEPA based adsorbents were higher than those of their PEI analogues with sorbent D having an equilibrium CO_2 capacity of 2.36 mmol g^{-1}.

The amine efficiency for sorbent A was 0.21 typical for PEI impregnated adsorbents. The amine efficiency of TEPA based adsorbents was greater that PEI based adsorbents due to the lower viscosity of the amine. PEI adsorbents have the lowest amine efficiencies attributed to pore blocking of small pores and sluggish diffusion through PEI films. The presence of SDS in sorbent B led to increases in amine efficiency. This could be related to the improve pore accessibility observed by nitrogen sorption allowing an increased number of adsorption sites. Sorbent C led to an increase in the adsorption of CO_2 however the effect was less than B. Little change in pore structure was observed between A and C suggesting C might offer additional CO_2 adsorption sites. The higher uptakes and breakthrough efficiencies for TEPA based adsorbents could be due to the increased mobility and reduced pore blocking of the TEPA based adsorbents. The presence of SDS in sorbent E led to an increase in amine efficiency compared to the signal component TEPA. This could be related to the increased accessibility of the pore structure as determined by nitrogen sorption. Sorbent F led to an increase in amine efficiency relative to signal component adsorbent D. This suggests that for this sample an increases number of adsorption sites are accessible.

The bed temperature was monitored throughout the experiment and a significant increase in the adsorbent temperature was detected (Figure 4.12). The bed temperature increased from 75 °C to 94 °C during the initial minute of adsorption. This was accompanied with the greatest derivative of CO_2 adsorption uptake. As the bed temperature decreases the rate of adsorption also decreases possibly as the majority of sites remaining are limited by the sluggish diffusion of CO_2 through the amines films.

As the temperature approaches 100 °C the desorption of CO_2 begins to be competitive with the adsorption under 15% CO_2 leading to a reduction in CO_2 uptake capacity [7]. The increases in bed temperature were proportional to the uptake capacity of the adsorbent with the materials possessing similar heat capacities. Increases in bed temperature would influence the rate of adsorption and mass transit throughout the sample leading to the rapid initial uptakes where the temperature is the greatest followed by diminishing uptakes as the adsorption progresses. Once the bed begins to cool the adsorption capacity would increase as the equilibrium shifts towards a greater proportion adsorbed on the material surface.

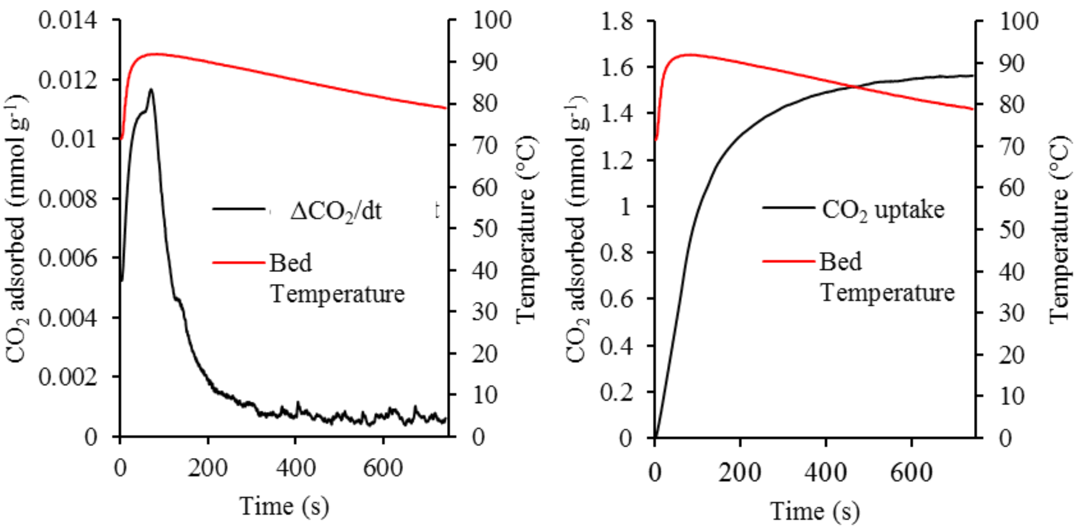

Figure 4.12. The adsorbent temperature profile and the amount of CO_2 adsorbed with time (left). The first derivative of the adsorbent temperature profile with the adsorbent temperature profile with time (right).

4.11. CO_2 adsorption in the presence of water

The influence of CO_2 uptake is the presence of water was investigated using a flow of 15% CO_2, 10% H_2O/N_2 at 75 °C (Section 3.4). Uptake profiles of the adsorbents under humid conditions are given in Figure 4.13, with equilibrium adsorption capacities given in Table 4.12. For sorbents A-C containing 25 % tertiary amines, water could lead to CO_2 adsorption onto these tertiary amine sites. The same is true for adsorbent F. However, this process is thought to be very slow and is not expected to a make a significant contribution in this study [21].

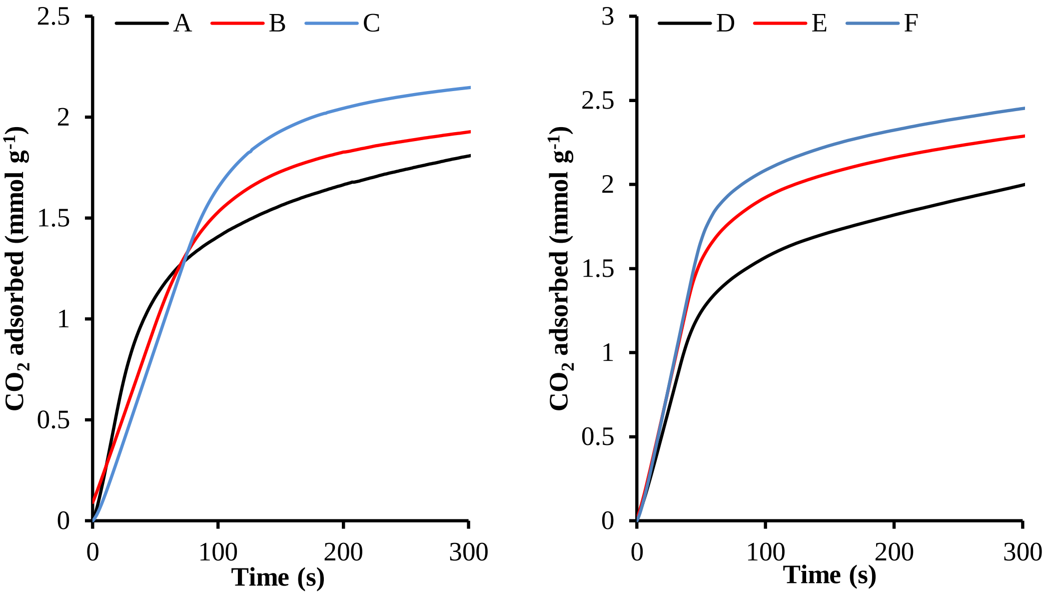

Figure 4.13. Fixed bed CO_2 adsorption experiments for PEI adsorbents A-C under 15 % CO_2/ 10%H_2O/N_2 at 75 °C (left) Fixed bed CO_2 adsorption experiments for TEPA adsorbents D-F under 15 % CO_2/ 10%H_2O/N_2 at 75 °C (right).

The presence of 10% water in the gas stream led to a 16% increase in uptake capacity for adsorbent A. The increase in amine efficiency suggests that a greater number of adsorption sites are available in the presence of water. This could be attributed to water disrupting the hydrogen bonding between the amines and the surface silanols or acting as a plasticiser, increasing the mobility of the amine chains [22]. A similar increase in adsorption capacity is observed for sorbent D suggesting a similar mode of action.

Adsorbents C and F containing TEA, exhibited the largest enhancement in CO_2 adsorption capacity under wet conditions. By contrast SDS containing adsorbents B and E exhibited the lowest increases in the presence of water. This suggests that the hydrophobicity of the surfactant may influence the role of water. A similar observation was noted by Wang *et al*. who noted ~ 20% increases in the adsorption capacity of binary surfactant-amine adsorbents [20]. Investigations by Sayari showed that PE-MCM-41 featuring high loadings of cetyltrimethylammonium bromide exhibited a reduction in CO_2 uptake in the presence of water [12]. It could be hypothesised that hydrophilic groups such as TEA facilitate the intrusion of water with the amine films, releasing a greater number of hydroxyl groups. Although increases in amines efficiency are present they are consistently below 0.5 after which point it would suggest a difference in the CO_2 adsorption mechanism.

Table 4.12. A summary of the CO_2 adsorption uptakes and amine efficiencies for adsorbents A-F.

Sorbent	**Dry CO_2 uptake (mmolg^{-1})[a]**	**Wet CO_2 uptake (mmolg^{-1})[a]**	**Dry amine efficiency (a.u.)**	**Wet amine efficiency (a.u.)**	**Enhancement by water (%)**
A	1.70	1.98	0.21	0.25	16.4
B	1.95	2.08	0.31	0.32	7.6
C	1.79	2.12	0.28	0.33	18.4
D	2.36	2.60	0.30	0.35	10.1
E	2.47	2.65	0.38	0.41	7.2
F	2.42	2.79	0.37	0.43	15.2

[a] The error for CO_2 adsorption experiments was determined to be +/- 3.7 %.

4.12 The effect of CO_2 partial pressure

The concentration of CO_2 in flue gas streams varies on the fuel of the powerplant with typical concentrations of 3% and 15% CO_2 for natural gas and coal fired powerstations respectively. To evaluate the influence of CO_2 partial pressure on adsorbents A-F CO_2 adsorption isotherms were conducted between 0.0001 – 0.95 P/P_0 CO_2 (Figure 4.14). The shape of the adsorption isotherms matches that observed in several literature reports for similar amine functionalised silicas [23, 24]. Between pressures of 0 - 0.06 P/P_0 the amount of CO_2 adsorbed increases rapidly with pressure. The isotherms do not fit Langmuir or Freundilch adsorption isotherms as physisorption is evident at increasing partial pressures of CO_2. The volume of CO_2 adsorbed at set pressures was consistently higher for surfactant included sorbents B and C compared to single component adsorbent A. The same trend was found for TEPA based adsorbents with sorbents E and F exhibiting a greater CO_2 uptake at set pressures compared to single component adsorbent D. These differences imply the addition of surfactants increases the number of adsorption sites. The quantity of CO_2 adsorbed was higher for TEPA based adsorbents that PEI owing to the order of magnitude difference in viscosity of the impregnated polymer. The amount of CO_2 adsorbed was high below 0.04, suggesting that these materials could be used for direct air capture of CO_2. Under static conditions of 313 K it appears that TEA bearing adsorbents blends adsorb more CO_2 than those containing SDS. This suggests that the TEA additive may present physisorption sites for CO_2 which become important at low adsorption temperatures.

The amine efficiencies are much greater than those recorded in the fixed bed reactor and TGA (Table 4.13). This can be attributed to the significant physisorption at high CO_2 partial pressures at 313 K. High amine efficiencies of up to 0.5 were reported under static adsorption conditions by Dao at similar temperatures [25].

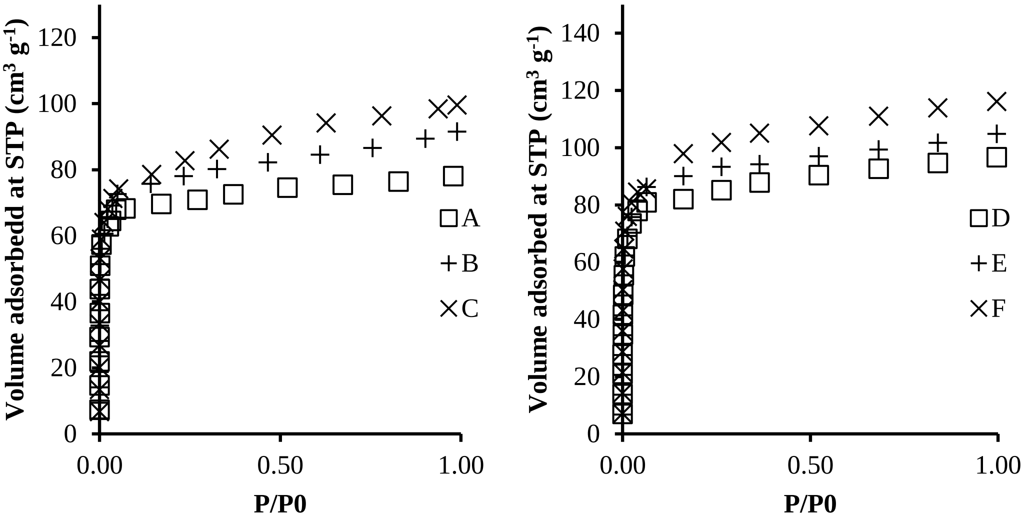

Figure 4.14. CO_2 adsorption isotherms of sorbents A-F measured at 313 K.

Table 4.13. Volumetric CO_2 adsorption capacities for adsorbents A-F.

Sorbent	Volumetric CO_2 uptake (mmol g^{-1})	Volumetric Amine efficiency
A	1.71	0.27
B	2.12	0.33
C	2.30	0.37
D	2.35	0.37
E	2.60	0.41
F	2.78	0.44

4.13 Influence of CO_2 adsorption temperature

The CO_2 uptakes were measured at set temperatures between 25 – 180 °C to determine the influence of additives on the optimum adsorption temperature (Figure 4.15). Given the exothermic nature of the CO_2 adsorption on amines, an increase in the adsorption temperature should lead to a decrease in the CO_2 uptake. However reports have noted peak CO_2 adsorption capacities at between 75 – 100 °C for impregnated PEI adsorbents [26]. Single component PEI adsorbent A exhibited a peak adsorption temperature at 100 °C under atmospheres of pure CO_2 with the extent of CO_2 adsorbed reducing significantly after 120 °C. Sorbents B and C exhibit maximum CO_2 adsorption capacities of 2.40 and 2.27 mmol g^{-1} respectively at 75 °C. The CO_2 adsorption capacity of both B and C decreased at temperatures above 100 °C. This suggests that a greater number of amine sites are accessible at 75 °C for surfactant loaded samples. For TEPA based adsorbent D the maximum adsorption capacity was recorded at 75 °C. For sorbent E the adsorption capacity of 2.78 mmol g^{-1} was attained at 75 °C. The peak adsorption temperature for adsorbent F was 2.71 mmol g^{-1} at 75 °C. There appeared to be little changes in adsorption capacity for all adsorbents between 130 – 180 °C. At lower temperatures sorbent C appeared to have higher adsorption capacities than B. This suggests that the presence of TEA provides additional sites for CO_2 adsorption. A similar trend is observed for sorbent F which also has features TEA.

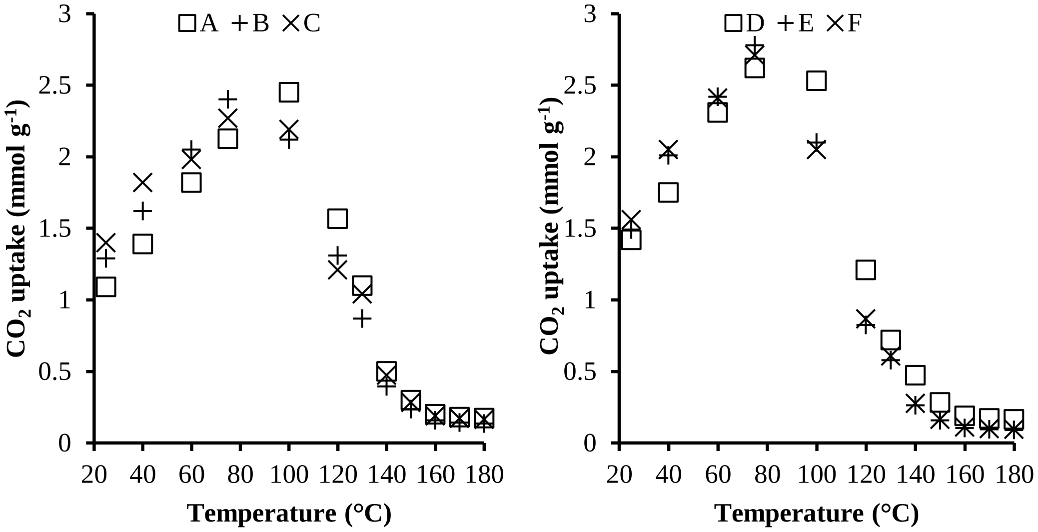

Figure 4.15. Influence of temperature on adsorption capacity for PEI (lef) and TEPA (right) based adsorbents under 100% CO_2.

4.14 Temperature programmed desorption

Temperature programmed desorption (TPD) was conducted to establish if there were any changes in adsorption mechanism or species formed in the presence of a surfactant. For adsorbent A, the peak desorption temperature was recorded at 374.15 K with a single broad peak responsible for all 8 potential amine sites (Figure 4.16). Comparing the peak shape to the theoretical peaks determined by Redhead, the peaks appear consistent with first order desorption. The desorption enthalpies (E_{des}) were calculated using the Redhead equation (Equation 4.2) [27].

$$E_{des} = RT_{max}\left(\ln\frac{v_1 T_{max}}{\beta} - ln\frac{\Delta E_{des}}{RT_{max}}\right) \qquad \text{Equation 4.2}$$

Where E_{des} is the enthalpy of desorption, R is the ideal gas constant, T_{max} is the temperature of the peak maximum, v_1 is the bond frequency, β is the heating rate. This method has been shown to provide an approximate measure of the enthalpy of desorption and as such should only be used as a guide. The value of E_{des} estimated for A was 88 kJmol^{-1} in agreement with literature values [28].

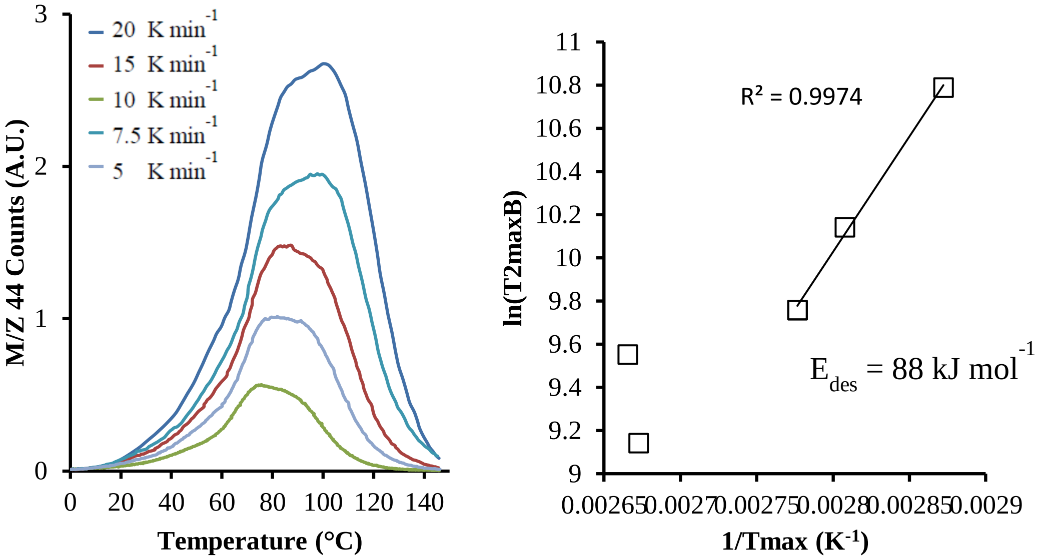

Figure 4.16. TPD of sorbent A conducted under a flow of Helium with β = 2.5-20 K min^{-1} (left).A Kissinger plot of sorbent A over a range of heating rates (right). Note: The error in the desorption enthalpy was determined to be +/- 4.6 kJ mol^{-1}.

Variation in the heading rate of sorbent A led to a shift in the observed maximum desorption temperature to higher temperatures with a retention of peak shape. A Kissinger plot assuming first order desorption was constructed. However, a linear plot could not be obtained throughout the whole temperature range (Figure 4.16). A tentative linear region can be drawn from β = 2.5-7.5 K min^{-1} which provides E_{des} as 88 kJ mol^{-1} similar to literature values. This suggests that at faster heating rates the sample was not at the specified temperature owing to thermal conductivity effects.

Sorbent B exhibited a T_{max} of 353.15 K (β = 10 K min^{-1}), approximately 15 K lower than single component adsorbent A (Figure 4.17, left). Two distinct peaks were present, separated by around 20 K suggesting a weaker and more strongly bound CO_2 species. At high heating rates the second peak dominates suggesting that heat effects through the sample may be a limiting factor. Construction of a Kissinger plot leads to an activation energy of 89.24 kJ mol^{-1} in agreement with literature values. Sorbent C had a T_{max} at 338K (β = 10 K min^{-1}) with a well-defined tail that diminished with increasing heating rate (Figure 4.17, right). A significant proportion of the CO_2 was found to adsorb at lower temperatures, suggesting the presence of a weakly bound CO_2 species.

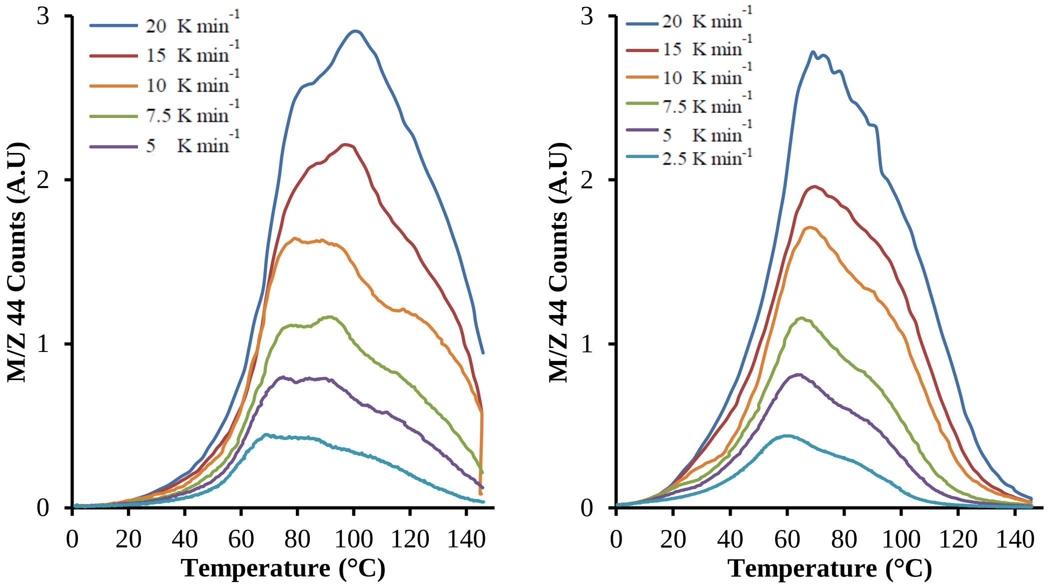

Figure 4.17. TPD of sorbent B conducted under a flow of Helium with β = 2.5-20 K min^{-1} (left) TPD of sorbent C conducted under a flow of Helium with β = 2.5-20 K min^{-1} (right).

Sorbent D presented two clear peaks in the temperature desorption programme at 344.15 K and 369.16 K (Figure 4.18). These two peaks were well resolved when β = 10 K min^{-1} however the peak at 344.15 K dominated at higher and lower heating rates. These peaks could be attributed to the primary and secondary amines sites present in the sample. An alternative hypothesis could suggest they are responsible for the diffusion of CO_2 through the amine polymer. The construction of a Kissinger plot does not yield a meaningful linear correlation. This suggests that the position in T_{max} at different heating rates cannot be attributed to a change in adsorption species and that thermal gradient effects are at play. Redhead analysis suggests that E_{des} is lower than PEI at 80 kJ mol^{-1}, however the literature precedent suggests the mechanism of uptake for PEI and TEPA is the same [29]. This suggest differences could be attributed to changes the in the diffusion of CO_2 through the films of amine.

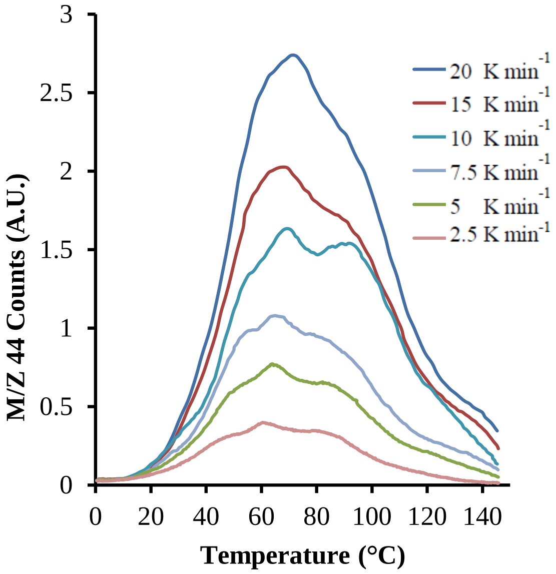

Figure 4.18. TPD of sorbent D conducted under a flow of Helium with β = 2.5-20 K min^{-1}.

Sorbent F containing SDS exhibited two distinct desorption peaks at 346.15 and 366.15 K when β = 10 K min^{-1} (Figure 4.19, left). These two peaks were resolved across all heating rates used. These peaks were similar for those reported for sorbent D. A Kissinger plot was constructed yielding a linear relationship for both peaks however the activation energies obtained were in the order of 200 kJ mol^{-1} suggesting an erroneous fit. Redhead analysis suggest that these species have a desorption enthalpy of 85 and 90 kJ mol^{-1} comparable to literature values. Such a large discrepancy suggests that mass transfer limitations are present.

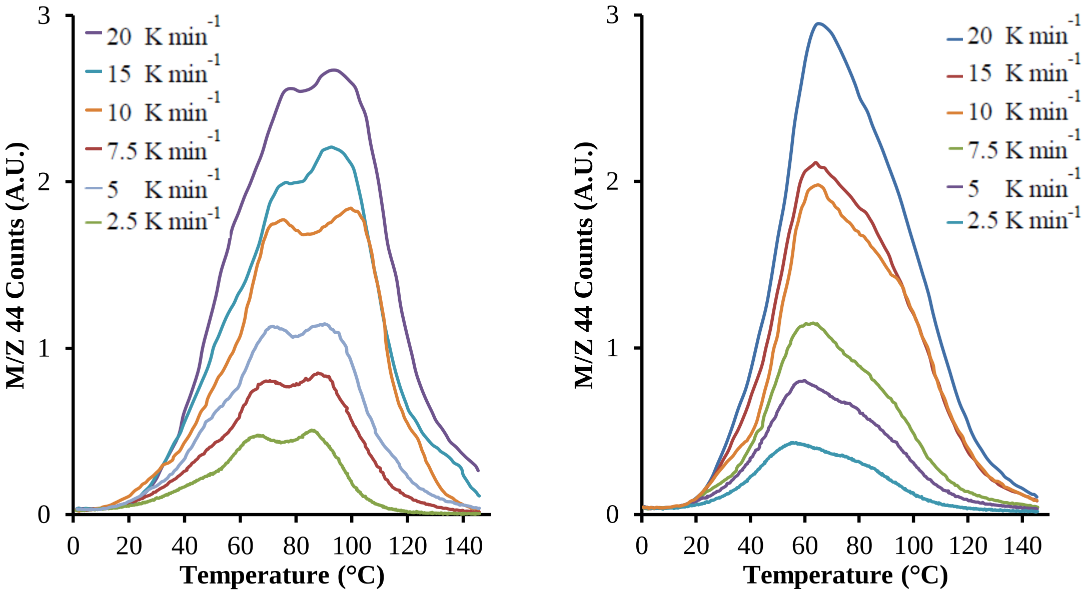

Figure 4.19. TPD of sorbent E conducted under a flow of Helium with β = 2.5-20 Kmin^{-1} (left) TPD of sorbent F conducted under a flow of Helium with β = 2.5-20 Kmin^{-1} (right).

The presence of TEA in sorbent F gives rise to a main peak at 338.15 K with a shoulder at higher temperature. It appears that the contribution that gave rise to higher temperature peak in D and E is diminished in F. Redhead analysis estimates E_{des} to be around. 85 kJ mol^{-1}. This suggests that in the presence of SDS, a greater proportion of the CO_2 can be removed at lower temperatures.

TPD analysis was completed on SDS and TEA impregnated onto Davisil 60 using the same experimental set up (Figure 4.20). 33wt% SDS on Davisil did not adsorb detectable amounts of CO_2. Conversely, 33wt% TEA physisorbed CO_2 with desorption peaking at 313 K. This suggests that the low temperature component in the TPD of sorbents C and F could partly be attributed to the physisorption of CO_2 on TEA sites.

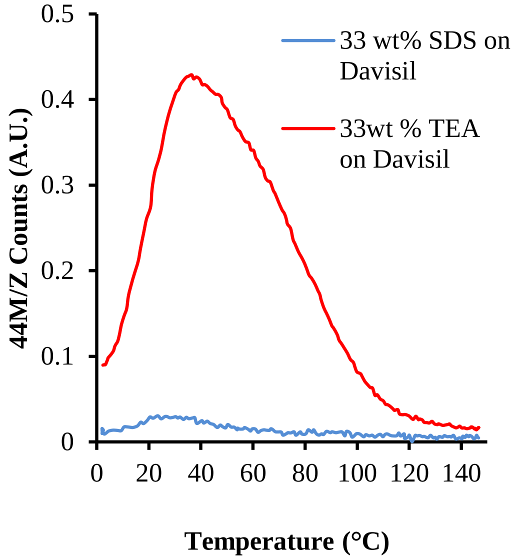

Figure 4.20. TPD of 33wt% SDS on Davisil 60 and 33wt% TEA on Davisil 60 conducted under a flow of He (50 ml min^{-1}) with β = 10 K min^{-1}.

4.15 DRIFTS of the species formed during CO_2 adsorption

To investigate any changes in the adsorption mechanism of CO_2 adsorption, *in-situ* diffuse reflectance adsorption spectroscopy (DRIFTS) was employed to monitor the species formed during the CO_2 adsorption. The spectra were referenced to samples under helium at the same temperature. Hence increasing bands correlate to the production of a new species whereas a reduction in such bands relates to the consumption of the specific species. Figure 4.20 shows the evolution of vibrational bands as the adsorption coordinate progresses for sorbent D. The adsorption of CO_2 on D led to a decrease in the bands at 3360 and 3290 cm^{-1} corresponding to the 1^{o} and 2^{o} amines decreased suggesting that both 1^{o} and 2^{o} amines were consumed in the adsorption of CO_2 [14]. A new band was produced at 3016 cm^{-1} relating to the stretch of an ammonium ion. This was accompanied by a corresponding ammonium ion bending band at 1630 cm^{-1}. Similarly to other reports the CH stretching bands at 2945 and 2845 cm^{-1} were suppressed during CO_2 adsorption [7]. A band at 3420 cm^{-1} was produced relating the NH stretch of carbamates species. This corresponds with peaks at 1560 and 1486 cm^{-1} which correspond to the symmetric and anti-symmetric stretches of a carbamates species. The bands produced at 1316 cm^{-1} correspond to a NCOO- skeletal vibration with 1407 cm^{-1} assigned to the C-N stretch of a carbamates species. The large band centred at 2500 cm^{-1} is attributed to the formation of zwitterionic species [17].

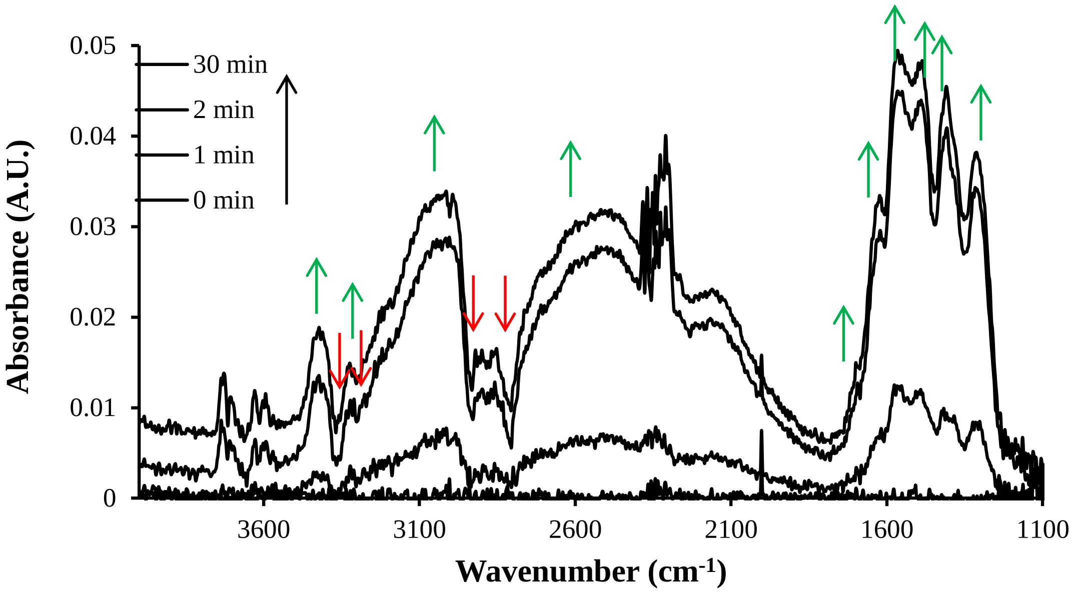

Figure 4.21. DRIFTS spectra of Sorbent D under a flow of 10% CO_2/He (100 ml min^{-1}) at 75 °C with increasing exposure time, referenced to Sorbent D under a flow of helium at 75 °C. Green arrows indicate increasing bands and red arrow diminishing bands.

To aid identification of the species the relative absorbance intensities of bands was plotted as a function of time shown in Figure 4.22. Here it is clear to see that there is a rapid increase in the amount of a carbamates bands at 1621, 1560, 1486, 1407 and 1316 cm^{-1} and that the relative increases in the bands are the same suggesting that they relate to the same species.

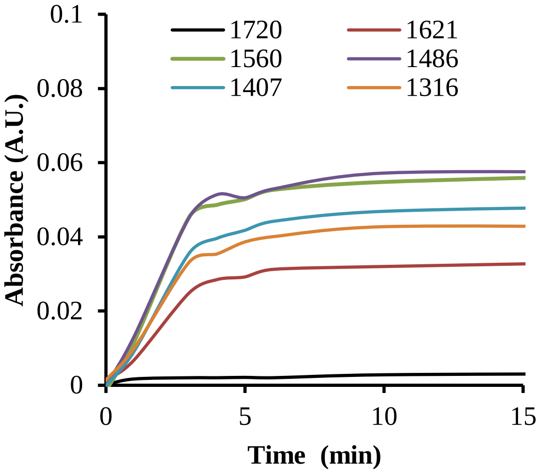

Figure 4.22. The intensity of carbamate bands present in Sorbent D under a flow of 10% CO_2/He (100 ml min^{-1}) at 75 °C.

The species formed from the CO_2 adsorption E and F were investigated under the same conditions as D. The spectra recorded after 30 min of CO_2 adsorption for E and F are compared to sorbent D in Figure 4.23. The same carbamate species is formed after CO_2 adsorption with identical bands formed at 1623, 1561, 1492, 1409 and 1315 cm^{-1}. Sorbents E and F appear to show a small additional adsorption band at 1719 cm^{-1} which is not present in sorbent D which can be attributed to the formation of carbamic acid (Figure 4.24).

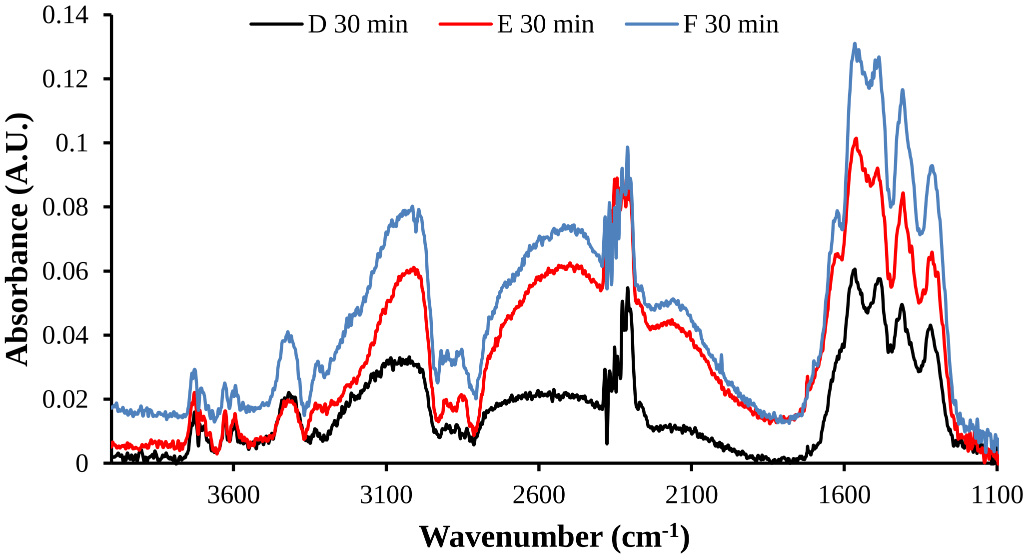

Figure 4.23. DRIFT spectra of sorbents D-F after exposure to 10% CO_2/He (100 ml min^{-1}) at 75 °C. Individual spectra are referenced to the same adsorbent under He at 75 °C.

Carbamic acid species have been shown to form on isolated amine sites where there is no additional amine group to lead to the formation of the carbamate [18, 30]. The large loadings of surfactant present in sorbents E and F could lead to an increase in the amount of isolated sites leading to the formation of a greater number of carbamic acid species. The adsorption of CO_2 onto the sites of carbamic acid would lead to an increase in the amine efficiency as they react in a 1:1 ratio between amine and CO_2. The relative intensity of adsorbent bands were plotted with time demonstrating that the bands responsible for the carbamate species form at the same rate. The rate of band formation of carbamic acid at 1719 cm^{-1} appears similar for adsorbents E and F suggesting there are no kinetic limitations or interconversion of such species (Figure 4.25). It should be noted the spectral contribution of carbamic acid is very small and as such is not expected to influence the CO_2 uptake behaviour.

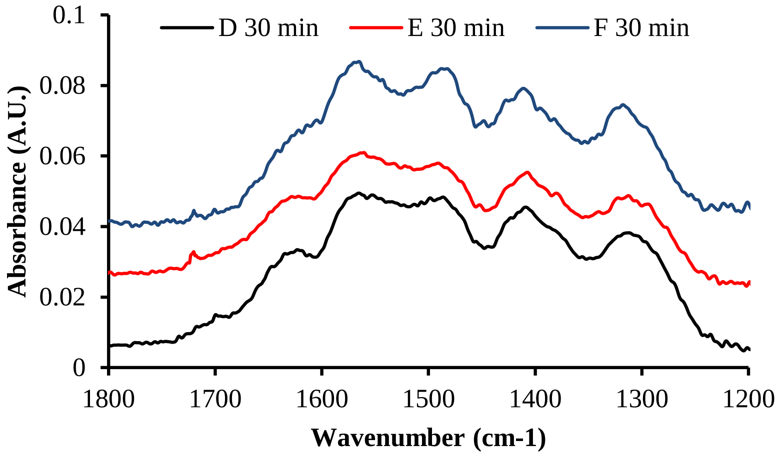

Figure 4.24. The carbonyl region of adsorbents D-F after CO_2 adsorption.

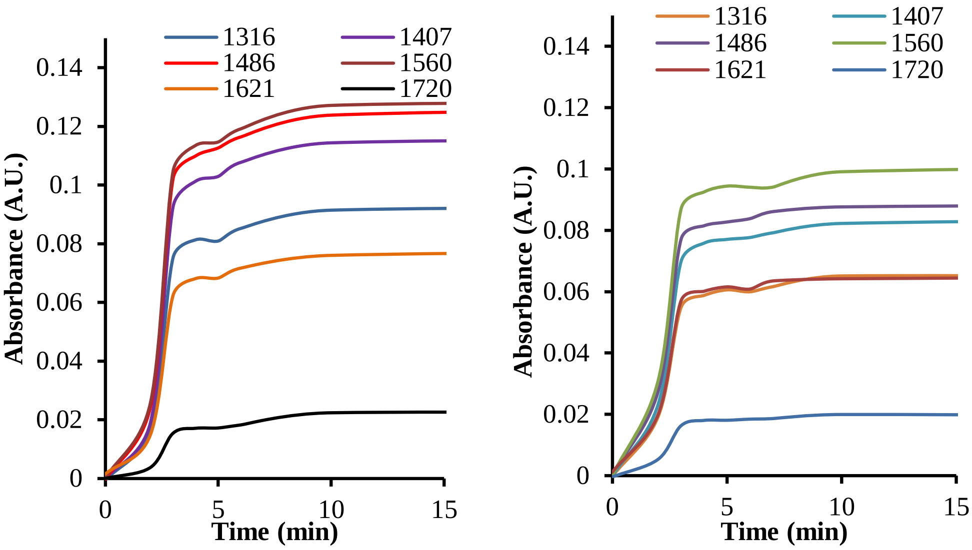

Figure 4.25. The intensity of carbamate bands present in Sorbent E under a flow of 10% CO_2/He (100 ml min^{-1}) at 75 °C (left) and sorbent D (right).

Basik *et al.* calculated the difference between DRIFTS adsorption spectra after the initial adsorption and once the system had equilibrated to probe whether there was a distribution between kinetic and thermodynamic adsorption species [14]. A similar approach was used by Didas *et al.* observed the formation of a bicarbonate species on materials in low amine coverage [30]. For sorbents D, E and F no change within the species formed between initial and equilibrated adsorption were observed. This analysis suggests that under dry adsorption conditions the presence of surfactant additives does not influence the mechanism of CO_2 adsorption. The same bands were present in sorbents D-F relating to the formation of alkylammonium carbamates.

4.16. ^{13}C SSNMR of the adsorbed CO_2 species

To fully evaluate the species former under CO_2 adsorption ^{13}C SSNMR was conducted on samples before and after adsorption of CO_2. Figure 4.26 shows the structure of adsorbents A-F after CO_2 adsorption. As can be seen the adsorption of CO_2 leads to the production of a peak 164.5 ppm corresponding to alkylammonium carbamate species [31]. No discernible change in the carbon backbone of the amine structure can be observed. The surfactant groups remain unchanged after CO_2

adsorption. This confirms that there is no change in the adsorption species in the presence of a surfactant species under dry gas conditions.

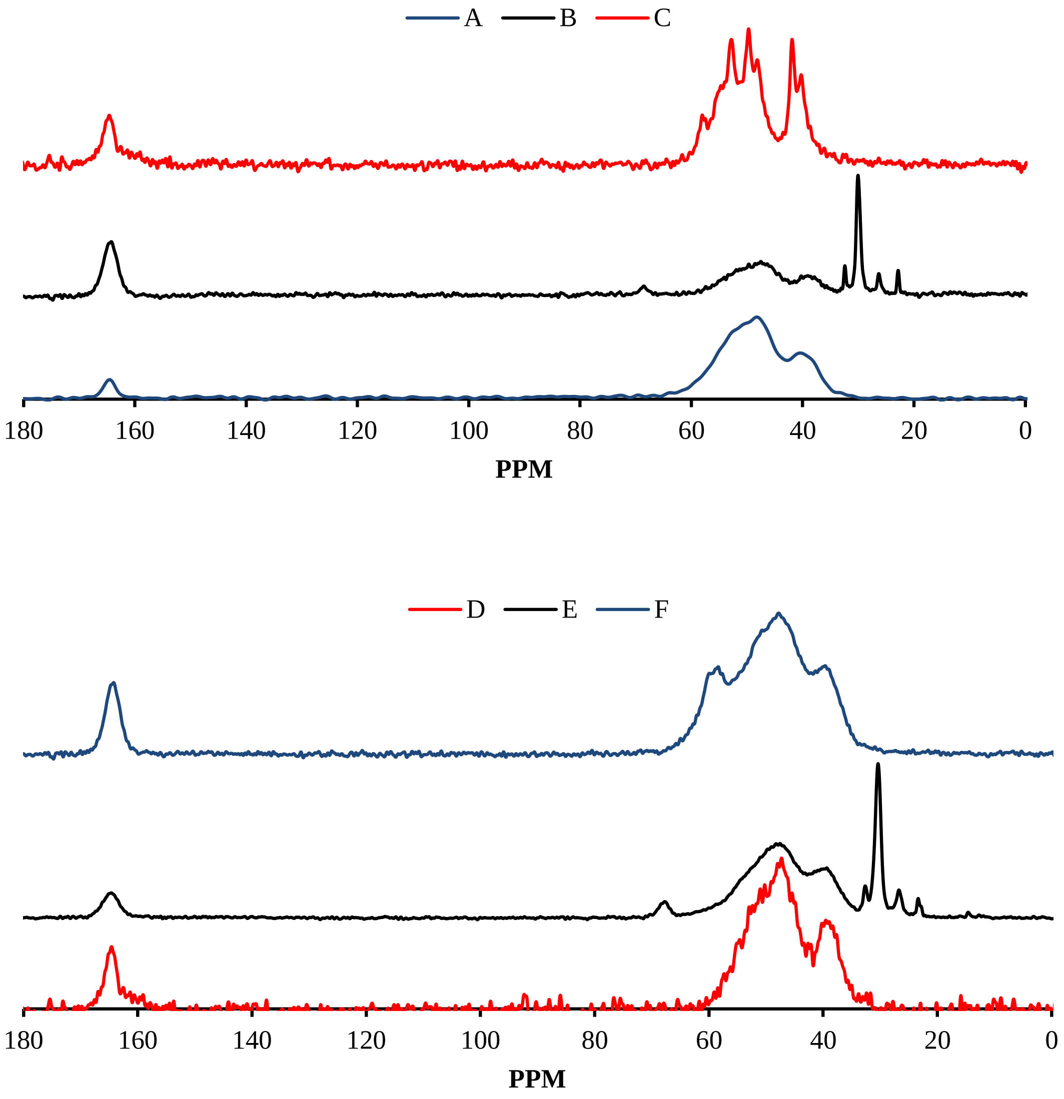

Figure 4.26. An overlaid ^{13}C SSNMR spectra of sorbents A-F before and after CO_2 adsorption. Spectra are offset to ensure spectra are easily comparable. Spectra are offset by 2.5E+08 to aid comparison.

4.17 Measuring the relative rate of CO_2 adsorption

Practical adsorption systems require rapid adsorption and desorption kinetics to ensure short sorption cycles to reduce the amount of material required. Silica supported amine adsorbents typically exhibit a rapid initial adsorption step followed by slow diffusion limited step [32]. The adsorption kinetics of sorbents A-F were measured by the pressure decay of CO_2 using volumetric sorption at 313.15 K at 0.0014 P/P_0 (Figure 4.27).

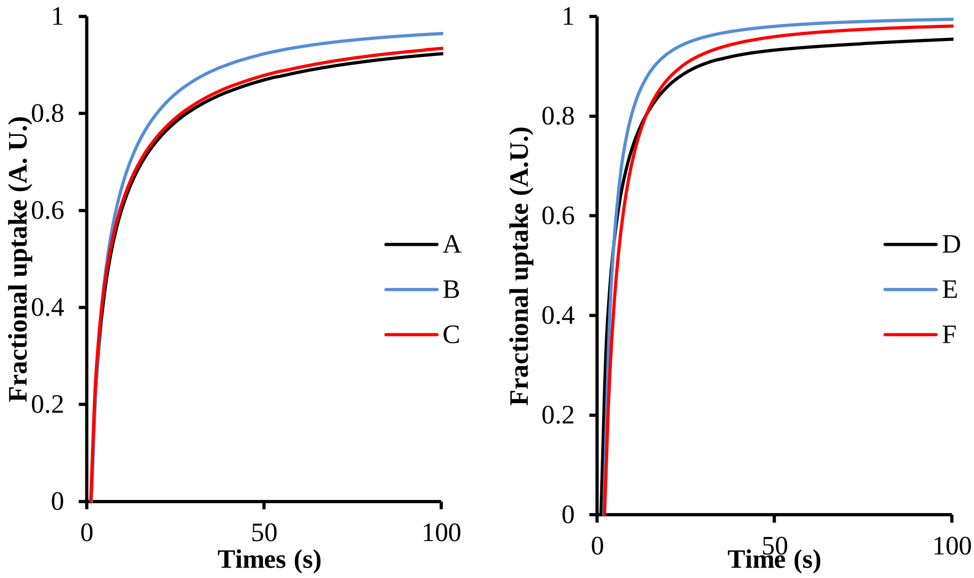

Figure 4.27. The fractional uptakes of adsorbents A-F collected at 313.5 K and 0.0014 P/P_0. All uptakes reach unity by 3000 seconds (not shown).

It is clear that TEPA based adsorbents have more rapid CO_2 adsorption than PEI based adsorbents. All adsorbents exhibit two stage adsorption kinetics with initial rapid CO_2 adsorption. This is followed by a region of slower adsorption where the CO_2 diffuses through the polymer. The activation energy of motion and viscosities measured earlier suggest that the rate of diffusion should be slower in the surfactant-amine mixtures. These kinetics show that this is not the case as the addition of SDS and TEA leads to an increase in the rate of CO_2 adsorption. Assuming the same products would be formed, this suggests that the presence of surfactants leads to an increased number of adsorption sites. The presence of surfactants could lead to a better dispersion of amine groups. This would lead to thinner films of amine at the surface which have been shown to react with CO_2 more readily [18, 30]. This can be related to the lower extent of pore blocking for surfactant included samples reported in Section 4.6.2. The incorporation of SDS into enhanced rates of uptake compared to TEA, which could be a reflected by the larger pore volume of the SDS adsorbents. These findings suggest that the presence of surfactant additives could be used to increase the rate of CO_2 adsorption of impregnated amine adsorbents.

4.18 Discussion

The findings from this chapter suggest that Davisil is a sensible support choice for solid adsorbents. Davisil supported polymeric amine adsorbents have a reduced CO_2 equilibrium adsorption capacity and slower rates of adsorption compared to their SBA-15 analogues. Nitrogen sorption in Section 4.6.2 showed that SBA-15 possess a higher BET surface area and pore volume that Davisil 60. Furthermore, STEM images show SBA-15 has a well ordered worm-like morphology compared to the disordered pore structure of the Davisil support. The reductions in the CO_2 adsorption uptakes are modest and the adsorption capacities below the required 3 mmol g^{-1}. However, given the lower cost and availability of commercial silica supports, these are likely to form the basis of practical solid sorbents.

The substitution of either PEI or TEPA for surfactants in the form of SDS or TEA led to improved adsorption uptakes under dry conditions. These increases in capacity are obtained with a lower amount of active amine component present in the sample, indicating that more amine sites are available to react. The effect of SDS led to increases in CO_2 uptake of 12.5 and 4.0 % for PEI and TEPA adsorbents respectively. The effect of TEA was lower leading to 5.2 and 2.3 % increases in CO_2 adsorption capacity for PEI and TEPA respectively. The increase in capacity are only slight, however the increases in amine efficiency are significant.

Others have argued that the role of additives may reduce the viscosity of the supported polymer phase, leading to faster CO_2 transit [11, 34]. In this study the use of saturation recovery ^{1}H SSNMR and shear viscosity measurements showed an increase in viscosity with surfactant additives. For purely liquid systems the Stokes-Einstein equation would predict that an increase in viscosity would lead to a decrease in the rate of diffusion of CO_2. This decreased rate of diffusion would also lead to a reduction in the equilibrium adsorption capacity of the adsorbents.

The increased amine efficiencies of TEPA adsorbents compared to PEI on identical supports could be rationalised by the lower viscosity of TEPA. As this study shows the presence of additives increases the viscosity of the amine and yields a greater CO_2 adsorption capacity. This is not what was expected and suggests that either a greater number of amine sites are accessible or that the enthalpy of adsorption is increasing.

DRIFTS conducted *in-situ* and post mortem ^{13}C SSNMR indicate that the same alkylammonium carbamate species is formed in all sorbents under dry adsorption conditions. DRIFTS found a small relative enhancement in the amount of carbamic acid found in surfactant containing samples E and F compared to single component adsorbent D. Carbamic acid is formed by the reaction of one CO_2 and one amine, stabilised through hydrogen bonding [14, 18]. The formation of such species occurs when there are no neighbouring amine groups to form a carbamate. When a large proportion of the amine groups are replaced with additives (B, C, E and F) the number of isolated sites that could form carbamic acid increase. As the reaction between an amine and carbamic acid is a 1:1 reaction the amine efficiency would increase. Carbamic acids have been shown to desorb at lower temperatures than carbamates [7]. However, the low intensity of the carbamic acid bands relative to the carbamate bands suggests that the fraction of carbamic species formed is low.

Redhead analysis of TPD spectra suggest that the enthalpy of desorption is between 85-90 kJ mol^{-1} consistent with alkylammonium carbamate formation found in other materials [35]. The T_{max} measured during TPD experiments decreased in the presence of surfactant additives suggesting that there were differences in the CO_2 desorption pathways. Studies have shown that the temperature required to desorb CO_2 from polymeric amine adsorbents is relative to the thickness of the amine polymer film [29]. This is caused by the CO_2 desorbing from one amine site and readsorbing on another, repeating this process until it reaches the exterior of the adsorbent. Hence a thinner film would lead to a faster rate of CO_2 diffusion. Similar to other studies two peaks were present in the TPD of sorbents A-F relating to strongly and weakly adsorbed CO_2. The ratio of these peaks was found to vary with the surfactant composition, with sorbents B and E desorbing CO_2 at predominantly lower temperatures. For sorbents C and F, the low temperature contribution may be due to the physisorption of CO_2 at TEA. The surfactant additives may lead to thinner, better dispersed amine films and thus limit the extent of readsorption during the desorption process leading to a lower apparent T_{max}. Furthermore the lower desorption temperatures could be due to the larger pore accessibility of SDS bearing adsorbents.

Investigations into the kinetics of CO_2 adsorption showed that the inclusion of surfactant additives led to an increase in the rate of adsorption. These differences suggest that the surfactant samples provide a greater number of accessible sites at a given adsorption temperature. The greatest enhancement in the kinetics was observed by SDS bearing sorbents B and E. The enhancement in the kinetics of adsorption correlates with the lower extent of pore blocking and larger average pore diameter of sorbents B and E. The presence of TEA did not appear to significantly influence the rate of uptake.

Many impregnated materials have pore blocking effects whereby the pore volume after impregnation is significantly lower than the difference between the volume of the organic component and that of the support [35]. This suggests the impregnation of the amine component leads to pore blockages, lower amine accessibility and hence lower adsorption capacities. The presence of the SDS additive appears to improve the dispersion of the PEI, leading to a greater fraction of available amine sites. The same trend was observed with sorbent E which exhibited a significant increase in pore size and pore volume.

For single component PEI the peak CO_2 adsorption temperature under 100 % CO_2 was 100 °C. The presence of surfactant additives in sorbents B and C led to a decrease in the peak adsorption temperature to 75 °C. This is concurrent with thinner layer of amine/surfactant mixture allowing a greater number of exposed amines sites at a given adsorption temperature. The adsorption of CO_2 at temperatures above 120 °C is less sensitive to the composition of adsorbents studied herein, with all adsorbents exhibiting low CO_2 adsorption capacities. The improved adsorption capacity of adsorbents B, C, E and F at 75 °C led to slight increases in the working capacity of adsorbents under purely temperature swing desorption.

The presence of water led to an increase in the equilibrium adsorption capacity of sorbents A-F. The enhancements in the presence of water appears to follow the trend TEA / amine polymer > single component amine polymer > SDS/amine polymer. Tertiary amine sites in TEA and PEI could react with CO_2

dissolved in water leading to an enhancement for these materials. However, the rate of carbonic acid formation in water is slow and as such the contributions from this mechanism of action are shown to be small. A possible explanation is a change in mechanism in the presence of water leading to the formation of bicarbonate species as oppose to alkylammonium carbonates. However such a species has only been shown to form at low surface coverages of amine and in small quantities [36].

It has been suggested that the water acts as a plasticiser reducing the viscosity of the amine, hence increasing the adsorption rate and equilibrium capacity of the adsorbents [11]. Water could disrupt hydrogen bonding interactions between the amine and the support, increasing the amount of accessible amines.

The two types of surfactant, SDS and TEA used in this study could mediate the interactions between water and impregnated amine polymer. The polar head groups of the SDS molecules could interact with the surface silanols or amine groups, extending a hydrophobic chain into the pore. This could limit the interactions between water and the amine leading to the lower increases of CO_2 adsorption capacity for SDS bearing adsorbents B and E in the presence of water. The presence of large amounts of hydrophobic alkyl chains within the pores of impregnated adsorbents has been shown to reduce the CO_2 uptakes in the presence of water [12]. This work by Sayari *et al*. incorporated a higher loading of hydrophobic group, suggesting a balance must be struck between improved amine dispersion and interactions with water. Conversely TEA can be regarded as hydrophilic and a significant proportion of this species could aid the interactions between water and the polymeric amine. This is reflected by adsorbents C and F exhibiting larger increases in the presence of water compared to the other adsorbents.

4.19 Conclusions

This Section has described an investigation into the behaviour of binary component PEI and TEPA adsorbents where 20% of the amine polymer has been replaced by SDS or TEA. It was found that the replacement of the amine polymer with SDS or TEA led to an increase in the amine efficiency, adsorption uptake and uptake kinetics. The presence of surfactant additives reduced pore blocking allowing a greater proportion of the amines sites to be accessible to CO_2.The nitrogen sorption data suggested that in the lower molecular weight TEPA based sorbent there was an increase in average pore size with surfactant addition. It was determined that the principal species formed under both dry and wet conditions was alkylammonium carbamates indicating that a change in adsorption mechanism was not underway. The use of saturation recovery SSNMR suggests that the viscosity of organic component increases with surfactant addition. This was confirmed by shear viscosity measurements suggesting that the surfactants led to a reduction in the amine viscosity.

The mode of action of SDS is to create a better dispersion of polymeric amine by mediating the interactions between the support and the polymeric amine. This leads to a greater proportion of thinner amine layers, which in turn yields enhanced amine accessibility and reduced desorption requirements. The presence of TEA appears to only marginally influence the dispersion of amine within the pores of the support. As such it offered little improvements in the rate of uptake compared to SDS. However, TEA was found to physisorb appreciable quantities of CO_2 at low temperatures and high CO_2 partial pressures. The presence of TEA led to increases in the adsorption capacity of CO_2 under humid adsorption conditions. This was attributed to its hydrophilic nature improving the uptake of water into the PEI film.

This chapter has uncovered the mode of action of two different surfactant additives. It is envisaged that this knowledge could be applied to numerous supports as a way of improving the amine dispersion and improving CO_2 adsorption behaviour.

4.20 References

1. M. B. Yue, L. B. Sun, Y. Cao, Z. J. Wang, Y. Wang, Q. Yu, J. H. Zhu, *Promoting the CO_2 adsorption in the amine-containing SBA-15 by hydoxyl group.* Microporous and Mesoporous Materials, 2008. **114**: p. 74.
2. D. S. Dao, H. Yamada, K. Yogo, *Large-Pore Mesostructured Silica Impregnated with Blended Amines for CO_2 Capture. Ind . Eng. Chem. Res.*, 2013. **52**: p. 13810.
3. C. M. Starkie, A. Amieiro-Fonseca, S. P. Rigby, T. C. Drage, E. H. Lester, *Surfactant Mediated CO_2 Adsorption; the Role of the Co-impregnation Species. Energy Procedia*, 2014. **63**: p. 2323.
4. A. Galarneau, H. Cambon, F. Di Renzo, F. Fajula, *True Microporosity and Surface Area of Mesoporous SBA-15 Silicas as a Function of Synthesis Temperature.* Langmuir, 2001. **17**: p. 8328.
5. V. Zeleňák, M. Badanićová, D. Halamová, J. Čejka, N. Murafa, G. Goerigk *Amine-modified ordered mesoporous silica: Effect of pore size on carbon dioxide capture.* Chemical Engineering Journal, 2008. **144**(2): p. 336-342.
6. D. Zhao, Q. Huo, J. Feng, B. F. Chmelka, G. D. Stucky, *Nonionic Triblock and Star Diblock Copolymer and Oligomeric Surfactant Syntheses of Highly Ordered, Hydrothermally Stable, Mesoporous Silica Structures. J. Am. Chem. Soc.*, 1998. **120**: p. 6024.
7. X. Xu, C. Song, J. M. Andresen, B. G. Miller, A. W. Scaroni, *Preparation and characterization of novel CO_2 "molecular basket" adsorbents based on polymer-modified mesoporous molecular sieve MCM-41. Microporous and Mesoporous Materials*, 2003. **62**: p. 29.
8. A. von Harpe, H. Peterson, Y. Li, T. Kissel, *Characterisation of commerical available and synthesized polyethyleneimines for gene delivery. J. Controlled Release*, 2000. **69**: p. 309.
9. J. H. Drese, S. Choi, R. P. Lively, W. J. Koros, D. J. Fauth, M. L. Gray, C. W. Jones, *Synthesis-Structure-Property Relationships for Hyperbranched Aminosilica CO_2 Adsorbents. Adv. Funct. Mater.*, 2009. **19**: p. 3821.
10. N. Linneen, R. Pfeffer, Y. S. Lin, *CO_2 capture using particulate silica aerogel immobilised with tetraethylenepentamine.* Microporous and Mesoporous Materials, 2013. **176**: p. 123.
11. D. S. Mebane, J. D. Kress, C. B. Storlie, D. J. Fauth, M. L.Gray, K. Li, *Transport, Zwitterions, and the Role of Water for CO_2 Adsorption in Mesoporous Silica-Supported Amine Sorbents. J. Phys. Chem. C*, 2013. **117**(26617).
12. A. Heydari-Gorji, Y. Belmbkhout, A. Sayari, *Polyethyleneimine-Impregnated Mesoporous Silica: Effect of Amine Loading and Surface Alkyl Chains on CO_2 Adsorption.* Langmuir, 2011. **27**: p. 12411.
13. *http://sdbs.db.aist.go.jp (National Institute of Advanced Industrial Science and Technology, Accessed 15.3.14.*
14. Z. Bacsik,, N. Ahlsten, A. Ziad, G. Zhao, A. E. Garcia-Bennett, B. Martín-Matute, N. Hedin,*Mechanisms and Kinetics for Sorption of CO2 on Bicontinuous Mesoporous Silica Modified with n-Propylamine.* Langmuir, 2011. **27**(17): p. 11118-11128.
15. Knöfel, C., et al., J. Phys. Chem. C, 2009. **113**: p. 21726.
16. X. Wang, V. Schwartz, J. C. Clark, X. Ma, S. H. Overbury, X. Xu, C. Song, *Infrared Study of CO2 Sorption over "Molecular Basket" Sorbent Consisting of Polyethylenimine-Modified Mesoporous Molecular Sieve.* J. Phys. Chem. C, 2009. **113**: p. 7260..
17. C. S. Srikanth, S .S. C. Chuang, *Infrared Study of Strongly and Weakly Adsorbed CO_2 on Fresh and Oxidatively Degraded Amine Sorbents.* J. Phys. Chem. C, 2013. **117**: p. 9196.

18. R. Sanz, G. Calleja, A. Arencibia, E. S. Sanz-Pérez, *Amino functionalized mesostructured SBA-15 silica for CO_2 capture: Exploring the relation between the adsorption capacity and the distribution of amino groups by TEM.* Microporous and Mesoporous Materials, 2012. **158**: p. 309.
19. J. Jeon, S. Kwak, *Variable-Temperature ^{7}Li Solid-State NMR Investigation of Li-Ion Mobility and Its Correlation with Conductivity in Pore-Filling Polymer Electrolytes for Secondary Batteries.* Macromolecules, 2006. **39**: p. 8027.
20. J. Wang, D. Long, H. Zhou, Q. Chen, X. Liu, L. Ling, *Surfactant promoted solid amine sorbents for CO_2 capture. Energy Environ. Sci.*, 2012. **5**: p. 5742.
21. F. A. Chowdhury, H. Yamada, T. Higashii, K. Goto, M. Onoda, *CO_2 Capture by Tertiary Amine Adsorbents: A Performance Comparison Study.* Ind . Eng. Chem. Res., 2013. **52**: p. 8323.
22. D. S. Mebane, J. D. Kress, C. B. Storlie, D. J. Fauth, M. L.Gray, K. Li, *Transport, Zwitterions, and the Role of Water for CO_2 Adsorption in Mesoporous Silica-Supported Amine Sorbents.* J. Phys. Chem. C, 2013. **117**: p. 26617.
23. R. Serna-Guerrero, E. Da'na, A. Sayari, *New Insights into the Interactions of CO_2 with Amine-Functionalized Silica. Ind . Eng. Chem. Res.*, 2008. **47**(23): p. 9406.
24. R. Serna-Guerrero, Y .Belmbkhout, A. Sayari, *Modeling CO_2 adsorption on amine-functionalized mesoporous silica: 1. A semi-empirical equilibrium model.* Chemical Engineering Journal, 2010. **161**: p. 173.
25. D. S. Dao, H. Yamada, K. Yogo, *Response Surface Optimisation of Impregnation of Blended Amines into Mesoporous Silica for High-Performance CO_2 Capture.* Energy & Fuels, 2015. **29**: p. 985.
26. X. Xu, C. Song, J. M. Andresen, B. G. Miller, A. W. Scaroni, *Novel Polyethyleneimine-Modified Mesoporous Molecular Sieve of MCM-41 Type as High Capacity Adsorbent For CO_2 Capture. Energy & Fuels*, 2002. **16**: p. 1463.
27. P. A. Redhead, *Thermal desorption of gases.* Vacuum, 1962. **12**: p. 203.
28. C. Knöfel, J. Descarpemtries, A. Benzaouia, V. Zeleňák, S. Mornet, P. L. Llewellyn, V. Hornebecq, *Functionalised micro-/mesoporous silica for the adsorption of carbon dioxide.* Microporous and Mesoporous Materials, 2006. **99**: p. 79.
29. W. C. Wilfong, C. S. Srikanth, S. C. Chuang, *In Situ ATR and DRIFTS Studies of the Nature of Adsorbed CO_2 on Tetraethylenepentamine Films.* ACS Appl. Mater. Interfaces, 2014. **6**: p. 13617.
30. S. A. Didas, M. A. Sakwa.-Novak, G. S. Foo, C. Sievers and C. W. Jones, *Effect of Amine Surface Coverage on the Co-Adsorption of CO and Water: Spectral Deconvolution of Adsorbed Species. J. Phys. Chem. Lett.*, 2014. **23**: p. 4194.
31. T. C. Drage, A. Arenillas, K. M Smith, C. E. Snape, *Thermal Stability of Polyethylenimine Based Carbon Dioxide Adsorbents and Its Influence on Selection of Regeneration Strategies.* Microporous and Mesoporous Materials, 2008. **116**: p. 504.
32. M. B. Yue, L. B. Sun, Y. Cao, Y. Wang, Z. J. Wang , J. H, Zhu, Efficent CO_2 Capturer Derived from As-Synthesized MCM-41 Modified with Amine. *Chem. -- Eur. J. 2008, 14, 3442*, 2008. **14**: p. 3442.
33. Y. Fan, Y. Labreche, R. P Lively, W. J. Koros, C. W. Jones, *Dynamic CO_2 Adsorption Performance of Internally Cooled Silica Supported Poly(ethylenimine) Hollow Fiber Sorbents.* AICHE J., 2014. **60**: p. 3878.
34. Y. G. Ko, S. S. Shin, U. S. Choi, *Primary, secondary, and tertiary amines for CO_2 capture: Designing for mesoporous CO_2 adsorbents.* Journal of Colloid and Interface Science, 2011. **361**: p. 594.
35. P. Bollini, N. A. Brunelli, S. A. Didas, C. W. Jones, *Dynamics of CO_2 Adsorption on Amine Adsorbents, 2. Insights into Adsorbnet Design.* Ind . Eng. Chem. Res., 2012. **51**: p. 15153.
36. S. A. Didas, M. A. Sakwa-Novak, G. S. Foo, C. Sievers and C. W. Jones, *Effect of Amine Surface Coverage on the Co-Adsorption of CO_2 and Water: Spectral Deconvolution of Adsorbed Species.* J. Phys. Chem. Lett., 2015. **5**: p. 4194.

CHAPTER FIVE

Hydrothermal stability of amine functionalized silica adsorbents

5.1 Introduction

The preceding chapter has shown that the CO_2 uptakes and kinetics of amine impregnated silica adsorbents can be improved by the addition of surfactants. Furthermore, a significant increase in the working capacity was observed implying a lower regeneration energy penalty. Impregnated amine polymers on silica supports can be considered a likely candidate material for post combustion capture systems. They exhibit high CO_2 adsorption capacities not adversely affected by the presence of water and can be regenerated under a range of conditions. In large scale power plants it seems sensible to use low grade steam to regenerate the adsorbents. The water and CO_2 mixture would be easy to separate yielding a stream of high purity CO_2. Only a small number of recent studies have considered the stability of solid adsorbents in the presence of steam or humid desorption conditions [1-4]. Within these reports deactivation has been attributed to amine leaching or reagglomerating in the pores of the support. Support degradation has also been shown to occur under aging of thin walled silica adsorbents in a sealed steam autoclave. The role of water on the deactivation pathway has not been thoroughly investigated. Considering that polyethyleneimines are water soluble and the lack of a formal covalent bond between the silica surface and impregnated amine polymers, one could anticipate that these adsorbents may be unstable over long timescales. This chapter investigates the mechanisms of amine functionalised silicas under humid adsorption and desorption conditions.

5.2 Adsorbents tested

The sorbents tested in this chapter and the abbreviations are given in Table 5.1. S-AP was prepared using the method outlined in Section 3.22 with all other adsorbents prepared using the procedure outlined in Section 3.20.

Table 5.1. The adsorbents used in this study.

Abbreviation	**Support**	**Amine**	**Organic loading (wt %)[a]**
S-PEI	Davisil 60	PEI 600[b]	32.9
S-TEPA	Davisil 60	TEPA[b]	32.8
S-PEI-H	Davisil 60	PEI 1800[b]	33.1
S-AP	Davisil 60	Amino propyl[c]	11.9
S-PEI-SP	Davisil 22	PEI 600[b]	32.8
S-PEI-LP	Davisil 150	PEI 600[b]	33.0

[a] Determined by TGA [b] functionalised by impregnation [c] covalently tethered.

5.3 Stability of impregnated amine sorbents over 100 dry CO_2 adsorption cycles

The stability of SBA-15 40 wt% TEPA and SBA- 15 40 wt% PEI under dry cycling conditions was investigated. These materials were characterised in Chapter 4. The sorbents were subjected to 100 cycles of adsorption under 100% CO_2 at 75 °C with regeneration conducted under N_2 at 120 °C (Figure 5.1). Pure CO_2 was chosen to better resolve the differences between fresh and aged adsorbents. Exposure to CO_2 results in mass gain, whilst changing to an inert flow and increasing the temperature to 120 °C leads to CO_2 desorption, evident by mass loss towards the mass of the dry, clean adsorbent. One hundred adsorption and desorption cycles led to a modest reduction in capacity for SBA-15 40 wt% PEI. The desorbed weight of SBA-15 40 wt% PEI increases with progressive cycles culminating in approximately 8.5 % of the CO_2 irreversibly adsorbed after 100 cycles.

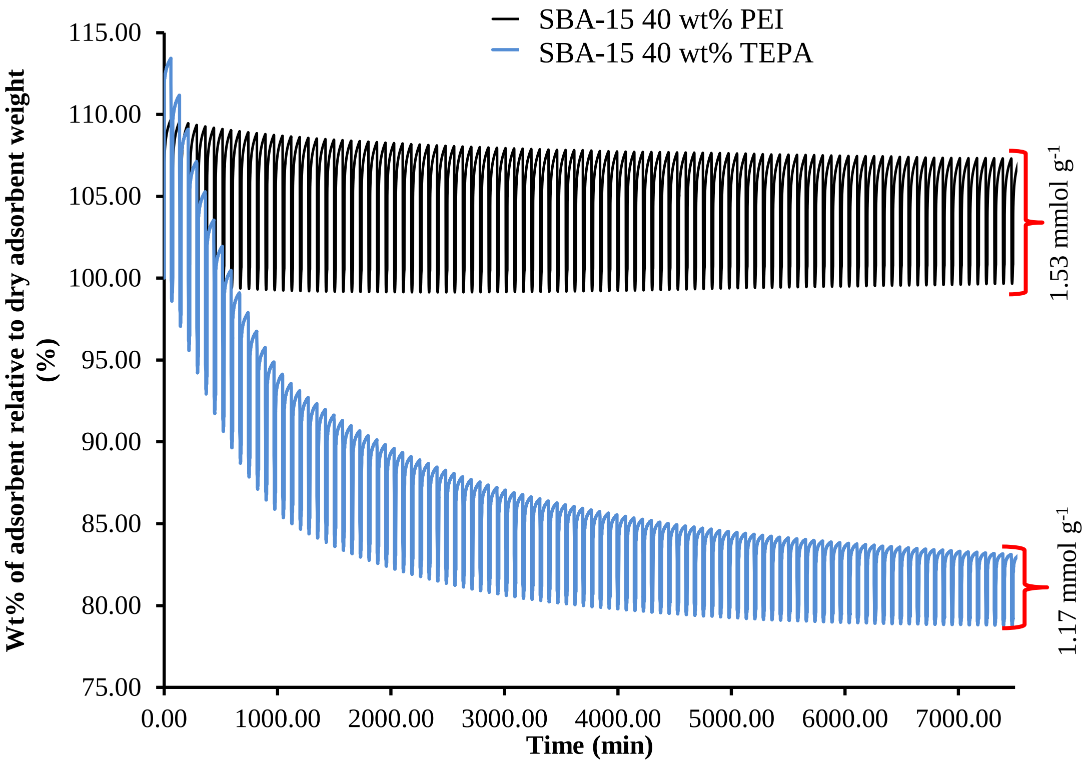

Figure 5.1. TGA mass profiles for SBA-15 40 wt% PEI and SBA-15 40wt% TEPA cycled between adsorption conditions (75 °C, 100% CO_2) and desorption conditions (120 °C, N_2). The initial adsorption capacities of SBA-15 40 wt% PEI and SBA-15 40 wt% TEPA were 2.46 and 3.21 mmol g^{-1} respectively.

The capacity of SBA-15 40 wt% PEI gradually reduced from 2.46 to1.56 mmol g^{-1} over successive cycles. This 36.8 % loss in CO_2 adsorption capacity is larger than which can be accounted for by urea formation alone. Akin to the increased diffusive resistance as the alkylammonium carbamate product formed during CO_2 adsorption onto PEI, the urea species could decrease the mobility amine polymer leading to a lower amine efficiency [5].

For SBA-15 40 wt% TEPA the desorbed mass of the adsorbent decreased with successive cycling. This is due to the impregnated amine evaporating from the porous support. These volatile losses do not follow a linear trend indicating not all amines are equivalent in the system. It is known that TEPA has a significant polydispersity featuring a proportion of triethlyenetetramine and pentaethylenhexamine (see Section 4). These species have lesser and greater volatilities than TEPA respectively. Furthermore, it is expected that the TEPA directly physisorbed onto the silica surface would require more energy to overcome the strong physisorption interaction, as opposed to TEPA located at the top of a multilayer. The reduction in CO_2 adsorption capacity for TEPA adsorbents was much greater than PEI sorbents with the former appearing uneconomical after only limited cycling. Evapouration of corrosive amines could be problematic when incorporated into a practical adsorption system. Regeneration at lower temperatures of TEPA adsorbents is possible, however this has been shown to take 2.5 times longer under an inert flow of nitrogen [6]. Regeneration using large amounts of sweep gas is impractical as it would require further CO_2 separation.

The degradation species of the sorbents under dry conditions was characterised by ^{13}C SSNMR with the CO_2 adsorbed from the final adsorption cycle (Figure 5.2). The peak at 164.5 ppm in SBA-15 40wt% PEI is assigned to alkylammonium carbamate, formed between two amine units and one CO_2 molecule. A second peak at 163 ppm is present which was assigned by Drage *et al.* as a thermally stable urea linkage [6]. The signal to noise ratio was much greater for SBA-15 40 wt% PEI than SBA-15 40 wt% TEPA due the increased retention of organic content. Asymmetrical peak broadening of the signal at 164.5 ppm is observed for SBA-15 40 wt% TEPA after 100 adsorption and desorption cycles, indicating the formation of a urea species.

Whilst there are an increasing number of reports of TEPA based adsorbents, it is demonstrated here and elsewhere that volatile losses of lower molecular weight TEPA adsorbents are significant under dry cycling conditions [7-9]. PEI adsorbents appear to offer enhanced stability under dry conditions, with a reduction in capacity attributed to urea formation [6]. The presence of water has been shown to inhibit the formation of urea [10]. This suggests that the principal deactivation of PEI and TEPA would be due to volatile losses.

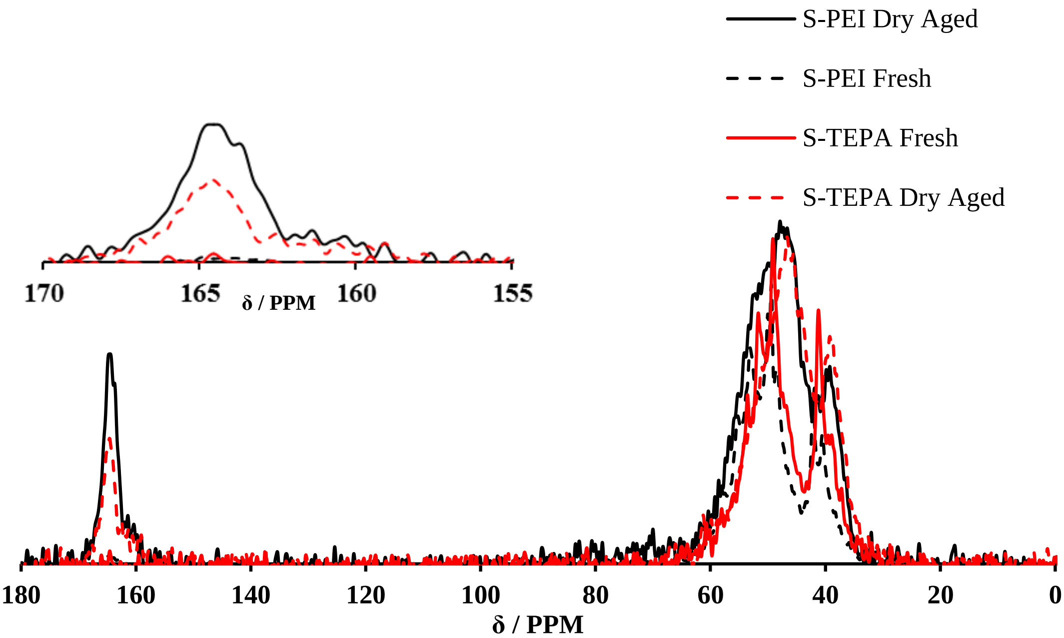

Figure 5.2. ^{13}C SSNMR MAS spectrum of SBA-15 40 wt% PEI and SBA-15 40wt% TEPA after cycling between 100 adsorption (75 °C, 100% CO_2, 60 min) and desorption (120 °C, N_2, 10 min) cycles. An expanded region of 155 – 170 ppm (inset).

5.4 Adsorbent stability under humid pseudo adsorption conditions

Regardless of whether steam regeneration is used to regenerate the adsorbents, solid adsorbents must be stable to water present in flue gas. The stability of the adsorbents, under pseudo-adsorption conditions of 10% H_2O / N_2 (1000 ml min^{-1}) at 75 °C for 24 h was investigated. A description of the experimental set up is given in Section 3.15. The influence of the molecular weight of the impregnated amine was investigated using the same batch of Davisil 60 support impregnated with 33 wt% of either TEPA (MW 189), PEI 600 (MW 600) or PEI 1800 (MW1800) denoted as S-TEPA, S-PEI, S-PEI-H respectively. Linear polyethyleneimines of any molecular weight were not studied as they exhibit poor CO_2 adsorption uptakes [11]. Larger molecular weight polyethlyeneimine polymers were not studied owing to their sluggish CO_2 adsorption properties and difficulties impregnating them into porous solids [12].

In a practical system the adsorbent would be exposed to the CO_2 rich stream until breakthrough is obtained, a process faster than the time taken to reach equilibrium. Assuming a solid residence time of 13 s for a fluidised bed adsorption system, 24 h of aging equates to the equivalent of 6646 adsorption cycles [13].

5.4.1 Stability of S-PEI under humid pseudo adsorption conditions

Aging of the S-PEI in the presence of 10% H_2O / N_2 (1000 ml min^{-1}) at 75 °C for 24 h led to marked decreases in the CO_2 adsorption capacity (Figure 5.3). Decreases in adsorption capacity were present after the first hour of aging. The equilibrium adsorption capacity further decreased with progressive aging, losing 37 % of its adsorption capacity after 24 h of aging. The amine efficiency decreased with aging as only part of the reduction in CO_2 adsorption capacity could be attributed to losses in amine loading observed by TGA (Table 5.2). Isothermal first order and second order kinetic models could not accurately represent the adsorption uptakes. To aid comparison of the kinetics with aging, fractional uptakes with aging are given in Figure 5.5. The adsorption halftime ($T_{1/2}$) increases with aging, suggesting that the amines in the pores are more accessible. However the lower adsorption capacity after aging suggests that a number of amine sites are completely inaccessible.

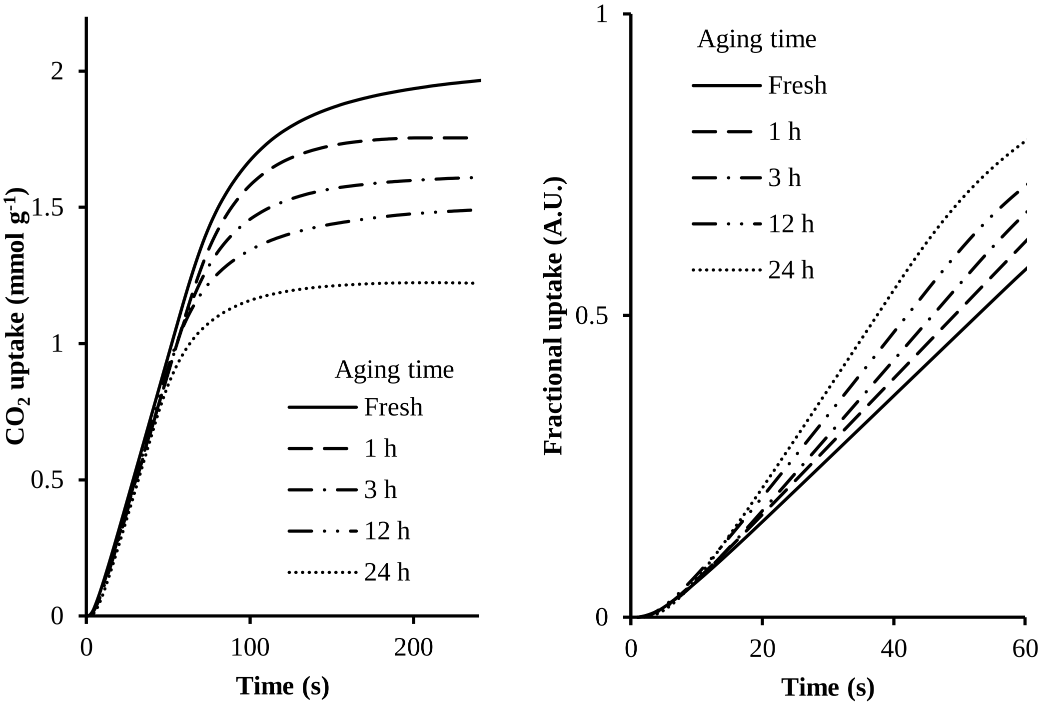

Figure 5.3. CO_2 adsorption uptakes of S-PEI at 75 °C under 15% CO_2, 10% H_2O/N_2 before and after under aging 10% H_2O/N_2 at 75 °C for 24 h (left). The change in fractional uptake with aging (right).

There appears to be no change in the amine structure as shown by the DRIFTS spectra before and after adsorption (Appendix A6). The bands at 3418, 3350 cm^{-1} correspond to the free primary and secondary amines with the bands at 2939, 2818 cm^{-1} attributed to the C-H stretches of the hydrocarbon backbone. The presence of a urea species at 1658 and 1560 cm^{-1} were not observed suggesting urea formation was not present. It has been suggested that the urea species can be hydrolysed in the presence of water to regenerate the amine [14].

Table 5.2. The influence of aging under pseudo-adsorption conditions on S-PEI.

Aging time (h)	**CO_2 capacity (mmol g^{-1})**	**% Original CO_2 uptake (%)**	**Adsorption $T_{1/2}$ (s)**	**Amine loading (wt. %)**	**Amine efficiency (a.u.)**
Fresh	1.96	100	50	32.9	0.25
1	1.75	89	43	N.D.[a]	N.D.[a]
3	1.60	81	41	N.D.[a]	N.D.[a]
12	1.49	76	36	N.D.[a]	N.D.[a]
24	1.22	62	28	30.1	0.17

[a] The sample was not removed from the reactor during the analysis, as such the organic content could not be determined.

Changes to the porous structure of the adsorbent were characterised by nitrogen sorption with the isotherms before and after aging under adsorption conditions presented in Figure 5.4. After aging in 10% H_2O / N_2 at 75 °C for 24 h the BET surface area and accessible pore volume increased. The extent of pore blocking before and after aging was determined and the results presented in Table 5.3. Aging led to an increase in pore volume present at 77 K. From close inspection of Figure 5.6 it can be seen that the relative pressure points of the isotherms overlay between 0 - 0.75 P/P_0. This suggests that the amine within these pores is unaffected by aging. However an increase in nitrogen adsorption is noted above 0.75 P/P_0 suggesting that aging has opened up larger pores that were previously filled by PEI. This increased accessibility after aging led to the increased rate of uptake as CO_2 diffusion is related to pore accessibility.

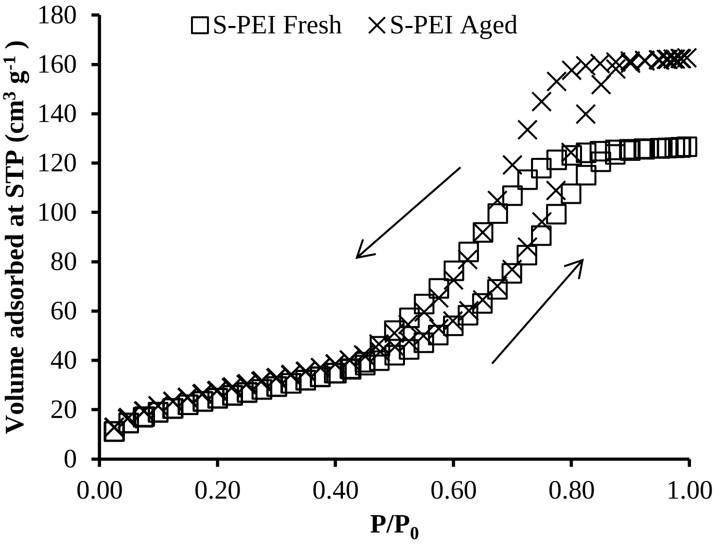

Figure 5.4. Nitrogen sorption isotherms of S-PEI before and after aging under 10% H_2O/ N_2 for 24 h at 75 °C.

Table 5.3. Differences in porosity of fresh and adsorption aged S-PEI.

Sorbent	BET Surface area (m^2 g^{-1})	BET C constant (a.u.)	Pore Volume (cm^3 g^{-1})	Inaccessible P_v (%)
S-PEI-Fresh	96.7 +/- 7.0	30.0	0.196 +/- 0.01	56.0
S-PEI-Aged	107 +/- 6.9	33.4	0.250 +/- 0.01	48.2

Figure 5.5 shows the BJH PSD of S-PEI before and after aging, highlighting an increase in the volume of pores between 8-10 nm. Coupled with the observed reductions in organic loading, it could be suggested that the PEI is removed from the largest pores first. As only a small proportion of amine is lost the amine could have reagglomerated into the smaller pores of the adsorbent. Amine agglomerated within the smaller pores of the adsorbent would be less accessible and hence a lower CO_2 adsorption capacity observed. This is similar to work by Hammache *et al.* who suggested that the reduction in capacity was caused by reagglomeration of the amine to yield pore blockages [3]. However the study by Hammache *et al.* did not observe leaching of the amine. In this work the adsorbents were tested for longer periods of time, with increased temperatures and with a greater gas flow rate. This suggests the amine may first reagglomerate before it leaches from the pores of the adsorbent.

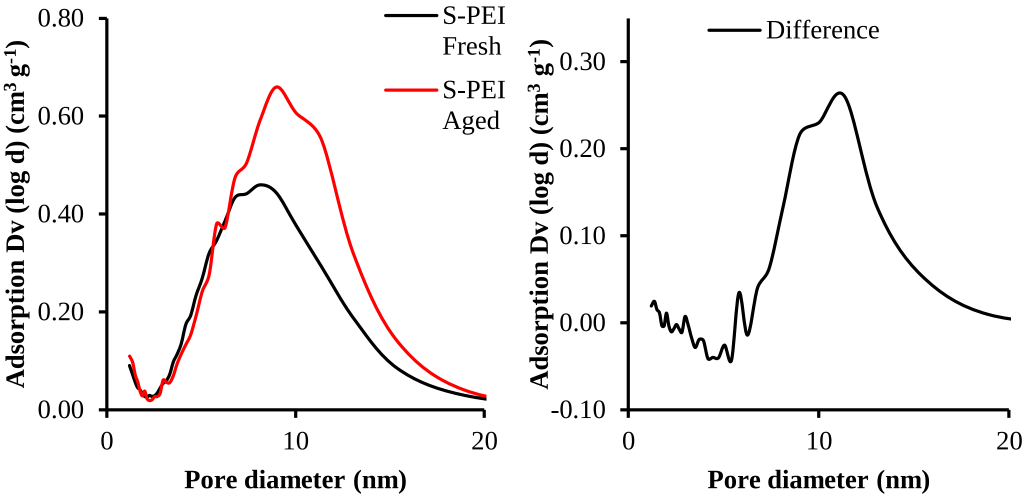

Figure 5.5. BJH PSD of S-PEI before and after pseudo-adsorption aging (left) The difference between the BJH adsorption pore size distributions with aging (right).

5.4.2 Stability of S-TEPA under humid pseudo adsorption conditions

Numerous authors have utilised TEPA based adsorbents, noting a much greater CO_2 adsorption capacity when compared to PEI based adsorbents [7, 15, 16]. Work from Chapter 5 indicated that lower molecular weight amines led to a lower extent of pore blocking allowing a greater proportion the amines to react. Furthermore, TEPA is less viscous than PEI enabling faster CO_2 transit through the polymer. Exposure of S-TEPA under conditions of 10% H_2O / N_2 at 75 °C for 24 h led to a reduction in the CO_2 adsorption capacities by 36 % (Figure 5.6, left). S-TEPA appeared more stable than S-PEI, suggesting that the additional desorption temperature ramps in the testing of S-PEI may influence the stability. Comparing the fractional uptakes of the S-TEPA before and after aging it is clear that the aged adsorbent had a faster rate of adsorption (Figure 5.6, right).

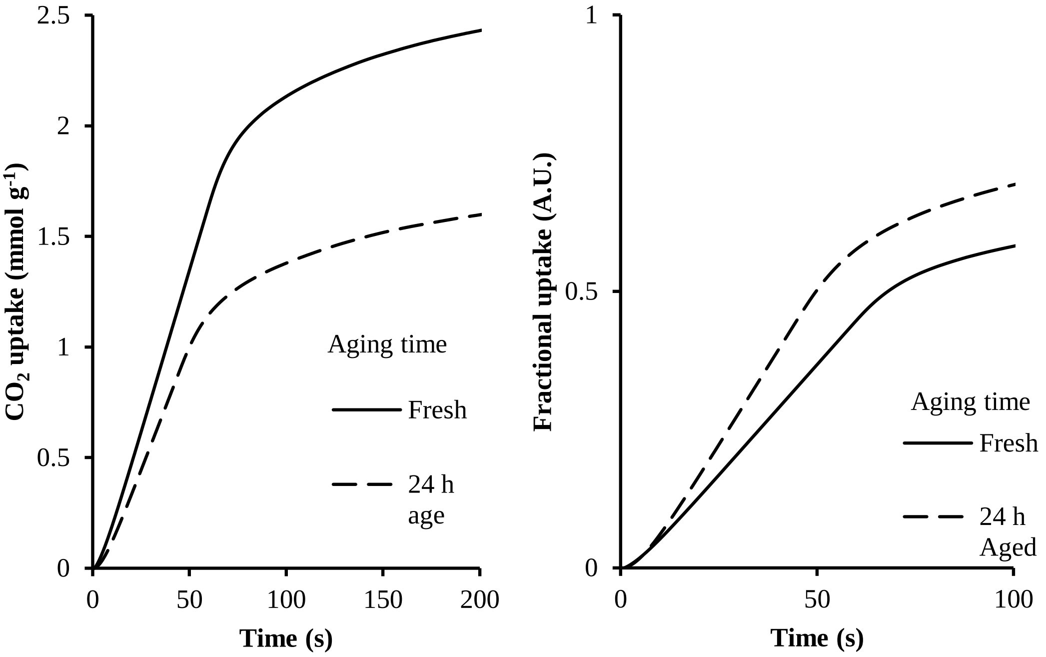

Figure 5.6. CO_2 adsorption uptakes of S-TEPA at 75 °C under 15% CO_2, 10% H_2O / N_2 before and after under aging 10% H_2O / N_2 at 75 °C for 24 h (left). The change in fractional uptake with aging (right).

The amine efficiency reduces from 0.30 to 0.23 after aging suggesting that increasing amounts of the amine are inaccessible after aging. The amount of amine loading was found to reduce significantly after the aging experiment (Table 5.4). This also correlated with a reduction in the adsorption $T_{1/2}$ suggesting that the fraction of amines remaining were more accessible.

DRIFTS spectroscopy of S-TEPA after aging indicated no change in chemical structure of the amine compared to the fresh amine adsorbent (Appendix A7). Nitrogen sorption isotherms of S-TEPA before and after aging show an increase in surface area, pore volume and average pore size with aging (Figure 5.7). This coincides with a loss of 14% of the impregnated TEPA from within the pores of the support. The extent of pore blocking was found to decrease after aging indicating that a greater proportion of the support was accessible to nitrogen at 77 K (Table 5.5). This correlates with the increase in adsorption kinetics observed but suggests that segments of the amine are agglomerated together as the amine efficiency decreases.

Table 5.4. The influence of aging under pseudo-adsorption conditions on S-TEPA.

Aging time (h)	**CO_2 capacity (mmol g^{-1})**	**% Original CO_2 uptake (%)**	**Adsorption $T_{1/2}$ (s)**	**Amine loading (wt. %)**	**Amine efficiency (a.u.)**
Fresh	2.32	100	63	32.8	0.30
24	1.53	64.8	50	28.3	0.22

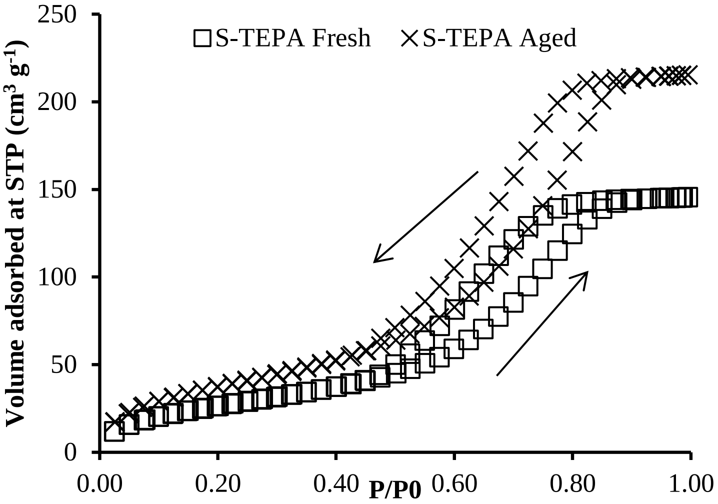

Figure 5.7. Nitrogen sorption isotherms of S-TEPA before and after aging under 10% H_2O / N_2 for 24 h at 75 °C.

Table 5.5. Differences in porosity of fresh and adsorption aged S-TEPA.

Sorbent	**BET Surface area (m^2 g^{-1})**	**BET C constant (a.u.)**	**Pore volume (cm^3 g^{-1})**	**Inaccessible P_v (%)**
S-TEPA-Fresh	103 +/- 7.4	30.0	0.23 +/- 0.01	50.7
S-TEPA-Aged	146 +/- 10.2	30.9	0.34 +/- 0.02	32.9

The BJH adsorption pore size distributions of S-TEPA before and after aging are given in Figure 5.8. In contrast to S-PEI, aging of S-TEPA gained porosity across all possible pore sizes. The loss of TEPA from the smaller pore sizes could be attributed to the increased volatility of the TEPA species.

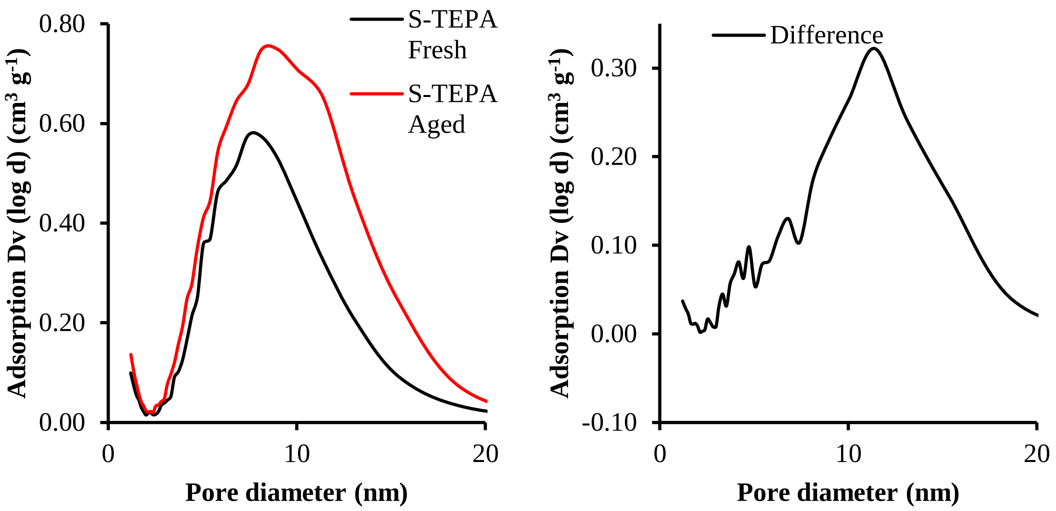

Figure 5.8. BJH PSD of S-TEPA before and after pseudo-adsorption aging (left) The difference between the BJH adsorption pore size distributions with aging (right).

5.4.3 Stability of S-PEI-H under humid pseudo adsorption conditions

The influence of aging under adsorption conditions of larger molecular weight PEI 1800 was investigated. Porous silica impregnated with PEI 1800 have shown increased stability under thermal aging experiments compared to PEI 600 [17]. The increased viscosity of PEI 1800 was found to restrict diffusion of CO_2 through the polymer. Exposure of S-PEI–H to 10 % H_2O / N_2 at 75 °C for 24 h led to a 3 % reduction in CO_2 adsorption capacity (Figure 5.9). Negligible changes in amine efficiency were observed suggesting S-PEI-H was stable under pseudo adsorption aging conditions (Table 5.6). Organic analysis confirmed no change in amine structure or loss of organic species (Appendix A8).

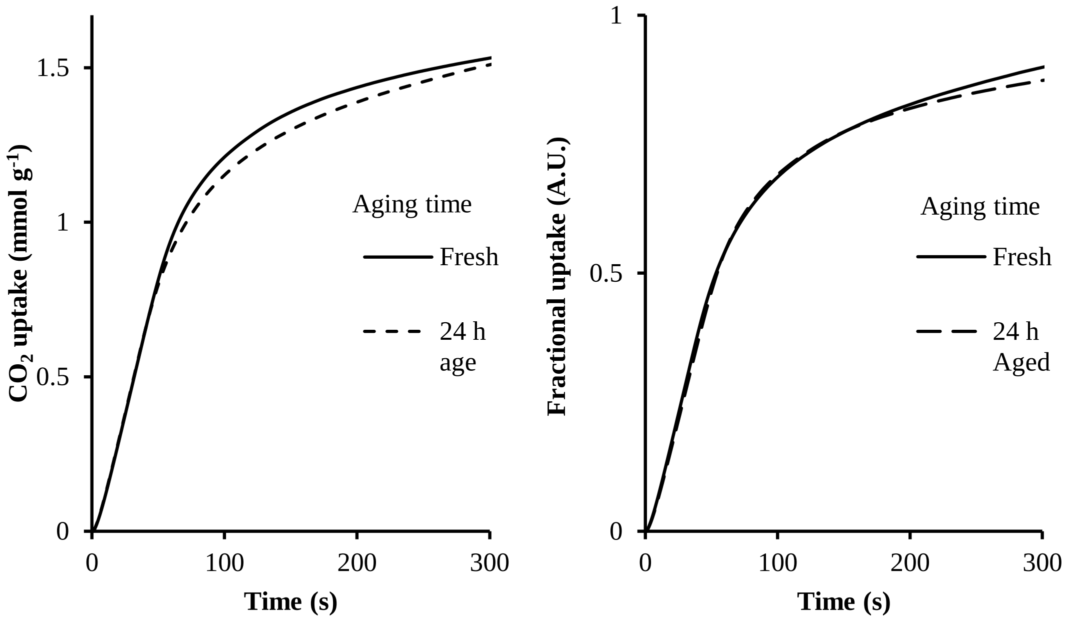

Figure 5.9. CO$_2$ adsorption uptakes of S-PEI-H at 75 °C under 15% CO$_2$, 10% H$_2$O/N$_2$ before and after under aging 10% H$_2$O / N$_2$ at 75 °C for 24 h (left). The change in fractional uptake with aging (right).

Table 5.6. The influence of aging under pseudo-adsorption conditions on S-PEI-H.

Aging time (h)	CO$_2$ capacity (mmol g^{-1})	% Original CO$_2$ uptake (%)	Adsorption T$_{1/2}$ (s)	Amine loading (wt. %)	Amine efficiency (a.u.)
Fresh	1.67	100	54	33.1	0.21
24	1.62	97	57	32.9	0.21

Changes in the porous structure of S-PEI-H before and after aging were investigated using nitrogen sorption (Figure 5.10). Fresh S-PEI-H exhibits cavitation evidenced by the kink in the desorption branch at 0.43 P/P$_0$. These inkbottle pores are removed after aging leading to an increase in average pore size of the adsorbent, suggesting that the amine had reagglomerated during aging. Aging under adsorption conditions led to a reduction in surface area from 144 to 110 m^2 g^{-1}, with marginal changes in pore volume observed (table 5.7). The BET C constant increased from 27.5 to 31.5 suggesting that a change in the amine coverage of the silica surface occurred.

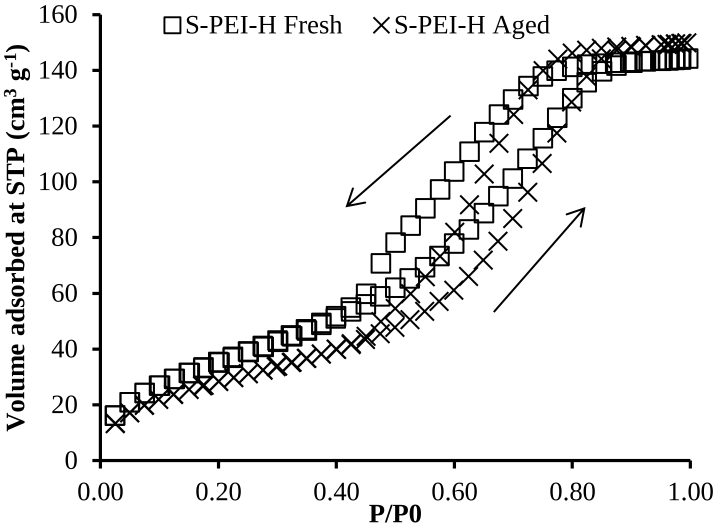

Figure 5.10. Nitrogen sorption isotherms of S-PEI-H before and after aging under 10% H_2O / N_2 for 24 h at 75 °C.

Table 5.7. A summary of the porosity properties of S-PEI-H after aging.

Sorbent	BET Surface area (m^2 g^{-1})	BET C constant (a.u.)	$V_{meas.}$ (cc g^{-1})	Inaccessible P_v (%)
S-PEI-H-Fresh	141 +/- 9.9	27.5	0.22 +/- 0.01	57.2
S-PEI-H-Aged	110 +/- 7.59	31.5	0.23 +/- 0.02	56.2

The organic loading remained constant before and after aging suggesting that no leaching is occurring. The extent of pore blocking remains the same between the two samples as this factor only takes into account the total pore volume of the adsorbent and the volume of the amine. The BJH adsorption pore size distribution is given in Figure 5.11, showing a reduction in the volume of pores below 5.4 nm followed by an increase in the volume of pores above 5.4 nm. This suggests that the amine has re-agglomerated from the largest pores into the smallest pores of the adsorbent.

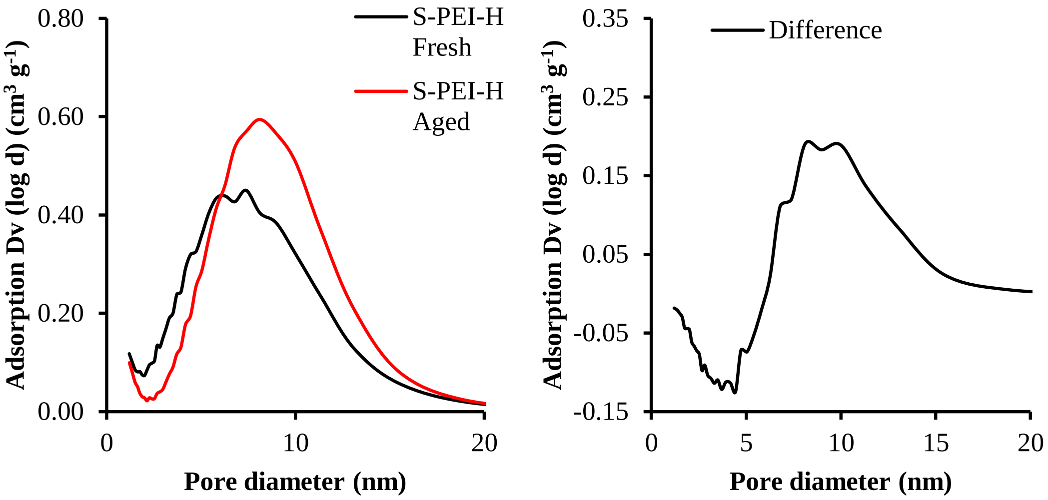

Figure 5.11. BJH PSD of S-TEPA before and after pseudo-adsorption aging (left) The difference between the BJH adsorption pore size distributions with aging (right).

5.5 The influence of pore size on the adsorbent stability under humid pseudo adsorption conditions.

The support has been shown to play a crucial role in amine accessibility and CO_2 adsorption capacities [18]. To investigate the role of pore size in sorbent stability, Davisil 22 and Davisil 150 silicas were used as supports for PEI 600. The properties of the supports used in the study are given in Table 5.8 and full isotherms are presented in Appendix A9. These materials possess a similar disordered pore structure to Davisil 60 with differences in pore sizes and pore volumes. The particle size was kept constant at 250-355 µm throughout this study.

Table 5.8. Properties of the supports used in this study.

Support	Surface area (m^2g^{-1}) [a]	Average pore size (nm)	Pore volume (cc g^{-1})	Particle size (µm)
Davisil 22	702.2[a]	2.6[b]	0.43+/-0.02	250-355
Davisil 60	516.4+/-14 [c]	8.2[d]	0.79+/-0.02	250-355
Davisil 150	288.6+/-7.2[c]	18.6[d]	1.06+/-0.02	250-355

[a] determined using T plot micropore analysis [b] Determined using DFT using N_2 at 77 K on silica (cylinder pore, NLDFT equilbrium model, the fitting error was less than 1% [c] BET surface areas with C constants of 83.8 and 91.2, following the order of the table. [d] BJH PSD.

5.5.1 Stability of S-PEI-LP under humid pseudo adsorption conditions

The CO_2 adsorption capacity of S-PEI-LP was greater than that of S-PEI in part to the greater amine accessibility provided by the larger pore sized support.

Larger pore silicas have enhanced amine accessibility over their small pore analogues facilitating a greater equilibrium CO_2 adsorption capacity [19]. Aging of S-PEI-LP under adsorption conditions led to a modest reduction in the CO_2 adsorption capacity (Figure 5.12, Table 5.9). The overall rate of adsorption does not appear to change significantly after aging despite a reduction in the amine loading present in the sample.

There was no change in chemical structure present during DRIFTS analysis suggesting no chemical degradation of the amine (Appendix A10). The porous structure of the adsorbent before and after aging was completed with nitrogen sorption with isotherms of the fresh and aged S-PEI-LP given in Figure 5.13.

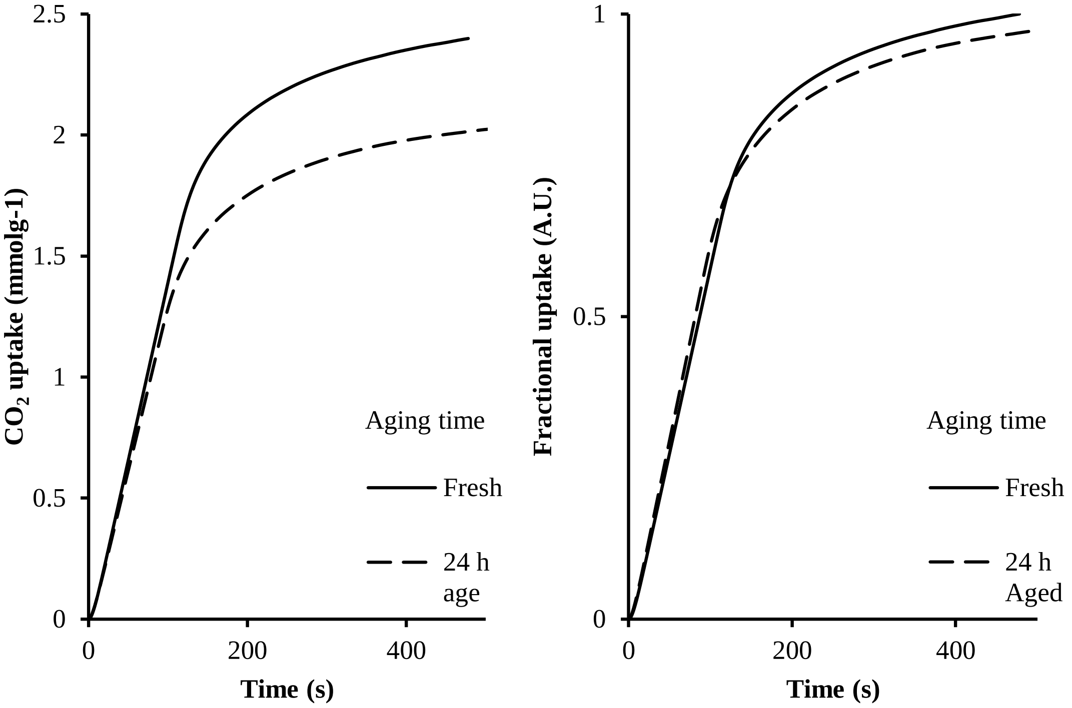

Figure 5.12. CO_2 adsorption uptakes of S-PEI-LP at 75 °C under 15% CO_2, 10 % H_2O / N_2 before and after under aging 10%H_2O / N_2 at 75 °C for 24 h (left). The change in fractional uptake with aging (right).

Table 5.9. The influence of aging under pseudo-adsorption conditions on S-PEI-LP.

Aging time (h)	CO_2 capacity (mmolg^{-1})	% Original CO_2 uptake (%)	Adsorption $T_{1/2}$ (s)	Amine loading (wt. %)	Amine efficiency (a.u.)
Fresh	2.39	100	93	33.0	0.30
24	2.07	86.6	91	29.1	0.30

The general features and appearance of the isotherms appear similar suggesting no significant changes in the porous structure occur. A slight increase in pore volume could be evidenced during aging, which can be attributed to the loss of amine from the support. Negligible changes in the extent of pore blocking occur after aging suggesting that that the loss of capacity is attributed to the fraction of amine lost through leaching with no amine agglomeration present is the sample (Table 5.10).

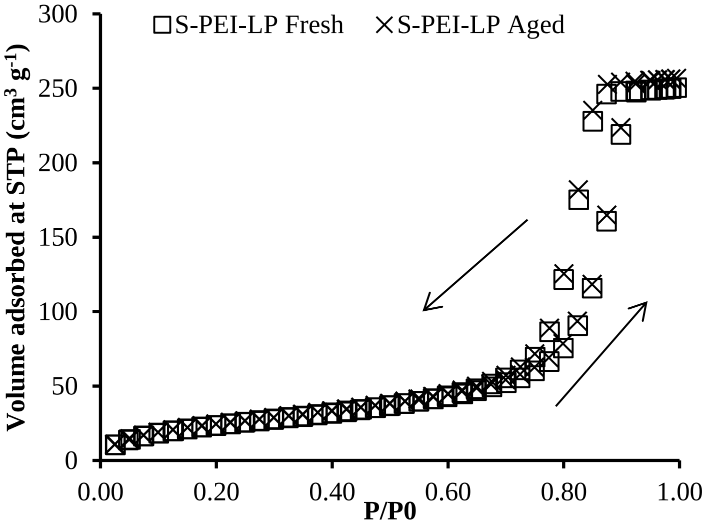

Figure: 5.13. Nitrogen sorption isotherms of S-PEI-H before and after aging under 10% H_2O / N_2 for 24 h at 75 °C.

Table 5.10. A summary of the porosity properties of S-PEI-LP after aging.

Sorbent	BET Surface area (m^2 g^{-1})	BET C constant (a.u.)	Pore volume (cm^3 g^{-1})	Inaccessible P_v (%)
S-PEI-LP-Fresh	91 +/- 5.7	35.0	0.38 +/- 0.02	16.8
S-PEI-LP-Aged	94 +/- 6.1	33.8	0.39 +/- 0.02	14.5

5.5.2 Stability of S-PEI-SP under humid pseudo adsorption conditions

As observed for many smaller pore supports, S-PEI-SP yielded a lower equilibrium CO_2 adsorption capacity and adsorption kinetics than its larger pore analogues [20, 21]. Part of this could be attributed to the high loading of amine in a support with little pore volume, leading to saturation of the support. S-PEI-SP appeared stable under aging under 10% H_2O / N_2 at 75 °C for 24 h with a marginal reduction in CO_2 adsorption capacity observed (Figure 5.14). The adsorption uptake of S-PEI-SP appeared to show a large a large linear region which could be due to the plug flow of CO_2 through the bed with little mass transit into the particles. No discernible changes in uptake kinetics or amine efficiency were observed after aging.

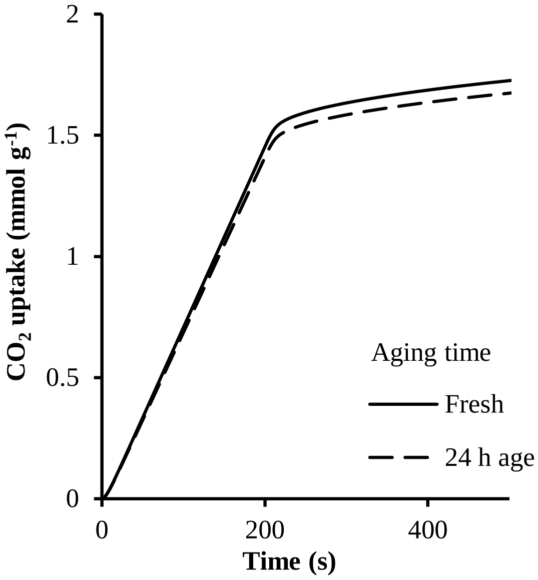

Figure 5.14. CO_2 adsorption uptakes of S-PEI-LP at 75 °C under 15% CO_2, 10 % H_2O / N_2 before and after under aging 10% H_2O / N_2 at 75 °C for 24 h.

DRIFTS analysis confirmed that the amine structure was unaltered during the course of the aging experiment (Appendix A11). The nitrogen adsorption isotherms of the sorbent yielded an essentially non-porous material at 77 K for both fresh and adsorption aged material (Appendix A12). This is consistent with literature reports of impregnated small pore adsorbents with pore blockages caused by the impregnation of amines [15]. The measured pore volume of ~0.01 cm^3 g^{-1} suggested that the majority of the porous nature of the material was inaccessible (Table 5.11). The organic loading of the material decreased by 3.2%, which could be attributed to amine being removed from the surface of the support. It appears that the pores were blocked with amine inhibiting the intrusion of water inside the pores of the adsorbent.

Table 5.11. Changes in amine accessibility for S-PEI-SP before and after aging.

Sorbent	Inaccessible P_V (%)	$V_{meas.}$ ($cm^3\ g^{-1}$)	$V_{support}$ ($cm^3\ g^{-1}$)	$V_{organic}$ ($cm^3\ g^{-1}$)
S-PEI-SP	95	0.01	0.55	0.34
S-PEI-SP Aged	95	0.01	0.55	0.33

5.6 Stability of covalently tethered S-AP under pseudo adsorption conditions

The stability of covalently tethered amines was investigated using aminopropyl functionalised silica (S-AP). Covalently tethered amines should possess greater stability, with degradation only possible from chemical deactivation or structural collapse of the support [4]. Aging of S-AP under 10% H_2O / N_2 at 75 °C for 24 h led to negligible changes in the CO_2 uptake (Figure 5.15). Nitrogen sorption of the aged adsorbent yielded no significant changes in pore structure, pore size or pore volume (Figure 5.16). Organic analysis before and after aging suggested that the organic component was not lost after aging. DRIFTS showed no change in amine structure after aging (Appendix A13).

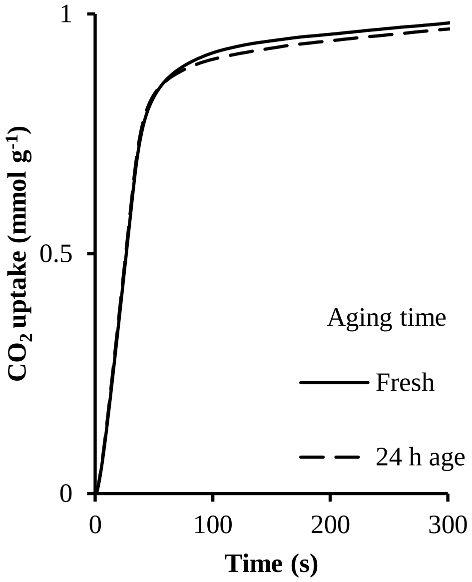

Figure 5.15. CO_2 adsorption uptakes of S-PEI-LP at 75 °C under 15 % CO_2, 10% H_2O / N_2 before and after under aging 10% H_2O / N_2 at 75 °C for 24 h.

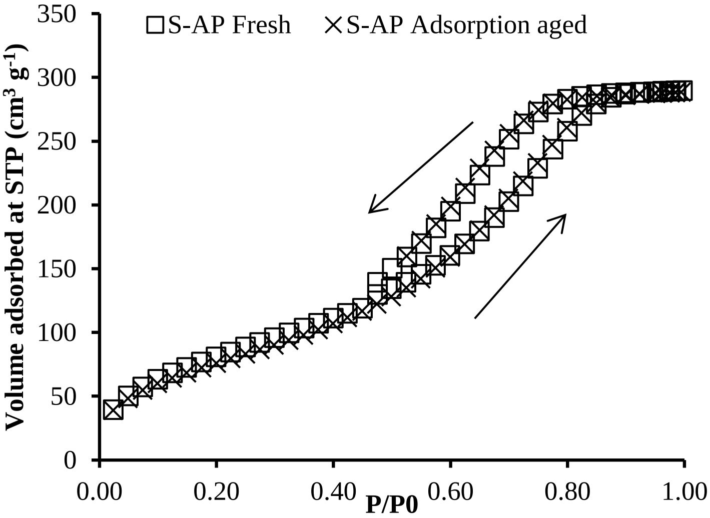

Figure 5.16. Nitrogen sorption of S-AP before and after aging under 10% H_2O / N_2, 75 °C for 24 h.

Table 5.12. A summary of the porosity properties of S-AP after aging.

Sorbent	BET Surface area (m^2 g^{-1})	BET C constant (a.u.)	Pore volume (cm^3 g^{-1})	Inaccessible P_v (%)
S-PEI-AP-Fresh	331 +/- 22.2	45.2	0.45 +/- 0.02	32.4
S-PEI-AP-Aged	315 +/- 16.1	43.4	0.44 +/- 0.02	33.9

5.7 Adsorbent stability under steam regeneration conditions

The stability of the adsorbents under steam regeneration conditions was conducted using a fixed bed reactor with 0.1g of sample exposed to 66% H_2O / He (100 ml min^{-1}) at 130 °C for 8 h. A description of the experimental set up is given in Section 3.16. The adsorption capacity of the adsorbents before and after desorption aging was conducted *ex-situ* using TGA under 15 % CO_2 at 75 °C (see Section 3.4). Assuming that steam regeneration takes 3 minutes for a 90% capture rate this experiment represents 160 steam regeneration cycles [22].

5.7.1 Stability of S-PEI under steam regeneration conditions

Steam aging of S-PEI led to a drastic loss in CO_2 adsorption capacity from 1.79 to 0.95 mmol g^{-1}, at which point these adsorbents become uneconomical (Figure 5.17). The rate of adsorption was faster with aged S-PEI attributed to the enhanced accessibility brought about by the loss of amines within the pores of the adsorbent. Analysis by TGA suggested a significant reduction in inorganic loading consistent with amine leaching form the pores of the adsorbent (Table 5.13).

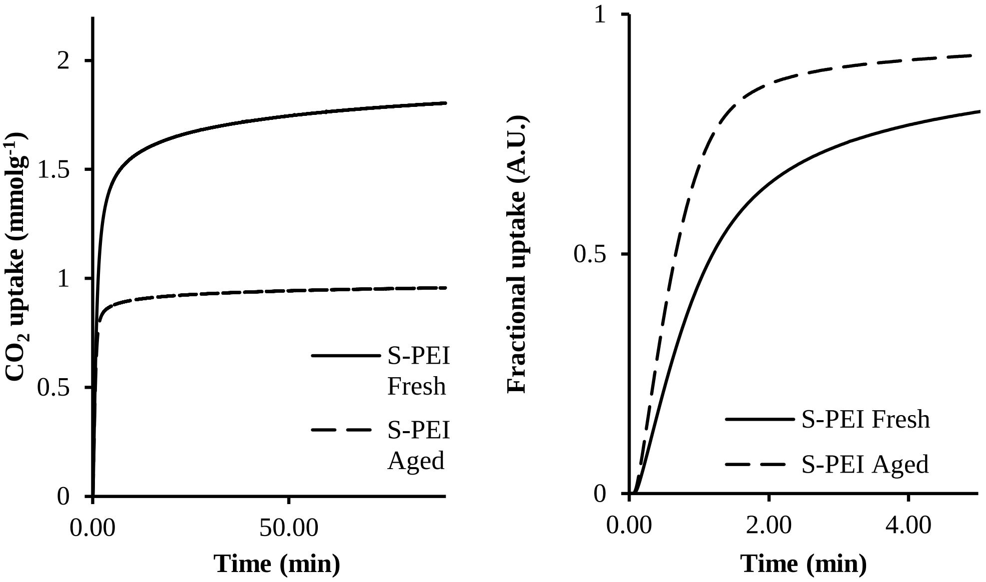

Figure 5.17. CO$_2$ uptakes for S-PEI before and after ageing under steam regeneration conditions (left). Fractional order uptakes of S-PEI before and after aging under steam regeneration conditions (right).

Table 5.13. The influence of steam regeneration on S-PEI.

Aging time (h)	CO$_2$ capacity (mmol g^{-1})	% Original CO$_2$ uptake (%)	Amine loading (wt. %)	Amine efficiency (a.u.)
Fresh	1.79	100	32.9	0.23
8	0.95	33	25.0	0.16

The origin of the degradation in S-PEI under pseudo-steam regeneration conditions was investigated by DRIFTS with no change in the chemical species ascertained (Appendix A6). A comparison of the nitrogen sorption data of the fresh and desorption aged S-PEI is presented in Figure 5.18.

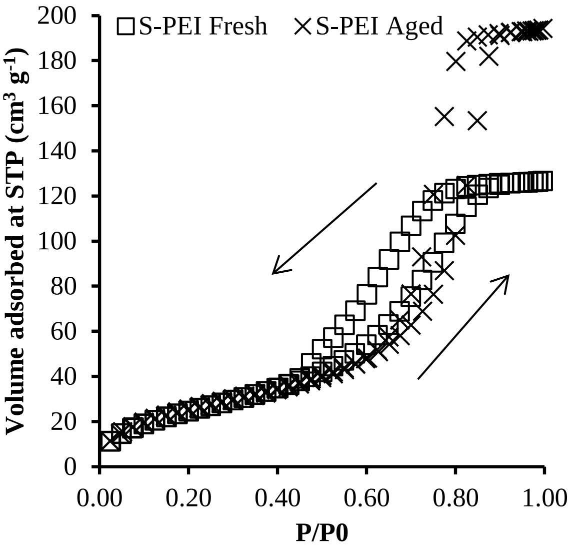

Figure 5.18. Nitrogen sorption isotherms of S-PEI- before and after aging under 66% H_2O / N_2 for 8 h at 130 °C.

Upon aging S-PEI under 66% H_2O / N_2 at 75 °C for 8 h there is a decrease in BET surface area, coupled with an increase in pore volume. The extent of pore blocking was significantly reduced after aging attributed to the loss of amine. (Table 5.14) The BJH PSD showed an increase in volume of pores above 8 nm S-PEI after aging, suggesting PEI leaching from the largest pores (Figure 5.19). A loss in the volume of pores below 8 nm is present suggesting that the PEI has migrated into small pores where there may be a greater sum of interactions between the PEI and silica support. This amine would be less accessible accounting for the reduction in amine efficiency observed after aging.

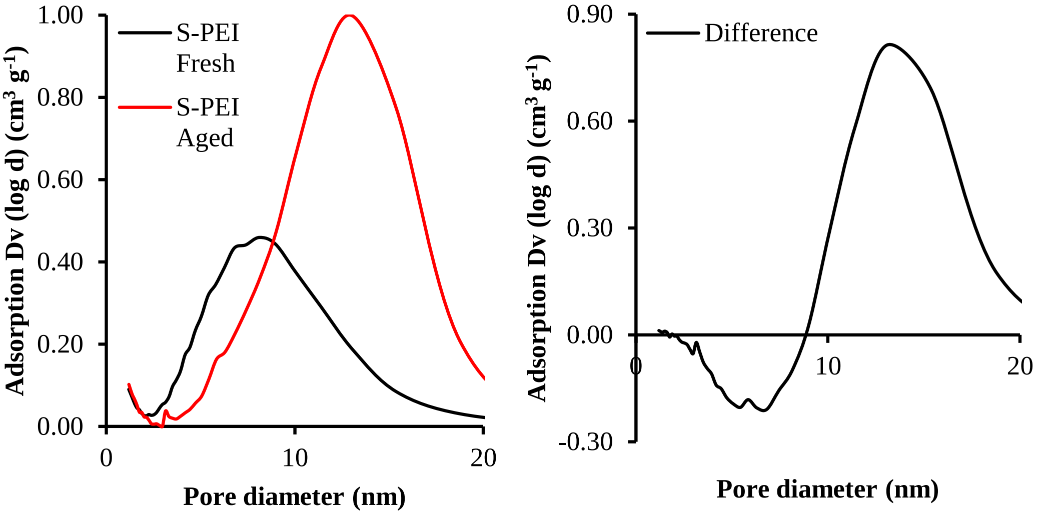

Figure 5.19. BJH adsorption pore size distribution of S-PEI before and after steam regeneration (left). The difference between the BJH adsorption pore size distributions (right).

Table 5.14. Changes in the porosity of S-PEI before and after aging under steam regeneration conditions.

Sorbent	BET Surface area (m^2 g^{-1})	BET C constant (a.u.)	Pore Volume (cm^3 g^{-1})	Inaccessible P_v (%)
S-PEI-Fresh	96.7 +/- 7.0	30.0	0.196 +/- 0.02	56.0
S-PEI-Aged	98.3 +/- 6.9	35.1	0.300 +/- 0.02	43.2

5.7.2 Stability of S-TEPA under steam regeneration conditions

Exposure of S-TEPA to 66% H_2O / N_2 at 130 °C for 8 h led to a 75% reduction in the CO_2 adsorption capacity of the adsorbent (Figure 5.20). The rate of adsorption for the aged adsorbent was significantly greater than that of the fresh adsorbent, however a large fraction of the amine was inaccessible for the aged sample evidenced by the reduction in amine efficiency from 0.30 to 0.12 (Table 5.15). A 41% loss of amine was observed via TGA confirming the instability of TEPA based adsorbents.

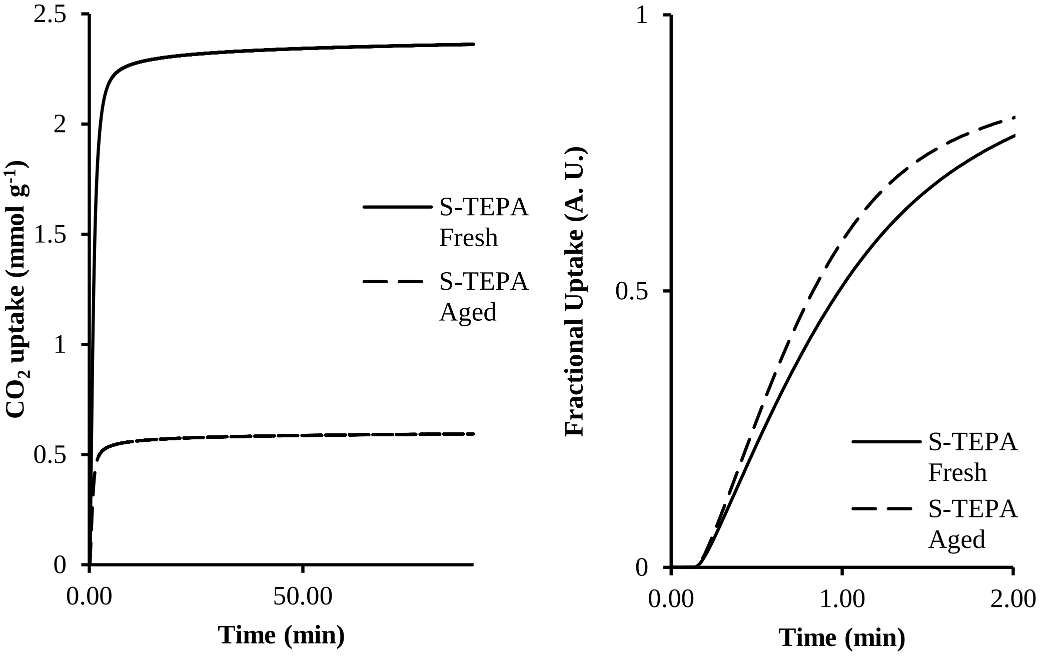

Figure 5.20. CO_2 uptakes for S-TEPA before and after ageing under steam regeneration conditions (left). Fractional order uptakes of S-TEPA before and after aging under steam regeneration conditions (right).

Table 5.15. The influence of steam regeneration on S-TEPA.

Aging time (h)	CO_2 capacity (mmol g^{-1})	% Original CO_2 uptake (%)	Amine loading (wt. %)	Amine efficiency (a.u.)
Fresh	2.36	100	32.8	0.30
24	0.59	25	19.1	0.12

The nitrogen sorption isotherm of the aged adsorbent shows a significant decrease in surface area and mesopore volume (Figure 5.21). The extent of pore blocking caused by the introduction of an amine increases with aging (Table 5.16). This indicates that either TEPA has agglomerated to the exterior of the adsorbent forming a diffusive layer or that mesostructured collapse is occurring [4]. When the S-TEPA was removed from the reactor it did not appear to have a greater proportion of amine on the surface in relation to any other adsorbent. The rate of decomposition of the S-TEPA is much greater than that of S-PEI this could be attributed to the increase in volatility of the TEPA species.

Table 5.16. Changes in the porosity of S-TEPA before and after aging.

Sorbent	BET Surface area (m^2 g^{-1})	BET C constant (a.u.)	Pore Volume (cm^3 g^{-1})	Inaccessible P_v (%)
S-TEPA-Fresh	103 +/- 7.4	30.0	0.23 +/- 0.02	50.7
S-TEPA-Aged	54 +/- 7.2	27.1	0.12 +/- 0.02	79.3

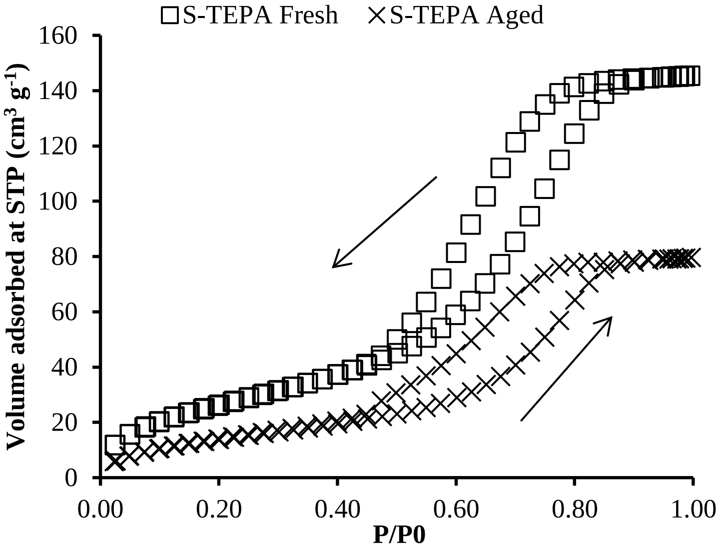

Figure 5.21. Nitrogen sorption isotherms of S-TEPA before and after aging under 66% H_2O / N_2 for 8 h at 130 °C.

The change in the BJH PSD after aging, showed a significant reduction in pore volume across all pore sizes (Figure 5.22). This loss of porosity is a stark contrast in the increases in porosity of S-PEI observed under similar conditions. This suggests that mesostructure collapse may have occurred. No organic degradation was observed via DRIFTS (Appendix A7).

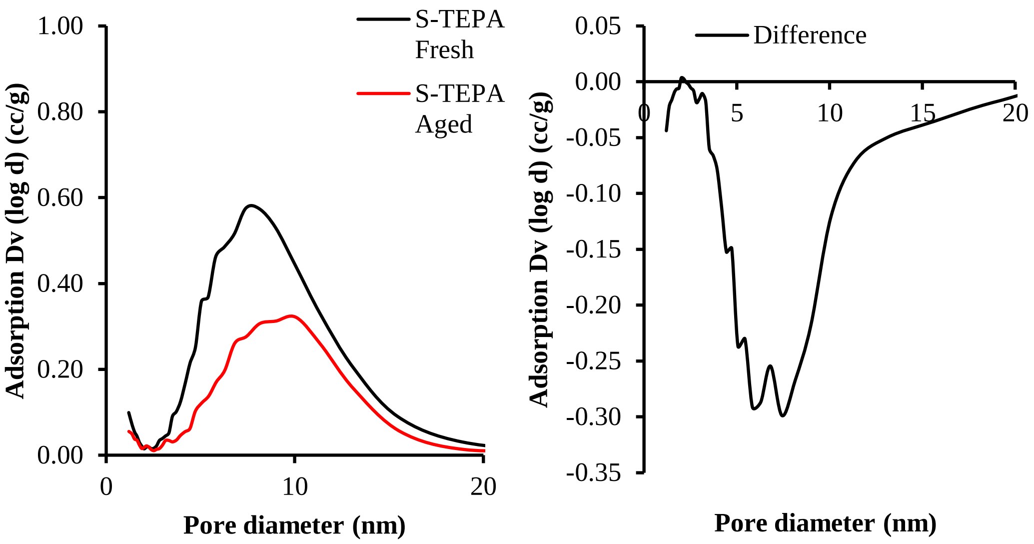

Figure 5.22. BJH adsorption pore size distribution of S-TEPA before and after steam regeneration (left). The difference between the BJH adsorption pore size distributions (right).

5.7.3 Stability of S-PEI-H under steam regeneration conditions

The heavier molecular weight of PEI 1800 used in the adsorbent S-PEI-H led to an increase in stability compared to S-TEPA and S-PEI after aging under 66% H_2O / N_2 at 130 °C for 8 h. Aging of S-PEI-H led to a reduction in CO_2 adsorption capacity of 19% (Figure 5.23). The amine efficiency decreased from 0.21 to 0.18 with aging suggesting that the remaining amine is less accessible (Table 5.17). No amine degradation was observed by DRIFTS (Appendix A8).

Table 5.17. The influence of steam regeneration on S-PEI-H.

Aging time (h)	CO_2 capacity (mmol g^{-1})	% Original CO_2 uptake (%)	Amine loading (wt. %)	Amine efficiency (a.u.)
Fresh	1.63	100	33.1	0.21
24	1.32	81.4	29.5	0.18

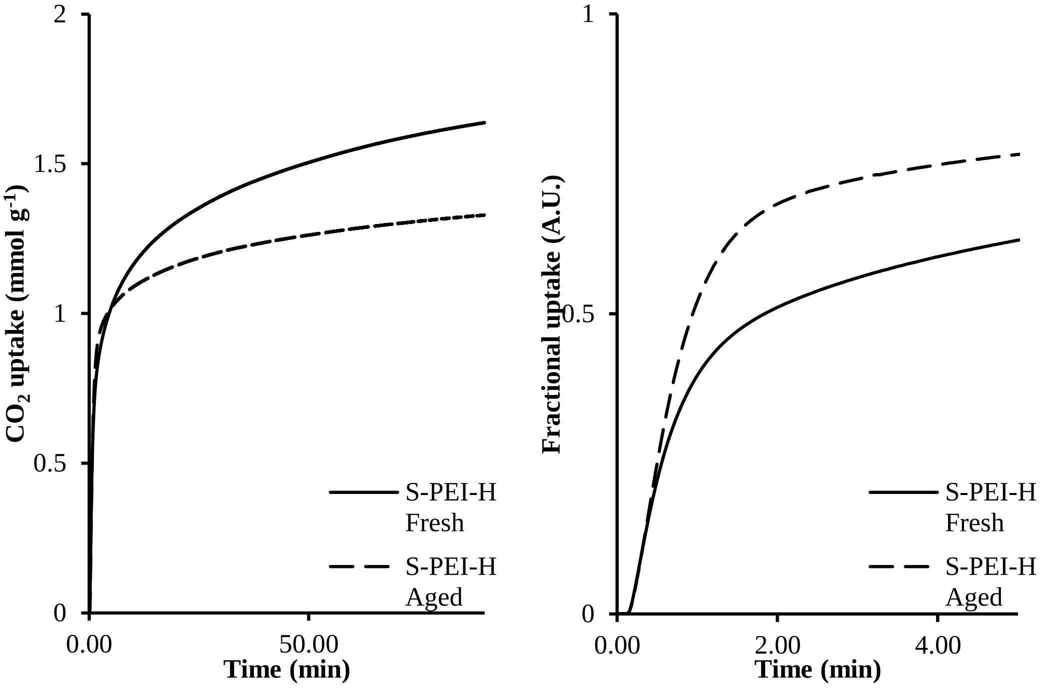

Figure 5.23. CO_2 uptakes for S-PEI-H before and after ageing under steam regeneration conditions (left).Fractional order uptakes of S-PEI-H before and after aging under steam regeneration conditions (right).

Nitrogen sorption of S-PEI-H after aging under desorption conditions showed a significant shift to larger pore sizes (Figure 5.24). This is coupled with a decrease in surface area a consequence of the loss of numerous smaller pores. The loss of hysteresis between 0.47-0.57 P/P_0 could be due to the changing geometry of the pores leading to reversible filling. This would be caused by PEI blocking off smaller pores part way down the channel. After aging the organic content was reduced from 33.1 wt% organic loading to 29.5 % organic loading correlating with the increase in pore volume observed for the steam aged S-PEI-H (Table 5.18).

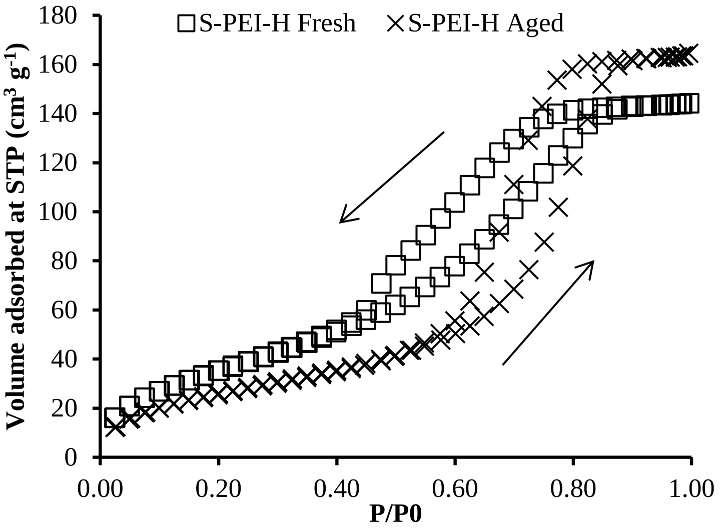

Figure 5.24. Nitrogen sorption isotherms of S-TEPA before and after aging under 66% H_2O / N_2 for 8 h at 130 °C.

Table 5.18. Changes in the porosity of S-PEI-H before and after aging.

Sorbent	BET Surface area (m^2 g^{-1})	BET C constant (a.u.)	Pore volume (cm^3 g^{-1})	Inaccessible P_v (%)
S-PEI-H-Fresh	141 +/- 9.9	27.5	0.22 +/- 0.01	57.2
S-PEI-H-Aged	110 +/- 7.59	34.9	0.25 +/- 0.02	48.0

BJH PSD of the fresh and aged materials are given below in Figure 5.25. After aging there is a loss of volume of pores below 7 nm with an increase in the volume of larger pores. This suggests that PEI is removed from the largest pores and that the smallest pore become occluded with amine. This suggests that heavier molecular weight PEI species appear to be unstable to steam aging.

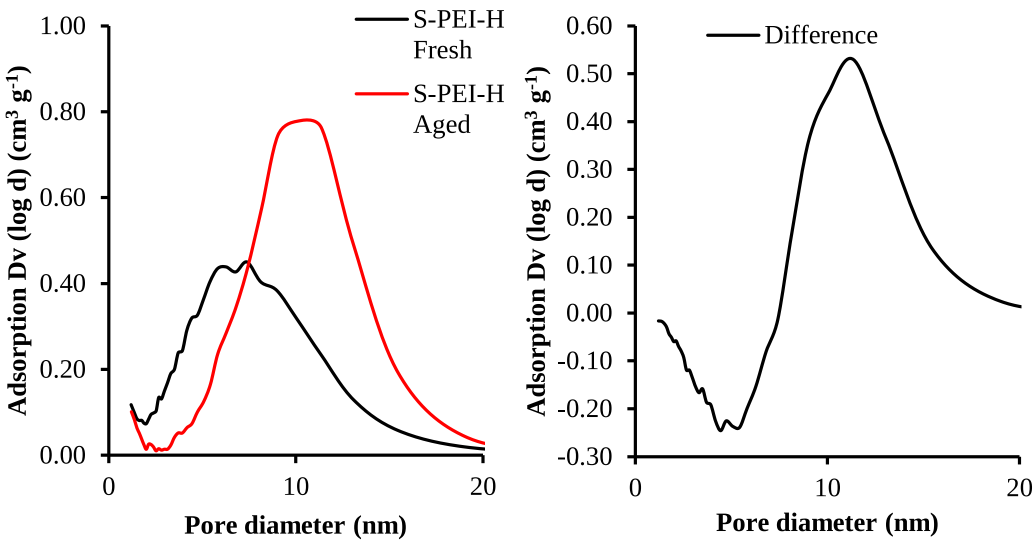

Figure 5.25. BJH adsorption pore size distribution of S-PEI-H before and after steam regeneration (left). The difference between the BJH adsorption pore size distributions (right).

5.7.4 Stability of S-PEI-LP under steam regeneration conditions

Aging of S-PEI-LP in the presence of 66% H_2O / N_2 at 130 °C for 8 h led to a reduction in CO_2 adsorption capacity of 40% (Figure 5.26). This reduction is capacity was accompanied with a reduction in amine efficiency from 0.30 to 0.23 (Table 5.19). Loss of the amine component was evident by a reduction in the organic loading of the sorbent from 33.1 to 25.7 wt%. The organic loses were similar to S-PEI suggesting that suggesting that the rate of leaching is insensitive to the pore size of the support. DRIFTS analysis confirmed no change in the amine adsorbent before and after aging (Appendix A10).

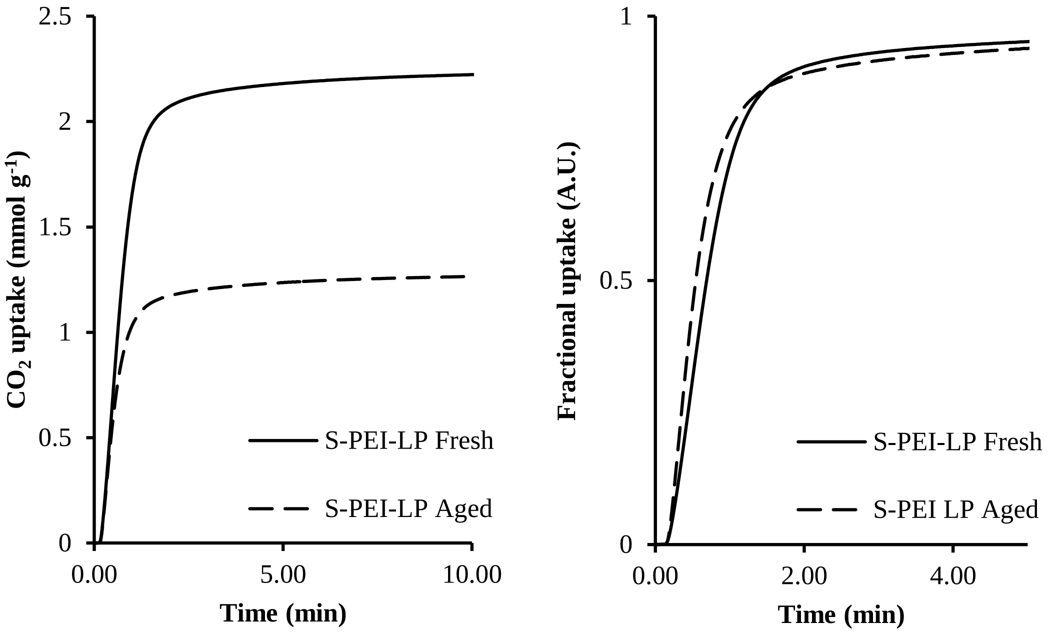

Figure 5.26. CO_2 uptakes for S-PEI-LP before and after ageing under steam regeneration conditions (left). Fractional order uptakes of S-PEI-H before and after aging under steam regeneration conditions (right).

Table 5.19. The influence of steam regeneration on S-PEI-H.

Aging time (h)	CO_2 capacity (mmol g^{-1})	% Original CO_2 uptake (%)	Amine loading (wt. %)	Amine efficiency (a.u.)
Fresh	2.38	100	33.1	0.30
8	1.43	60	25.7	0.23

Nitrogen sorption isotherms of S-PEI-LP before and after aging under desorption conditions is given below in Figure 5.27. Aging led to a slight increase in surface area for 91 to 120 m^2 g^{-1} with a marked increase in pore volume consistent with the reduction in organic loading (Table 5.20).

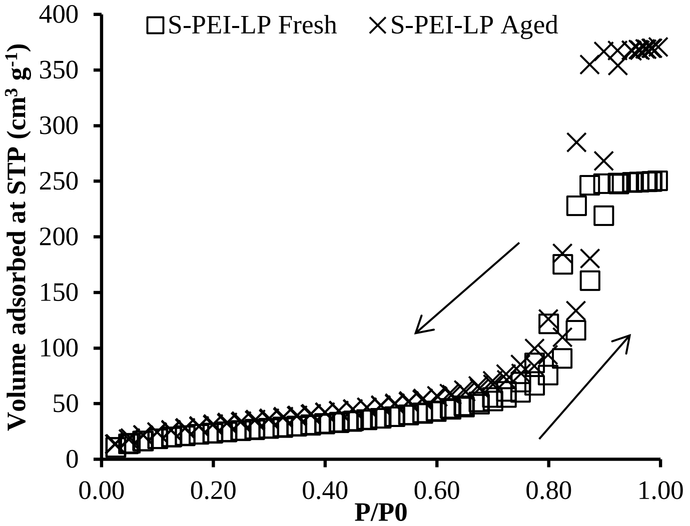

Figure 5.27. Nitrogen sorption isotherms of S-PEI-LP before and after aging under 66% H_2O / N_2 for 8 h at 130 °C.

Table 5.20. Changes in the porosity of S-PEI-LP before and after aging.

Sorbent	BET Surface area ($m^2\ g^{-1}$)	BET C constant (a.u.)	Pore volume ($cm^3\ g^{-1}$)	Inaccessible P_v (%)
S-PEI-LP-Fresh	91 +/- 5.7	35.0	0.38 +/- 0.02	44.9
S-PEI-LP-Aged	120 +/- 7.16	36.8	0.57 +/- 0.03	24.0

Figure 5.28 compares the BJH adsorption pore size distribution showing a clear increase in the volume of the larger pores. This suggests that the PEI is removed from the largest pores of S-PEI-LP with none agglomerating within the smallest pores. This finding suggests that PEI only reagglomerates within pores below 6 nm. This would explain the larger capacity of S-PEI-LP after aging compared to S-PEI. In S-PEI-LP none of the amine reagglomerates into the smallest pores where it cannot efficiently adsorb CO_2.

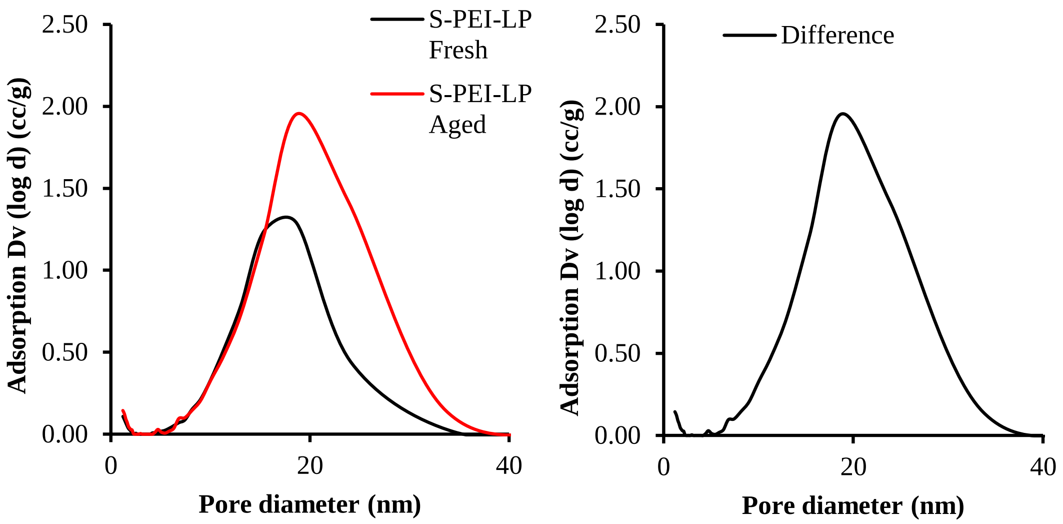

Figure 5.28. BJH PSD of S-PEI-LP before and after steam regeneration (left). The difference between the BJH adsorption pore size distributions (right).

5.7.5 Stability of S-PEI-SP under steam regeneration conditions

Aging of S-PEI-SP under 66% H_2O / N_2 at 130 °C for 8 h led to a reduction in the CO_2 adsorption capacity by 24% (Figure 5.29). This reduction in capacity was accompanied with a reduction in amine efficiency from 0.22 to 0.17. There was also reduction in the overall rate of adsorption after aging under desorption conditions. Only a small amount of amines leached from the pores of the adsorbent, suggesting that the amine saturated pores restricted the intrusion of water (Table 5.21).

Table 5.21. Changes in amine accessibility for S-PEI-SP before and after aging.

Aging time (h)	CO_2 capacity (mmol g^{-1})	% Original CO_2 uptake (%)	Amine loading (wt. %)	Amine efficiency (a.u.)
Fresh	1.72	100	32.8	0.22
24	1.32	76	29.7	0.17

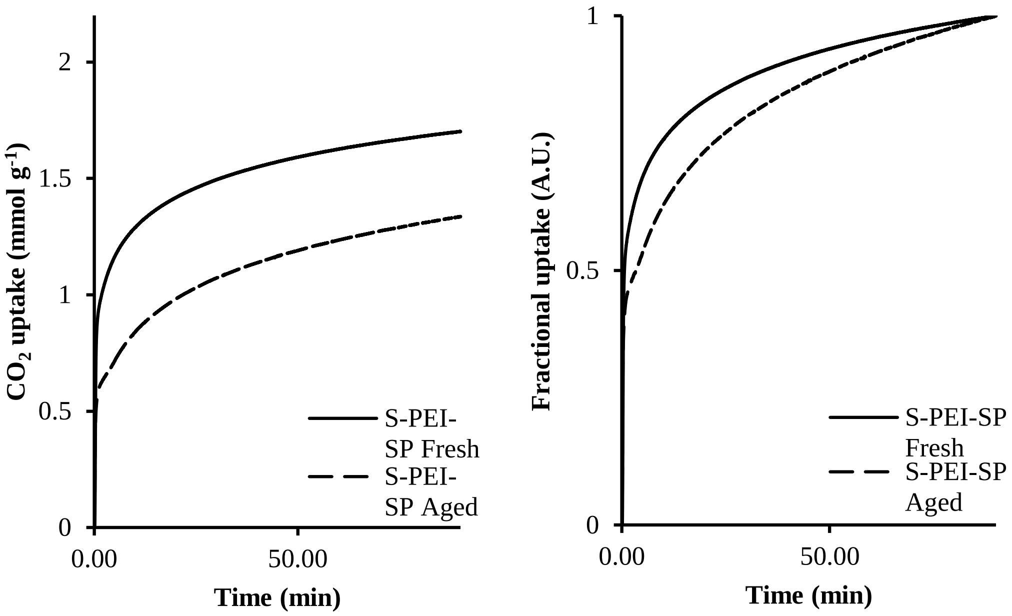

Figure 5.29. CO_2 uptakes for S-PEI-SP before and after ageing under steam regeneration conditions (left).Fractional order uptakes of S-PEI-SP before and after aging under steam regeneration conditions (right).

A combination of the low porosity of the sample and small quantity of the sample yielded no sensible nitrogen sorption data. The particles appeared to be non-porous to nitrogen at 77 K, suggesting the pores remained amine filled after aging (Appendix A12). Organic analysis indicated a marginal mass loss from 33 to 29.7 wt% which is assigned to amine leaching from the exterior and pores of the support. Amine degradation was not observed with DRIFTS (Appendix A11).

5.7.6 Stability of S-AP under steam regeneration conditions

Covalently tethered S-AP aged under a flow of 66% H_2O / N_2 at 130 °C for 8 h exhibited a 11% reduction in CO_2 adsorption capacity (Figure 5.30). With regard to Figure 5.30, the increase in the mass peaking at 2 min is caused by rocking motion of the pan as the gas is switched over. This is a consequence of the small amount of low density sample used in the experiment. A contributing factor could also be the heat of adsorption causing the sample temperature to increase, leading to desorption of CO_2, with subsequent re-adsorption after the sample has cooled down. TGA analysis showed no loss of organic component and DRIFTS spectroscopy yielded no degradation of the amine species (Appendix A13).

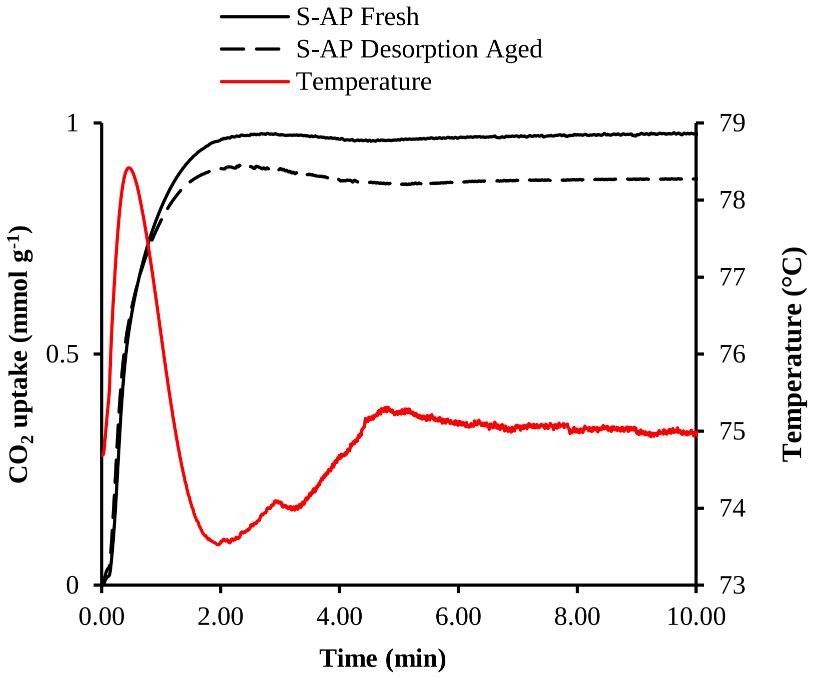

Figure 5.30. CO_2 uptakes for S-AP before and after ageing under steam regeneration conditions.

Aging of S-AP under 66% H_2O / N_2 at 130 °C for 8 h led to a slight reduction in surface area from 310 m^2g^{-1} to 290 m^2g^{-1},with a corresponding decrease in BET C constant from 45 to 35 (Table 5.22). This suggests that a change in the surface structure is occurring however the error associated with the measurements could negate the discrepancies between samples. The nitrogen sorption isotherms of S-AP suggest that the pore structure remains similar after aging, with a marginal increase in pore volume (Figure 5.31). Degradation of aminopropyl functionalised silcas with partial coverage have also been reported in the literature [22]. Condensation of water within the pores of the adsorbent could lead to localised concentrations of a high pH solution, conditions suitable for silica hydrolysis. In impregnated amines adsorbents there is little to no exposed silica however given the incomplete coverage of S-AP exposed silica sites may remain.

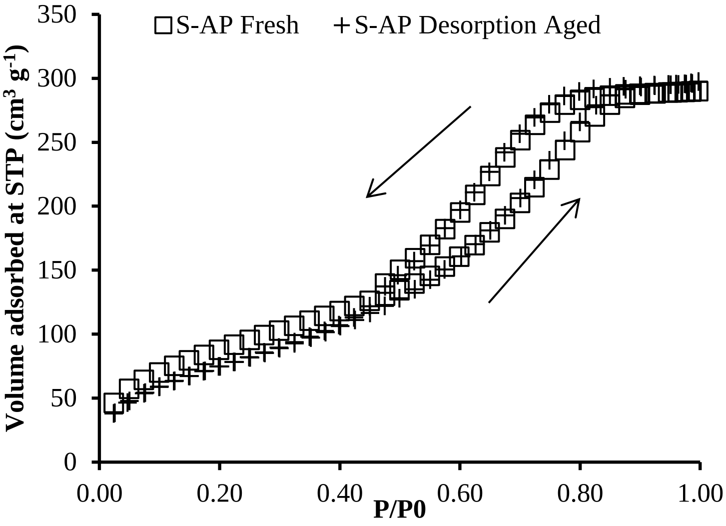

Figure 5.31. Nitrogen sorption isotherms of S-AP before and after aging under 66% H_2O / N_2 for 8 h at 130 °C.

Table 5.22. Changes in the porosity of S-AP before and after aging.

Sorbent	BET Surface area ($m^2 g^{-1}$)	BET C constant (a.u.)	Pore Volume ($cm^3 g^{-1}$)	Inaccessible P_v (%)
S-PEI-AP-Fresh	331 +/- 22.2	45.2	0.45 +/- 0.02	32.4
S-PEI-AP-Aged	288 +/- 17.9	35.2	0.46 +/- 0.02	33.9

5.8 Investigation into support degradation

To investigate whether degradation of the support could lead to a reduction in the CO_2 capacity of the adsorbents, fresh Davisil 60 silica was aged under identical conditions. Davisil 60 was aged under both pseudo adsorption and steam regenerations and the changes in structure investigated by nitrogen sorption. No discernible changes in the bare silica support are observed by nitrogen sorption experiments as shown in Table 5.23. Full isotherms can be found in Appendix A14.

Table 5.23. The influence of aging of the porosity of Davisil 60.

Extent of aging	BET Surface area ($m^2\ g^{-1}$)	BET C constant (a.u.)	Pore volume ($cm^3\ g^{-1}$)	BJH PSD (nm)
Fresh	516.4 +/- 22.2	83.8	0.79 +/- 0.04	8.2
Adsorption aged	524 +/- 17.9	81.4	0.79 +/- 0.04	8.3
Desorption aged	518.1 +/-14.1	83.2	0.79 +/- 0.04	8.0

To investigate changes in silica species ^{29}Si SSNMR was employed to investigate any changes in the silica sites present after aging. Cross-polarisation ^{29}Si NMR of Davisil 60 shows the presence of Q2, Q3 and Q4 silica sites, this analysis is not quantitative but can be used to see observe the formation of Q1 sites or indicate changes in the relative Q2 and Q3 ratios. After aging under adsorption and desorption conditions no change in the Q2 and Q3 ratios is observed (Figure 5.32).

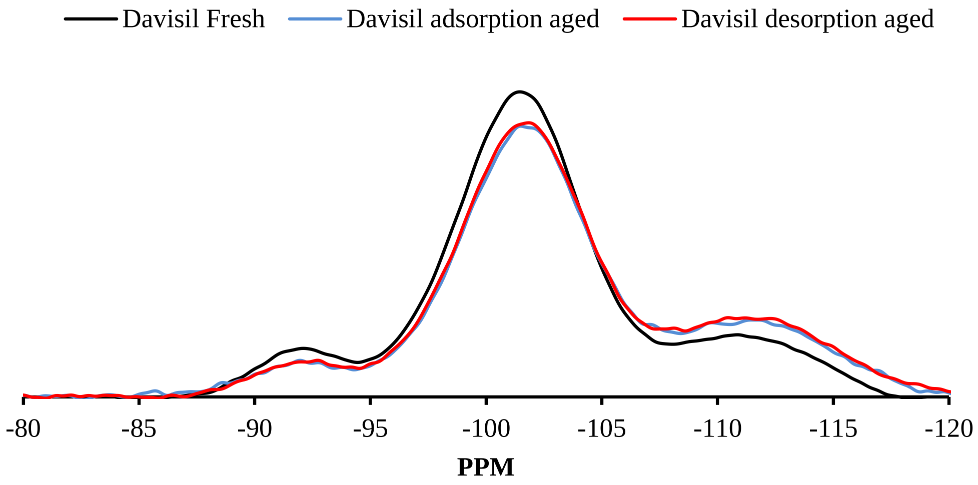

Figure 5.32. ^{29}Si MAS CP SSNMR of unfunctionalised Davisil support exposed to adsorption (10% H_2O / N_2, 75°C, 24 h) and desorption (66% H_2O / N_2, 130 °C, 8 h) aging conditions.

After impregnation of amine polymer the signal corresponding to Q2 sites diminished, rationalised as the surface sites where the amine binds to the surface of silica. It is known that high pH environments can lead to the dissolution of silica surfaces [23]. To elucidate if the presence of the amine affected the decomposition

^{29}Si SSNMR was conducted before and after aging of S-PEI sorbent under desorption aging conditions (Figure 5.33). Negligible changes in the silica structure were observed after adsorption aging conditions. Furthermore, STEM images showed amine agglomerations on the surface but no obvious support degradation (Appendix A15 and A16).

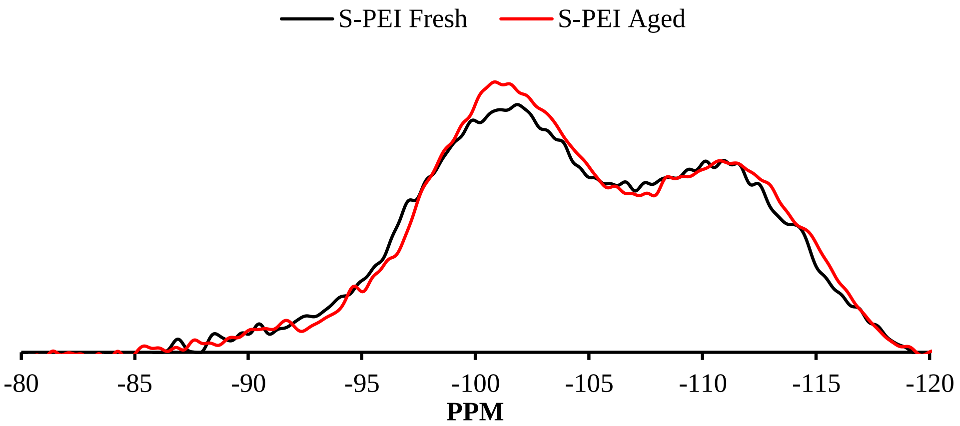

Figure 5.33. ^{29}Si MAS CP SSNMR of S-PEI before and after aging under 66% H_2O / N_2 at 130 °C for 8 h).

5.9 Discussion

In this chapter silica supported amine sorbents were aged in the presence of water under both pseudo adsorption and steam regeneration conditions. Cycling of SBA-15 40 wt% PEI and SBA-15 40 wt% TEPA over 100 CO_2 adsorption and desorption cycles under dry gas conditions led to significant reductions in CO_2 adsorption capacity. The higher weight molecular weight PEI adsorbent showed the formation of thermally stable urea species during cycling [6]. Urea species form in instances where two neighbouring amine groups have the correct steric geometry to be able to form a stable urea species by the elimination of water (Equations 5.1 and 5.2).

$R_2NH_2^+ + R_2COO^- \leftrightarrow R_2\,NCONR_2 + H_2O$ Equation 5.1

$2R_2NH + CO_2 \leftrightarrow R_2NCONR_2 + H_2O$ Equation 5.2

The reduction in capacity of S-PEI was 35%, assuming that 2.5% of the amine is a urea species this would lead to a reduction in capacity of 5% leaving a 30% reduction in capacity unaccounted for. Similar to the assumed reduction in viscosity for the alkylammonium carbamate product formed between CO_2 and PEI, formation of urea species could produce crosslinking between PEI molecules leading to a reduction in amine accessibility. The reduction in amine efficiency with progressive aging suggests that a proportion of the amine is becoming inaccessible. No evidence of PEI loss from the support was observed, which is attributed to the low vapour pressure of the average PEI unit. The narrow PDI of the PEI used in this study suggests that volatile losses from lower molecular weight components of the PEI would not be problematic.

SBA-15 40 wt% TEPA exhibited a reduction in adsorption capacity from 3.2 to 1.53 mmol g^{-1} after 100 cycles. The dry mass of the sorbent decreased by 20 % after cycling as impregnated TEPA was volatilising from the sample. Commercial TEPA consists of a mixture of triethylenetetraamine (TETA), pentaethylenehexamine (PEHA) and tetraethylenepentamine (TEPA) giving rise to a significant polydispersity index. Single component vapour pressures of these amines are below 0.01 mm Hg at 20 °C, however under desorption conditions of 130 °C the vapour pressure is no longer negligible and steady losses due to evapouration could be expected [24]. Owing to the significant quantities of TEPA loaded on the adsorbent multilayers of amine are expected. TEPA molecules at the top of a multilayer or the exterior of adsorbent may behave similarly to bulk TEPA and evapourate. A small amount of urea species was observed suggesting that the formation of urea species in not restricted to tertiary amine sites. Owing to the mass losses from volatilisation of the amine component the estimation of the extent of urea conversion could not be accurately determined.

The thermal stability of PEI and TEPA under nitrogen is presented in Figure 5.34. with the onset of evapouration of TEPA beginning at 150 °C evidenced by the negative heat flow suggesting an endothermic transition such as evapouration. PEI exhibited much greater thermal stability with the onset of evaporation occurring at 290 °C, with the majority of the PEI mass loss above 347 °C. The slight mass loss from PEI at 60 °C can be attributed to the desorption of water or pre-adsorbed CO_2.

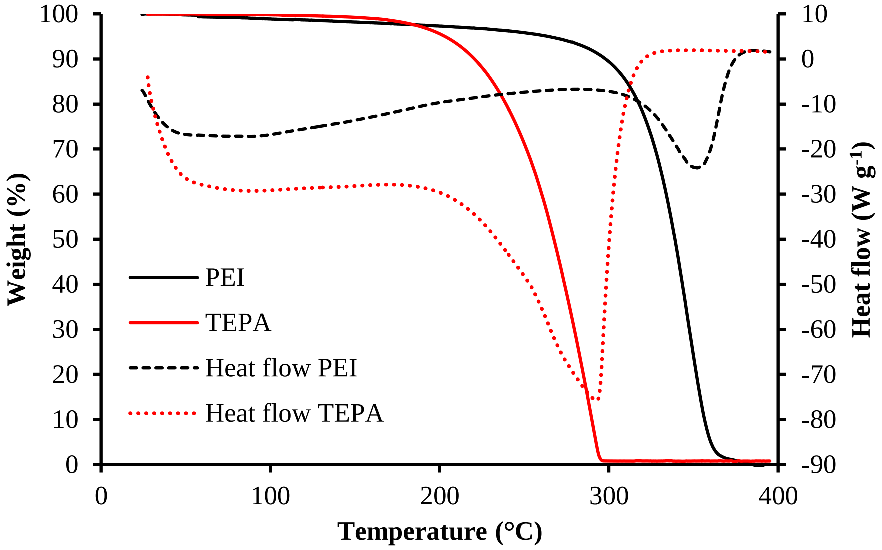

Figure 5.34. The thermal stability of TEPA and PEI (MW 600) determined by TGA.

Under realistic operating conditions, the flue gas stream will contain between 5-15 % water. Furthermore if steam-regeneration is employed then excellent hydrothermal stability is required. Recent reports suggest that liquid water within the pores of the adsorbent solubilises the impregnated amine causing it be washed out of the pores [2]. The Kelvin equation (Equation 5.3) was used to determine the relative pressure of water that would be required to condense water within the pores (Figure 5.35).

$$ln\left(\frac{P}{P_0}\right) = -\frac{2\gamma V_m cos\theta}{RT(r_p)}$$ Equation 5.3

Where P is the actual vapour pressure, P_0 is the saturation vapour pressure, γ is the surface tension, V_m is the molar volume, θ is the contact angle, R is the universal gas constant, T is the temperature and r_p is the pore radius. The determination of the contact angle porous adsorbents is difficult hence two scenarios were considered. Scenario one where the pore was considered perfectly wetting and a second scenario assuming a contact angle of 45 ° as observed for PEI films over silica surfaces [25].

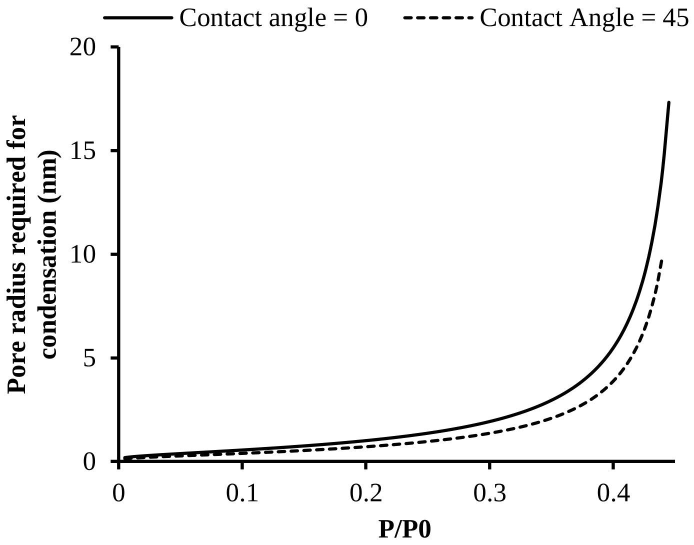

Figure 5.35. Minimum pore diameters for capillary condensation estimated from the Kelvin equation for differing pressures of water at 80 °C. The saturation pressure for water at 80 °C is 0.465 atm.

As can been seen under the adsorption aging conditions (P = 0.1 atm, T = 80 °C) condensation would be spontaneous in pores with diameters below 1.2 nm for a material with a contact angle of 0 ° (Figure 5.35). For a surface bound polyethlyeneimine film the increased contact angle would mean that condensation would not occur in pores below 0.8 nm. At adsorption temperatures the condensation of water would not occur until the partial pressure of water exceeded 0.35 atm, far in excess of any power station flue gas stream. Water would still be expected to adsorb on the surface of the adsorbent and to an extent multilayers could form but filling of the pore with water would not occur. The pore size for the condensation of water under the steam desorption conditions used (66% H_2O / N_2, 130 °C) was calculated (Figure 5.36). Condensation of water within the pores of the adsorbent would become spontaneous in all pores below 1,200 nm for a perfectly wetting surface and 850 nm for a PEI film. This analysis suggests that the principal difference between aging under adsorption and steam regeneration conditions is the spontaneous condensation of water within the pores of the adsorbent. Given the large radii necessary for condensation to occur and the irregular surface and resultant packing of the adsorbents, water could condense between the particles of the adsorbent. This could provide an additional concentration gradient for the amine to be removed from within the pores of the adsorbent.

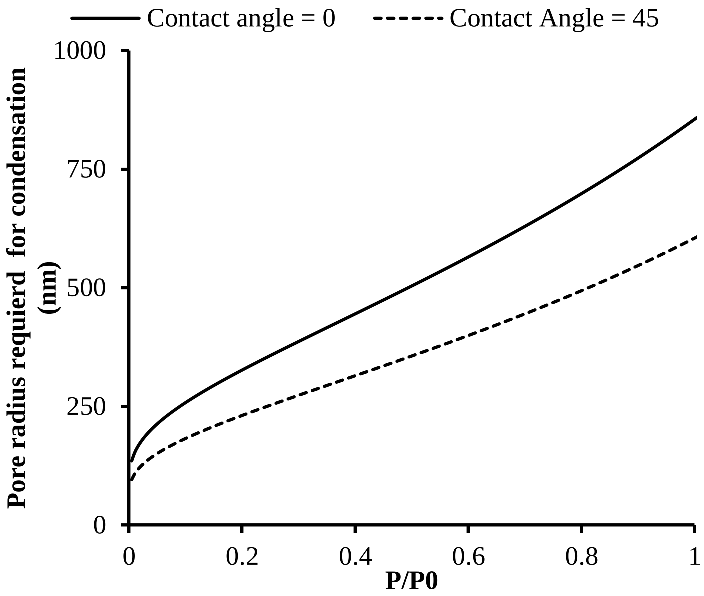

Figure 5.36. Minimum pore diameters for capillary condensation estimated from the Kelvin equation for differing pressures of water at 130 °C. The saturation pressure for water at 130 °C is 2.70 atm.

DRIFTS confirmed that no chemical changes in the amine structure were present after aging. This suggests that cause of deactivation under aging is related to leaching or dispersion of amine on the support. The amine molecular weight appears to influence the stability of silica impregnated amine adsorbents based on the same support. TEPA based adsorbents exhibit poor stability in the presence of aging under adsorption and desorption conditions which can be partly accounted for by leaching of the amine component. The extent of leaching is much more pronounced under desorption conditions attributed to the increased vapour pressure of the TEPA species at higher temperatures. Under adsorption conditions the BJH average pore size increases consistent with loss of amine from the largest pores only. The pore structure after aging under desorption conditions shows a large reduction in pore volume across all pores sizes. This is consistent with a breakdown of the silica support or an amine film forming over the surface of the particle. The condensation of water within the pores of the adsorbent under desorption conditions could provide a pathway for leaching via dissolution of the TEPA into water. Once a significant amount of TEPA has been removed from the pores exposing the silica surface, a mixture of condensed water and basic amines within the pores could led to hydrolysis of the silica support. The reduction in amine efficiency of S-TEPA after aging reinforces the idea of structural collapse as the remaining amine is less accessible. Similar mesostructured collapse was found to occur for amine impregnated mesocellular foam aged in a sealed autoclave [4].

Adsorbent S-PEI did not show volatile losses during aging in dry conditions, with urea formation being the sole deactivation pathway. Aging under pseudo-adsorption conditions led to a small amount of amine leaching from the amine. The PEI appeared to be selectively removed from the largest pores of the adsorbent whist unaffected in pores below 6nm.

Aging under desorption conditions increased leaching of the active amine component suggesting that capillary condensation of water enhances the rate of amine leaching. The volume of pores above 6 nm increased after aging consistent with leaching of amine from the largest pores. A reduction in the volume of pores below 6 nm suggests that the remaining amine has agglomerated mostly within the smaller pores of the adsorbent. In principle it would be more stable owing to the greater sum of interactions. Fauth *et al.* reasoned that losses in amine efficiency after aging were due to the re-agglomeration of PEI within the pores of the adsorbents [26]. Later work by Hammache *et al.* observed losses due to both re-agglomeration and PEI leaching [3]. Support degradation was not significant for this sample suggesting that not enough amine had been removed to expose the silica surface. It could be rationalised that until a bare silica surface is exposed the presence of multilayers of amine increase the stability of the silica.

Leaching of amine was not observed for S-PEI-H after aging under adsorption conditions but was present after aging under desorption conditions. The extent of leaching was lower than that of the lower molecular weight amines. Aging of the sample under adsorption conditions led to a reduction in the volume of pores between 4 - 8 nm and a larger increase in the volume of pores above 8 nm. Given that very little amine material was lost this suggests that the heavy molecular weight PEI had reagglomerated within the smallest pores of the adsorbent. This is also consistent with the reductions in amine efficiency observed as the amine in the smaller pores would be less accessible. Aging under desorption conditions led to larger reductions in amine efficiency and CO_2 adsorption capacity compared to aging under desorption conditions. Changes in the pore structure of S-PEI-H showed a reduced volume in small pores bellow 7 nm and an increase in pore volume for pores larger than 7 nm. This is consistent with the amine reaggolmerating within the small pores whilst leaching from the largest pores.

There appears to be a correlation between amine molecular weight and stability under adsorption and desorption conditions. This could be attributed to the differences in solubility of the larger molecular weight amine polymers. The amine polymers are likely to adopt a configuration maximising the interactions between nitrogen atoms and the surface of the silica support. The sum of these interactions would be greater for polymers of greater molecular weight hence the rate of solubilisation would be slower.

The effect of pore size has been shown to have a significant effect in the uptake capacity and amine efficiency of the adsorbents [18]. Aging of S-PEI LP led to only a slight reduction in capacity under adsorption conditions with negligible changes in porous structure or organic loading. The lack of amine reagglomeration for this sample contrasts with that of smaller pore adsorbents suggesting that the smaller pores are required for amine re-agglomeration to be significant. Aging under desorption conditions led to an increase in surface area and pore volume. The extent of leaching was similar to S-PEI suggesting that the nature of the rate of leaching is dependent on the molecular weight. This suggests that capillary condensation of water within the pores of the adsorbent follows the same mechanism of leaching present in the smaller pore sized silica. The overall capacity of S-PEI-LP remained greater than that of S-PEI owing to the fact that amines could not become occluded in small pores. Amines agglomerated with the smallest pores of the adsorbent appear to be less effective at capturing CO_2 as they are less accessible.

S-PEI-SP appeared to exhibit greater stability than larger pore sized adsorbents retaining almost all of the adsorption capacity after aging under adsorption conditions. The pores of the S-PEI-SP were inaccessible to nitrogen at 77 K suggesting that the amine blocked access to the pores. This suggests that water intrusion into the pores is a component of amine deactivation. During aging under desorption conditions the CO_2 adsorption capacity of the adsorbent was reduced, with a slight reduction in amine loading observed. The extent of amine leaching was lower compared to larger pore sized adsorbents. This could be a culmination of the amine being more strongly held within the smaller pore adsorbent or the limited intrusion of water owing to the number of pore blockages. It is expected that as water can intrude into the pores the rate of amine leaching would increase. Inaccessibility to N_2 at 77 K coupled with a reduction in amine efficiency after aging under desorption conditions suggests that the amine has reagglomerated yielding a significant amount of pore blocking.

Covalently functionalised S-AP did not show any form of degradation under pseudo-adsorption conditions owing to the covalent interaction between the organic component and the support. The degradation of S-AP under steam regeneration conditions was a surprising result as the high coverage of covalently bound species would be expected to offer the silica phase a degree of protection from hydrolysis [27, 28]. It is known that the amino propyl groups of the silica interact strongly with the silica surface owing to the strong acid base interaction and incomplete coverage of the silica surface [29]. As the pores are filled with water under steam regeneration conditions it is expected that these surface bound amines could create a basic environment where the silica becomes slowly hydrolysed at exposed silica sites. This silica degradation could account for the loss in surface area and CO_2 adsorption capacity. A similar effect has been observed for covalently grafted aminopropyl groups regenerated in steam but with a more thinner walled silica structure [22].

For the adsorbents that remain highly loaded with amines during aging, it is expected that this amine would prevent access of water to the silica surface. Silica support degradation is characterised with a reduction in BET surface area and pore volume. The adsorbents featured in this study typically exhibit an increase in surface area and pore volume after aging. This suggests that amine leaching is occurring as opposed to support degradation. Exposure of the bare support under similar conditions did not yield significant changes in the structure of the adsorbent. This was also observed by Gray *et al.* using a commercial silica gel Cariact G10 who noted no support degradation after steam aging conditions. Indeed SBA-15 has been reported to be stable at temperature is the present of steam at similar pressures used in this study [30, 31]. In the presence of water and over extended periods of time some degradation of silica supports is to be expected, with such degradation acerbated in the presence of steam. Silica volatilisation and redeposition is a kinetically limited process and under the conditions used in post combustion systems is not likely to be a contributing factor to support degradation. Furthermore, the relatively short times in the study may not be sufficient to yield tangible support degradation [32].

The temperature at which the aging was conducted is expected to increase the rate of degradation as reported by Li *et. al.* who noted an accelerated loss of sorbent degradation with increasing temperature [4]. Increased temperatures would decrease the viscosity of the polymer components facilitating the re-agglomeration of the amine adsorbents. Furthermore increasing the temperature would increase the rate of dissolution of the amine component into the condensed water. During the aging of S-PEI under pseudo adsorption conditions the adsorbent was found to deteriorate faster than S-TEPA. The capacity of this sample was cycled 5 times between the aging conditions (10% H_2O / N_2, 75 °C) and desorption conditions (10% H_2O / N_2, 75 °C). This was to allow the CO_2 uptake to be measured at various points in time. This suggests that temperature cycling between adsorption and desorption conditions may have an impact on the stability of impregnated adsorbents.

5.10 Conclusion

This chapter investigated the mechanism for deactivation of polyamine impregnated mesoporous silica adsorbents under pseudo adsorption and steam regeneration conditions. Preparation and degradation of a range of adsorbents bearing different amine molecular weights and pore structures has allowed a structure activity relationship to be constructed. The observations presented herein suggest that a combination of amine reagglomeration and leaching is responsible for the deactivation of the adsorbents. The rate of amine leaching was found to be dependent on the aging conditions used. Aging under steam regeneration conditions was found to degrade the adsorbents more so than humid adsorption conditions. This is thought to be due to the spontaneous capillary condensation of water within the pores of the adsorbent. The polymer molecular weight was shown to correlate with adsorbent stability, with lower molecular weight amines possessing increased water solubility. The observation of amine leaching present in this chapter is ascribed to more aggressive testing conditions used in comparison to studies that observed smaller amounts of leaching.

Once a critical amount of the amine has been removed from the pores yielding an exposed silica surface, support hydrolysis and redeposition can occur. It is though the condensation of water in the pores solubilised the amine leading to a highly basic solution which in turn hydrolysed the exposed regions of the silica support. This degradation of the silica support leads to a significant decline in the performance of the adsorbent.

The distribution of the amine varies with aging as the amine adopts a more stable configuration, filling the smallest pores of the adsorbent to maximise the number of interactions between the amine and the silica support. Once the amines become occluded within the smallest pores of the adsorbent they are less accessible leading to a reduction in amine efficiency and hence uptake capacity of the adsorbent. For PEI 600 this agglomeration only occurs in pores below 6 nm. In instances where larger pore supports were used no agglomeration was observed.

This chapter highlights the lack of long term stability of impregnated amine adsorbents to steam regeneration, a barrier which must be surmounted for the practical application of impregnated amine silica adsorbents.

5.11 References

1. J. C. Hicks, J. H. Drese, D. J. Fauth, M. L. Gray, G. Qi, C. W. Jones, *Designing Adsorbents for CO_2 Capture from Flue Gas-Hyperbranched Aminosilicas Capable of Capturing CO_2 Reversibly.* J. Am. Chem. Soc., 2008. **130**: p. 2902.
2. W. C. Wilfong, B. W. Kail, M. L. Gray, *Rapid Screening of Immobilized Amine CO_2 Sorbents for Steam Stability by Their Direct Contact with Liquid H_2O.* ChemSusChem, 2015. **8**: p. 2041.
3. S. Hammache, J. S. Hoffman, M. L. Gray, D. J. Fauth, B. H. Howard, H. W. Pennline, *Comprehensive Study of Steam on Polyethyleneimine on Silica for CO_2 Capture.* Energy & Fuels, 2013. **27**: p. 6899.
4. W. Li, P. Bollini, S. A. Didas, S. Choi, J. H. Drese, C. W. Jones, *Structural Changes of Silica Mesocellular Foam Supported Amine-Functionalized CO_2 Adsorbents Upon Exposure to Steam.* ACS Appl. Mater. Interfaces, 2010. **2**: p. 3363.
5. J. Zhao, F. Simeon, Y. Wang, G. Luo, T. A. Hatton, *Polyethylenimine-impregnated siliceous mesocellular foam particles as high capacity CO_2 adsorbents.* RSC Adv. , 2012. **2**: p. 6509.
6. T. C. Drage, A. Arenillas, K. M Smith, C. E. Snape, *Thermal Stability of Polyethylenimine Based Carbon Dioxide Adsorbents and Its Influence on Selection of Regeneration Strategies.* Microporous and Mesoporous Materials, 2008. **116**: p. 504.
7. X. Feng, G. Hu, G. XIe, Y. Xie, J. Lu, M. Luo, *Tetraethylenepentamine-Modified Siliceous Mesocellular Foam (MCF) for CO_2 Capture.* Ind. Eng. Chem. Res., 2013. **52**: p. 4221.
8. W. C. Wilfong, C. S. Srikanth, S. C. Chuang, *In Situ ATR and DRIFTS Studies of the Nature of Adsorbed CO_2 on Tetraethylenepentamine Films.* ACS Appl. Mater. Interfaces, 2014. **6**: p. 13617.
9. M. Yao, Y. Dong, X. Hu, X. Feng, A. Jia, G. Xie, G. Hu, M. Luo, *Tetraethylenepentamine-Modified Silica Nanotubes for Low-Temperature CO_2 Capture.* Energy Fuels, 2013. **27**: p. 7673.
10. A. Sayari, Y. Belmabkhout, *Stabilization of Amine-Containing Adsorbents: Dramatic Effect of Water Vapor.* J. Am. Chem. Soc., 2010. **132**: p. 6312.
11. D. J. N. Subagyono, Z. Liang, G. P. Knowles, A. L. Chaffe, *Amine modified mesocellular siliceous foam (MCF) as a sorbent for CO_2.* Chem Eng Res Des, 2011. **89**: p. 1647.
12. X. Yan, L .Zhang, Y. Zhang, K. Qiao, Z. Yan , S. Komarneni, *Amine-modified mesocellular silica foams for CO_2 capture.* Chemical Engineering Journal, 2011. **168**: p. 918.
13. W. Zhang, H. Liu, C. Sun, T. C. Drage, C. E. Snape, *Performance of Polyethyleneimine-silica adsorbent for post-combustion CO_2 capture in a bubbling fluidized bed.* Chemical Engineering Journal, 2014. **251**: p. 293.
14. A. Sayari, Y.Belmabkhout, *Stabilization of Amine-Containing CO_2 Adsorbents: Dramatic Effect of Water Vapor. J. Am. Chem. Soc.*, 2010. **132**: p. 6312.
15. N. N. Linneen, R. Pfeffer, Y. S. Lin, *Amine Distribution and Carbon Dioxide Sorption Performance of Amine Coated Silica Aerogel Sorbents: Effect of Synthesis Methods.* Ind . Eng. Chem. Res., 2013. **52**: p. 14671.

16. G. Qi, Y. Wang, L. Estevez, X. Duan, N. Anako, A. A. Park, W. Li, C. W. Jones, E. P. Giannelis, *High efficiency nanocomposite sorbents for CO_2 capture based on amine-functionalized mesoporous capsules.* Energy Environ. Sci., 2011. **4**(444).
17. A. Heydari-Gorji, A. Sayari, *Thermal, Oxidative, and CO_2 - Induced Degradation of Supported Polyethyleneimine Adsorbents.* Ind . Eng. Chem. Res., 2012. **51**: p. 6887.
18. V. Zeleňák, M. Badanićová, D. Halamová, J. Čejka, N. Murafa, G. Goerigk, *Amine-modified ordered mesoporous silica: Effect of pore size on carbon dioxide capture.* Chemical Engineering Journal, 2008. **144**(2): p. 336-342.
19. D. S. Dao, H. Yamada, K. Yogo, *Large-Pore Mesostructured Silica Impregnated with Blended Amines for CO_2 Capture. Ind . Eng. Chem. Res.*, 2013. **52**: p. 13810.
20. X. Xu, C. Song, J. M. Andresen, B. G. Miller, A. W. Scaroni, *Novel Polyethyleneimine-Modified Mesoporous Molecular Sieve of MCM-41 Type as High Capacity Adsorbent For CO_2 Capture. Energy & Fuels*, 2002. **16**: p. 1463.
21. X. Xu, C. Song, J. M. Andresen, B. G. Miller, A. W. Scaroni, *Preparation and characterization of novel CO_2 "molecular basket" adsorbents based on polymer-modified mesoporous molecular sieve MCM-41. Microporous and Mesoporous Materials*, 2003. **62**: p. 29.
22. W. Li, S. Choi, J. H. Drese, M. Hornbostel, G. Krishnan, P. M. Eisenberger, C. W. Jones, *Steam-Stripping for Regeneration of Supported Amine-Based CO_2 Adsorbents. ChemSusChem*, 2010. **3**: p. 899.
23. R. K. Iler, *The Chemistry of Silica.* John Wiley & Sons, New York, 1979.
24. Huntsman Corporation , *Ethyleneamines A Global Profile of Products and Services.* Huntsman Corporation, 2007.
25. G. Dacarro, L. Cucca, P. Grisoli, P. Pallavicini, M. Patrini, A. Taglietti, *Monolayers of polyethilenimine on flat glass: a versatile platform for cations coordination and nanoparticles grafting in the preparation of antibacterial surfaces.* Dalton Trans., 2012. **41**: p. 2456.
26. D. J. Fauth, M. L. Gray, H. W. Pennline, *Investigation of Porous Silica Supported Mixed-Amine Sorbents for Post-Combustion CO_2 Capture.* Energy Fuels, 2011. **26**: p. 2483.
27. A. Matsumoto, K. Tsutsumi, K. Schumacher, K. K. Unger, *Surface Functionalization and Stabilisation of Mesoporous Silica Spheres by Silanization and Their Adsorption Characteristics.* Langmuir, 2002. **18**: p. 4014.
28. T. Tatsumi, K. A. Koyano, Y. Tanaja, S. Nakata, *Stabilization of M41S Materials by Trimethylsilyation.* Stud. Surf. Sci. Catal., 1998. **117**: p. 143.
29. Z. Bacsik,, N. Ahlsten, A. Ziad, G. Zhao, A. E. Garcia-Bennett, B. Martín-Matute, N. Hedin, *Mechanisms and Kinetics for Sorption of CO2 on Bicontinuous Mesoporous Silica Modified with n-Propylamine.* Langmuir, 2011. **27**(17): p. 11118-11128.
30. F. Zhang, Y. Yang, H. Yang, Y. Meng, C. Yu, B. To, D. Zhao, *Understanding the Effect of Wall strucutre on the Hydrothermal Stability of Mesostructured Silica SBA-15.* J. Phys. Chem. B, 2005. **109**: p. 8723.
31. Q. Li, Z. Wu, B. Tu, S. S. Park, C. Ha, D. Zhao, *Highly hydrothermal stability of ordered mesoporous aluminosilicates Al-SBA-15 with high Si/Al ratio.* Microporous and Mesoporous Materials, 2010. **135**: p. 95.

32. W. Chaikittislip, H. Kim, C. W. Jones, *Mesoporous Alumina-Supported Amines as Potential Steam-Stable Adsorbents for Capturing* CO_2 *from Simulated Flue Gas and Ambient Air*. Energy Fuels, 2011. **25**: p. 5528.

CHAPTER SIX

Post functionalisation of impregnated silica adsorbents with hydrophobic silanes

6.1 Introduction

Chapter 5 concluded that both impregnated and covalently tethered amine functionalised silicas are unstable under steam regeneration conditions. The mechanism of deactivation was due to the impregnated amine solubilising and leaching from the pores of the adsorbent. Reagglomeration of the amine within the smallest pores of the adsorbent, where they are less accessible also contributed to deactivation. Leaching of amine polymer from the pores of the adsorbent would be problematic in practical adsorption systems. It was found that the stability of the amine was proportional to the molecular weight of the amine adsorbent. In instances where lower molecular weight TEPA was impregnated the extent of amine dissolution was much greater and the support became degraded. Support degradation was also suggested for covalently grafted 3-aminopropyltrimethoxysilane with an incomplete coverage of silica. It is believed that when the bare silica surface is exposed in the presence of both amines and condensed water within the pores, the high pH environment hydrolyses the silica support.

Owing to the economic benefits of steam regeneration and lack of suitable alternatives, there is a clear a need for steam stable adsorbents. Work by Chaikittislip *et al*. investigated amine impregnated mesoporous alumina as a method of increasing the steam stability of the adsorbents, rationalising alumina to be a more stable support [1]. They noted an apparent increase in the stability of 30 wt % PEI on alumina adsorbents than 25 wt% PEI on silica. However the differences in stability could be attributed to the differences in accessible pore volume. This was demonstrated by the stability of S-PEI-SP in Chapter 6. Given the limited information and the importance of the support in adsorbent stability, it is difficult to ascertain whether alumina supports do increase the stability of impregnated amines adsorbents.

Given the lack of stability of impregnated and grafted adsorbents investigated in Chapter 5 the concept of installing a barrier around the exterior of the adsorbent particles was explored. The aim being to selectively functionalise the exterior and pore mouths of the support with hydrophobic groups. This would prevent leaching of the active amine component and may reduce the rate at which water enters the pores. It can be envisaged that the amine polymer will not interact with hydrophobic groups in the same way as surface silanols, which may led to an energy barrier towards leaching.

6.2 Design of adsorbents

In this investigation four different alkoxysilanes were grafted onto S-PEI using the preparation described in Section 3.21. The 4 silanes are given in Figure 6.1. These silanes were selected to provide a range of surface energies and condensation rates. Sterically demanding silanes were chosen to inhibit the deposition of the silanes within the pores of the adsorbents. A similar strategy was used to selectivity functionalise the pore mouths of zeolite L, with the grafting groups too bulky to enter the pores [2]. The presence of guest species in porous silicas has been shown restrict access to the internal pore structure. This has been used to selectively functionalise the exterior of silica particles [3-5]. Given the large pore size of the support used in this study some of the silanes would be able to enter the pores. The polymeric amine was used to block access to hydrolysable silica sites within the pores leading to selective functionalisation at the exterior surface and pore mouths of the particles. Chlorosilanes were avoided owing to the evolved HCl deactivating the amines and requiring extensive washing which may strip the amine from the support.

Triethoxyphenylsilane

Trimethoxy(octyl)silane

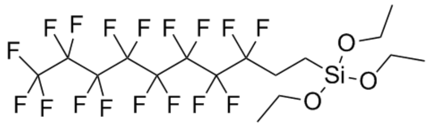

1H,1H,2H,2H-Perfluorodecyltriethoxysilane

Hexadecyltrimethoxysilane

Figure 6.1. The 4 alkyoxysilanes that were grafted onto the surface onto the S-PEI adsorbent.

Long chain alkyl groups are commonly used to create hydrophobic surfaces yielding a contact angle on a clean silica surface greater than 100 ° [6]. Octylsilane also has a much lower steric requirement than hexadecylsilane which is anticipated to have a larger contact angle. The fluorinated silane was chosen as it is expected to have larger steric demands with a very high contact angle and should be the most hydrophilic. Phenyl groups are present in many structures that adsorb CO_2 which may offer additional sites for CO_2 adsorption.

6.3 Characterisation of adsorbents

The characterisation of the barrier coated adsorbents was conducted by ^{13}C SSNMR, nitrogen sorption, organic analysis and DRIFTS. The extent of silane loading was confirmed by TGA, with an additional mass gain proportional to the amount of alkoxysilane added to the S-PEI (Table 6.1). The silane loading (mmol g^{-1}) was calculated using the mass difference between the S-PEI and the silane coated adsorbent divided by the molecular weight of the hydrolysed silane. The greatest loading of silane was attained using triethoxyphenylsilane owing to the smallest steric footprint of the silane. The greater extent of loading is also attributed to the increased rate of hydrolysis of less sterically hindered silanes. Although the silane loading increases with increasing amounts of silane present in the system this does not infer that the silica surface is not completely covered. Trialkoxysilanes are known to auto-condense leading to the formation of oligomers which can then attach to the silica surface [7]. The second highest loading was obtained for octylsilane functionalised sorbents following the rationale for steric arguments. The third highest loading was obtained for hexadecyltrimethoxysilane functionalised sorbents. This silane would offer a similar steric bulk to that of perfluorodecylsilane however, the methoxy groups would be more reactive. The lowest loading was achieved with the sterically demanding perflurodecyltriethoxysilane functionalised adsorbents.

The organic structure of the supported adsorbents was confirmed by ^{13}C and ^{29}Si SSNMR. These confirmed the structure of the amine and coating were not perturbed during the coating process and that bands associated with amine degradation were not present.

Table 6.1. The amount of silane loaded on the adsorbents.

Sorbent	**Organic loading (wt%)**	**MW silane after hydrolysis**	**Mass of silane (wt%)**	**Silane loading (mmol g^{-1})**
S-PEI	32.9	n/a	n/a	n/a
S-PEI-O-L	36.4	114.13	3.5	0.31
S-PEI-O-M	37.0	114.13	4.1	0.35
S-PEI-O-H	37.6	114.13	4.6	0.39
S-PEI-H-L	39.0	256.26	6.1	0.23
S-PEI-H-M	39.6	256.26	6.7	0.26
S-PEI-H-H	40.1	256.26	7.2	0.27
S-PEI-F-L	40.0	475.24	7.1	0.14
S-PEI-F-M	43.2	475.24	10.3	0.21
S-PEI-F-L	44.9	475.24	12.0	0.25
S-PEI-P-L	36.0	108.04	3.1	0.28
S-PEI-P-M	37.9	108.04	5.0	0.46
S-PEI-P-H	39.1	108.04	6.2	0.56

^{29}Si SSNMR are provided in Appendix A17 and show the presence of a Si-C signal in each adsorbent. No signal was observed for a Si-N species across all samples suggesting that the grafting was chemoselective for the surface silanols. The ^{13}C SSNMR spectra of octylsilane coated adsorbents show additional bands at 14.1, 23.2, 30.2 and 33.1 ppm confirming the presence of the octyl chains (Figure 6.2). For perfluorodecylsilane functionalised adsorbents additional peaks appeared at 3.1, 25.6 ppm representing the C-H groups α and β to the Si atom. A weak signal was present between 110-120 ppm, indicative of a C-F species. Owing to the cross-polarisation SSNMR used the signal intensity of these C-F species these is low. For hexadecylsilane functionalised adsorbents the presence of peaks at 14.7, 23.9, 30.6 and 32.9 ppm are responsible for the long hydrocarbon chain. The presence of grafted phenyl species was determined by the aromatic bands at 128.0 and 134.9 ppm.

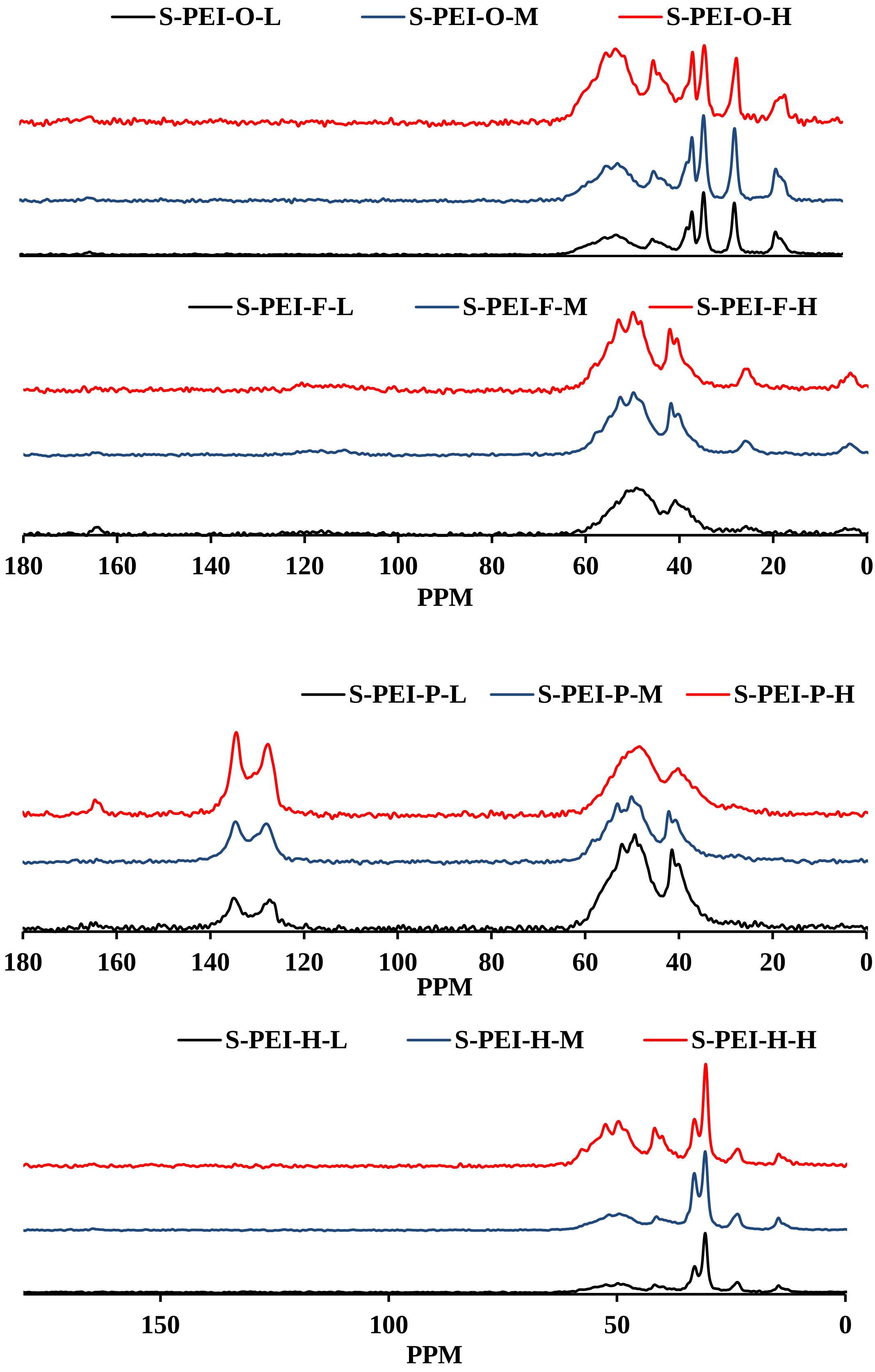

Figure 6.2. ^{13}C SSNMR of the silane modified S-PEI species used in this study.

DRIFTS was used to determine the presence of the coating with a representative spectra given in Figure 6.3. The spectra confirm that the amine has not degraded during the grating process. Slight increases in absorbance are present at ~2930 cm^{-1} for S-PEI-O-M, S-PEI-H-M and S-PEI-P-M relative to S-PEI. This is due to the C-H stretches of these silane groups. The bands corresponding to C-C aromatic stretches or C-F stretches are likely to be obscured by the vibrational bands of the amine and silica respectively.

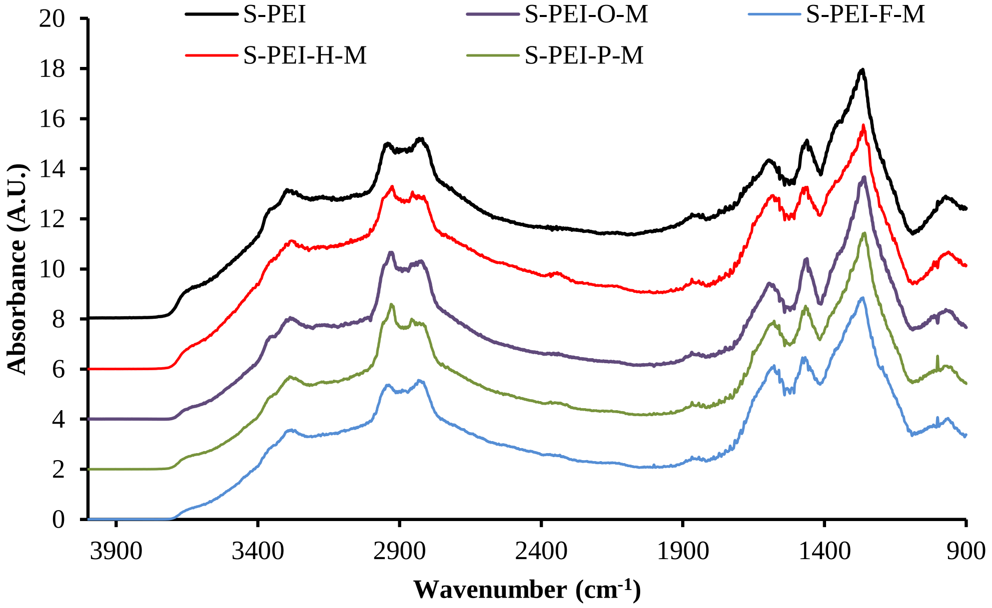

Figure 6.3. Single beam DRIFT spectra comparing the vibration bands of S-PEI and S-PEI-O-M, S-PEI-F-M, S-PEI-H-M and S-PEI-P-M. Referenced to KBr.

6.4 CO_2 adsorption capacities

The effect of the silane coatings on the CO_2 uptakes was determined under 100% CO_2 using the TGA method given in Section 3.4. Both dry and humid adsorption capacities were recorded under 15% CO_2 / N_2, and 15% CO_2, 10% H_2O / N_2 using the fixed bed reactor described in Section 3.3.

6.4.1 CO_2 adsorption of trimethoxy(octyl)silane functionalised S-PEI

Increasing loadings of the octyl silane coating led to a reduction in the CO_2 uptake capacities of the adsorbents (Figure 6.4). Furthermore, the rate of overall rate of CO_2 uptake is inversely proportional to the octylsilane loading. The silane coated adsorbents exhibited typical two-stage kinetics; a kinetically limited regime followed by diffusion limited CO_2 adsorption. For silane coated adsorbents it can be seen that a lower fraction of the CO_2 is occurring in the kinetically limited regime with a greater proportion being diffusion limited. The amine efficiencies normalised for the silane loading, were 0.26, 0.24 and 0.20 for S-PEI-O-L, S-PEI-O-M and S-PEI-O-H respectively. This suggests that increasing octyl silane coatings restricts access to amine groups.

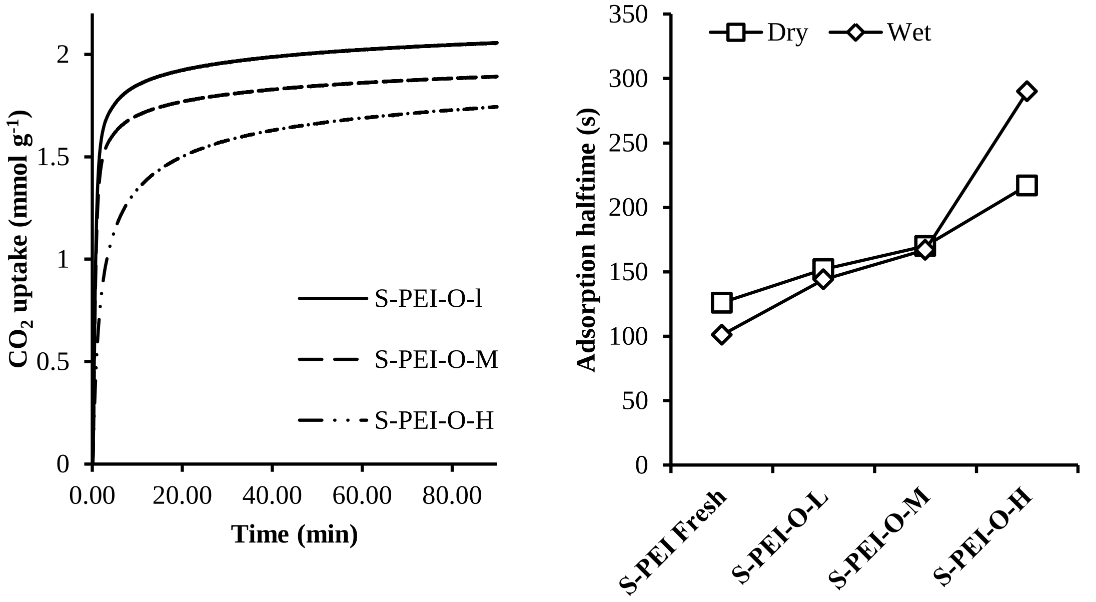

Figure 6.4. CO_2 adsorption uptakes of S-PEI coated with various amounts of octyltrimethoxysilane under 100 % CO_2, 75 °C (left) The effect of water on the adsorption halftimes at 75 °C under 15% CO_2 /N_2 and 15% CO_2 / N_2, 10% H_2O (right).

Under realistic operating conditions the concentration of H_2O in flue gas is typically between 5 and 15 %. To investigate the influence of a hydrophobic coating CO_2 adsorption was conducted under 15 % CO_2 in the presence of 10% water using a packed bed adsorption column described in Section 3.3. The enhancement in adsorption capacity under humid desorption conditions was inversely proportional to the octylsilane loading. For the lowest extent of octyl coating the fractional uptake of humidified CO_2 is greater than dry CO_2. For S-PEI-O-M the rates of adsorption under both dry and wet gas are similar, however with high octylsilane loadings the rate of adsorption is faster for dry analysis conditions. This could be due to a film of water forming over the particles leading to increased diffusional resistance of CO_2 into the pores of the adsorbent. A reduction in CO_2 breakthrough time of impregnated adsorbents co-impregnated with hydrophobic groups under humid gas flows was observed by Wang *et al.* [8]. The slight decreases in adsorption halftime under humid CO_2 observed in this study could be due to lower amounts of hydrophobic groups and their location on the particle. Furthermore there are differences in the concentration of water used and a different reactor design.

Table 6.2. The influence of water on the equilibrium CO_2 uptakes of octylsilane coated adsorbents.

Sorbent	Dry CO_2 uptake (mmolg^{-1})[a]	Amine efficiency (a.u.)	Wet enhancement (%)[b]
S-PEI-O-L	2.05	0.26	11.7
S-PEI-O-M	1.90	0.24	5.8
S-PEI-O-H	1.62	0.21	0.1

[a] Determined using TGA under 100 %CO_2 at 75 °C [b] The relative increase between 15%CO_2/N_2 and 15% CO_2, 10% H_2O/ N_2 determined in the fixed bed reactor at 75 °C.

6.4.2 CO_2 adsorption of perflurodecyltrimethoxysilane functionalised S-PEI

Increasing loadings of the perfluorodecylsilane led to a reduction in the CO_2 adsorption capacity (Figure 6.5). The adsorption halftime increased with silane loading suggesting a lower accessibility of amines at higher silane loadings. The amine efficiencies normalised for the silane loading, were 0.27, 0.23 and 0.20 for S-PEI-F-L, S-PEI-F-M and S-PEI-F-H respectively. The reduction in adsorption capacity, rate and amine efficiency indicate that a greater proportion of the amine was inaccessible with increasing silane loading.

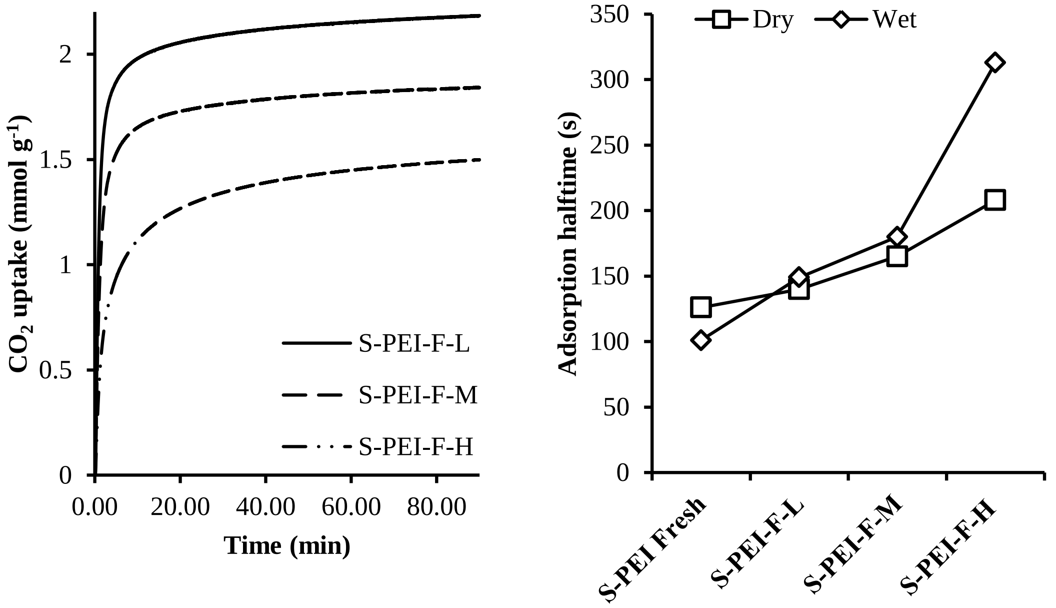

Figure 6.5. CO_2 adsorption uptakes of S-PEI coated with various amounts of perfluorodecyltriethoxysilane under 100 % CO_2, 75 °C (left) The effect of water on the adsorption half times at 75 °C under 15 % CO_2 / N_2 and 10% CO_2, 10% H_2O / N_2 (right).

The CO_2 adsorption capacity of S-PEI-F-L is greater than that of S-PEI-O-L which can be related to the lower amount of silane present in the material. The presence of 10% H_2O in the incoming gas stream led to an increase in the CO_2 adsorption capacity of 7.1 % for S-PEI-F-L. For S-PEI-F-M there was no significant difference in the equilibrium adsorption capacities under both dry and humid adsorption conditions. For the highest loading of fluorinated silane, the equilibrium adsorption capacity was reduced by 2.4 % in the presence of water. The adsorption halftime increased for all fluorinated silane loadings under wet conditions. The magnitude of this effect was greater for increased silane loadings. This could be attributed to water forming a resistive film over the pores of the adsorbent.

Table 6.3. The influence of water on the equilibrium CO_2 uptakes of perfluorodecylsilane coated adsorbents.

Sorbent	**Dry CO_2 uptake (mmol g^{-1})[a]**	**Amine efficiency (a.u.)**	**Wet enhancement (%)[b]**
S-PEI-F-L	2.18	0.28	7.2
S-PEI-F-M	1.84	0.23	-0.2
S-PEI-F-H	1.49	0.19	-2.4

[a] Determined using TGA under 100 %CO_2 at 75 °C [b] The relative increase between 15%CO_2/N_2 and 15% CO_2, 10% H_2O/ N_2 determined in the fixed bed reactor at 75 °C.

6.4.3 CO_2 adsorption hexadecyltrimethoxysilane functionalised S-PEI

Increasing loadings of the hexadecyltrimethoxysilane led to a reduction in the equilibrium CO_2 adsorption capacity (Figure 6.6). The adsorption halftimes were proportional to silane loading suggesting silane restricted access to the amine. The amine efficiencies corrected for differences in silane loading decreased with silane loading are 0.27, 0.23 and 0.17 for low, medium and high loadings of hexadecyltrimethoxysilane. This suggests that a greater proportion of the amine was inaccessible with increasing silane loading.

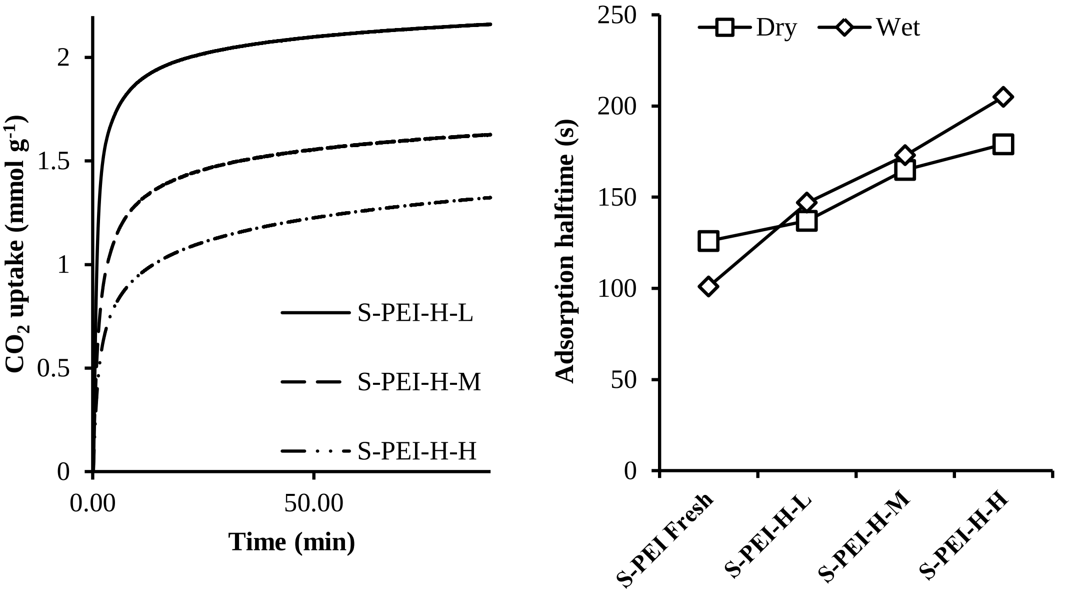

Figure 6.6. CO_2 adsorption uptakes of S-PEI coated with various amounts of hexadecyltrimethoxysilane under 100% CO_2, 75 °C (left) The effect of water on the adsorption half times at 75 °C under 15% CO_2 / N_2 and 15% CO_2 10% H_2O / N_2 (right).

Under humid adsorption conditions the CO_2 adsorption capacity for S-PEI-H-L increased by 7.9 %. Increasing levels of hexadecylsilane loading led to distinct reductions in CO_2 adsorption under humid conditions relative to dry conditions. The adsorption halftimes were increased in the presence of water for all hexadecylsilane functionalised adsorbents. This suggests the hydrophobic water formed a film over the surface of the adsorbents, reducing the rate of uptake.

Table 6.4. The influence of water on the equilibrium CO_2 uptakes of hexadecylsilane functionalised adsorbents.

Sorbent	Dry CO_2 uptake (mmol g^{-1})[a]	Amine efficiency (a.u.)	Wet enhancement (%)[b]
S-PEI-H-L	2.15	0.27	7.9
S-PEI-H-M	1.74	0.23	-4.2
S-PEI-H-H	1.33	0.17	-25.4

[a] Determined using TGA under 100 %CO_2 at 75 °C [b] The relative increase between 15%CO_2/N_2 and 15% CO_2, 10% H_2O/ N_2 determined in the fixed bed reactor at 75 °C.

6.4.4 CO_2 adsorption triethoxyphenylsilane functionalised S-PEI

Increasing loadings of phenylsilane led to a reduction in the CO_2 adsorption capacity (Figure 6.7). The adsorption halftimes appear to decrease for increasing silane loading suggesting that the inclusion of the silane is restricting access to the amine adsorption sites. The amine efficiencies were 0.29, 0.23 and 0.22 for S-PEI-P-L, S-PEI-P-M and S-PEI-P-H respectively. The CO_2 uptake of S-PEI-P-L was the highest reported for the silane functionalised adsorbents. This is attributed to the low loading of the least sterically bulky silane.

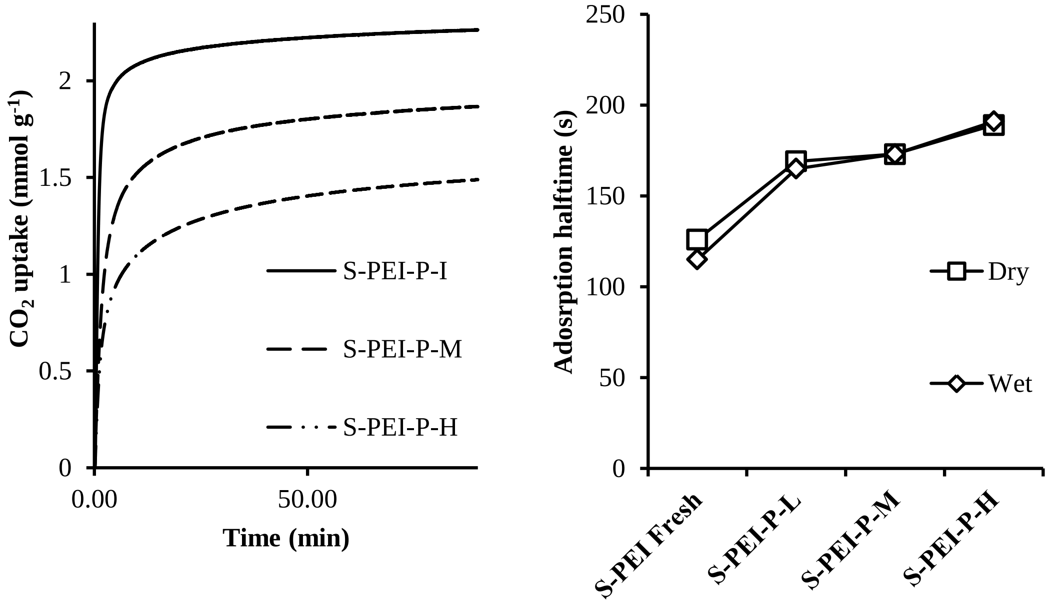

Figure 6.7. CO_2 adsorption uptakes of S-PEI coated with various amounts of triethoxyphenylsilane under 100% CO_2, 75 °C (left) The effect of water on the adsorption half times at 75 °C under 15% CO_2 / N_2 or 15% CO_2, 10% H_2O / N_2 (right).

The CO_2 adsorption capacity for phenyl coated adsorbents increased relative to the adsorption capacities measured under dry adsorption conditions. Under humid adsorption conditions the CO_2 adsorption capacity increased 13.2% for S-PEI-P-L and 8.8% and 6.0% for S-PEI-P-M and S-PEI-P-H respectively. The fractional uptakes of CO_2 adsorption in the presence of water suggest that the presence of water does not adversely affect the adsorption of CO_2.

Table 6.5. The influence of water on the equilibrium CO_2 uptakes of phenylsilane functionalised adsorbents.

Sorbent	**Dry CO_2 uptake (mmolg^{-1})[a]**	**Amine efficiency (a.u.)**	**Wet enhancement (%)[b]**
S-PEI-P-L	2.26	0.29	13.2
S-PEI-P-M	1.86	0.24	8.8
S-PEI-P-H	1.74	0.22	6.0

[a] Determined using TGA under 100 %CO_2 at 75 °C [b] The relative increase between 15%CO_2/N_2 and 15% CO_2, 10% H_2O/ N_2 determined in the fixed bed reactor at 75 °C.

All silane coated sorbents possessed a reduced CO_2 sorption capacity compared to S-PEI, coupled with a reduction in the overall uptake kinetics. Within the different loadings of the same silane structure it can be seen that increasing amounts of silane led to a reduction in the CO_2 adsorption capacity. This is accompanied with a reduction in adsorption rate. The relative rate of adsorption proceeds from fastest to slowest phenyl, octyl, fluoryl and hexadecylsilanes for the most highly loaded adsorbents. This could be related to the steric increasing requirements of the silanes. It is apparent that the presence of increased amounts of silane coating decreases the observed rate of uptake as well as the equilibrium capacity in the presence of 10% H_2O. This could be attributed to the formation of a resistive film of water over the hydrophobic adsorbent inhibiting the diffusion of CO_2 within the pores of the adsorbent. Alternatively this could be attributed to constriction around the mouth of the pores of the adsorbents restricting the adsorption of CO_2.

6.5 Pore structure characterisation of post functionalised S-PEI adsorbents

Changes to the porous structure of the adsorbents after the addition of various barrier coatings was investigated by nitrogen sorption.

6.5.1 Pore structure characterisation of trimethoxy(octyl)silane functionalised S-PEI

Nitrogen sorption isotherms of octylsilane functionalised adsorbents are presented below in Figure 6.8 and summarised in Table 6.6. It can be seen that increasing extents of silane coating led to a reduction in surface area and pore volume. The decreases in surface area and pore volume are greater than which can be rationalised by mass gain from silane addition. For adsorbents with high octylsilane loading the presence of ink well pores was observed from a kink in the desorption branch at 0.45 P/P_0. The effect is less pronounced that ordered materials such as SBA-16 or vycor glass as studied by Neimark *et al.* owing to the wider range of pore sizes present in the material [9].

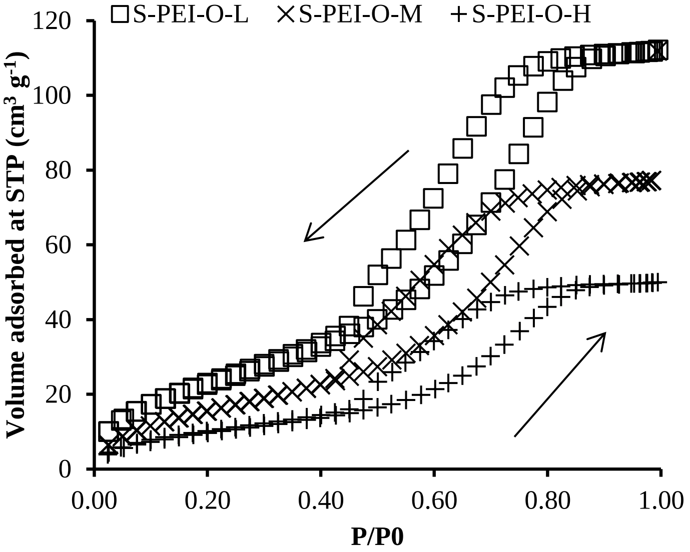

Figure 6.8. Nitrogen sorption of S-PEI-O-L, S-PEI-O-M and S-PEI-O-H at 77 K.

Table 6.6. A summary of the porosity of phenylsilane coated adsorbents.

Sorbent	**BET surface area (m^2g^{-1})**	**BET C constant (a.u.)**	**Pore volume ($cm^3\,g^{-1}$)**	**Inaccessible P_v (%)**
S-PEI-O-L	91 +/- 7.7	25	0.17 +/- 0.01	59.7
S-PEI-O-M	53 +/- 4.4	26	0.12 +/- 0.01	71.1
S-PEI-O-H	44 +/- 3.8	25	0.08 +/- 0.01	80.5

The presence of partial cavitation and change in hysteresis between the uncoated and coated samples suggests that the silane is present near the pore mouths of the adsorbents. The BET C constant is 83.8 for bare Davisil support and 30 for S-PEI, which is accounted for by the significant differences in the energy of adsorption of nitrogen on the bare SiO_2 surface and a PEI coated surface. For S-PEI-O-L, S-PEI-O-M and S-PEI-O-H the C constant reduces to 25. This shift suggests that the nitrogen is adsorbing onto a surface with a slightly different enthalpy of adsorption. This could be assigned to the nitrogen adsorbing onto the hydrocarbon chains of the octylsilane. The magnitude of the C constant does not change with increasing silane loading indicating that the changes in surface energy are slight. The BJH PSD does not appear to change with increasing loadings suggesting that the silane coating does not intrude into the pores of the adsorbent (Figure 6.9). A reduction in pore volume is evident over all pore sizes with increasing silane loading rationalising the reduction in amine accessibility.

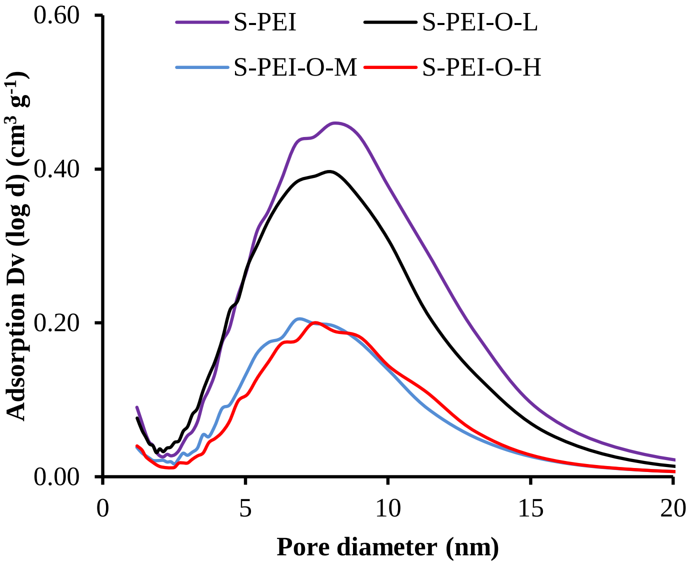

Figure 6.9. BJH PSD of octylsilane functionalised S-PEI with a range of silane loadings.

6.5.2 Pore structure characterisation of perfluorodecyltriethoxysilane functionalised S-PEI

Nitrogen sorption isotherms of perfluorodecylsilane functionalised sorbents are presented in Figure 6.10 and summarised in Table 6.7. Increasing levels of silane loading led to a significant reduction in surface area and pore volume greater than which can be attributed to mass gain alone. This suggests that silane deposition may lead to a degree of pore blocking. S-PEI-F-H has lost a significant amount of pore volume suggesting that silanes may have condensed within the pores of the adsorbent. Partial cavitation is observed for all perfluorodecylsilane adsorbents suggesting that at least a portion of the silane is located near the pore mouths.

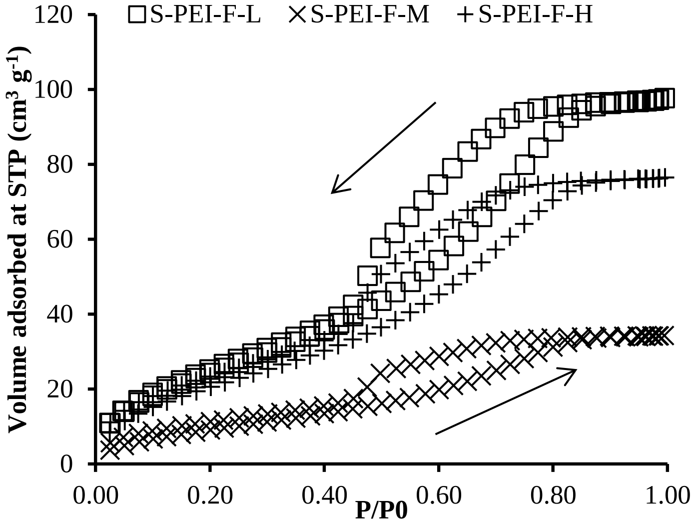

Figure 6.10. Nitrogen sorption of S-PEI-F-L, S-PEI-F-M and S-PEI-F-H at 77 K.

Table 6.7. A summary of the porosity of perfluorodecylsilane functionalised adsorbents.

Sorbent	BET surface area (m^2g^{-1})	BET C constant (a.u.)	Pore volume ($cm^3\ g^{-1}$)	Inaccessible P_v (%)
S-PEI-F-L	99.9 +/- 9.5	22	0.15 +/- 0.01	61.2
S-PEI-F-M	86.1+/- 9.4	19	0.11 +/- 0.01	68.9
S-PEI-F-H	37.2 +/- 3.6	21	0.05 +/- 0.01	85.1

The BET C constant for silane modified adsorbents did not vary significantly with increasing silane concentrations and remained lower than that of S-PEI. This suggests that there were little changes in the overall surface energy with increasing silane loadings. The BJH PSD indicated that the introduction of the fluorinated silane led to a slight reduction in the volume of the largest sized pores. (Figure 6.11). The reduction in pore volume suggests increasing silane concentrations lead to increasing amounts of poor blocking.

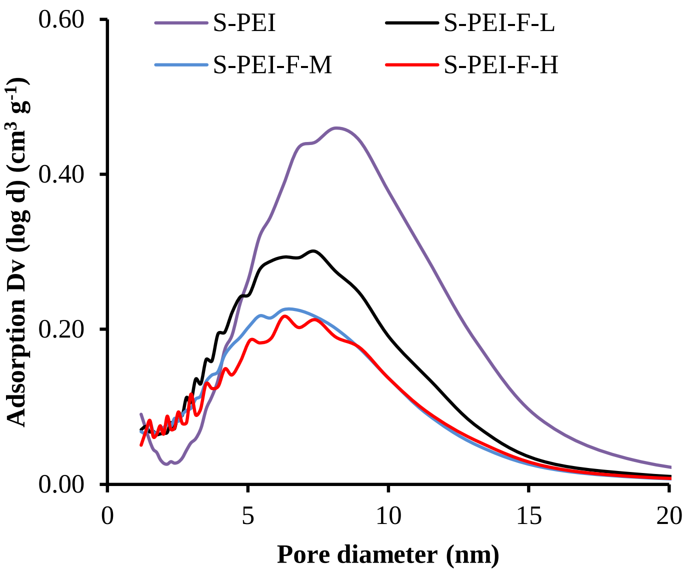

Figure 6.11. BJH PSD of perfluorodecylsilane functionalised S-PEI with a range of silane loadings.

6.5.3 Pore structure characterisation of hexadecyltrimethoxysilane functionalised S-PEI

Nitrogen isotherms of hexadecylsilane functionalised adsorbents are given below in Figure 6.12 with a summary presented in Table 6.8. Similar to other adsorbents increasing concentrations of silane lead to a reduction in pore volume and surface area. The BET C constants have little variation with silane loading suggesting that the overall surface energy is not changing significantly with increasing silane loading. Partial cavitation is also present for the silane loaded adsorbents suggesting that a portion of the silane is located at the pores mouths of the adsorbents. Both S-PEI-H-M and S-PEI-H-H exhibit large reductions in pore volume compared to S-PEI. This suggests that a fraction of the silane may be residing within the pores of the adsorbent.

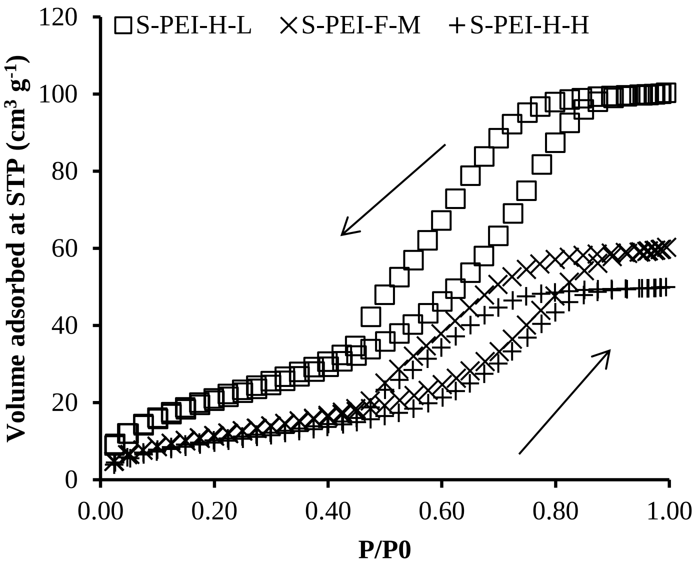

Figure 6.12. Nitrogen sorption of S-PEI-H-L, S-PEI-H-M and S-PEI-H-H at 77 K.

Table 6.8. A summary of the porosity of hexadecylsilane functionalised adsorbents.

Sorbent	**BET surface area (m^2g^{-1})**	**BET C constant (a.u.)**	**Pore volume ($cm^3 g^{-1}$)**	**Inaccessible P_v (%)**
S-PEI-H-L	81.2 +/- 8.9	28	0.16 +/- 0.01	59.6
S-PEI-H-M	46.5+/- 4.1	24	0.09 +/- 0.01	67.9
S-PEI-H-H	38.3 +/-3.2	26	0.07 +/- 0.01	81.8

The BJH PSD with increasing loadings of silane is given below in Figure 6.13. Comparing the relative pore sizes it appears that S-PEI-H-M and S-PEI-H-H have a slightly lower average pore size that the other adsorbents. This suggests that some of the silane may be located within the pores of the adsorbent. This would explain the large reduction in porosity obtained for these two adsorbents.

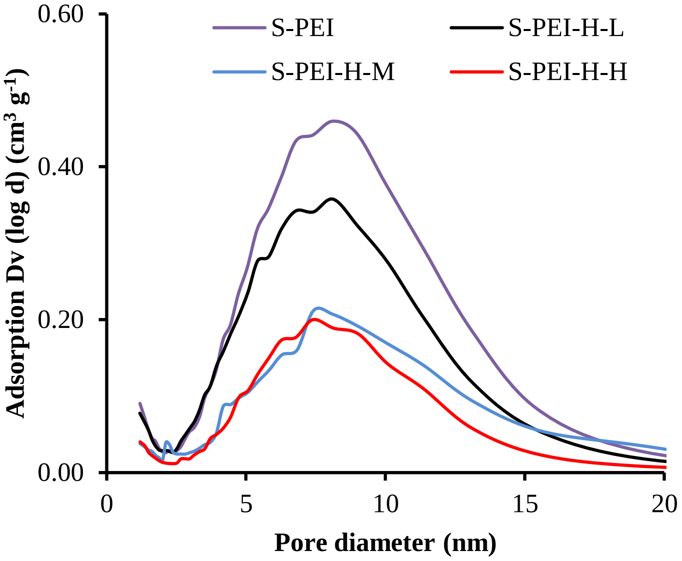

Figure 6.13. BJH PSD of hexadecylsilane functionalised S-PEI with a range of silane loadings.

6.5.4. Pore structure characterisation of triethoxyphenylsilane functionalised S-PEI

Nitrogen sorption isotherms of phenylsilane functionalised adsorbents are given in Figure 6.14 and derived data summarised in Table 6.9. It was found that increasing levels of silane loading led to a reduction in the surface area and pore volume of the adsorbent. The C constant of the BET equation showed little variation with increasing silane loading suggesting that the nature of the surface was not changing.

Table 6.9. A summary of the porosity of phenylsilane functionalised adsorbents.

Sorbent	BET surface area (m^2g^{-1})	BET C constant (a.u.)	Pore volume ($cm^3 g^{-1}$)	Inaccessible P_v (%)
S-PEI-P-L	81.7 +/- 6.5	27	0.15 +/- 0.01	64.8
S-PEI-P-M	63.0+/- 5.0	27	0.11 +/- 0.01	73.0
S-PEI-P-H	49.1 +/- 4.7	22	0.09 +/- 0.01	77.2

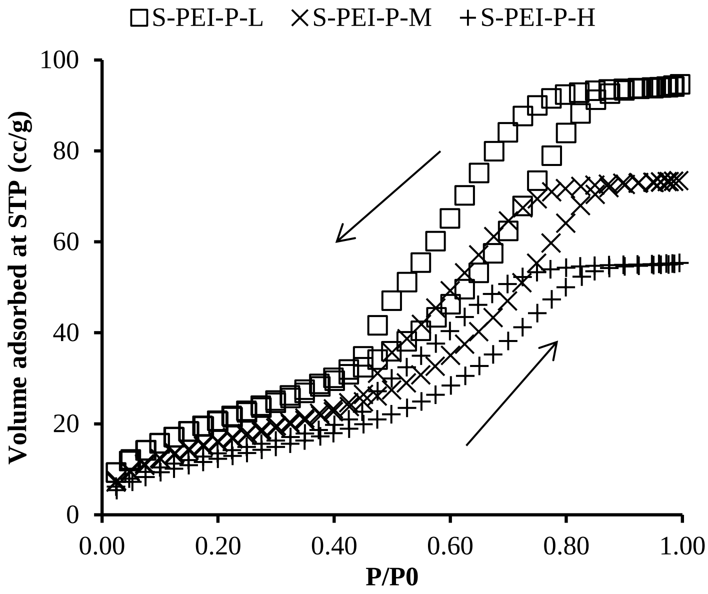

Figure 6.14. Nitrogen sorption of S-PEI-P-L, S-PEI-P-M and S-PEI-P-H.

The BJH PSD shows a shift to slightly lower pore sizes with increased silane loadings (Figure 6.15). This suggests that silane is present either around the pore mouths or within the pores of the adsorbent. A clear reduction in the total pore volume was observed over all pore sizes with increasing silane loading.

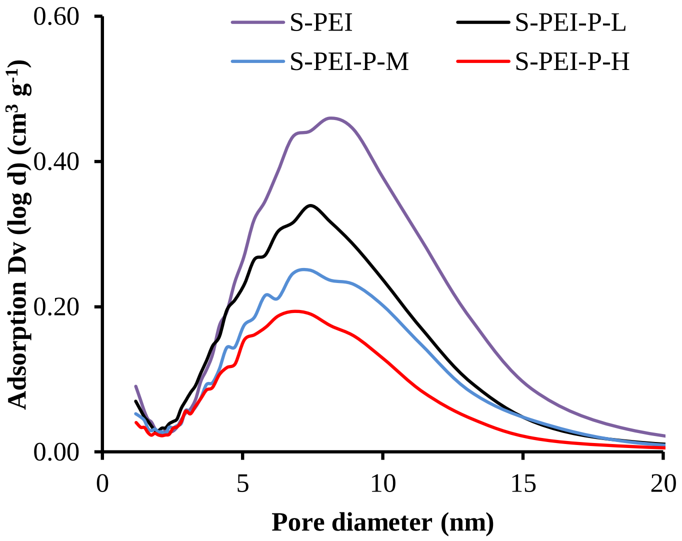

Figure 6.15. BJH PSD of phenylsilane functionalised S-PEI with a range of silane loadings.

6.6 Aging of silane modified S-PEI adsorbents under steam regeneration conditions

The adsorbents developed in this chapter were submitted to aging under steam regeneration conditions of 66% H_2O / N_2 at 130 °C for 8 h, as described in Section 3.22. CO_2 adsorption capacities before and after aging were measured using the TGA method described in Section 3.4 under 100 % CO_2 at 75 °C. The overall rate of adsorption was compared using TGA uptake curves as the time take to 0.8 fractional uptake.

6.6.1 Stability of trimethoxy(octyl)silane functionalised S-PEI under steam regeneration conditions

Steam regeneration aging of octylsilane coated adsorbents led to reductions in the CO_2 adsorption capacities of all sorbents irrespective of silane loading (Figure 6.16). The retention the CO_2 adsorption capacity was 90, 91 and 92 % for low, medium and high amounts of trimethoxy(octyl)silane loading respectively. This compares favourably to that of S-PEI which retained 55 % of its CO_2 uptake after identical aging. This suggests that increasing silane loading from 0.31 leads to only marginal gains in the stability of the adsorbents. The time taken to reach 80% of the adsorbents capacity appears to increase after aging suggesting the amine is less accessible (Figure 6.16). This change in time to 80 % uptake appears to proportional to the silane loading.

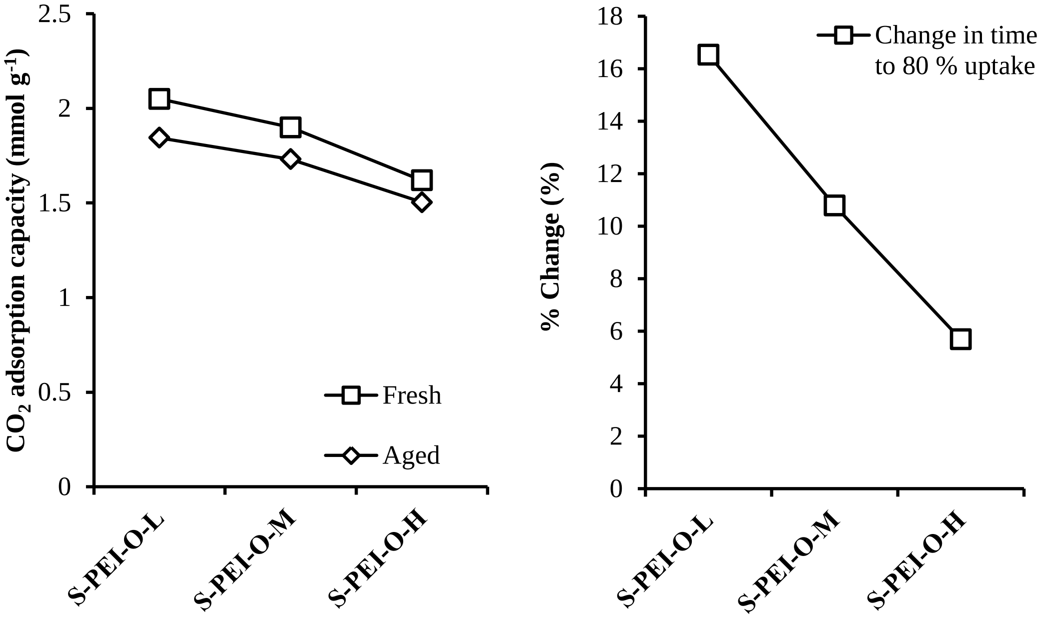

Figure 6.16. CO_2 adsorption uptakes of octylsilane functionalised adsorbents before and after steam aging conducted under 100% CO_2 at 75 °C (left). Changes in the time taken to reach 80 % CO_2 uptake under 100% CO_2 at 75 °C (right) .

Changes in the porous properties of the adsorbents were characterised by nitrogen sorption. Complete isotherms can be found in Appendix A18 - A20 with a summary of the relevant details provided in Table 6.10. The BET surface area deceased for the S-PEI-O-L coupled a reduction in the organic loading of the material. The amount of organic losses appear greater for S-PEI-O-M and S-PEI-O-H than S-PEI-O-L.

Table 6.10. Changes in the porosity of the octylsilane coated adsorbents after aging.

Sorbent	**BET Surface area (m^2 g^{-1})**		**Pore Volume (cm^3 g^{-1})**		**Organic**
	Fresh	**Aged**	**Fresh**	**Aged**	**loss (%)**
S-PEI-O-L	91 +/-7.7	80 +/-6.8	0.17 +/-0.01	0.16 +/-0.01	6.1
S-PEI-O-M	53 +/-4.4	74 +/-6.1	0.12 +/-0.01	0.15 +/-0.01	10.6
S-PEI-O-H	44 +/-3.8	55 +/-4.7	0.08 +/-0.01	0.10 +/-0.01	10.3

Note: The BET C constants did not change after aging.

Considering the BJH PSD of S-PEI-O-L it can be seen that the average pore size increases with aging. This suggests that amine is lost from the largest pores of the adsorbent similar to the deactivation of S-PEI (Figure 6.17). There also appears to be a loss in the volume in pores below 8 nm suggesting that PEI is agglomerating within these pores. The reduction in surface area could be attributed to the amine reagglomerating within the smallest pores meaning they are inaccessible to nitrogen at 77 K. This is a similar mechanism to the aging of S-PEI reported in Chapter 5. This would lead to a reduction in the accessibility of the amine under adsorption conditions accounting for the increase in time taken to reach 80 % capacity. The BET surface area and pore volume of S-PEI-O-M and S-PEI-O-H increase with aging. This is accompanied by an increase in the amount of organic losses. This suggests that for these adsorbents unstable organics are being removed from the support. This could be due to octylsilane oligomers being washed from the pores of adsorbent. These could be formed by the condensation of trimethoxy(octyl)silane within the pores of the adsorbent independent of the silica surface. The BJH PSD of S-PEI-O-M and S-PEI-O-H show pore volume increases overall all pore sizes, which could be due to the removal of weakly bound guest such as a silane oligomer. DRIFTS indicated no change in organic structure was present after aging for all levels of silane loading (Appendix A21).

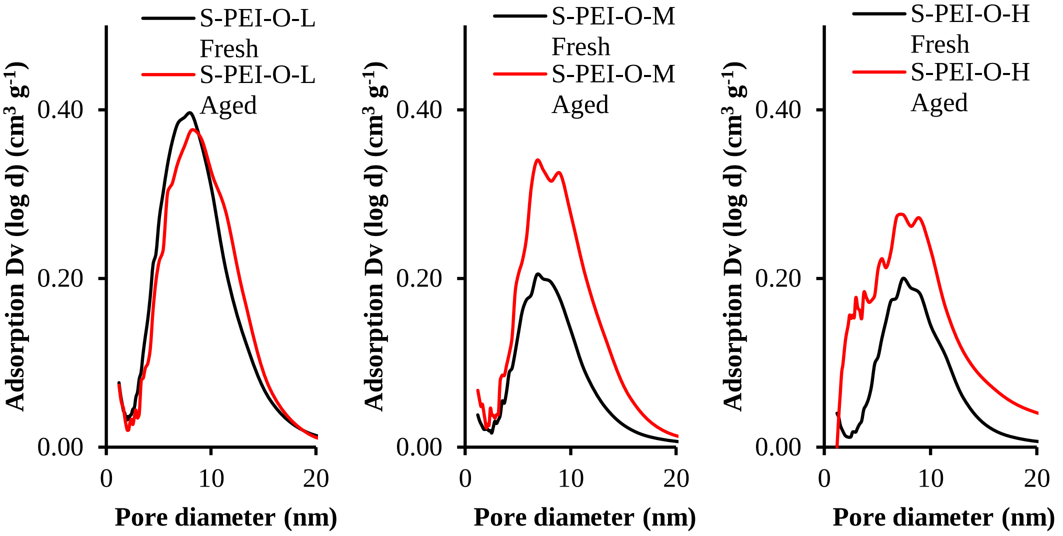

Figure 6.17. BJH PSD for octylsilane coated adsorbents before and after aging under steam regeneration conditions.

6.6.2 Stability of perfluorodecyltriethoxysilane functionalised S-PEI under steam regeneration conditions

Aging of the perfluorodecylsilane functionalised adsorbents under 66% H_2O / N_2 at 130 °C for 8 h led to a reduction in capacity for all adsorbents (Figure 6.18). The retention the CO_2 adsorption capacity was 96% for S-PEI-F-L and S-PEI-F-M respectively. The time taken for S-PEI-F-L and S-PEI-F-M to reach 80 % of their total uptake capacity increased slightly after aging. Interestingly S-PEI-F-H exhibited an increase in the CO_2 adsorption capacity after aging as well as a decrease in the time to 80% of the total uptake capacity.

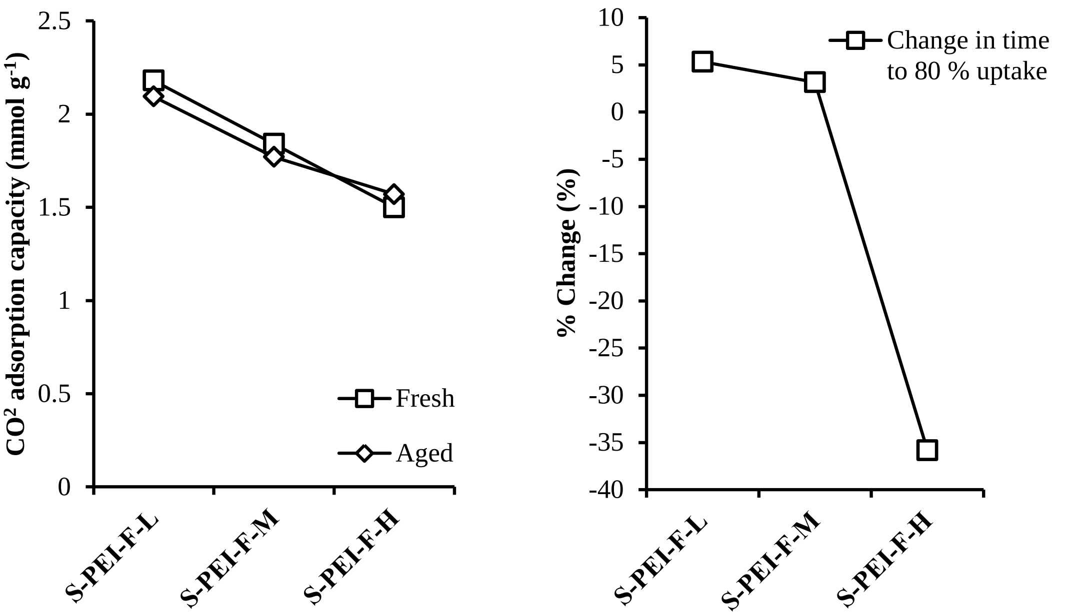

Figure 6.18. CO_2 adsorption uptakes of perfluorodecylsilane functionalised adsorbents before and after steam aging conducted under 100 % CO_2 at 75 °C (left). Changes in the time taken to reach 80% CO_2 uptake under 100% CO_2 at 75 °C (right).

Changes to the structure of the adsorbents after aging were determined using nitrogen sorption and are summarised in Table 6.11. Full isotherms can be found in Appendix A22-A24. Aging of S-PEI-F-L led a reduction in surface area with negligible change in pore volume.

Table 6.11. Changes in the porosity of the perfluorodecyl coated adsorbents after aging.

Sorbent	BET Surface area (m^2 g^{-1})		Pore Volume (cm^3 g^{-1})		Organic loss (%)
	Fresh	Aged	Fresh	Aged	
S-PEI-F-L	99.0 +/-9.4	89 +/-8.53	0.15 +/-0.01	0.16 +/-0.01	6.3
S-PEI-F-M	86.1 +/-9.4	98 +/-10.9	0.11 +/-0.01	0.12 +/-0.01	3.1
S-PEI-F-H	37.2 +/-3.6	78 +/-7.8	0.05 +/-0.01	0.15 +/-0.01	10.2

Note: The BET C constants did not change after aging.

The BJH PSD of S-PEI-F-L showed that aging led to loss in the volume of pores below 6 nm and an increase in volume of pores greater than 6 nm. This suggests that the PEI had agglomerated within the smallest pores of the adsorbent and was removed from the largest pores. Aging of S-PEI-F-M led to little change in the structure of the adsorbent with a small amount of increasing pore volume for pores above 8 nm consistent with minimal amine leaching. This adsorbent appeared to be highly stable with 3.1 % of the organic material lost after aging. Aging of S-PEI-F-H led to an increase in pore volume and BET surface area. The BJH adsorption pore size distribution leads to an increase in volume across all pore sizes. This suggests a weakly interacting guest such as silane oligomers are present within the pores of the adsorbent and are removed after aging. This would explain the increase in rate and adsorption capacity observed after aging. DRIFTS suggested no change in organic structure with aging (Appendix A25).

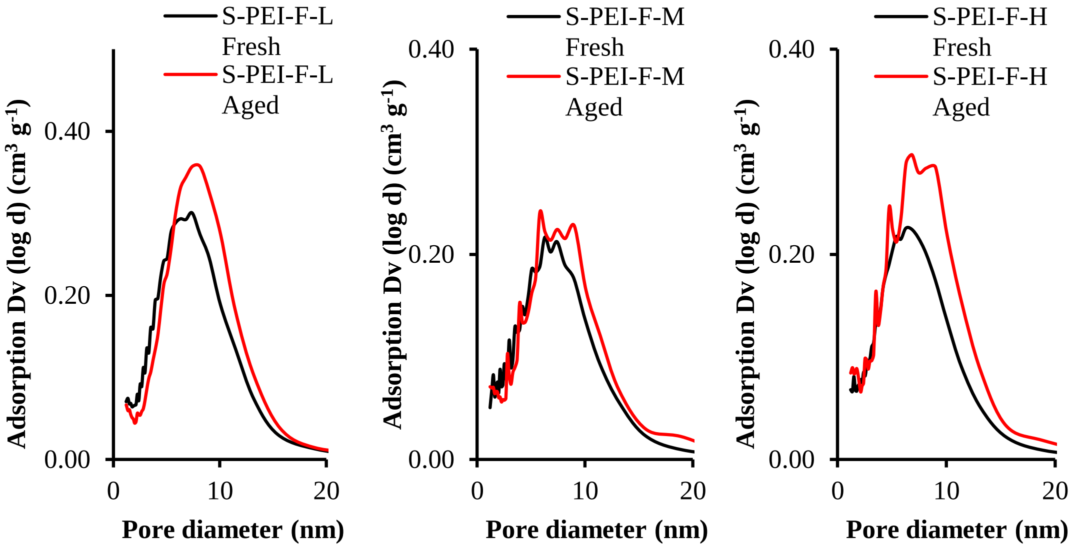

Figure 6.19. BJH PSD for perfluorodecylsilane coated adsorbents before and after aging under steam regeneration conditions.

6.6.3 Stability of hexadecyltrimethoxysilane functionalised S-PEI under steam regeneration conditions

Aging of hexadecylsilane functionalised adsorbents under 66% H_2O / N_2 at 130 °C for 8 h led was conducted and the CO_2 adsorption capacity measured before and after the aging (Figure 6.20). The retention the CO_2 adsorption capacity was 90 and 94 % for S-PEI-F-L and S-PEI-F-M respectively. Similar to S-PEI-F-H, S-PEI-H-H exhibited a 26% increase in the CO_2 adsorption capacity after aging. This increase in capacity was also coupled with a significant reduction in the time taken to reach 80 % of the uptake capacity. This suggests that the amine species in S-PEI-H-H becomes more accessible after aging.

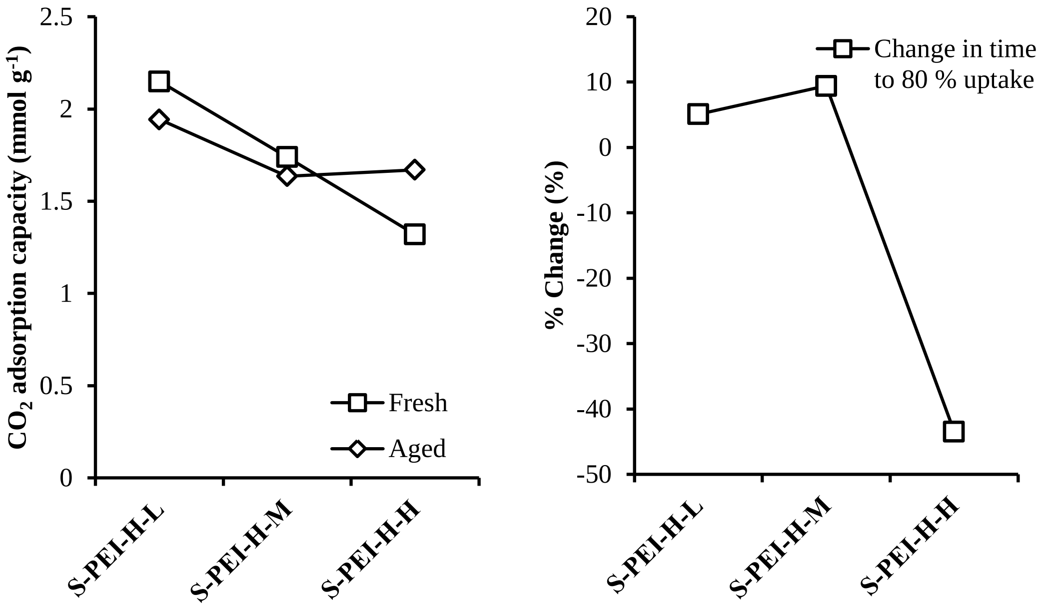

Figure 6.20. CO_2 adsorption uptakes of hexadecylsilane functionalised adsorbents before and after steam aging conducted under 100% CO_2 at 75 °C (left). Changes in the time taken to reach 80% CO_2 uptake under 100% CO_2 at 75 °C (right).

Changes to in the porous structure of the adsorbents were characterised by nitrogen sorption (Table 6.12, Appendix A26 - A28). Aging of S-PEI-H-L led to a reduction in surface are coupled with an increase in the average BJH PSD (Figure 6.21). For S-PEI-H-L there was a loss of volume in pores below 7 nm suggesting PEI had reagglomerated within the smallest pores of the adsorbent. An increase in pore volume at larger pore sizes suggested that amine was selectively removed from the largest pores. Aging of S-PEI-H-M led to small changes in surface area and pore volume with an increase in the average BJH PSD. Coupled with the slight changes in organic loading and surface area this suggests a small amount of amine leaching. The pore structure of S-PEI-H-H changed significantly after aging, with increases in both surface area and pore volume. The BJH adsorption pore size distribution shows that the increases in volume were present over all pore sizes suggesting the removal of a weakly interacting guest. The removal of the guest led to increased amine accessibility and hence a larger CO_2 adsorption capacity. DRIFTS suggested no change in structure after aging (Appendix A29).

Table 6.12. Changes in the porosity of the hexadecyl coated adsorbents after aging.

Sorbent	**BET Surface area ($m^2 g^{-1}$)**		**Pore Volume ($cm^3 g^{-1}$)**		**Organic loss (%)**
	Fresh	**Aged**	**Fresh**	**Aged**	
S-PEI-H-L	81.2+/-8.9	68.6 +/-5.3	0.16 +/-0.01	0.16 +/-0.01	6.6
S-PEI-H-M	46.5+/-4.1	49.1 +/-4.4	0.09 +/-0.01	0.10 +/-0.01	10.3
S-PEI-H-H	38.3+/-3.2	78.5 +/-6.5	0.07 +/-0.01	0.16 +/-0.01	15.2

Note: The BET C constant did not change significantly after aging.

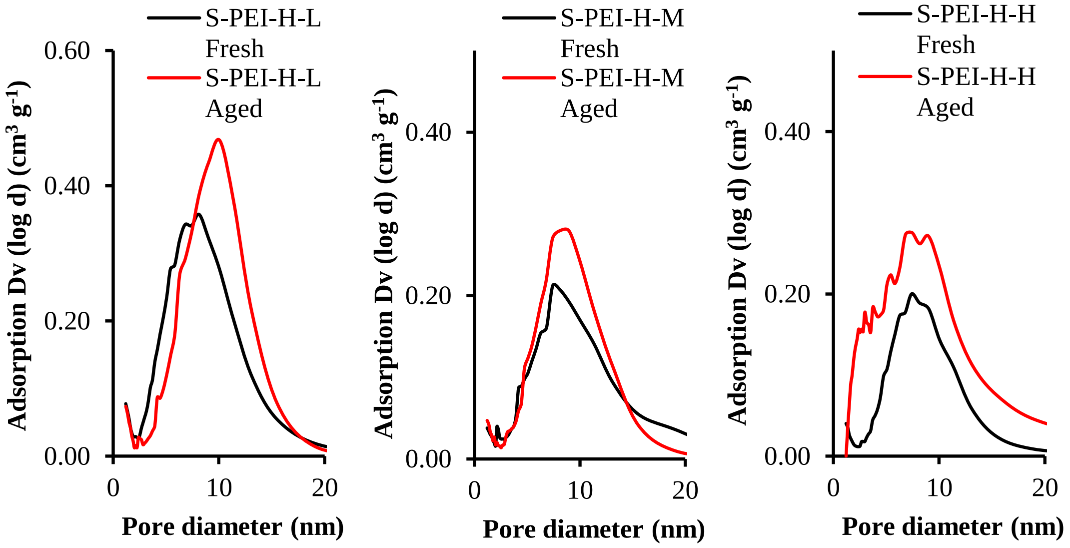

Figure 6.21. BJH PSD for hexadecyl coated adsorbents before and after aging under steam regeneration conditions.

6.6.4 Stability of triethoxyphenylsilane functionalised S-PEI under steam regeneration conditions

Aging of the phenylsilane functionalised adsorbents, under 66% H_2O / N_2 at 130 °C for 8 h led to a reduction in CO_2 uptake for all adsorbents (Figure 6.22). The retention of CO_2 uptake after aging was 80, 87 and 93 % for S-PEI-P-L, S-PEI-P-M and S-PEI-P-H, respectively. The relative change in the time taken for the adsorbent to reach 80 % of its equilibrium adsorption capacity appeared to correlate with phenylsilane loading. S-PEI-P-L and S-PEI-P-M exhibited an increase in the time to 80% CO_2 of adsorption capacity. S-PEI-H observed a decrease in the time to 80% uptake but unlike S-PEI-F-H and S-PEI-H-H, exhibited a reduction in total CO_2 uptake.

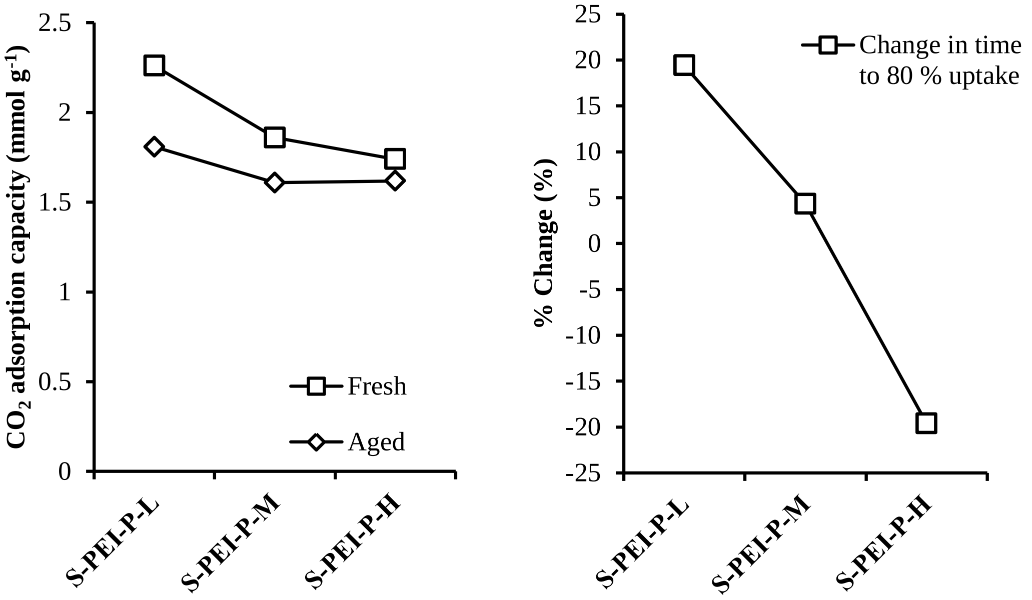

Figure 6.22. CO_2 adsorption uptakes of phenylsilane functionalised adsorbents before and after steam aging conducted under 100% CO_2 at 75 °C (left). Changes in the time taken to reach 80% CO_2 uptake under 100% CO_2 at 75 °C (right).

Changes to the porous nature of the adsorbents after aging were characterised by nitrogen adsorption and are summarised in Table 6.13. Full nitrogen sorption isotherms are given in Appendix A30 - 32 Aging led to reduction in the surface area of S-PEI-P-L with little change in pore volume. The BJH PSD of S-PEI-P-L showed an increase in the volume of pores larger than 8 nm (Figure 6.23). This was coupled with a reduction in the volume of pores below 8 nm. It appears that the amine is agglomerating within the smallest pores of the adsorbent where they are less accessible to CO_2. Organic analysis confirms that a proportion of amine has leached from the pores of the adsorbent. Aging of S-PEI-P-M gave a small increase pore volume and shift in the BJH PSD to larger pores suggests that PEI has leached from the pores of the adsorbent. This is confirmed by the reduction in organic loading after aging. For S-PEI-P-H there is little change in the pore structure with a marginal increase in pore volume. The BJH PSD of S-PEI-P-H is consistent with the removal of silane oligomers evident by the increase in volume across all pore sizes. DRIFTS confirmed no degradation of the organic species (Appendix A33).

Table 6.13. Changes in the porosity of the phenyl coated adsorbents after aging.

Sorbent	**BET Surface area ($m^2 g^{-1}$)**		**Pore Volume ($cm^3 g^{-1}$)**		**Organic**
	Fresh	**Aged**	**Fresh**	**Aged**	**loss (%)**
S-PEI-P-L	81.7+/-6.5	69.8 +/-5.6	0.15 +/-0.01	0.15 +/-0.01	8.7
S-PEI-P-M	63.0+/-5.0	57.7 +/-4.6	0.11 +/-0.01	0.12 +/-0.01	4.8
S-PEI-P-H	49.1+/-4.7	51.2 +/-4.2	0.09 +/-0.01	0.10 +/-0.01	6.9

Note: The BET C constant increased from 22 to 27 for S-PEI-P-H. No changes were observed for other samples.

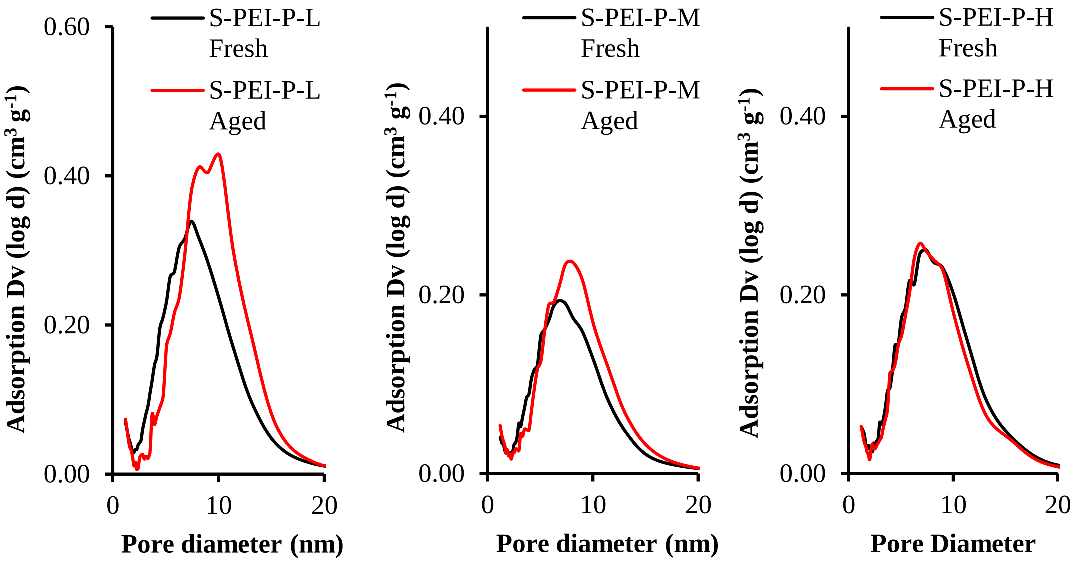

Figure 6.23. BJH PSD for phenyl coated adsorbents before and after aging under steam regeneration conditions.

6.7 Equilibrium water adsorption of S-PEI and S-PEI-F-H

Water adsorption isotherms were completed at 298 K to ascertain if the surface functionality of the adsorbents influenced the sorbent interaction with water. The water adsorption of S-PEI and S-PEI-F-M are compared in Figure 6.23. Both S-PEI and S-PEI-F-M exhibit type III adsorption isotherm with increasing condensation as P/P_0 approaches unity. Between 0.4 – 0.8 P/P_0 the amount of water adsorbed was slightly lower on S-PEI-F-M than S-PEI. Between 0 – 0.3 P/P_0 both adsorbents appear to adsorb similar amounts of water. Above 0.8 P/P_0 condensation of water between particle grains and the pores of the particles would become spontaneous as the partial pressure tends to the saturation pressure of water. To understand if the difference in water uptakes could be related to the surface area of the adsorbents the isotherms were normalised for surface area (Figure 6.24). When normalised for surface area S-PEI-F-M appears to adsorb less water overall and in the range 0-0.3 P/P_0 S-PEI. The difference in water uptake were slight from the limited samples analysed, suggested that the introduction of a silane coating may lead a lower uptake of water. However it is not clear if this effect is due the surface functionality or change in pore structure of the adsorbents.

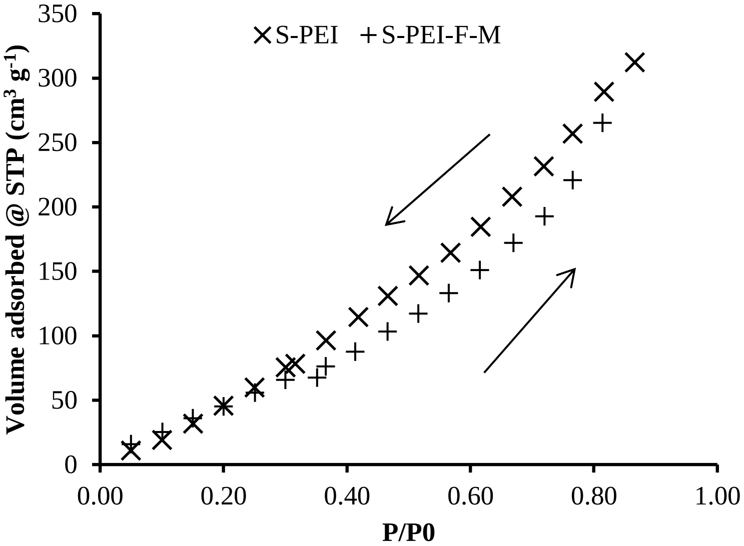

Figure 6.24. Water adsorption isotherm of S-PEI and S-PEI-F-M at 298 K.

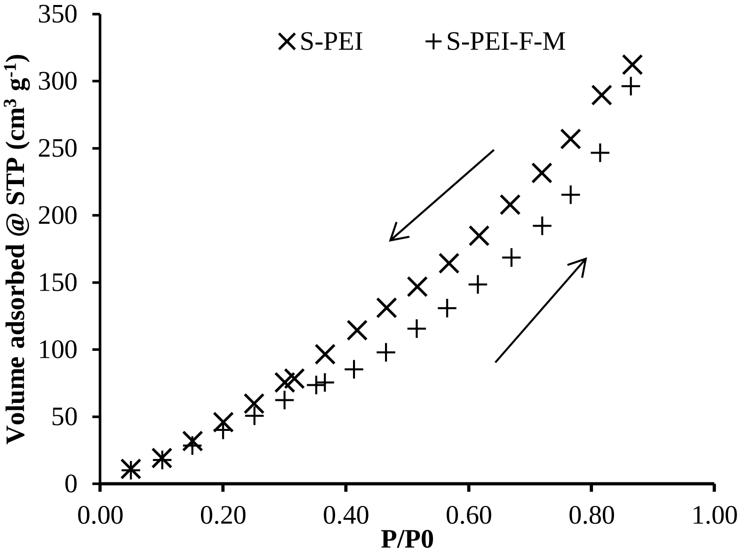

Figure 6.25. Water adsorption isotherm of S-PEI and S-PEI-F-M normalised for surface area of S-PEI at 298 K.

6.8 Dynamic water sorption of S-PEI and S-PEI-F-M

In a realistic operating process the adsorption of water is unlikely to reach equilibrium and as such the kinetics of water adsorption were investigated using dynamic vapour sorption. The rate of water uptake was determined at 333 K with a relative humidity step change between 30 and 33 RH and 87 to 90 RH (Section

3.18). The equilibrium water uptakes are given in Table 6.14 and the equilibrium water uptakes appear to correlate with the volumetric measurements.

Table 6.14. Water adsorption onto S-PEI and S-PEI-F-M determined using dynamic vapour sorption at 333 K.

Adsorbent	**Water uptake (wt%)**		**Surface area corrected uptake (wt%)**	
	33% RH	**90 %RH**	**33 % RH**	**90 %RH**
S-PEI	5.1	27.9	5.1	27.9
S-PEI-F-M	3.8	23.1	4.2	25.6

The fractional uptake of water adsorption between 30 and 33 RH shows that the presence of the barrier coating reduces the rate of water uptake (Figure 6.25). This suggests that the hydrothermal barrier coating may limit the intrusion of water into the porous of the adsorbent. This is turn could lead to a decrease in the rate of solubilisation of the amine polymer, which would reduce the amount of amine leaching. However, it is not clear if the coating imparts any selectivity over that of water as the rate of CO_2 uptake of S-PEI-F-M is lower than that of S-PEI.

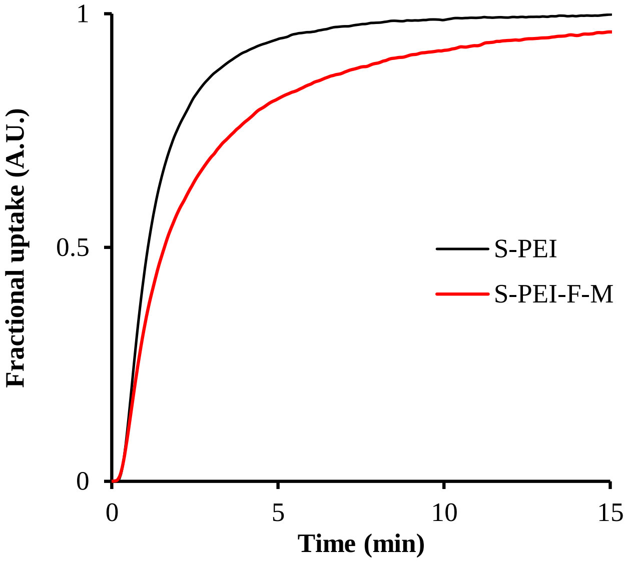

Figure 6.26. The fractional uptake of water of S-PEI and S-PEI-F-M at 60 °C, with a 30 to 33 RH step.

6.9 Discussion

This chapter has described the post functionalisation of S-PEI with a range of hydrophobic silanes. It was shown that by variation of the amount of silane used in the synthesis the amount of silane loading could be varied. Increasing levels of silane led to a reduction in the CO_2 adsorption capacity. For target silane loadings of 1 mmol g^{-1} (S-PEI-X-H, where X = O, F, H or P) there appears to be a guest species within the pores of the adsorbent which has little affinity for the pores. This is tentatively assigned to the formation of silane oligomers independent of the pore surface. The gentle washing conditions used in the preparation were insufficient to remove silanes trapped within the pores of the adsorbent. For S-PEI-F-H and S-PEI-H-H a weakly interacting guest was removed from the pores during steam regeneration aging. This was evidenced by a large increase in the volume of pores over all pore sizes. Furthermore, in instances where this was thought to occur, steam regeneration aging led to increases in CO_2 adsorption uptake of S-PEI-F-H and S-PEI-H-H. However, these materials offer slow rates of adsorption and uneconomical CO_2 uptakes.

As no significant gains in particle size were introduced by silane deposition, the materials would occupy the same volume in a reactor as S-PEI. Hence reporting the capacity on a volumetric basis negating for the mass of the silane is reasonable. The CO_2 capacities measured were corrected for the amount of silane present in the sorbent (Figure 6.27).

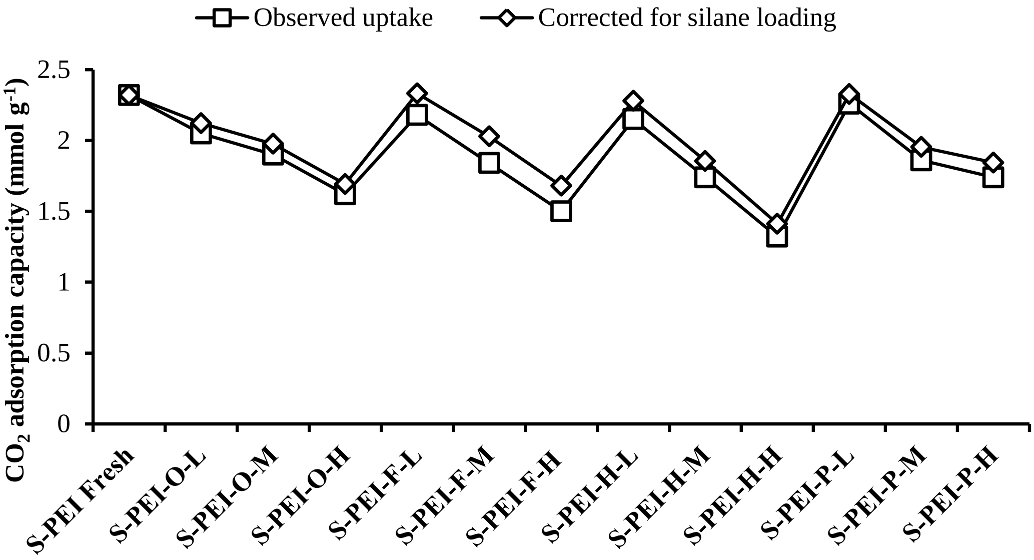

Figure 6.27. Observed and corrected CO_2 adsorption capacities accounting for the increased mass from silane loading.

From this analysis it is clear that for the lowest loadings of silane, access to the amine component is largely unaffected. Increasing levels of silane loading for all silane functionalities led to a reduction in CO_2 adsorption capacity on a volumetric basis. ^{13}C and ^{29}Si SSNMR confirm that the silanes were chemoselective for the surface silanols and did not react with the amine polymer. Under the conditions used to deposit the silane it is expected that the vast majority of the silane reacts with surface hydroxyl species or condenses with other silanes. Hence the losses in capacity were due to pore blockages and constriction used caused by silane deposition [7]. This was confirmed by nitrogen sorption experiments that showed losses in pore volume with increasing silane loading.

The relative rates of CO_2 uptake were compared by the time taken for the CO_2 uptake capacity to reach 80 % of its final equilibrium adsorption capacity (Figure 6.28). This point was chosen as above 80 % uptake, the rate slows as it becomes limited by the diffusion of CO_2 through the amine. In practical adsorption systems the adsorbents may be used exclusively in this rapid adsorption range. S-PEI had the fastest rate of adsorption, followed by the sorbents functionalised with the lowest levels of silane functionalisation.

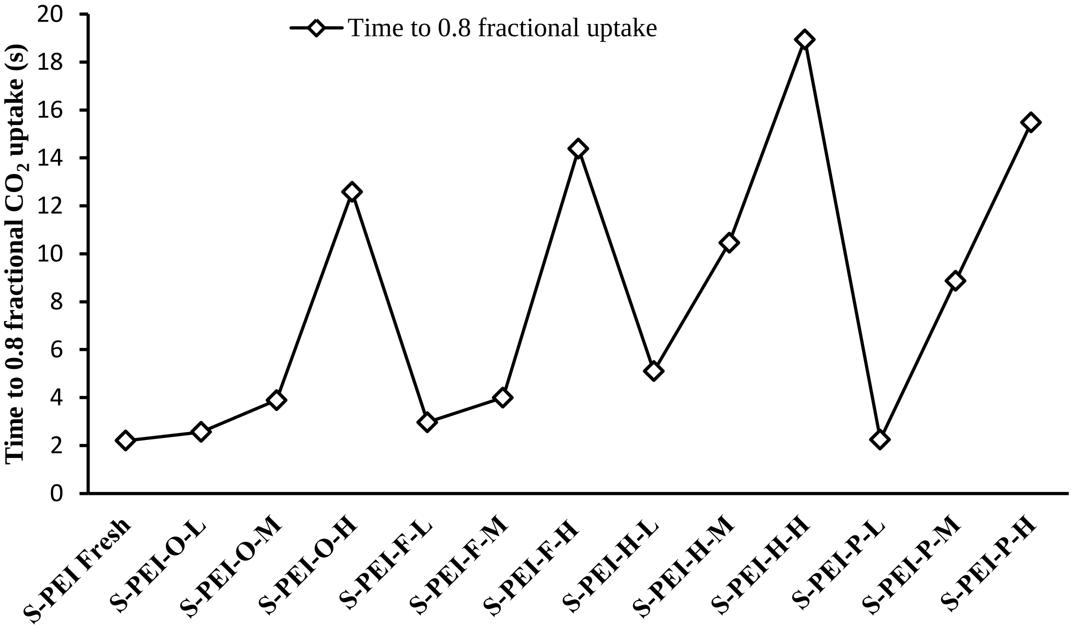

Figure 6.28. The time taken to reach 80% of the equilibrium adsorption capacity of silane coated adsorbents under 100% CO_2 at 75 ° C.

Increasing amounts of silane loading led to a reduction in the rate of CO_2 adsorption, with sorbents S-PEI-X-H (where X = O, F, H or P) taking in excess of 12 min to reach 80 % uptake. Such times are not practical in real world applications. These reductions in adsorption capacity and kinetics can be attributed to pore blocking and constriction caused by the condensation of multilayers of silane. The same pore blocking and pore constriction may also increase the stability of the adsorbents by reducing the rate of water intrusion. There is an apparent trade-off between increasing stability and practical rates of CO_2 adsorption.

The overall rate of CO_2 adsorption of the silane functionalised adsorbents differed in the presence of humid gas streams. A slight rate enhancement was observed for S-PEI and the lowest extents of silane coated adsorbents, albeit to a lower extent than S-PEI. As the silane loading increased the enhancement in CO_2

uptake capacities under humid adsorption conditions are reduced. This is coupled with an increasing adsorption halftime. This reduction in enhancement could be due to the formation of a resistive film of water over the outside of the hydrophobic particles. Dynamic vapour sorption measurements showed that S-PEI-F-M had a slower rate of water adsorption compared to S-PEI. This suggests the presence of hydrophobic groups may lead to the formation of a diffusive film over the surface of the particles. This film would restrict the transit of CO_2 within the pores of the adsorbent. Secondly, this would limit the amount of water within the pores, reducing the uptake enhancements frequently observed in the present of water. Literature reports suggest that at low levels of water in the feed stream, no enhancements in uptake capacity were observed [10]. This suggests that a certain concentration of water needs to be inside the pores to provide a beneficial effect. In cases where silane oligomers have formed, this could also reduce the passage of water into the adsorbent.

As discussed previously in Chapter 6, the CO_2 adsorption capacity of S-PEI was reduced after aging under a flow of 66% H_2O / He at 130 °C for 8 h. Steam aging of S-PEI led to a reduction in the adsorption capacity of 45 % (Figure 6.29). The origin of this reduction was proposed to be the condensation of water within the pores of the adsorbent leading to solubilisation of the amine. This solubilised amine could then leach out of the adsorbent. Further losses in adsorption capacities were also caused by reagglomeration of the amine within the smallest pores of the adsorbent. These mechanisms provided a significant reduction in the adsorption capacity of S-PEI after aging.

Post functionalisation of S-PEI with a target loading of 0.33 mmol g^{-1} of silane (S-PEI-X-L, where X = O, F, H or P) led to adsorbents with improved steam stability compared to S-PEI. These low loaded silane materials offered enhanced stability compared to S-PEI with retentions of capacity following the order S-PEI-F >S-PEI-H = S-PEI-O > S-PEI-P. Evidence of partial degradation was present with S-PEI-X-L adsorbents degrading in a manner similar to that observed by S-PEI. Aging of these materials led to a reduction in the volume of pores below 8 nm and an increase in pore volume above 8 nm. This suggests that the PEI is leaching from the largest pores of the adsorbent and becoming occluded in the smallest pores.

Increasing the target silane loading to 0.66 mmol g^{-1} (S-PEI-X-M, where X = O, F, H or P) led to adsorbents with a high retention of CO_2 adsorption capacities. S-PEI-F-M showed negligible change in pore structure with minimal organic losses after leaching. Furthermore this adsorbent exhibited reasonable adsorption rates with a slightly reduced CO_2 uptake capacity. S-PEI-P-M appeared to partially deactivate by reagglomeration and leaching in a similar manner to S-PEI. Aging of S-PEI-O-M led to a high retention in CO_2 uptake with aging but showed increases in pore volume across all pore sizes. This suggests the formation of silane oligomers coupled with amine leaching. S-PEI-H-M did lead to high levels of stability but possessed sluggish rates of adsorption.

At the highest target silane of 1 mmol g^{-1} (S-PEI-X-H, where X = O, F , H or P) led to adsorbents with low CO_2 adsorption capacities and slow rates of adsorption. With the exception of S-PEI-P-H, these adsorbents appeared to show the formation of silane oligomers within the pores of the adsorbents. S-PEI-P-H was the most stable of the phenylsilane functionalised adsorbents, however it possessed low rates of adsorption and low CO_2 uptake.

Perfluorodecylsilane modified sorbents appeared to possess the greatest levels of stability with S-PEI-F-L and S-PEI-F-M retaining 96 % of their CO_2 capacity after aging (Figure 6.29). These groups were the most hydrophobic of those studied with a contact angle on a clean silica surface of ~135 ° [6]. S-PEI-F-L appeared to show evidence of reagglomeration and leaching suggesting this sorbent would degrade over extended periods of testing.

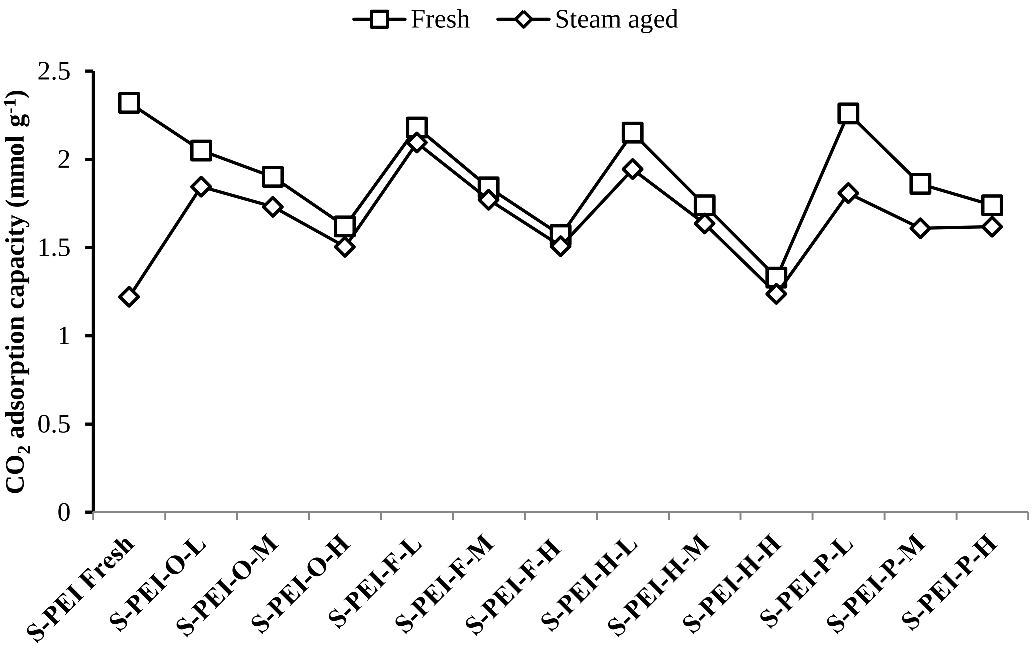

Figure 6.29. A comparison of the CO_2 adsorption capacities of different adsorbents before and after aging under 66% H_2O / N_2, 130 °C, 8 h. Measured under 100% CO_2 at 75 °C.

The hydrophobic layer does not entirely prevent leaching as it is predominantly located around the exterior and pore mouths of the particle. This hydrophobic coating constricting the pore mouths would retard the passage of water within the pores and would only be a kinetic barrier. This is evidenced by the reduction is adsorption rates in the presence of water due to the formation of a diffusive film. Water would still be able to percolate into the pores and condensation could occur within the PEI films causing them to dissolve. It could be expected that the rate of solubilisation of the polymer would be reduced in adsorbents coated with hydrophobic silanes owing to the slower intrusion of water into the pores. This reduced rate of solubilisation appears to lead to a decrease rate of amine leaching. This is turn appears to provide additional stability under aging in the presence of steam. However, it appears the increased stability comes at the expense of slower adsorption rates and lower CO_2 uptake capacities.

6.10 Conclusions

This chapter investigated the effect of introducing a silane coating to PEI impregnated silica adsorbents on their CO_2 uptake behaviour and stability under steam regeneration conditions. Previous work presented in Chapter 5 identified that the condensation of water within the pores of the adsorbent was a key factor in the degradation of adsorbents. The leaching of polymeric amines within practical solid adsorption systems could be highly problematic. This contribution suggests that the incorporation of a silane barrier coating of the adsorbents leads to a significant increase in the stability of the adsorbents under steam regeneration. The origin of this stability appears to be related to the changes in pore mouths of the adsorbents. Furthermore the rate of water adsorption appears reduced suggesting that the adsorption of water and hence dissolution of the amine polymer would be reduced.

The rate of amine leaching was greatly reduced with the inclusion of a barrier coating suggesting that silane modification was an effective method to address amine leaching. The origin of deactivation due to amine reagglomerating within the pores of the adsorbent was also present.

The inclusion of a silane coating leads to a partial reduction in the adsorption capacity. This can be attributed to the porous coating increasing the support mass per active amine and retarding the access of CO_2. For sorbents with highly loaded amounts of silane the rate of CO_2 adsorption is severely restricted suggesting that multilayers of silane have deposited within the pores of the adsorbent.

The findings from this chapter suggest there is an interplay between the hydrophobic silane loading, hydrothermal stability and favourable CO_2 adsorption properties. This investigation showed that post functionalisation is a viable method of increasing the stability of adsorbents in the presence of steam regeneration. This study has also shown that the use of post functionalisation needs to be carefully controlled so that the favourable adsorption properties of the adsorbent are not lost.

6.11 References

1. W. Chaikittislip, H. Kim, C. W. Jones, *Mesoporous Alumina-Supported Amines as Potential Steam-Stable Adsorbents for Capturing CO_2 from Simulated Flue Gas and Ambient Air.* Energy Fuels, 2011. **25**: p. 5528.
2. D. Brühwiler, G. Calzaferri, T. Torres, J. H. Ramm, N. Gartmann, L. Dieu, I. López-Duarte, M. V. Martinez-Diaz, *Nanochannels for supramolecular organisation of luminsent guests.* J. Mater. Chem., 2009. **19**: p. 8040.
3. F. de Juan, E. RuizHitzky, *Selective Functionalization of Mesoporous Silica.* Adv. Mater., 2000. **12**: p. 430.
4. S. Kim, J. Ida, V. V. Guliants, J. Y. S. Lin, *Tailoring Pore Properties of MCM-48 Silica for Selective Adsorption of CO_2.* J. Phys. Chem. B, 2005. **109**: p. 6287.
5. N. Gartmann, D. Brühwiler, *Controlling and Imaging the Fuctional-Group Distribution on Mesoporous SIlica.* Chem. Mater., 2009. **48**: p. 1433.
6. B. Arkles,*Hydrophobicity, Hydrophilicity and Silane Surface Modification.* Gelest Inc., 2006.
7. E. P. Plueddemann, *Silane Coupling Agents Second Edition.* Springer Science+Business Media New York, 1991.
8. J. Wang, D. Long, H. Zhou, Q. Chen, X. Liu, L. Ling, *Surfactant promoted solid amine sorbents for CO_2 capture. Energy Environ. Sci.*, 2012. **5**: p. 5742.
9. M. Thommes, B. Smarsly, M. Groenewolt, P. I. Ravikovitch and A. V. Neimark, *Adsorption Hystersis of Nitrogen and Argon in Pore Networks and Characterisation of Novel Micro- and Mesoporous Silicas.* Langmuir, 2006. **22**: p. 756
10. A. Heydari-Gorji, Y. Belmbkhout., A. Sayari, Polyethyleneimine-Impregnated Mesoporous Silica: Effect of Amine Loading and Surface Alkyl Chains on CO2 Adsorption. Langmuir, 2011. **27**: p. 12411.

CHAPTER SEVEN

Conclusions and Future Work

7.1 Conclusions

The first aim of this thesis was to characterise and improve the hydrothermal stability of amine functionalised silicas. To date limited work has been completed regarding the stability of amine functionalised silicas under steam regeneration conditions. This thesis describes a comprehensive set of experiments mimicking adsorbent stability with respect to water under both adsorption and steam desorption conditions.

Aging of both impregnated and covalently tethered amine adsorbents in the presence of water led to significant reductions in CO_2 adsorption capacities of the adsorbents. The adsorbents appeared less stable under steam regeneration conditions than humid adsorption conditions. It appeared that the capillary condensation of water within the pores of the adsorbent led to increased amounts of degradation.

Studying a range of ethlylenediamine polymer molecular weights and support pore sizes, a mechanism of deactivation was presented. For impregnated amine adsorbents amine leaches from the pores of the adsorbent and is removed from the largest pores first. This was evidenced by increasing pore volume at larger pore sizes determined using nitrogen sorption. However amine leaching was not able to account for the entire loss in capacity observed. It was found that the impregnated polymers re-agglomerate within the smallest pores of the adsorbent. It is believed that in their agglomerated state the amines are less accessible to CO_2.

The rate of leaching was found to be proportional to the molecular weight of the amine polymer. This suggests that the solubilisation of the polymer in the presence of water is crucial. Aging of TEPA impregnated adsorbents under steam regeneration conditions led to a loss in pore volume and surface area suggesting degradation of the silica support. This material also had the highest amount of leaching, suggesting that high loadings of amine polymer protect the silica from degradation. The capillary condensation of water within the pores of the adsorbent could lead to dissolution of the amines forming a localised high pH solution. In the presence of exposed silica sites this could lead to silica hydrolysis and mesostructure degradation.

Covalently tethered amines were also found to be unstable in the presence of steam with slight reductions in adsorption capacity observed after aging. This was attributed to the incomplete coverage of the organic groups that led to exposed silica sites. These exposed silica sites could be hydrolysed by a localised solution of high pH within the pores of the adsorbent.

It was found that supports with little accessible volume exhibited good stability in the presence of steam, concluding that water must intrude into the pores for deactivation to occur. Supports with an average pore size of 20 nm appeared to deactivate solely by leaching with no amine agglomeration present. This suggests for PEI 600, there is a critical pore size required for stable agglomeration to occur.

Pore accessibility to water was found to be a crucial factor influencing the stability of adsorbents under steam regeneration conditions. A series of adsorbents were designed to enhance the stability of the amine impregnated silica adsorbents. These consisted of impregnated amine adsorbents post functionalised with a range of hydrophobic organosilanes at the exterior and pore mouths of the adsorbents. A method was developed to deposit these silanes onto the external surface of the adsorbent without the leaching of the active polymeric amine. The introduction of these groups led to an increase in the steam stability of the adsorbents.

It appeared that deposition of all silane groups led to an increase in steam stability with the magnitude of the effect proportional to the nature of the silane used. Aging of adsorbents with the hydrophobic barrier layer were still found to have reduced CO_2 adsorption capacities after aging. However, the stability was greatly enhanced over unfuctionalised adsorbents. The largest retention in CO_2 adsorption capacities after aging under steam regeneration conditions was found to be for S-PEI coated with perflurodecyltriethoxysilane. This adsorbent retained 96% CO_2 adsorption capacity with minimal changes in organic loading after aging. Although many of the adsorbents appeared to offer greater stability compared to S-PEI, degradation due to amine reagglomeration was present. Loss in adsorption capacity for silane coated S-PEI was also due to small amounts of amine leaching from the pores of the adsorbent.

Use of dynamic vapour adsorption experiments showed that the presence of large hydrophobic silanes on the exterior of the particle led to a reduction in the rate of water adsorption into the pores of the sorbent. This would lead to a reduced rate of solubilisation of the amine component and hence improve adsorbent stability. The presence of a silane coating could also provide a higher energy surface, restricting the migration of the polymer outside the pores of the adsorbent.

When S-PEI was treated with 1 mmol g^{-1} of either hexadecyltrimethoxysilane or perfluorodecyltriethoxysilane a large reduction in pore volume and CO_2 uptake was observed. Aging of these materials led to an increase in pore volume and CO_2 uptake suggesting silanes had condensed independently of the support, forming aggregates with the pores. This suggests that an optimum amount of silane coverage exists with too little only a small benefit, with too much leading to increase pore constriction.

The effect of silane coating led to reductions in CO_2 adsorption capacity, with increasing levels of silane loading yielding further reductions in CO_2 uptake. This was attributed to the silanes causing pore blockages. Whilst offering significant increases in stability under steam regeneration, highly loaded silane coated S-PEI led to large reductions in the rate of uptake of CO_2. Furthermore, it was found that high levels of silane coating reduced the rate of CO_2 adsorption in the presence of water. This was thought to be due to a diffusive film of water forming of the surface of the adsorbent particle.

The impact of this work highlights the critical issue of steam stability of amine impregnated adsorbents. This is an essential requirement if steam regeneration is to be used as a regeneration strategy. This thesis has demonstrated that post functionalisation of PEI impregnated adsorbents offer significant increases in steam stability. However there appears to be a trade-off between increased stability and desirable CO_2 adsorption properties.

A second objective of this thesis was to understand the role additive molecules have in tuning the CO_2 adsorption properties of impregnated adsorbents. A first of a kind study into the mobility of silica supported polymeric amine adsorbents was conducted using saturation recovery ^{1}H SSNMR. This suggested that the addition of surfactant species increased the viscosity of the amine blends. It was found using ^{13}C SSNMR and *in-situ* DRIFTS spectroscopy, that there was no change in adsorption mechanism in the presence of surfactant additives under dry adsorption conditions. Using a combination of nitrogen sorption, TPD and CO_2 adsorption experiments it was established that the role of the surfactant was dependent on its functionality. The incorporation of TEA was found to only slightly influence the dispersion of the amine but was shown to present physisorption sites for CO_2. The incorporation of SDS led to the production of better dispersed, thinner layers of amine on the adsorbent surface. This gave rise to a greater number of accessible sites leading to an increase in the rate and amount of CO_2 adsorbed. Additionally the presence of these thin, well dispersed layers of amine facilitate the regeneration requirements allowing shorter regeneration cycles at lower temperatures.

It is expected that the understanding of surfactant addition would be a straightforward method of improving the CO_2 uptakes and kinetics of other silica supports. Furthermore, these adsorbents exhibited increased CO_2 adsorption capacities with less amine polymer. Given the greatly reduced cost of surfactant additives compared to the PEI, this could be a method of reducing the cost of the adsorbents.

This thesis has advanced the knowledge and understanding of amine functionalised silica adsorbents. The application and development of the ideas and materials herein allow the design of solid supported amine adsorbents that have greater stability and improved CO_2 adsorption properties.

.

7.2 Future work

7.2.1 Preliminary investigation into free radical polymerisation within the pores of mesoporous silica relevant to post combustion carbon capture

Amines have been polymerised onto the surface of porous silicas by the polymerisation of aziridine onto a silica surface. [1-3] These materials were shown to be stable is the presence of water with their CO_2 capacities enhanced in the presence of water. Owing to the high loadings of amine incorporated into the adsorbent a high extent of silica coverage could be envisaged. Owing to the high reactivity of the aziridine monomer the polymerisation is uncontrolled leading to pore blockages and patchy coverage of amine groups.

Surface polymerised adsorbents with a greater level of control were reported by Qi *et al.*, producing covalently tethered ethylenediamines by polymerising 2-methyl-2oxazoline in the presence of 3-iodopropyltrimethoxysilane [4]. The adsorbents were found to be stable under repeated cycling and performed well under simulated flue gas conditions. The long term stability of these adsorbents in the presence of water was not reported.

These findings suggest that polymerisation of amine bearing groups could be an efficient method of introducing high levels of functionality. Building on this work a preliminary study was conducted using a silica supported free radical initiator and polymerising a reactive monomer into the pores of adsorbent. It is hypothesised that by using commonly available monomers this could be a method of producing low cost adsorbents. The experimental details of the sorbents produced by this process can be found in Sections 3.22 and 3.23. The initiator functionalised silica was polymerised with vinylbezenyl chloride (VBC) with a range of loadings followed by a subsequent reaction with ethylendiamine (EDA) yielding functionalised adsorbents (Figure 7.1).

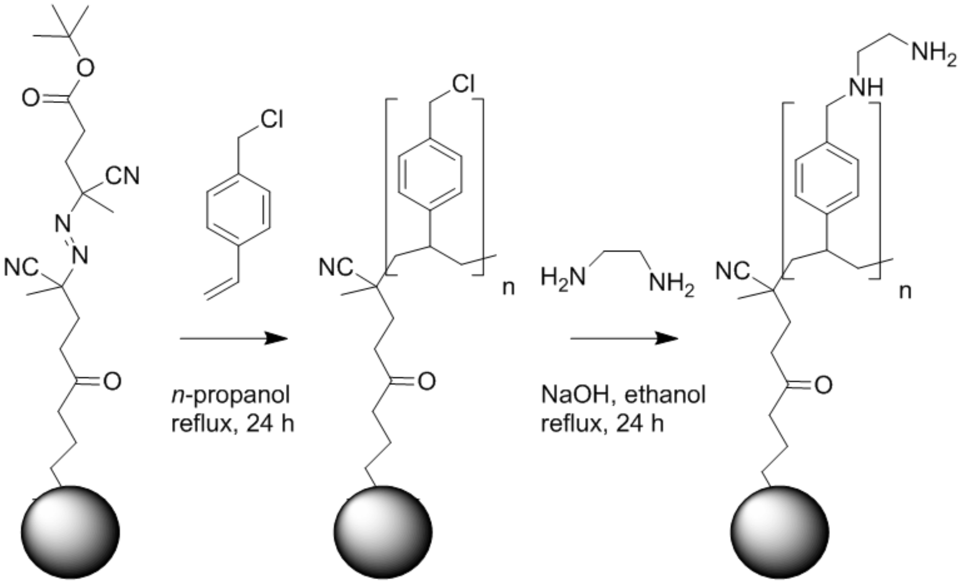

Figure 7.1. The synthesis silica supported amines using free radical polymerisation.

The polymerisation of VBC yielded gains in the organic loading of the adsorbents, with the loading obtained proportional to the concentration of monomer (Table 7.1). After functionalisation with ethylenediamine the surface polymerised materials were found to exhibit favourable CO_2 adsorption properties under 100 % CO_2 at 75 °C (Table 7.1). These adsorption capacities are comparable to those of grafted adsorbents. Attempts to graft additional monomer and hence achieve a higher amine loading were unsuccessful with the greatest CO_2 adsorption capacity observed for a silica monomer ratio of 1:1.

Table 7.1. The organic loading and CO_2 adsorption capacity of silica supported amines using free radical polymerisation.

Sorbent	Silica : monomer ratio	Organic loading (wt%)	CO_2 uptake (mmol g^{-1})
S-Poly 0.25 VBC EDA	1:0.25	15.2	0.88
S-Poly 0.5 VBC EDA	1:0.5	21.3	1.1
S-Poly 1 VBC EDA	1:1	27.1	1.57
S-Poly 2 VBC EDA	2:1	32.7	0.37
S-Poly 4 VBC EDA	4:1	36.2	0.273

Nitrogen sorption confirmed that increasing levels of VBC loading led to a reduction in the porosity of the support (Appendix A34). This is likely to be associated with polymerisation occurring at the pore mouths of the adsorbents. Furthermore inspection of ^{13}C SSNMR before and after ethylenediamine functionalisation appeared to suggest that not all of the benzylchloride groups had reacted (Appendix 35).

This preliminary work suggests that if the polymerisation could be controlled, this could be an efficient method of incorporating high levels of amine loaded materials into the pores of the adsorbent. Furthermore, a large number of monomers and their derivatives that could be functionalised in this way. This process has the potential to incorporate a wide range of functionalities on the silica surface with high levels of loading.

7.2.2 Future work on the hydrothermal stability of amine functionalised silica adsorbents

This thesis has highlighted the importance of adsorbent stability in the presence of water under both adsorption and stream regeneration conditions. Given the proposed benefit of steam regeneration a clear need for hydrothermally stable adsorbents exists. In this thesis S-TEPA was aged under pseudo steam regeneration conditions which led to a reduction in pore volume and amine efficiency. This is a stark contrast to other impregnated amine adsorbents which displayed increases in pore volume and surface area as a consequence of amine leaching from the support. Owing to the lower molecular weight of TEPA compared to PEI, this test could be argued to be an accelerated aging test of heavier molecular weight amine polymers. To facilitate the creation of next generation adsorbents the origin of this deactivation needs to be understood. Two causes of degradation are possible namely, support degradation or more simply an amine film depositing on the surface. There is a highly probability that both pathways could be occurring.

Previous investigations into impregnated silicas in the presence of steam have argued both support degradation and support stability [5, 6]. Whilst examples such as these are useful there has been no thorough spectroscopic investigation into the potential support breakdown. With this in mind an investigation into the possible degradation pathways would be beneficial. By using a range of templated mesoporous silicas such as MCM-41, SBA-15 and the like the extent of support breakdown could be investigated by small angle X-ray scattering (SAXS). Hence adsorbents would be aged in a manner similar to that which is presented in this thesis and the structure identified at set points during aging. One limitation in the work of this thesis is that adsorbents were only aged under 66% H_2O for 8 h. An improved study would allow aging for longer periods of time to gather a firm grasp of adsorbent stability and the degradation mechanism. In addition to SAXS, the breakdown of ordered mesoporous supported amines could also be characterised by electron microscopy and ^{29}Si SSNMR. A selection of ordered silica supports with differing pore sizes, wall thicknesses and surface functionality could be studied.

Such a structure-stability relationship would be of great utility in designing the next generation of amine supported adsorbents.

On a similar theme, this thesis only investigated the steam stability of adsorbents in the presence of nitrogen at a largely constant temperature. However the cycling of temperatures and changes in the moisture content between adsorption and desorption may have an effect on amine re-agglomeration and leaching. The zwitterionic alkylammonium carbamate product formed during CO_2 would have differing physical properties to the amine. This species may leach or agglomerate at a different rate to the unreacted amine and should be investigated.

7.2.3 Future work on the role of surfactant additives in amine impregnated silica adsorbents

This thesis and others have shown that surfactant additives can enhance the CO_2 adsorption properties of impregnated amine adsorbents [7-12]. The role of additives with respect to both hydrothermal and flue gas contaminant stability warrants investigation. Experiments in this thesis suggest that some surfactant additives influence the enhancement of CO_2 uptake in the presence of water. Hence it is hypothesised that amines co-impregnated with surfactants could offer enhanced hydrothermally stability. Furthermore, the surfactants may prevent leaching and reagglomeration of the amine which has been shown in this thesis to be a significant deactivation mechanism.

7.3 References

1. J. H. Drese, S. Choi, R. P. Lively, W. J. Koros, D. J. Fauth, M. L. Gray, C. W. Jones, *Synthesis-Structure-Property Relationships for Hyperbranched Aminosilica* CO_2 *Adsorbents. Adv. Funct. Mater.*, 2009. **19**: p. 3821.
2. J. C. Hicks, J. H. Drese, D. J. Fauth, M. L. Gray, G. Qi, C. W. Jones, *Designing Adsorbents for* CO_2 *Capture from Flue Gas-Hyperbranched Aminosilicas Capable of Capturing* CO_2 *Reversibly.* J. Am. Chem. Soc., 2008. **130**: p. 2902.
3. H. J. Kim, J. H. Drese, J. W. Park, *A Hyperbranched Poly(ethyleneimine) Grown on Surfaces.* Journal of Colloid and Interface Science, 2000. **227**: p. 247.
4. G. Qi, L. Fu, E. P. Giannelis, *Sponges with covalently tethered amines for high-efficiency carbon capture.* Nat Commun, 2015. **5**: p. 5796.
5. W. Li, P. Bollini, S. A. Didas, S. Choi, J. H. Drese, C. W. Jones, *Structural Changes of Silica Mesocellular Foam Supported Amine-Functionalized* CO_2 *Adsorbents Upon Exposure to Steam.* ACS Appl. Mater. Interfaces, 2010. **2**: p. 3363.
6. S. Hammache, J. S. Hoffman, M. L. Gray, D. J. Fauth, B. H. Howard, H. W. Pennline, *Comprehensive Study of Steam on Polyethyleneimine on Silica for* CO_2 *Capture.* Energy & Fuels, 2013. **27**: p. 6899.
7. D. S. Dao, H. Yidetaka, K. Yogo, *Large-Pore Mesostructured Silica Impregnated with Blended Amines for* CO_2 *Capture. Ind . Eng. Chem. Res.*, 2013. **52**: p. 13810.
8. D.S. Dao, H. Yidetaka, K. Yogo, *Response Surface Optimisation of Impregnation of Blended Amines into Mesoporous Silica for High-Performance* CO_2 *Capture.* Energy & Fuels, 2015. **29**: p. 985.
9. A. Heydari-Gorji, Y. Belmabkhout, A. Sayari, *Polyethyleneimine-Impregnated Mesoporous Silica: Effect of Amine Loading and Surface Alkyl Chains on* CO_2 *Adsorption.* Langmuir, 2011. **27**: p. 12411.
10. M. B. Yue, L. B. Sun, Y. Cao, Z. J. Wang, Y. Wang, Q. Yu, J. H. Zhu, *Promoting the* CO_2 *adsorption in the amine-containing SBA-15 by hydoxyl group.* Microporous and Mesoporous Materials, 2008. **114**: p. 74.
11. J. Wang, D. Long, H. Zhou, Q. Chen, X. Liu, L. Ling, *Surfactant promoted solid amine sorbents for* CO_2 *capture. Energy Environ. Sci.*, 2012. **5**: p. 5742.
12. W. Yan, J. Tang, Z. Bian, J. Hu, H. Liu, *Carbon Dioxide Capture by Amine-Impregnated Mesocellular-Foam-Containing Template. Ind . Eng. Chem. Res.*, 2012. **51**: p. 3653.

CHAPTER EIGHT

Appendix

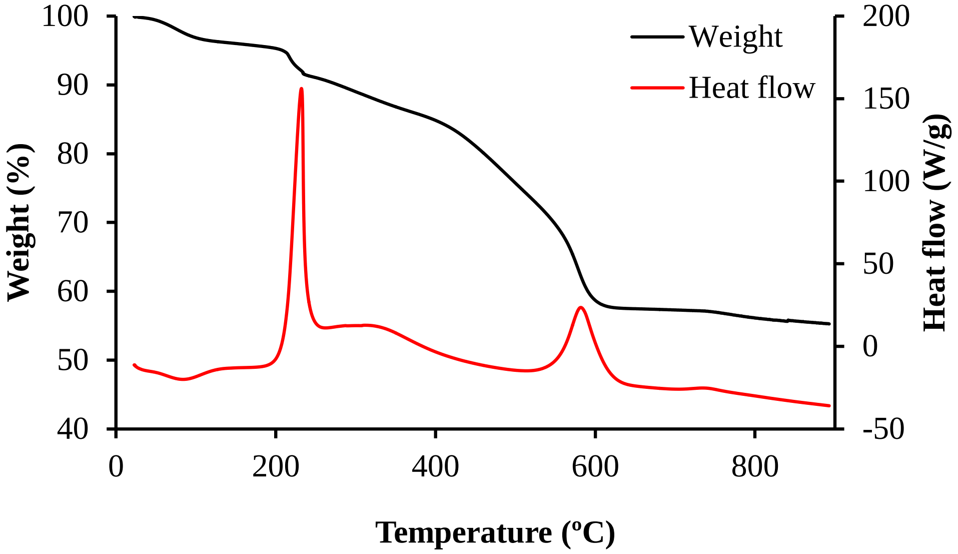

Figure A1. TGA of SBA-15 40 wt% PEI.

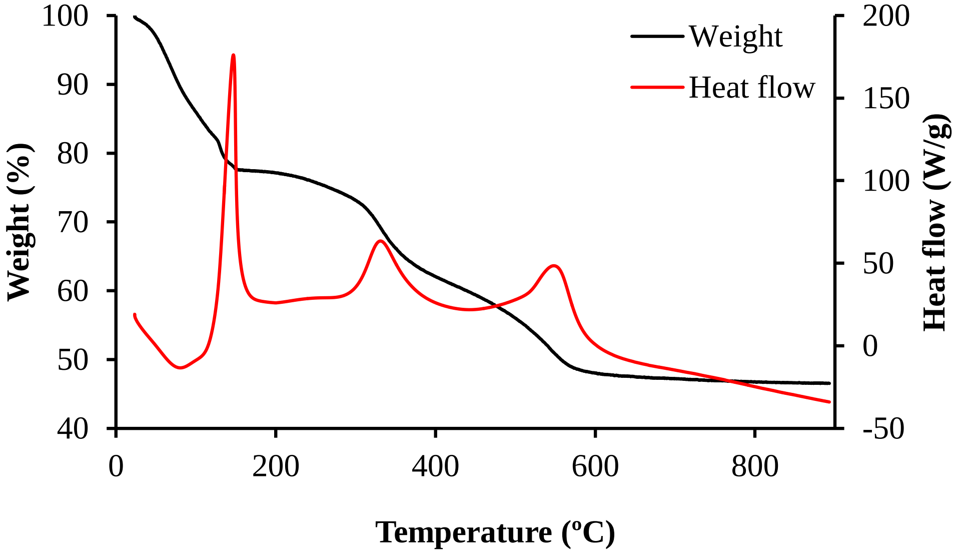

Figure A2. TGA of SBA-15 40 wt% TEPA.

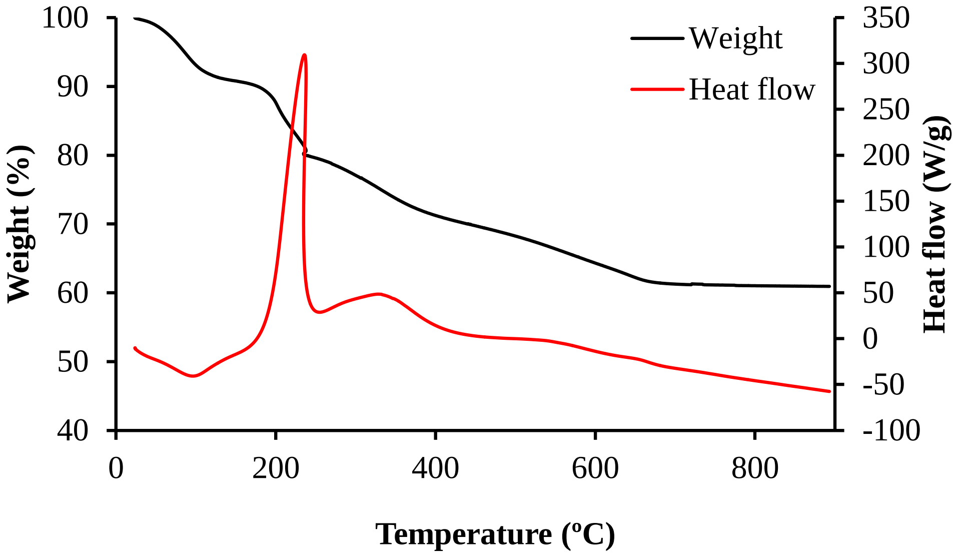

Figure A3. TGA of Davisil 33 wt% TEPA.

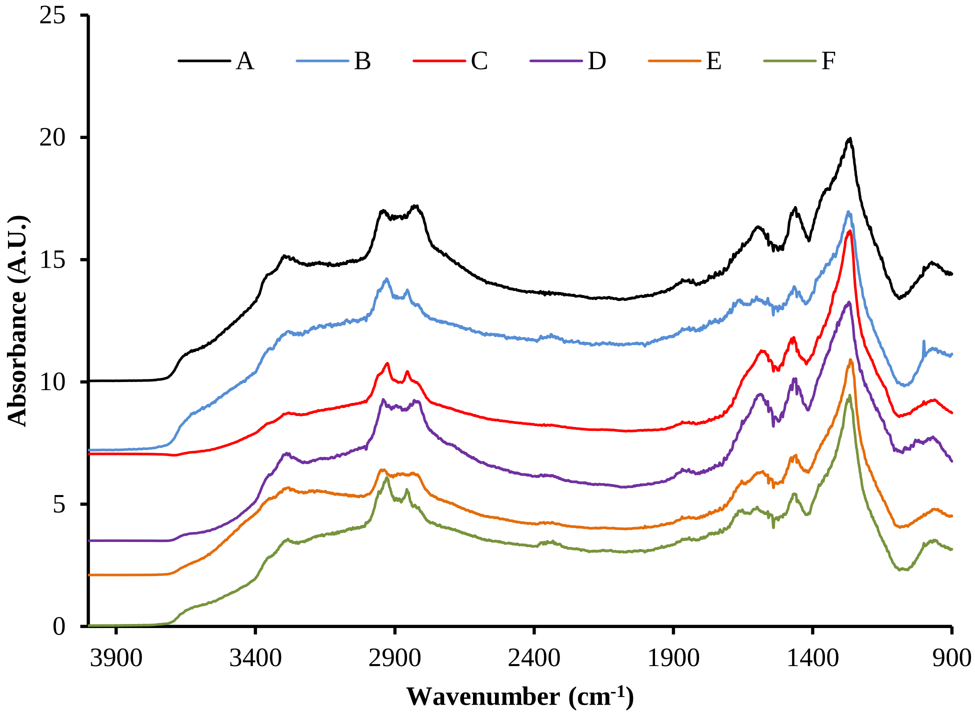

Figure A4. DRIFT spectra of adsorbents A-F referenced to KBr. Spectra are offset to aid comparison.

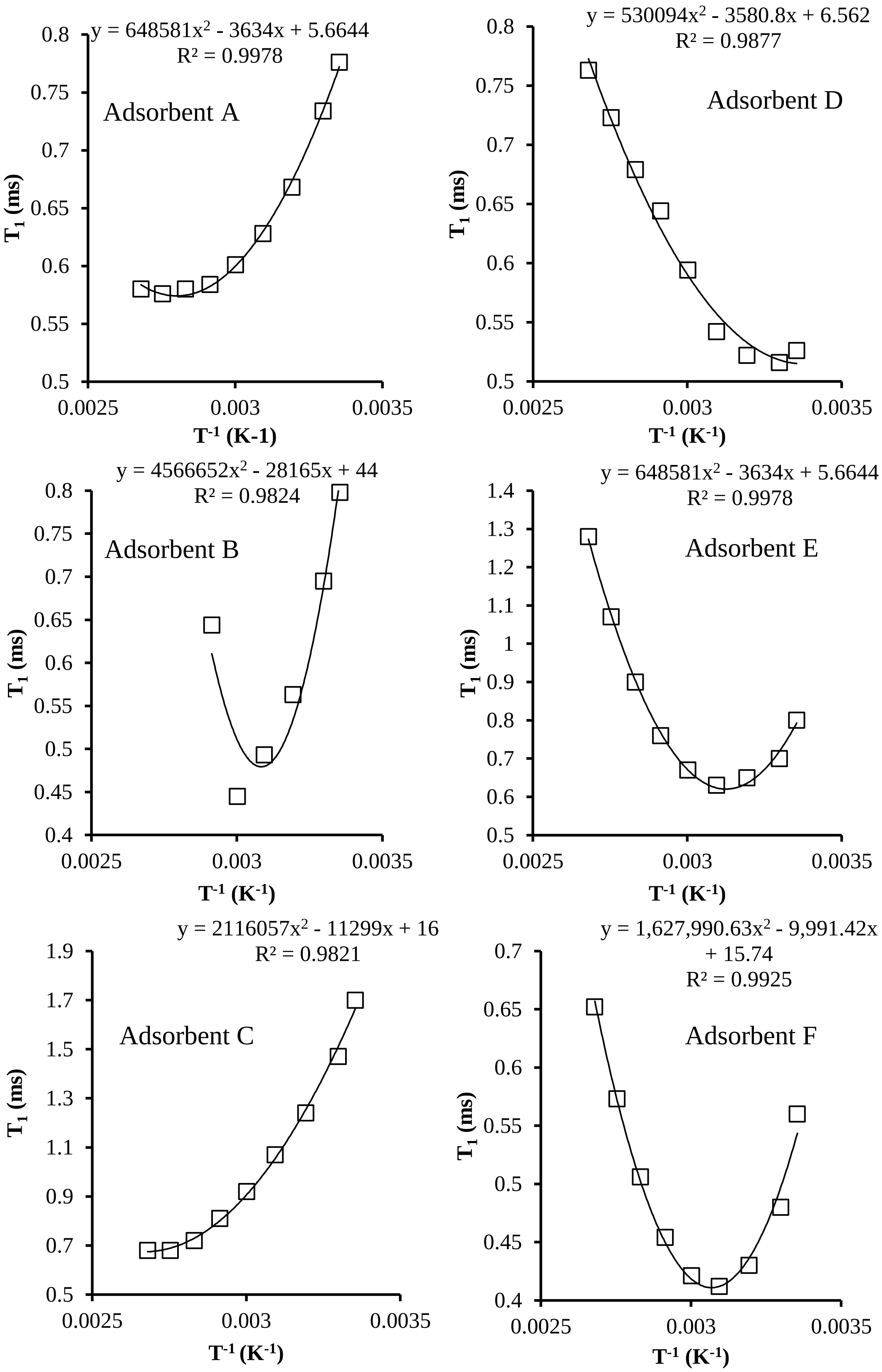

Figure A5. Plots of T_1 vs T^{-1} fitted with 2nd order polynomials for adsorbents A-F.

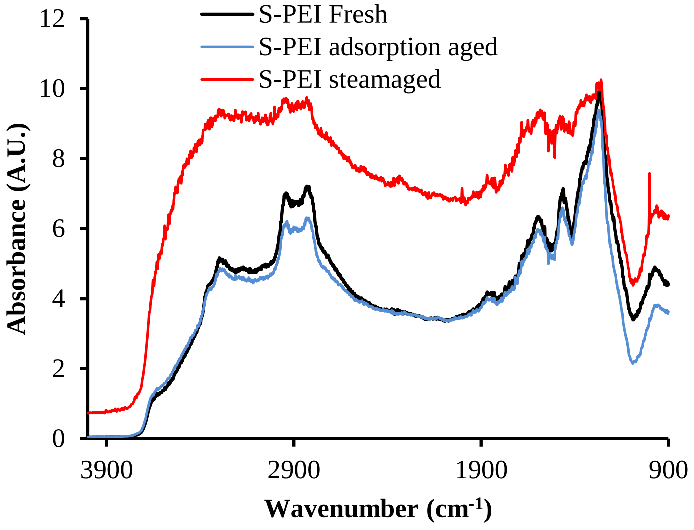

Figure A6. DRIFT spectra of S-PEI before and after aging under humid pseudo adsorption conditions and steam regeneration conditions. Referenced to KBr.

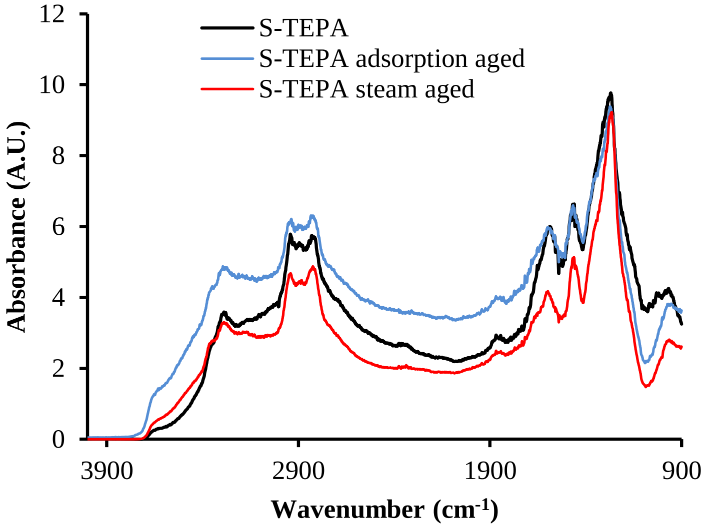

Figure A7. DRIFT spectra of S-TEPA before and after aging under humid pseudo adsorption conditions and steam regeneration conditions. Referenced to KBr.

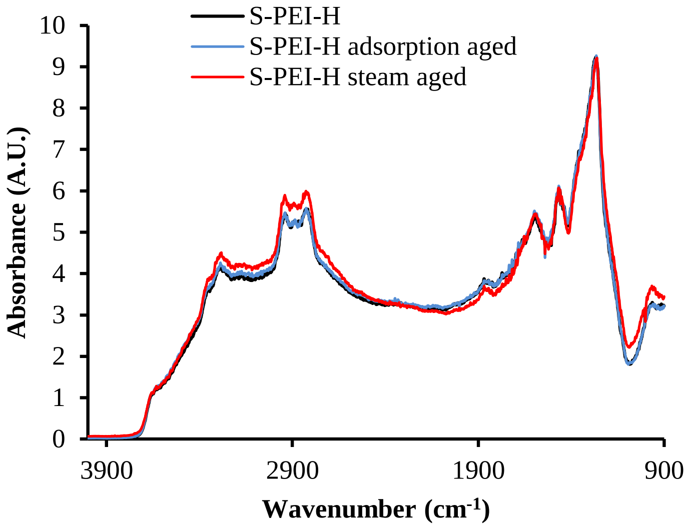

Figure A8. DRIFT spectra of S-PEI-H before and after aging under humid pseudo adsorption conditions and steam regeneration conditions. Referenced to KBr.

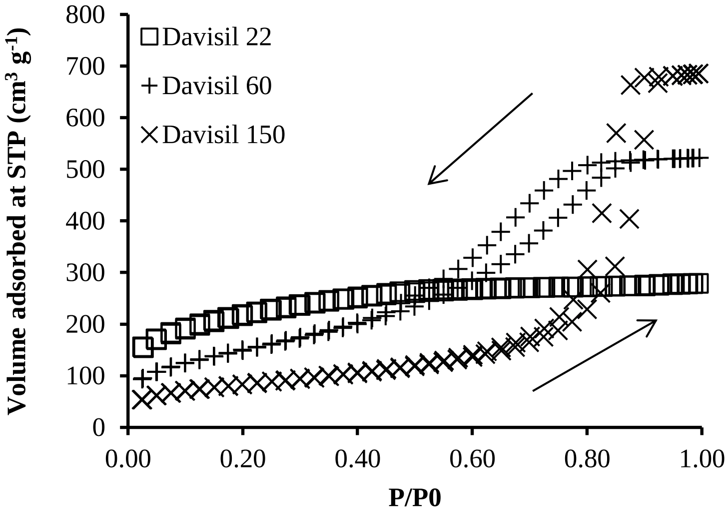

Figure A9. Nitrogen sorption isotherms of Davisil 22, Davisil 60 and Davisil 150 at 77 K.

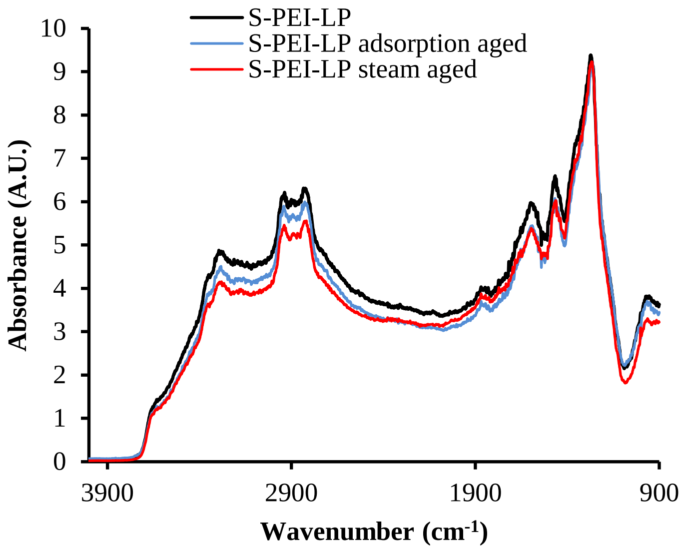

Figure A10. DRIFT spectra of S-PEI-LP before and after aging under humid pseudo adsorption conditions and steam regeneration conditions. Referenced to KBr.

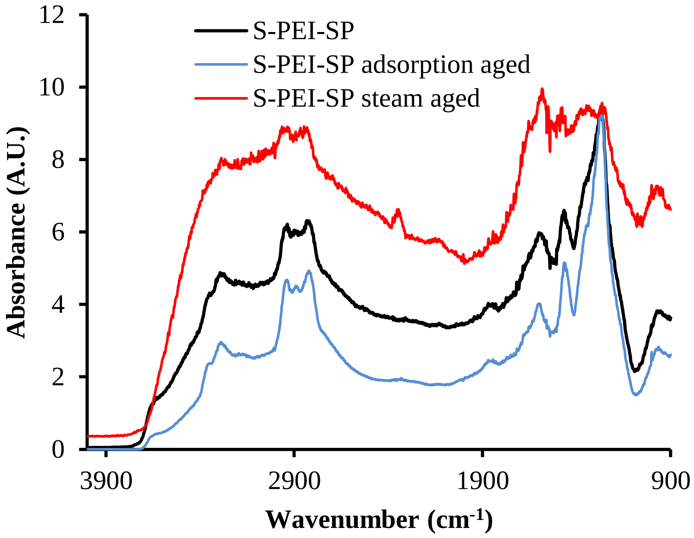

Figure A11. DRIFT spectra of S-PEI-SP before and after aging under humid pseudo adsorption conditions and steam regeneration conditions. Referenced to KBr.

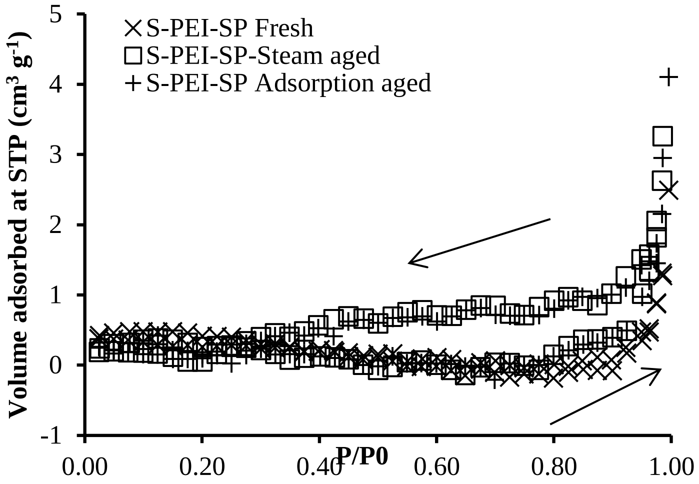

Figure A12. Nitrogen sorption isotherms of S-PEI-SP, before and after aging under pseudo adsorption conditions and pseudo regeneration conditions.

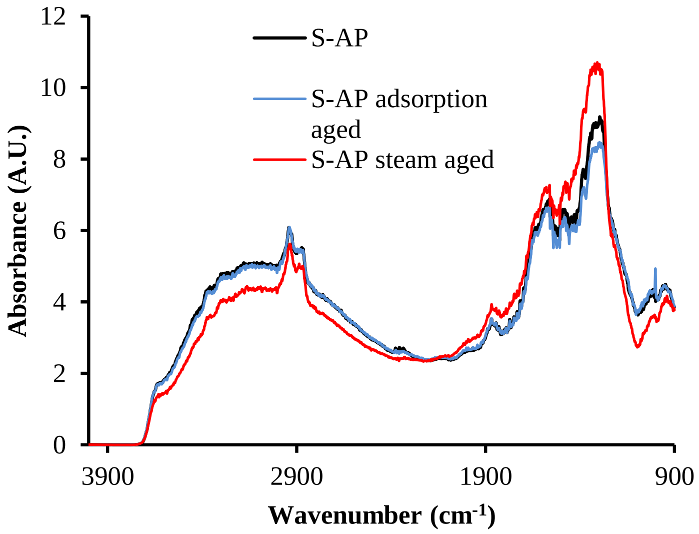

Figure A13. DRIFT spectra of S-PEI-AP before and after aging under humid pseudo adsorption conditions and steam regeneration conditions. Referenced to KBr.

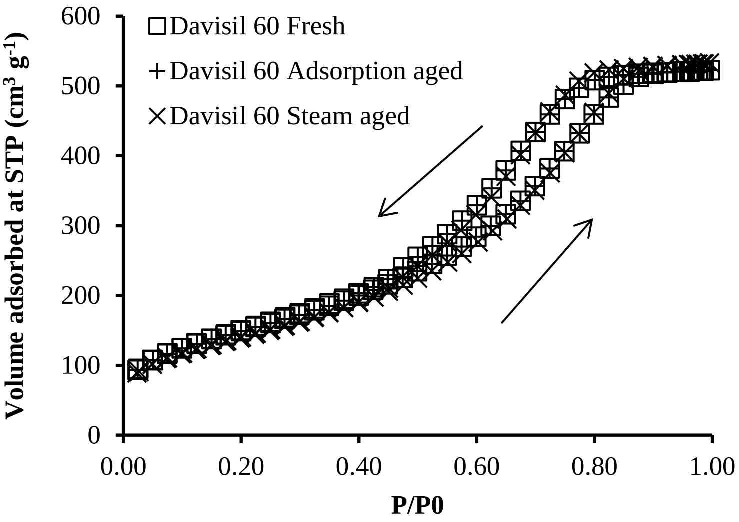

Figure A14. Nitrogen sorption isotherm of Davisil 60 before and after aging under pseudo adsorption and steam regeneration conditions.

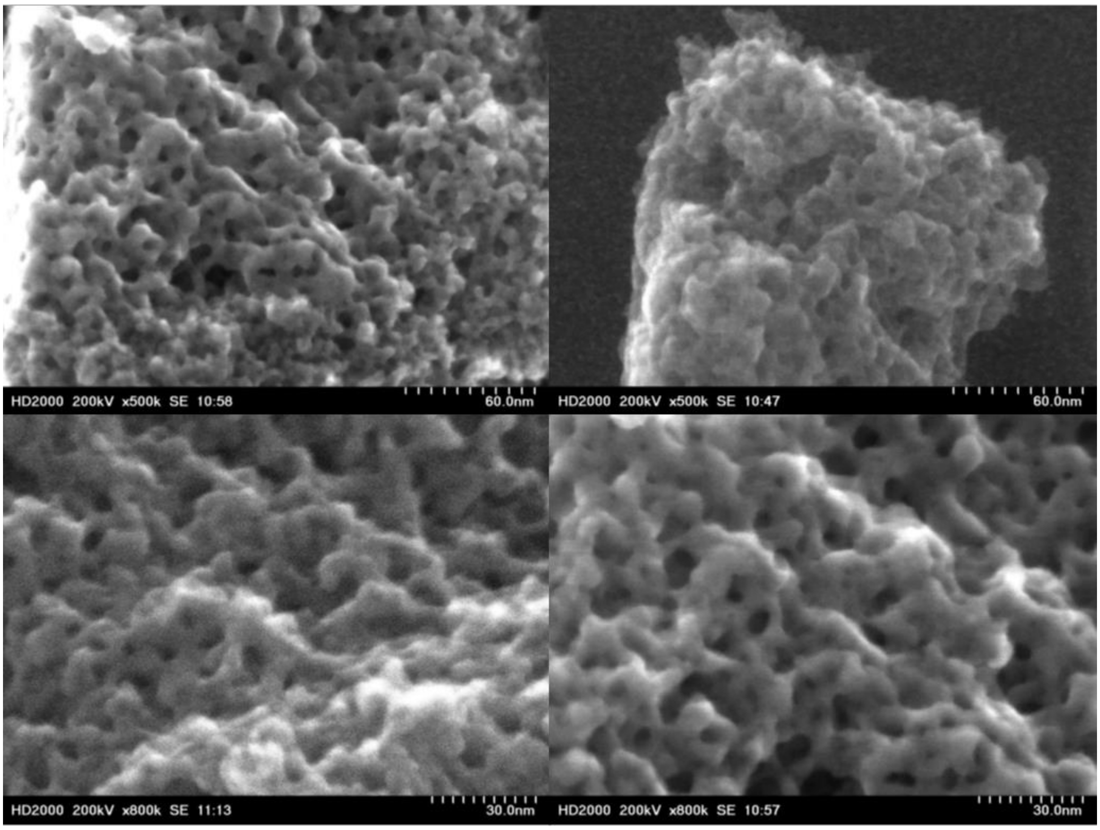

Figure A15. STEM images of S-PEI fresh.

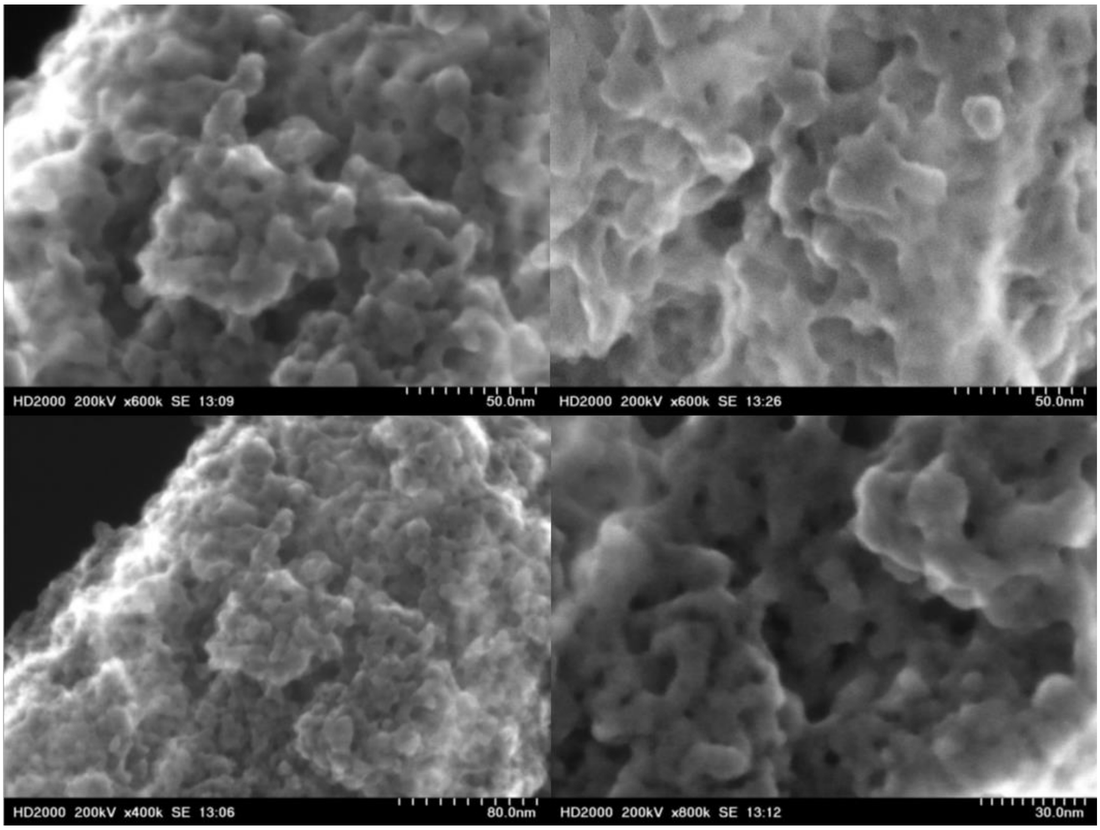

Figure A16. STEM images of S-PEI after steam aging.

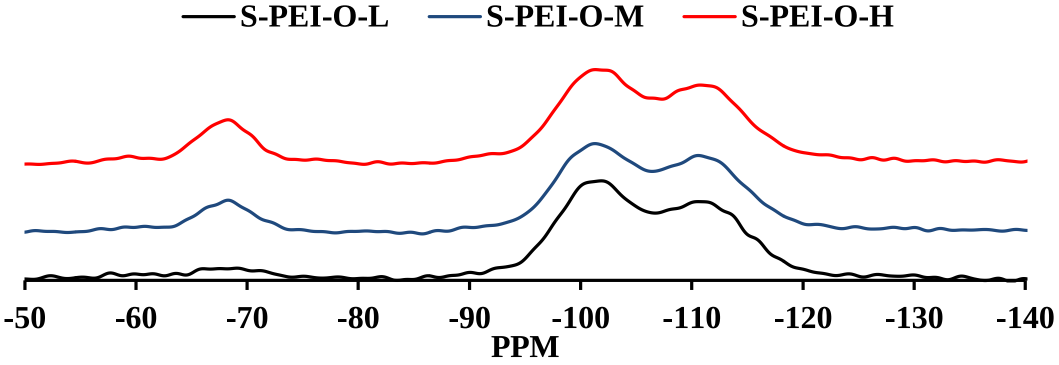

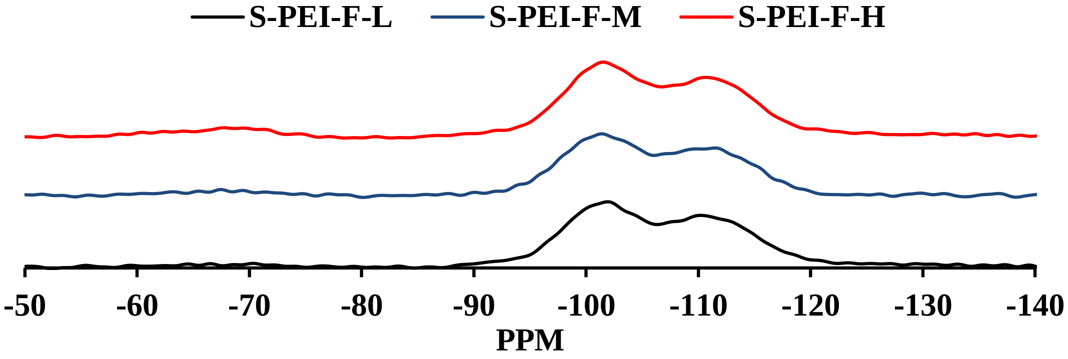

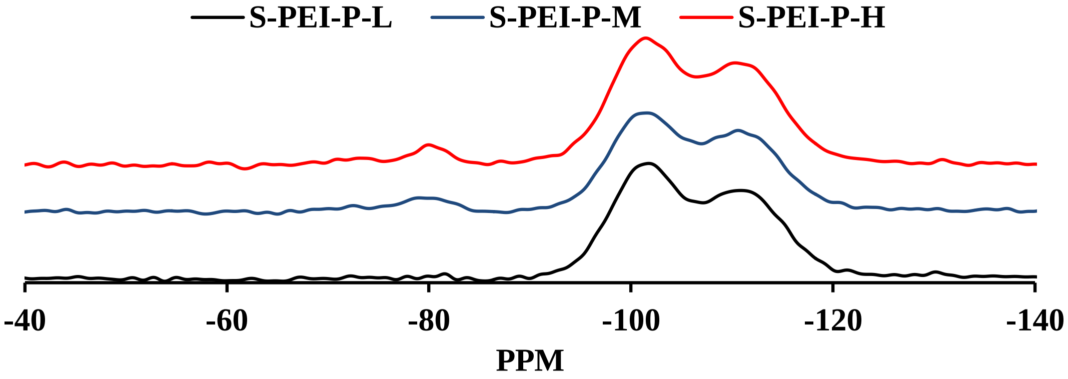

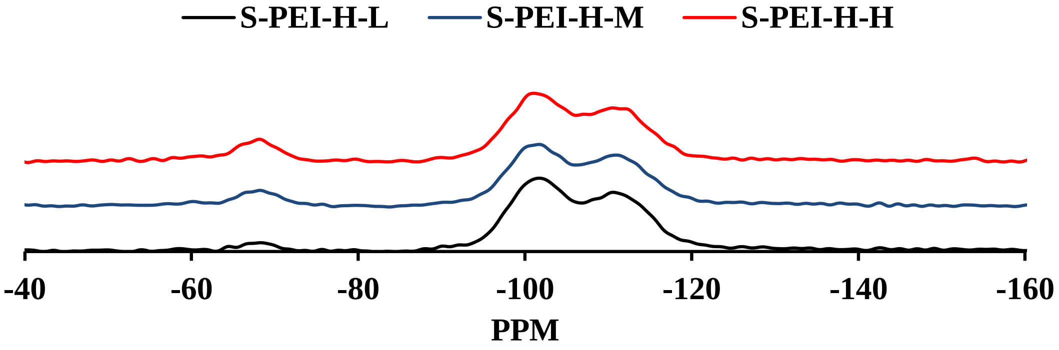

Figure A17. CP MAS ^{29}Si SSNMR silane functionalised S-PEI adsorbents.

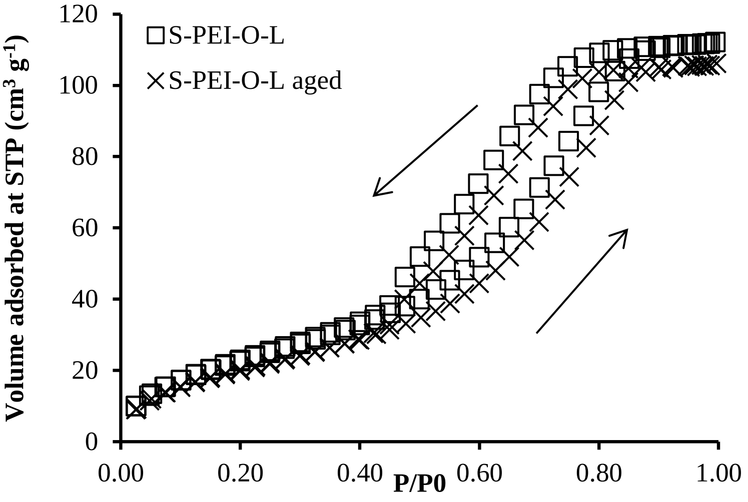

Figure A18. Nitrogen sorption isotherms S-PEI-O-L before and after steam regeneration.

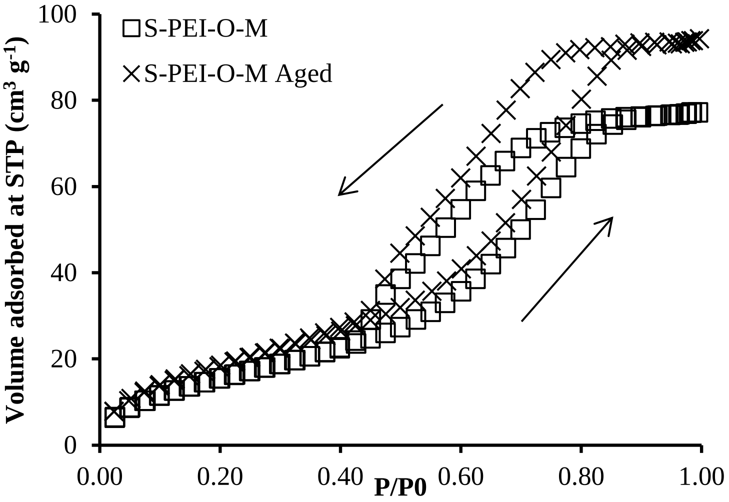

Figure A19. Nitrogen sorption isotherms S-PEI-O-M before and after steam regeneration.

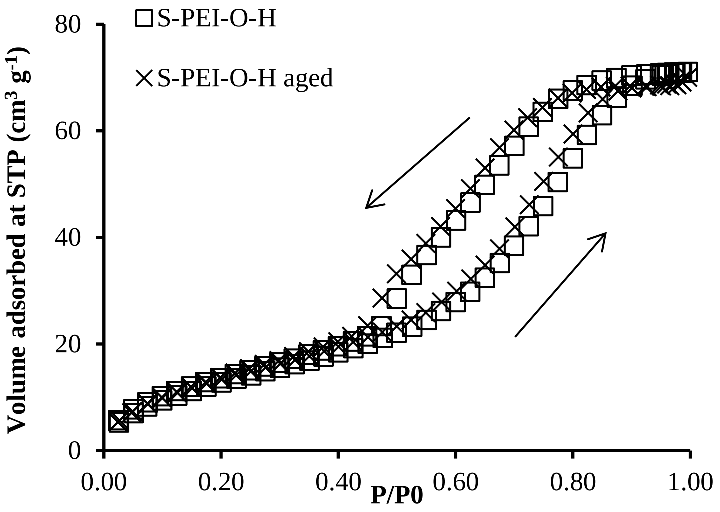

Figure A20. Nitrogen sorption isotherms S-PEI-O-H before and after steam regeneration.

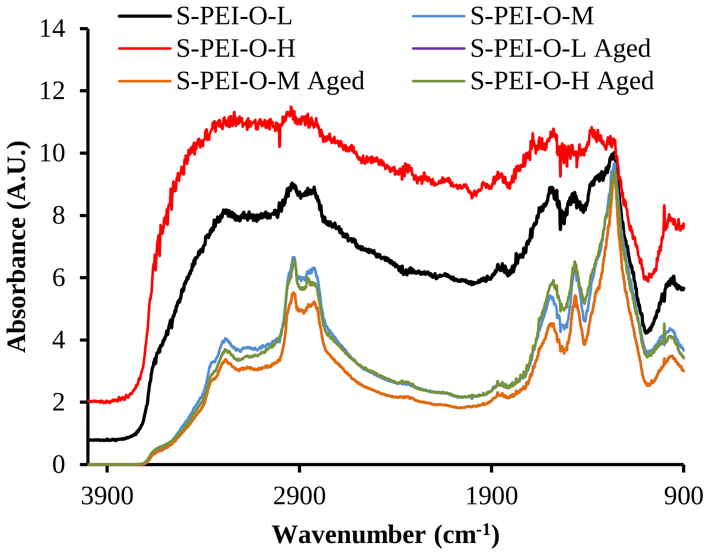

Figure A21. DRIFT spectra of triethoxy(octyl)silane adsorbents before and after aging.

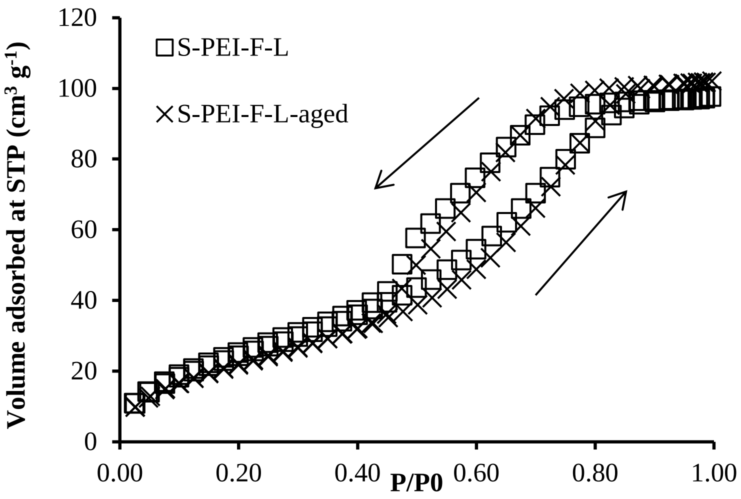

Figure A22. Nitrogen sorption isotherms S-PEI-F-L before and after steam regeneration.

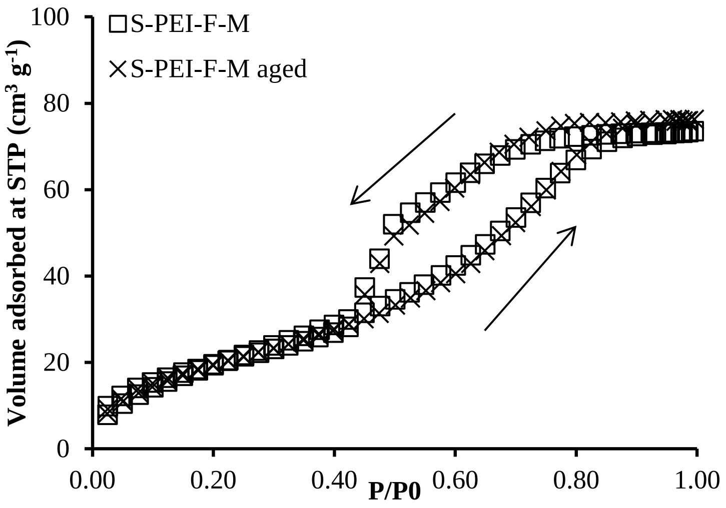

Figure A23. Nitrogen sorption isotherms S-PEI-F-M before and after steam regeneration.

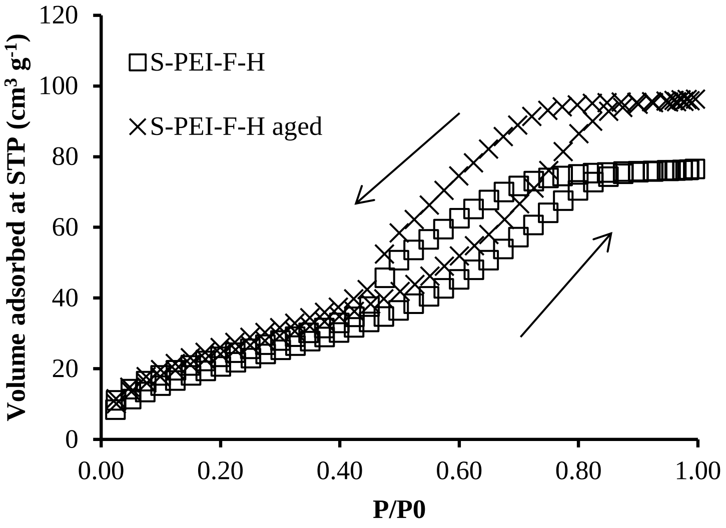

Figure A24. Nitrogen sorption isotherms S-PEI-F-H before and after steam regeneration.

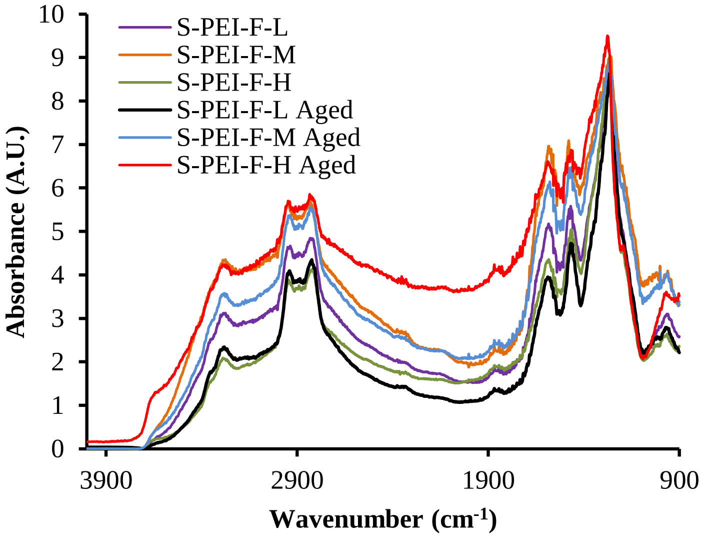

Figure A25. DRIFT spectra of perfluorodecylsilane functionalised adsorbents before and after aging.

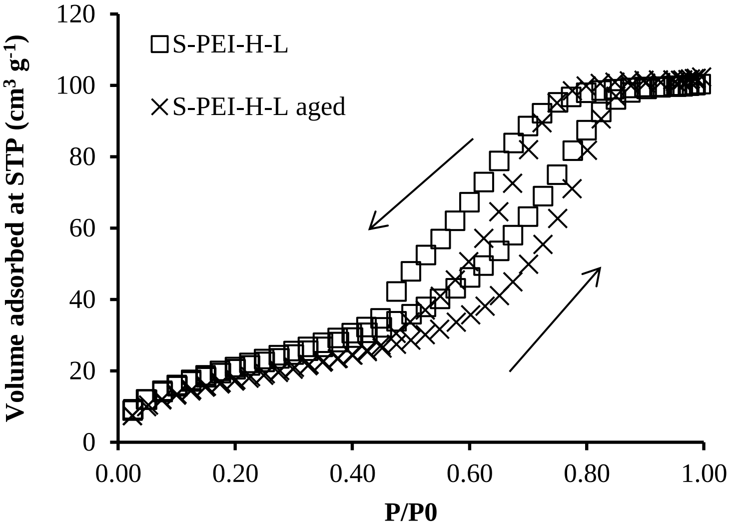

Figure A26. Nitrogen sorption isotherms S-PEI-H-L before and after steam regeneration.

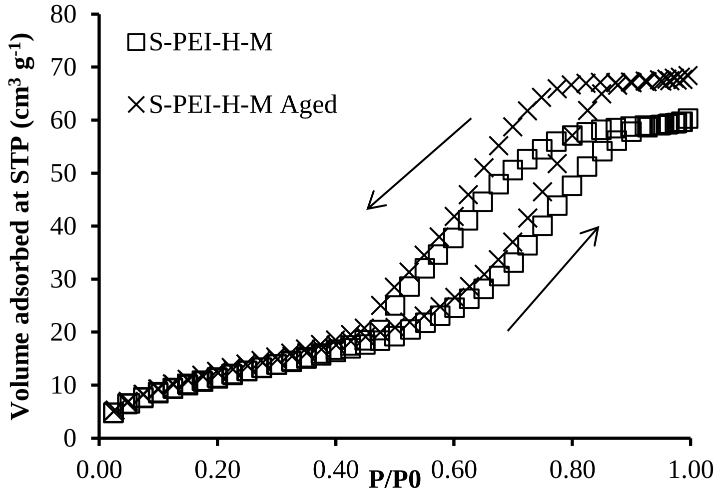

Figure A27. Nitrogen sorption isotherms S-PEI-H-M before and after steam regeneration.

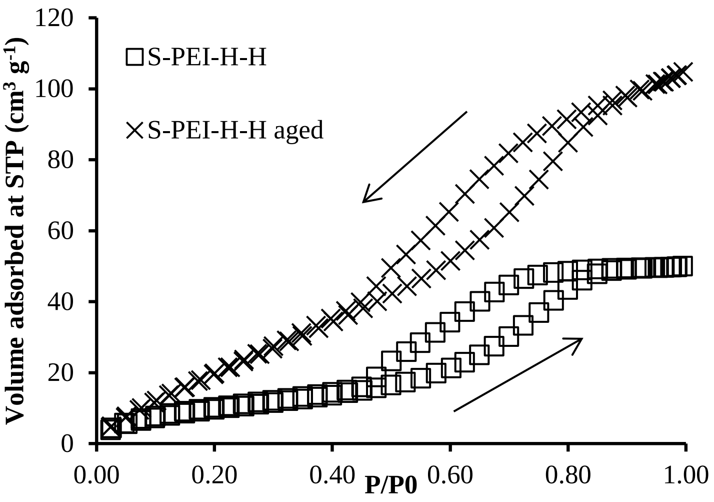

Figure A28. Nitrogen sorption isotherms S-PEI-H-H before and after steam regeneration.

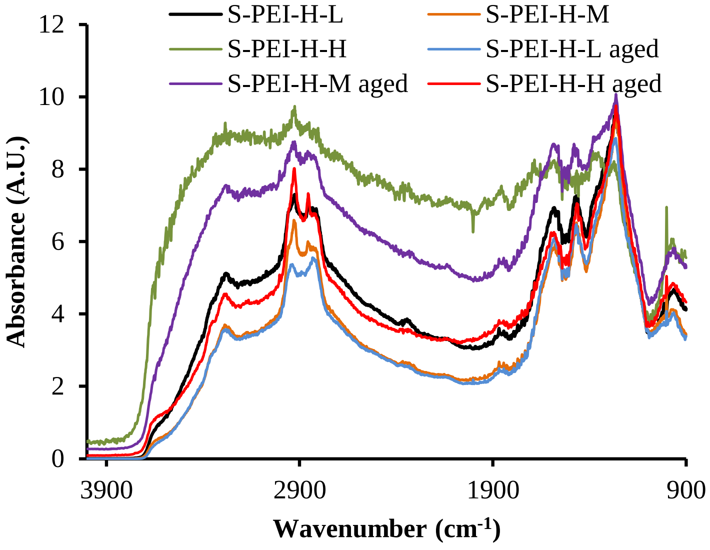

Figure A29. DRIFT spectra of hexadecylsilane functionalised adsorbents before and after aging.

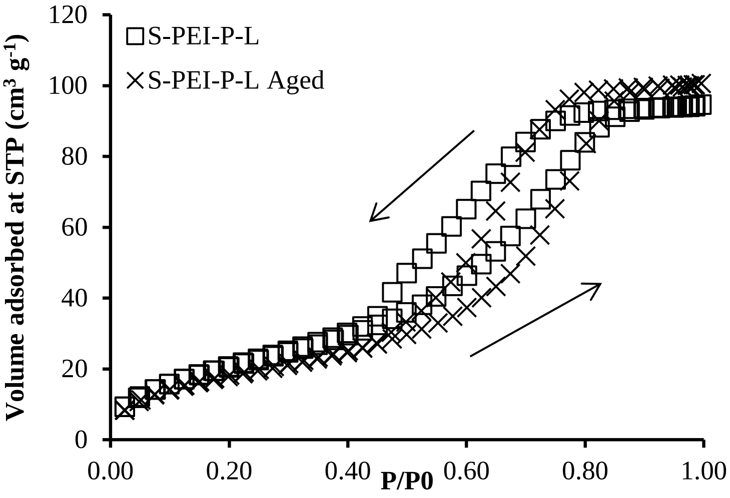

Figure A30. Nitrogen sorption isotherms S-PEI-P-L before and after steam regeneration.

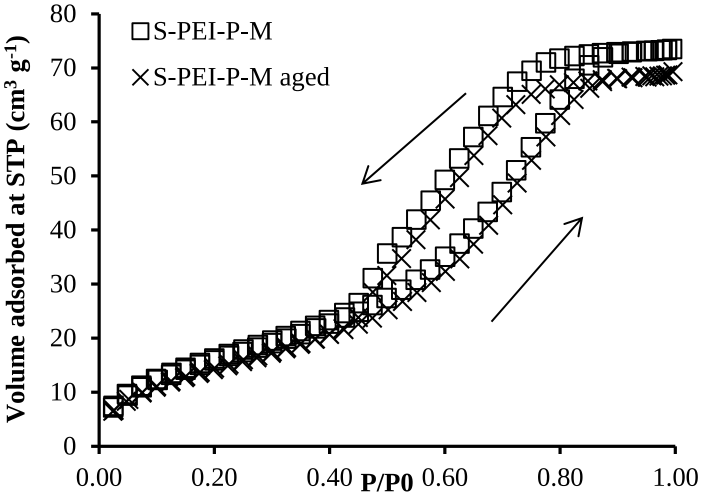

Figure A31. Nitrogen sorption isotherms S-PEI-P-M before and after steam regeneration.

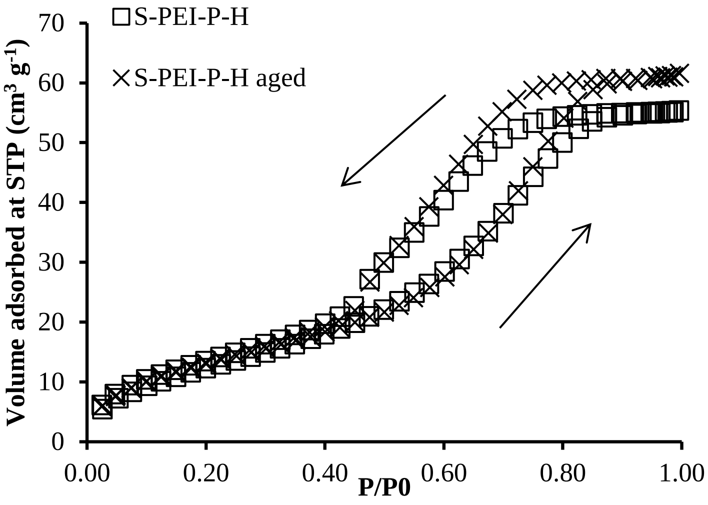

Figure A32. Nitrogen sorption isotherms S-PEI-P-H before and after steam regeneration.

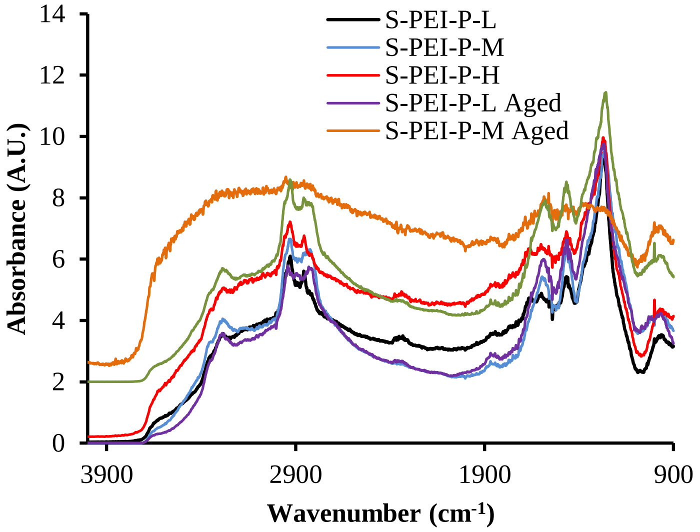

Figure A33. DRIFT spectra of phenylsilane functionalised adsorbents before and after aging.

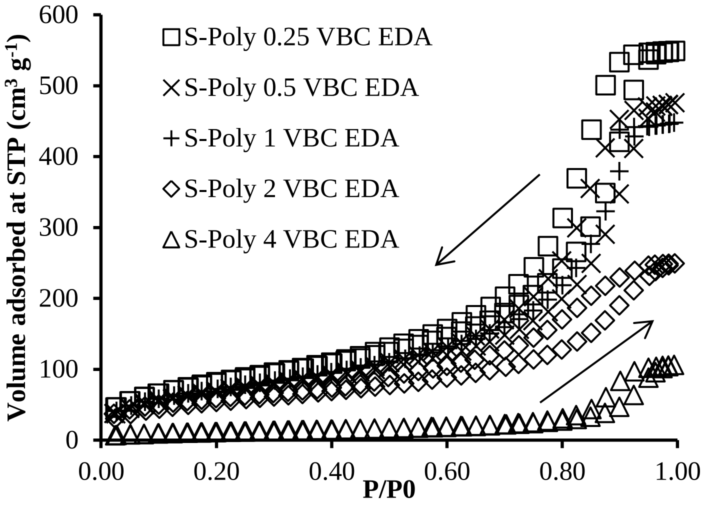

Figure A34. Nitrogen sorption isotherms of free radical polymerised adsorbents.

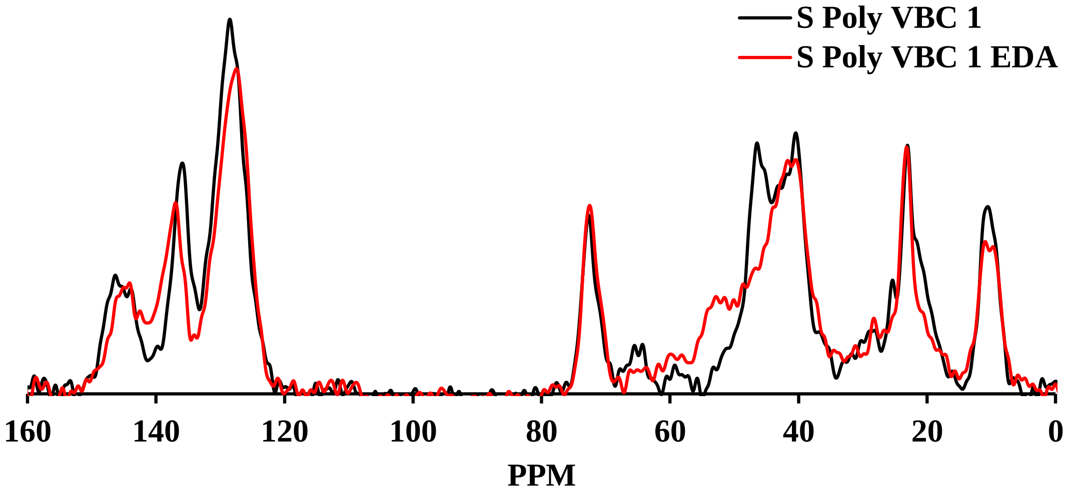

Figure A35. SSNMR of S-Poly VBC before and after functionalisation with ethylenediamine.